Modelling and estimating tree and forest resources of the Dry Afromontane forests in South-central Ethiopia using field and remotely sensed data

Modellering og estimering av tre- og skogressurser i de tørre afromontane skogene i det sør-sentrale Etiopia ved bruk av feltinventering og fjernmåling

Zerihun Asrat Kutie

Modelling and estimating tree and forest resources of the Dry Afromontane forests in South-central Ethiopia using field and remotely sensed data
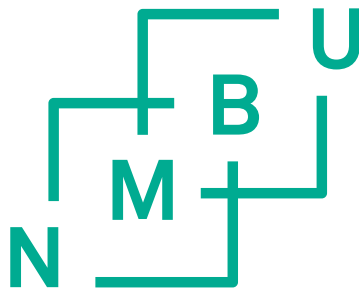
Modellering og estimering av tre- og skogressurser i de tørre afromontane skogene i det sør-sentrale Etiopia ved bruk av feltinventering og fjernmåling

Philosophiae Doctor (PhD) Thesis

Zerihun Asrat Kutie

Norwegian University of Life Sciences
Faculty of Environmental Sciences and Natural Resource Management

Ås 2020

PhD Supervisors:

Professor Terje Gobakken
Faculty of Environmental Sciences and Natural Resource Management
Norwegian University of Life Sciences
P.O. Box 5003, NO - 1432 Ås,
Norway

Professor Tron Eid
Faculty of Environmental Sciences and Natural Resource Management
Norwegian University of Life Sciences
P.O. Box 5003, NO - 1432 Ås,
Norway

Professor Erik Næsset
Faculty of Environmental Sciences and Natural Resource Management
Norwegian University of Life Sciences
P.O. Box 5003, NO - 1432 Ås,
Norway

Research professor Hans Ole Ørka
Faculty of Environmental Sciences and Natural Resource Management
Norwegian University of Life Sciences
P.O. Box 5003, NO - 1432 Ås,
Norway

Associate Professor Mesele Negash
Wondo Genet college of Forestry and Natural Resources
Hawassa University
P.O. Box 128, Shashemene,
Ethiopia

PhD Evaluation Committee

Professor Henrik Meilby
Department of Food and Resource Economics
University of Copenhagen
Rolighedsvej 23, 1958 Fredriksberg C,
Denmark

Professor Timo Erkki Tokola
School of Forest Sciences
University of Eastern Finland
P.O. Box 111, FI-80101 Joensuu,
Finland

Dr Meley Mekonen Rannestad
Faculty of Environmental Sciences and Natural Resource Management
Norwegian University of Life Sciences
P.O. Box 5003, NO - 1432 Ås,
Norway

Acknowledgements

Contents

Abstract

For effective forest management missions, the presence of accurate information about the forest resources is indispensable. However, the absence of such relevant information for most natural forests in Ethiopia have been challenging the success of management efforts. Lack of appropriate methods, models and data are usually the bottleneck for the availability of the required information. This thesis thus, aimed at identifying and evaluating methods and providing models and data required for estimating tree and forest resources to enhance forest management decision-making. In Paper I, suitability of satellite images for forest area and canopy cover estimation based on visual image interpretation was evaluated. PlanetScope, RapidEye and Sentinel-2 imageries were used under different forest conditions in Ethiopia. Promising results were obtained where the required forest area and canopy cover estimates of large forest areas can be determined with relatively less time than field-based survey. When choosing satellite images, the spatial resolution should be considered carefully. Particularly for densely forested areas finer resolution images should be used. Imageries with high temporal resolution enhance estimation results by offering relatively more cloud free images. In Paper II, models for quantifying basic tree biometric properties including total tree and section volumes were developed and wood basic density data for 30 tree species in Dry Afromontane forests of south-central Ethiopia were documented. The models and data may also be applied to other similar forests. In Paper III, aboveground tree biomass prediction options were assessed for the study sites. The newly developed models are accurate and flexible in application depending on the availability of data from forest inventory. Models developed previously elsewhere were evaluated on our data and generally large prediction errors were observed. Indirect biomass prediction option from volume, using biomass expansion factor and wood basic density, was also assessed and found to be less accurate than the direct method using the newly developed models. Finally, Paper IV assessed the use of satellite images of Landsat 8, Sentinel-2 and PlanetScope for biomass estimation. The biomass model developed in Paper III was used to calculate ground reference values for the 111 systematically distributed sample plots. As a first practical experience for this type of forest in Ethiopia, the possible best spectral and textural variables to be used in biomass prediction models were identified for the respective image types. Model-assisted aboveground biomass estimation method in all the three imageries cases improved estimation efficiency compared to the purely field-based estimation. The estimation efficiency gain from Sentinel-2 was much larger than the others. In general, though further research still required on some gap areas, the developed models along with documented data and evaluated methods in this thesis may have strong practical implications to enhance forest management decision-making including the implementation of REDD+ MRV programs in the Dry Afromontane forests in Ethiopia.

List of papers

The PhD thesis is based on the papers listed below and are referred to by their roman numbers (I-IV).

Paper I

Asrat, Z., Taddese, H., Ørka, H.O., Gobakken, T., Burud, I., Næsset, E., 2018. Estimation of forest area and canopy cover based on visual interpretation of satellite images in Ethiopia. *Land*, 7(3), 92.

Paper II

Asrat, Z., Eid, T., Gobakken, T., Negash, M., Modelling and quantifying tree biometric properties of Dry Afromontane forests of South-central Ethiopia. (In press).

Paper III

Asrat, Z., Eid, T., Gobakken, T., Negash, M., Aboveground tree biomass prediction options for the Dry Afromontane forests in South-central Ethiopia. *Forest Ecology and Management*, 473, 118335.

Paper IV

Taddese, H., Asrat, Z., Burud, I., Gobakken, T., Ørka, H.O., Dick, B.Ø., Næsset, E., Use of remotely sensed data to enhance estimation of aboveground biomass for the Dry Afromontane forest in South-central Ethiopia. (manuscript).

x

1.0. Introduction

1.1. General background

Around 50% of all the land areas on the earth can potentially support forests (Grace et al., 2014); while today's forest cover only about 31% (4.06 billion ha) of the land, as vast areas have been cleared (FAO, 2020). Forest covers of the world have been changing over time. Between the years 1990 and 2020 the global forest cover has shrunk by 178 million ha, though the overall rate of deforestation has slowed down. However, the ways in which the forest areas have changed over those decades is interestingly important. While net forest areas have increased in some parts of the world mainly Europe and Asia since 1990, by far the largest forest area conversion to other land uses between 1990 and 2020 occurred in the tropics of Africa and South America, which has shown losses in every measurement period of the global forest resource assessment (FAO, 2020).

Forests in the tropics account for 45% of the global forest area (FAO, 2020). Various forest types such as rainforests, montane forests, dry forests, woodlands, mangroves, etc. are found in the tropics (Brandon, 2014). Tropical forests play a pivotal role of socio-economic and ecological significance from local to the global perspectives, hence supporting directly or indirectly the livelihoods of several millions (Hewson et al., 2014; FAO and UNEP, 2020). The forests have been sequestering large carbon quantities and they are a huge store of carbon stocks. Though the reported figures have some variations, tropical forests stored more than 270 Pg of carbon (e.g. Pan et al., 2011; Grace et al., 2014). Embracing many of terrestrial species, the forests also maintain higher levels of biodiversity than any other forests on the planet (Brandon, 2014). Products and services like timber, fuel wood, water purifications, as well as cultural and religious values of tropical forests are huge. However, tropical forests are suffering from severe deforestation and forest degradation, primarily caused by anthropogenic activities like timber and fuel wood extraction, conversion of the forest areas to agricultural lands, mining, and infrastructure development (Venter and Koh, 2012). Deforestation and forest degradation in the tropics exacerbate loss of biodiversity and increase in global carbon emissions (FAO and UNEP, 2020).

Coordinated efforts have been made globally towards sustainable management and utilization of the resources. A compensation-based policy mechanism: Reducing Emissions from Deforestation and forest Degradation, and the sustainable management of forests, and the conservation and enhancement of forest carbon stocks (REDD+) was established, so as to address the issues and concerns over the conservation of tropical forest and to mitigate adverse effects of carbon emissions on global climate change. The REDD+ evolved gradually into its latest

form and contents. First it was introduced to the United Nations Framework Convention on Climate Change (UNFCCC) in 2005 as reduced emission from deforestation (RED), at the 11th Conference of Parties in Montreal (Hewson et al., 2014). Under the REDD+ mechanism, participating developing countries are supposed to receive payments for their verified achievement in reducing carbon emissions from forest related activities as well as enhancing the removal of the carbon from the atmosphere (Goetz et al., 2015). This mechanism has been accepted as a low cost and promising approach for mitigating climate change (Angelsen and Brockhaus, 2009) that also may secure several ecological functions of forests, including biodiversity conservation. Many developing countries have been adopting REDD+ programs, and the number has increased significantly since the initial introduction under the UNFCCC. Though the REDD+ program, has been adopted and implemented in several countries, some key aspects of the REDD+ yet need to be solved in many of the developing tropical countries. For instance, establishing efficient and credible Measurement, Reporting, and Verification (MRV) systems and conducting proper national forest monitoring and assessment tasks have been challenging (Gizachew et al., 2017), while they are significantly important since payments for carbon offsets under the REDD+ mechanism are made based on the estimates of forest carbon stocks and changes (Mattsson et al., 2012; Goetz et al., 2015).

The Good Practice Guidelines (GPG) by the Intergovernmental Panel on Climate Change (IPCC) provide guidance on estimation methods at different levels of details (i.e. Tier 1, 2 and 3) in which a Tier represents a level of methodological complexity (IPCC, 2006). For the methods in the sector of Agriculture, Forestry and Other Land Uses, the GPG provides a framework of Tier structure. Accordingly, Tier 1 is the simplest alternative to apply, which utilizes globally available activity data and makes use of default equations and values that are directly provided by the IPCC. Relatively higher uncertainties are associated with Tier 1 as compared to the other higher Tiers. On the other hand, Tier 2 utilizes country- or region-specific data for the most important land-use categories, while Tier 3 utilizes high order methods including models and inventory measurement systems that are tailored for the country specific conditions (IPCC, 2006).

Tree biomass, volume, wood basic density, etc. are among important components in greenhouse gas (GHG) inventories carried out in forestry as outlined by the IPCC's GPG. The IPCC encourages countries to apply higher Tiers by developing their country-specific emissions factors, such as allometric models for more accurate biomass estimation (Penman et al., 2003; IPCC, 2006; Petrokofsky et al., 2012). Accurate biomass estimations are essential for computing carbon stock in forests. The MRV system is thus responsible for ensuring such accurate estimations in

the REDD+ programs implementation. Biomass estimations can be done based on field survey or remote sensing assisted approaches (Lu, 2006). Even though, the field-based survey approach is an accurate method for estimation of biomass; it is time consuming, labour intensive, and difficult to implement in remote forest areas and areas with large geographic extent with reasonable cost and precision (Saarela et al., 2015; Næsset et al., 2016). Therefore, integration of the field-based survey with a remote sensing assisted approach is sought. Accordingly, methods integrating remotely sensed data have gained wider acceptance for biomass and other forest attributes estimations, due to their potential to overcome the limitations of using solely field-based approach. Moreover, remotely sensed data can provide a holistic view over large areas and enhance the efficiency and usefulness of limited conventional field-based methods (Sinha et al., 2015). There are, however, technical (capacity) and resource (infrastructure) limitations in most developing countries to fully benefit from the advancement of remote sensing technologies (Singh, 2013).

In addition to forest biomass and volume parameters, proper and accurate estimation methods for forest area and forest cover change are significantly important for the REDD+ programs as well as for the regular forest management and monitoring practices. For instance, establishing a forest reference level (FRL), that serve as benchmark for REDD+ programs, requires knowing the state of the forest and forest cover changes. This refers to the deforestation and afforestation conditions that result in forest area changes. Therefore, it is mandatory for REDD+ undertakings to accurately estimate the current status of a forest and its spatio-temporal change through a more rigorous methodology that results in a reliable estimate as outlined in the IPCC's GPG (Penman, 2003). Remotely sensed data are, therefore, considered fundamental and play crucial role in the development of cost-efficient methods for estimations of forest parameters (e.g. biomass and forest cover/area) needed in REDD+ programs (Asner et al., 2012, Næsset et al., 2016). Thus, it will be important to understand and quantify the contribution of different remotely sensed data in improving the estimates of the parameters of interest under different forest conditions, as this may shape investment decisions in development of cost efficient MRV systems in the tropical countries.

1.2. Forests and their management in Ethiopia

Ethiopia is a country located in the east African region with an area of over one million square kilometres. It has diverse topographic features with altitudes ranging from about 125 m b.s.l. to over 4500 m a.s.l., having more landmass above 2000 m than any other country in Africa. The highlands that possess Afromontane vegetations were separated by the East African Rift Valley into the eastern and western highlands (Friis et al., 2010). The altitudinal variations and

associated agroecological zones have resulted in the formation of different types of vegetations. Floristic analyses of the country have revealed that there were up to 7,000 estimated higher plant species out of which about 12% are estimated to be endemic (Gebre-Egziabher 1991; Vivero et al., 2006). Friis et al. (2010) categorized the vegetations in Ethiopia into twelve major types. For the purposes of FRL report compilation and conducting the national forest inventory, the vegetation classes were formed in to four main biome types, i.e., Moist Afromontane, Dry Afromontane, *Acacia-Commiphora* and *Combretum-Terminalia* (UN-REDD, 2017). The Dry Afromontane forests, where most of the studies in this thesis were conducted, are distributed over the north-central, central and south-central highlands of the country where the altitude ranges between 1500 – 3400 m.a.s.l with tree species of *Juniperus procera*, *Afrocarpus falcatus*, *Olea europaea*, *Croton macrostachyus* and *Ficus species,* dominating the upper canopy while the middle and lower canopy are usually occupied by *Allophylus abyssinicus*, *Apodytes dimidiata*, *Bersama abyssinica*, *Cassipourea malosana*, *Celtis africana*, *Chionanthus mildbraedii* and *Dombeya torrida* (Friis et al. 2010).

Forests supply most of the wood products for domestic use, as well as large volume of diverse non-wood forest products, in addition to their ecological functions. It has never been easy, however, to get reliable estimates on the state of forest cover and forest cover change, growing stock volume, biomass, etc. in Ethiopia (Singh, 2013). There were limited and conflicting information, partly attributed to varied definitions of forest and methodological inconsistencies. The Woody Biomass Inventory Strategic Planning Project (WBISPP) report was the only comprehensive source of information on forests in Ethiopia, which estimated that around 4.07 million ha of Ethiopia's land was covered by high forest, that accounts to about 3.56% of the total land area (WBISPP, 2005). In another report, FAO (2010) estimated that total forest cover was about 12.29 million ha, which is about 11% of the total land area. On the other hand, recently the forest cover of the country was reported to be 15.5% (UN-REDD, 2017; Bekele et al., 2018). A recently released report of the national forest inventory (NFI) now also serves as a source of information (MEFCC, 2018a). The average annual forest loss was estimated to be about 92,000 ha per year, where the main drivers of deforestation and forest degradation were expansion of agriculture land, intensive fuel wood consumption, illegal timber processing and forest fires (UN-REDD, 2017). According to a document from the government (FDRE, 2011), if actions are not taken to change the traditional development path, an area of 9 million hectares might be deforested between the years 2010 and 2030.

Ethiopia has been striving to conserve its forests and minimize deforestation and forest degradation by implementing different forest management schemes such as participatory forest

management, area exclosures, biosphere reserves, etc. at various geographic scales (Lemenih and Kassa, 2014; Lemenih et al, 2015; NABU, 2017). Moreover, Ethiopia has chosen REDD+ as a climate change mitigation mechanism for the forest sector. The REDD+ was evolved as an integral part of the Climate Resilient Green Economy (CRGE) strategy, which provides an ambitious cross-sectoral plan for achieving the economic transition without increasing current levels of GHG emissions. The strategy identified forestry as one of the sectors having the largest abatement potential. Therefore, protecting and re-establishing forests for their economic and ecosystem services including carbon stocks is one of the pillars of the CRGE strategy, and REDD+ has been selected as one of the initiatives for fast-track implementation to achieve CRGE objectives (FDRE, 2011). Since Ethiopia first initiated the REDD+ process at national level by requesting to participate in the World Bank's Forest Carbon Partnership Facility in 2008, several stepwise milestone activities have been conducted. It has designed and conducted NFI, which was finalized and reported in 2018 (MEFCC, 2018a). The country has also established and submitted its updated FRL report in 2017, which was prepared in the context of results-based payments for REDD+ implementation. The FRL quantified activity data (deforestation and afforestation) and indicated the GHG considered (i.e. CO_2) by pools (i.e. aboveground, belowground, and deadwood biomass); based on historical average data between 2000 and 2013 (UN-REDD, 2017). It is expected and emphasized also in the report that the relevant forest information will be updated periodically applying relevant state of the art quantification methods and options.

Sound and broad-based forest management decisions under any management schemes require accurate information of the forest resources, which in turn depend on the availabilities of accurate measurement, prediction and estimation processes. Therefore, the implementation of REDD+ activities should be measured, reported and verified using appropriate national forest monitoring systems with proper combinations of remotely sensed and ground-based inventory techniques. In addition, such systems serve as bases for formulating policy measures and adapting management techniques, also provide information to evaluate the success of implemented policies and programs. However, currently prediction models for biomass, volume, etc. and other data that are relevant for estimating forest parameters such as carbon stocks, are not sufficiently available in Ethiopia. Furthermore, despite the potential of the remote sensing-assisted methods for REDD+ related issues as well as conventional forest management aspects, there has been limited studies in relation to all forest types in Ethiopia. As a result, the Tier-3 approach to carbon inventory that was proposed by the IPCC has been challenging to implement in Ethiopia.

2.0. Objective

The main objective of this thesis was to identify and evaluate methods as well as provide models and inputs data required for estimating tree and forest resources to enhance forest management decision-making and support implementations of the REDD+ MRV system in Ethiopia. The specific objectives of the thesis, addressed through the four papers, were:

1. To assess feasibility of satellite images for forest area and canopy cover estimation based on visual image interpretation. (Paper I)

2. To develop models for tree volume and other biometric properties (height, diameter at breast height and bark thickness) and to document wood basic density data for trees in Dry Afromontane forest of south-central Ethiopia. (Paper II)

3. To evaluate aboveground biomass prediction options for trees in Dry Afromontane forests of south-central Ethiopia. (Paper III)

4. To evaluate application of remotely sensed optical satellite images data for aboveground biomass estimation in the Dry Afromontane forests of south-central Ethiopia. (Paper IV)

3.0. Conceptual framework

Figure 1 shows the conceptual framework of this thesis including the workflow and interdependences between the main activities (objectives). Data were obtained by integrating sample plot inventory, destructive sampling and remote sensing. In the sample plot inventories variables such as tree height (ht), diameter at breast height (dbh), diameter at stump height (dsh) and bark thickness (bt) are measured. From this, information about the forest population are generated and used as basis for selecting trees for destructive sampling. The measurements from sample plot inventories are also used for modelling ht-dbh, dbh-dsh and bt-dbh relationships. Data from destructive sampling of trees are used for modelling total tree and sections volume and aboveground biomass (AGB). In addition, wood basic density (wbd) data are compiled and documented from the harvested sample trees. Remotely sensed data, optical satellite images in this case, are used to enhance forest area, forest biomass and canopy cover estimations. For a forest biomass estimation, using different satellite images, individual tree and plot data from sample plot inventory are used along with the developed individual tree AGB and ht-dbh models as well as wbd data to derive biomass estimates at plot level. The biomass at plot level is later used to calibrate models based on data extracted from the satellite images. Forest area and canopy cover estimations are carried out based on visual interpretation of the different satellite images. Different statistical modelling and analyses techniques are applied to develop the models and assess their performances, and to evaluate estimation methods for forest biomass, forest area and canopy cover. The results of the thesis are given as models, methods and data that will enhance forest management decision-making including the implementations of REDD+ MRV programs.
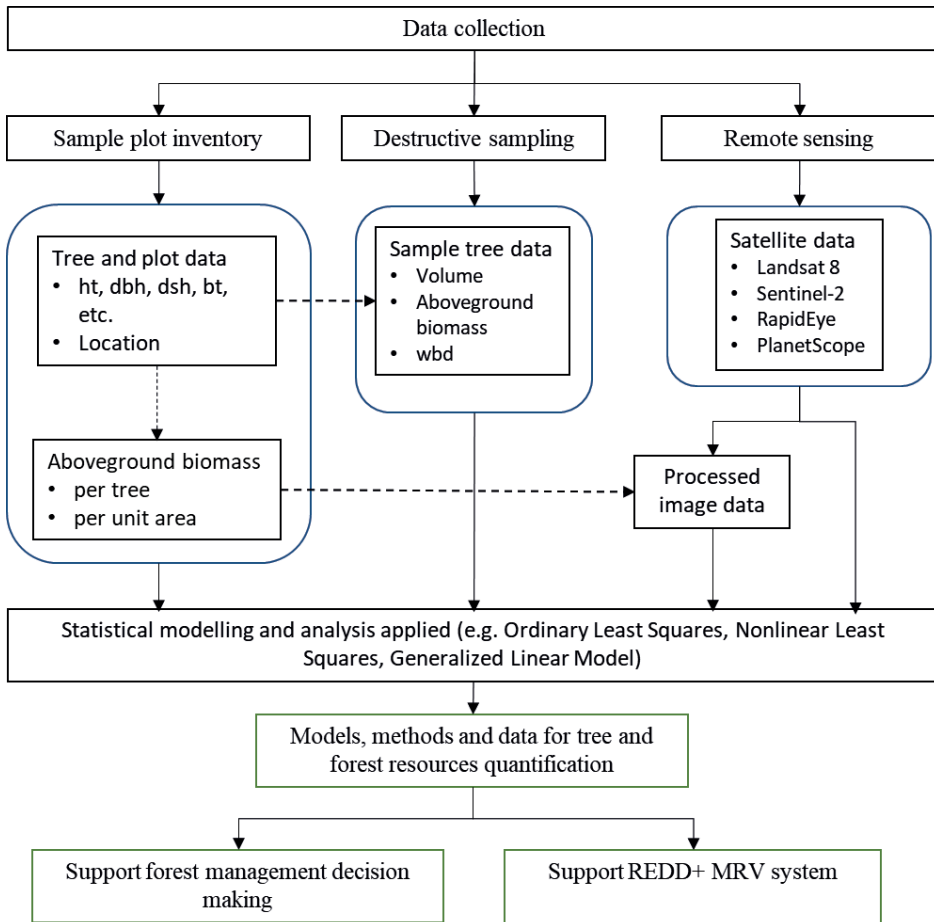
Figure 1. Conceptual framework for the thesis.

4.0. Motivation

4.1. Forest area and canopy cover estimation

Information about forest area is among the crucial inputs for forest management decisions. Forest area estimates essentially facilitate quantification of resources up on which forest management and utilization activities, such as, production planning, making marketing decisions, setting and evaluating policies, etc. are based. Hence, there is always a constant demand for accurate and up to date information on forest area estimates at a local, regional, and national scale (Deppe, 1998). In addition, in REDD+ implementations, where countries are required to report their contribution of climate change mitigation efforts to access result-based payments, accurate and consistent information on forest area and forest area change are important. In a basic methodological approach of estimating greenhouse gas emissions and removals, activity data are multiplied with emission factors, coefficients that quantify emissions per unit area such as tons of CO_2 equivalent per ha (Penman et al., 2003). In this regard forest area change estimates (i.e. activity data), which often provide information on the extent of human activity resulting in emissions from deforestation and forest degradation or removals from afforestation, are basic inputs. For effective assessment of the forest area and forest area change the presence of working definition of forest is also mandatory. Usually, a comprehensive forest definition includes threshold values for quantitative variables including minimum area, minimum crown cover percent, minimum tree height, and minimum width. Thus, crown or canopy cover estimate, which is the proportion of the land covered by the vertical projection of tree crowns, also plays a significant role in forest management for various decisions related to silviculture and utilization of the forests in addition to qualifying the forest definition (Korhonen et al., 2006).

Forest area determination may be done via mapping approaches such as digital processing of remotely sensed data (e.g. satellite images) which results in a map that shows the spatial arrangement of the forest patches. In some past and current practices of forest cover assessment and land use/land cover (LULC) mapping in Ethiopia, digital image classification and mapping methods are practiced (e.g., Kindu et al., 2013; Hailemariam et al., 2016). However, digital image classification and mapping methods in general require a high level of technical skills, and in most cases, technical software (Bey et al., 2016). Furthermore, the spectral similarity of land-cover classes is also challenging. As a result, the wider application and use of such methodologies for large-scale activities such as nationwide assessment could be problematic. Consequently, estimates and reports from most developing tropical countries including Ethiopia have been highly uncertain, hence necessitating for suitable actions to be taken (IPCC, 2006; Singh, 2013). Alternatively, forest area and canopy cover estimates may be obtained through statistical

sampling either observed in the field or from remotely sensed imageries by visual interpretation. To maximize from visual image interpretation method and overcome the drawbacks of digital image processing, some platforms and open source software such as Geo-Wiki, VIEW-IT, Sky Truth and Collect Earth have been developed and used (Clark and Aide, 2011; Fritz et al, 2012; Bey et al., 2016). The software packages have been used for interpretation of satellite imagery with different spatial resolutions under different forest conditions to provide reference data for forest area and forest cover change estimates (Potapov et al., 2014; Sannier et al., 2014). The application of some of the software packages is associated with the use of very high-resolution images, which are often known to have a small geographic scope and an irregular time interval of acquisition, in turn limiting its utility for large areas. On the other hand, Landsat images that are available at global scale, have relatively low spatial and temporal resolutions. Therefore, since forest conditions and properties of the imageries, could potentially influence estimates, it is important to evaluate different types of satellite images under different forest conditions to provide guidelines for using such tools at a national level.

The main objective of Paper I was thus to identify and evaluate the use of alternative types of satellite images for forest area and canopy cover estimation based on visual image interpretation under different forest conditions in Ethiopia.

4.2. Basic models and data for tree biometric properties

Availability of basic tree biometric data like ht, dbh, bt, volume, biomass and wbd, are critical for enhanced forest management decision-making. Some of the variables are obtained through observation while others are determined using appropriate models. In forest management tree height data are usually needed for estimation of tree volume, biomass, site index, etc. Unlike diameter, which is easily measured for all trees, measuring height is more difficult, time consuming, costly and prone to measurement errors (Larjavaara and Muller-Landau, 2013). Thus, height measurement for all trees on sample plots in any given forest inventory task may not be feasible. Therefore, ht-dbh models developed from sample trees data are commonly used to predict missing heights (West, 2015; Mugasha et al., 2013a; 2019). In the same line established dbh-dsh relationship provide an opportunity to quantify volume or biomass losses from previous harvest or damage where only dsh can be measured (Corral-Rivas et al., 2007; Özçelik et al., 2010). Furthermore, quantifying bark thickness of trees by means of an established bt-dbh relationship might be useful either to assess the volume of solid wood to be used for construction materials or volume of bark to be used for energy purposes, spices or medicine (van Laar and Akça, 2007; Kershaw et al., 2017).

Volume data are important to describe present forest resources, also as a variable in growth and yield models for predicting future growing stocks. Impacts of harvest and silvicultural practices may be evaluated in terms of changes in growing stock volume (Vanclay, 1994; Weiskittel et al., 2011). Volume data may also be used to determine biomass using expansion and conversion factors (Lindner and Karjalainen, 2007; Bollandsås et al., 2016). In Ethiopia there is a recent growing concern for sustainable management and utilization, including sustainable timber harvesting, of natural forests particularly in a participatory forest management scheme as opposed to protection-oriented measures which have led to intensification of illegal logging practice (Lemeneh et al., 2015; Ayele et al., 2018; MEFCC, 2018b). In this regard, despite the relevance of volume models (i.e. total tree and sections volume models), currently there is no volume model developed for the natural forests in Ethiopia apart from a few species-specific models for plantations (Henry et al., 2011). As a result, default form factor of 0.5 has been used to estimate tree volume along with dbh and ht (e.g. Sisay et al., 2017).

Information on wbd of trees have been used to facilitate forest management decisions. It is used as basis for characterizing tree species from a wood utilization point of view (Chave et al., 2009; Missanjo and Matsumura, 2016), and may also have management implications since larger wbd indicates better wood quality for fuel (Githiomi and Kariuki, 2010) and better resistance to severe abiotic disturbance factors (Chave et al., 2009). Wood basic density may also be used to predict biomass either when using allometric models (Chave et al., 2014; Njana et al., 2016) or along with biomass expansion factors and volume data (Bollandsås et al., 2016). Since wbd varies with tree height and age, and among tree sections, species, sites, and other environmental factors (Githiomi and Kariuki, 2010; Henry et al. 2010; Ubuy et al., 2018a; Tesfaye et al., 2019), it should be determined and documented in such a way that addresses these variations.

The main objective of Paper II was therefore to provide models and data that can be used as tools for quantifying biometric tree properties (i.e. ht, dbh, bt, volume and wbd) and in this way facilitating a sustainable management and use of the forest resources in the Dry Afromontane forests of south-central Ethiopia.

4.3. Aboveground tree biomass prediction options

Information about tree biomass is important in forestry to understand how tree growth occur by producing biomass through photosynthesis, to quantify products such as wood for fuel or pulp and to determine how much carbon is sequestered in forests as a result of trees taking carbon dioxide from the atmosphere (Köhl et al., 2006; West, 2015). In line with climate change and subsequent efforts to mitigate that, accurate biomass and carbon stock estimation methods

have become a concern of the global community (e.g. Brown, 2002; IPCC, 2006). Aboveground biomass, one of the five carbon pools in a forest ecosystem, has the largest carbon storage potential in the tropical forests (Pan et al., 2011). Biomass estimations are often carried out either on ground-based survey or using remotely sensed auxiliary data. In any case the presence of accurate individual tree biomass prediction option is fundamental to predict biomass of trees observed in the field sample plots, which then further aggregated and analysed or used as ground reference for remote sensing-based estimation (Temesgen et al., 2015). Tree biomass prediction options could be direct, using existing or new allometric models, or indirect, using conversion factors. Allometric models are constructed based on relationships between trees AGB and measurable tree variables (e.g. dbh, ht, wbd, etc.). The relationships are explored empirically from calibration data where AGB has been directly measured by destructive sampling along with measurements of the predictor variables (Bollandsås et al., 2016).

A review by Henry et al. (2011) on biomass models in sub-Saharan Africa showed that most of the available models in Ethiopia are limited to a few *Eucalyptus* species in plantations, while about 98% of the species remained uncovered. Recently some species-specific models for natural forests have been developed (e.g. Tesfaye et al., 2016; Kebede and Soromessa, 2018; Daba and Soromessa, 2019). A few mixed-species general biomass models also exist in some parts of the country and certain forest conditions (Eshete and Ståhl, 1998; Mokria et al., 2018; Ubuy et al., 2018b). Except for Tetemke et al. (2019), who developed mixed-species models including ten tree species for the Dry Afromontane forests in northern Ethiopia, no such models exist for this type of forests. As a result, pan-tropical models (Brown, 1997; Chave et al., 2005; 2014) have been commonly used (e.g. MEFCC, 2018a; Gebeyehu et al., 2019). Ethiopia's FRL report also recommends the pan-tropical biomass model developed by Chave et al. (2014) to be applied across all forest types due to lack of existing biomass models in the country (UN-REDD, 2017). In addition to direct prediction of tree biomass using allometric models, biomass may be predicted indirectly from volume using a biomass expansion factor (BEF) and wbd (Brown, 1997).

The main objective of Paper III was therefore to explore different aboveground tree biomass prediction options for Dry Afromontane forests in south-central Ethiopia by using the direct method based on new and previously developed models and the indirect method based on volume, BEF and wbd. The newly developed models are accompanied by covariance matrices for the parameter estimates to enable assessment of model related uncertainties in large area forest biomass estimation.

4.4. Aboveground forest biomass estimation using remotely sensed data

Application of remote sensing techniques in forestry enhanced availability of information needed for forest management at different spatial scales and temporal dimensions including the development and implementations of efficient REDD+ MRV system. Remote sensing technologies have advanced over the last few decades and became vital tools for enhancing quality and ensuring accessibility of spatial information to users across the world. Following the advancement, there are many sources of useful remotely sensed data for estimation of forest parameters such as biomass. Remotely sensed data applied in forestry have been mainly obtained from sources such as, optical satellite imageries, airborne laser scanning, and radio detection and ranging (Kumar et al., 2015). Also, aerial images such as from unmanned aerial vehicles (UAV) have become important source of information (e.g. Kachamba et al., 2016a; Puliti et al., 2018), however, UAV acquisitions are still restricted to relatively small areas due to some limiting factors such as battery consumption and flight regulations. For biomass estimations, some previous studies have shown that application of remotely sensed data can help reducing field-based efforts with enhanced precision of estimates (e.g. Næsset et al., 2016). Using remotely sensed data for biomass estimation first requires development of prediction model based on sample plot forest inventories data to be used as reference biomass (ground reference). The reference data will be regressed against variables extracted from remotely sensed data for the respective sample plots. The developed model will then be applied for biomass estimation over the entire study area.

Landsat and Sentinel-2 imageries are some examples of optical satellite data that have been used for biomass estimation, and are also freely accessible data (Woodcock et al., 2008; Malenovský, et al., 2012). In addition, PlanetScope imageries are among potentially applicable commercial satellite remote sensing data, with high-resolution and daily basis provision. These satellite imageries have been used widely in different parts of the world in forestry for the purposes of biomass estimations (e.g. Gizachew et al., 2016; Næsset et al., 2016; Baloloy et al., 2018; Chen et al., 2018). However so far, except some efforts related to the use of optical satellite images for land cover classification and mapping, for the Dry Afromontane forests in south-central part or elsewhere in Ethiopia, data from the above-mentioned satellite missions have never been used to assess forest biomass. Hence, no practical experience exists for this type forest in this regard.

Therefore, the main objective of Paper IV was to explore what kind of relevant variables may be extracted from the different satellite programs (i.e. Landsat 8, Sentinel-2 and PlanetScope) for biomass prediction modelling and to evaluate to what extent such remotely sensed data may improve the precision of biomass estimates beyond the precision obtained in a pure field-based estimation for the Dry Afromontane forest in south-central Ethiopia.

5.0. Materials and methods

5.1. Study sites

For Paper I, seven different sites (A, B, ..., G) distributed throughout Ethiopia (Table 1, Figure 2a) were considered. The selected sites are of different biomes having either a tree gain or loss history. The rest of the papers concentrated in one of the seven sites in south-central Ethiopia (i.e. site A, Table 1, Figure 2b). Specifically, Paper II and III were based on data from the Dry Afromontane forests of Degaga-Gambo and Wondo Genet sites, while Paper IV focused on Degaga-Gambo site only (Figure 2b). The Degaga-Gambo and Wondo Genet sites are located on the eastern escarpment of the Great Ethiopian Rift Valley. The areas have a bimodal rainfall distribution with the short rainy season between March and May and the main rainy season between July and September. The Degaga-Gambo forest extends from 38°45' to 38°56' E longitude and from 7°13' to 7°33' N latitude, with a total area of about 14176 ha out of which 12580 ha is natural forest. The elevation ranges from about 2100 to 2700 m.a.s.l. while the mean annual rainfall and temperature are 1245 mm and 14.9 ℃, respectively. The soils are generally classified as Mollic Nitisols and Humic Umbrisols, respectively, at lower and upper altitudes (Fritzsche et al., 2007). Similarly, Wondo Genet forest extends from 38°37' to 38°39' E longitude and from 7°6' to 7°7' N latitude. The natural forest has an area of about 390 ha with an altitudinal range from about 1850 to 2400 m.a.s.l and the soils are mainly classified as Mollic Andosols (Erikson and Stern, 1987). The mean annual rainfall and temperature are 1123 mm and 17.6 ℃, respectively.

Table 1. Description of the study sites for Paper I.

Site	Biome type	Condition of forest in the area*
A	*Acacia-Commiphora* and partly Dry Afromontane	Both tree gain and loss of similar magnitude
B	Moist Afromontane	Characterized by more tree loss
C	Partly Moist Afromontane and partly *Acacia-Commiphora*	Characterized by more tree loss but very little gain
D	Moist Afromontane	Characterized by more tree loss
E	Moist Afromontane	Both tree gain and loss of similar magnitude
F	Dry Afromontane	Characterized by tree gain
G	*Combretum-Terminalia*	Characterized by more tree loss

* Source: Global Forest Watch (www.globalforestwatch.org).
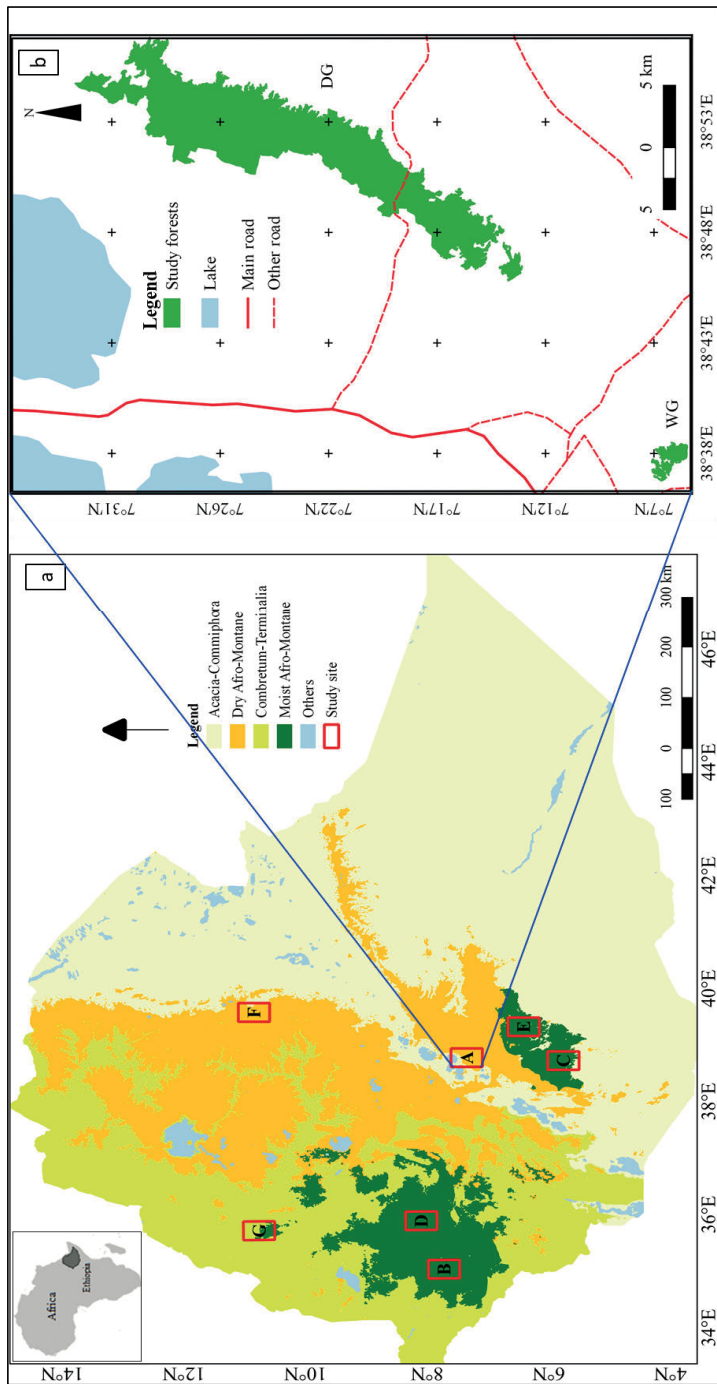
Figure 2. Map of the study sites: Paper I was based on the seven study sites, i.e. A to G in panel (a); Paper II and III were based on the two forest sites DG (Degaga-Gambo) and WG (Wondo Genet) in panel (b); and Paper IV was based on Degaga-Gambo site.

15

5.2. Data collection

5.2.1. Sample plot inventory data

Ground based sample plot inventories were carried out in the natural forests of both Degaga-Gambo and Wondo Genet sites, where a total of 65 and 42 circular plots with a size of 1000 and 400 m^2 were surveyed in the sites, respectively. In the plots all trees were identified for species name and measured for dbh. The data were used in tree selection for destructive sampling for Paper II and III. Up to 10 trees were further sampled and measured for dbh, dsh, ht and bt in each plot and the data were used partly in Paper II and IV. The maximum dbh encountered was 270 cm and totally 71 tree species were observed out of which 60 tree species were included in the sample trees (n=1345). For Paper IV, which was entirely carried out in Degaga-Gambo site including the 65 plots from the natural forest and other plots from plantations, cropland and open areas, a total of 111 plots were surveyed. Handheld global positioning system (GPS) receiver was used to navigate to the pre-defined locations of the plots. More precise coordinates of the plot centres were determined using differential GPS and global navigation satellite system (GLONASS) measurements. Two Topcon legacy-E +40 dual frequency receivers were used as base station and as a rover field unit. The receivers record pseudo-range and carrier phase of GPS and GLONASS. The base station was set up at Wondo Genet College of Forestry and Natural Resources campus. The Euclidean distance between the base station and the plot centres ranged between 21.7 and 57.2 km with an average distance of 41.8 km. For determining the position of the base station using precise point positioning, the GPS and GLONASS data were recorded continuously for more than 24 hours (Kouba, 2009). At the plot centres, the rover field unit was mounted on a 2.98 m carbon rod and recorded for 41.5 minutes on average using a one-second logging rate. The recordings were post-processed using the Magnet tools software (Topcon Positioning Systems Inc). The standard error of the post-processed planimetric plot coordinates reported by the Magnet tools software ranged from 0.017 to 1.111 m with a mean of 0.232 m.

5.2.2. Destructive sampling data

The information obtained from the sample plot inventories were used to secure appropriate distribution of sample trees across sizes and species. Accordingly, 63 trees (i.e. 32 and 31 from Degaga-Gambo and Wondo Genet sites, respectively) were destructively sampled from 30 tree species that represented about 87% of the total basal area of the forest. The selection also considered tree distribution across the diameter ranges from 5 cm to ≥ 105 cm (i.e. 5 – 15 cm, 15 – 25 cm, ..., ≥ 105 cm) as well as spatial and altitudinal variations. Prior to felling trees were measured for dbh and dsh with a calliper or diameter tape, ht with a Haglöf VL5 hypsometer and crown width (crw) with a measuring tape.

Selected trees were cut down at stump height (0.3 m aboveground) and sorted into merchantable stem, branch and foliage (twigs, leaves and fruits). Merchantable stem is a tree trunk up to 10 cm top diameter for all trees with dbh ≥ 15 cm. Branch includes all branches with diameter ≥ 2 cm, the top logs with diameter < 10 cm and trees having dbh < 15 cm. Smaller branches < 2 cm considered as part of foliage. The merchantable stem was marked and crosscut into shorter logs, and then for each log the length (m) and mid diameter (cm) were measured for determination of volume. Weight (kg) was also observed using a hanging balance scale (0 - 200 kg capacity) for biomass determination. The volume (m^3) of each log was determined by multiplying the mid cross-section area by its length. The volume and weight of each branch billet were determined similarly. Finally, for Paper II the merchantable stem volume (V_{ms}) and branch volume (V_{br}) were obtained by summing the volume of all logs of the respective sections; while the total tree volume (V_{tot}) is the sum of merchantable stem and branch volume. The total fresh weights of the merchantable stem and branches were also obtained by the summation of the weights of logs in each respective section. The fresh weight of foliage was obtained by observing and adding up the weights of each bundle. The fresh weights are basis for determining dry weight biomass used in Paper III.

5.2.3. Sub-sampling and laboratory work

For wbd (Paper II) and biomass (Paper III) determination, wood sub-samples (wood discs of about 3-4 cm in length) were collected from each harvested tree. For the stem section, six sub-samples were collected, i.e. two sub-samples from dbh position, and from middle and upper parts of the stem. Three of the sub-samples, one from each position were used for wbd and the last three for biomass determination. For branches also six sub-samples (three sub-samples each for wbd and biomass determination) were collected per tree (i.e. two sub-samples each from big, medium and small sized branches). For some small trees with few and small sized branches, only two sub-sample (one sub-sample for each wbd and biomass) were collected for the branch section. In case of large trees, where it was not practical to take the whole wood disc, the sub-samples were taken with an effort to represent all the bark, sapwood and heartwood sections (Williamson and Wiemann 2010). Small bundles of foliage samples were also taken from each sample tree. Totally, 791 sub-samples (364 for wbd and 427 for biomass) were collected. All the sub-samples were brought to laboratory with airtight plastic bags. Green volumes of sub-samples for wbd were determined by water displacement after peeling off the bark, and fresh weights for biomass sub-samples determined using sensitive digital balance scale. The sub-samples were then dried in an oven at a temperature of 103 ℃ by monitoring and weighing it recurrently every 24 hours until a constant mass was attained. Then, wbd was determined as the ratio of oven dry weight (g) to the green volume (cm^3) for each sub-sample.

Finally, the average dry to fresh weight biomass ratios were determined for the stem, branch and foliage sections, and used to convert the fresh weights of their respective sections into dry weights. The total tree aboveground dry weight biomass (AGB_t) was aggregated from merchantable stem biomass (B_{ms}), branch biomass (B_{br}) and foliage biomass (B_f).

5.2.4. Remotely sensed data

In Paper I, applications of optical satellite images of PlanetScope, RapidEye and Sentinel-2 (Table 2) were evaluated for forest area and canopy cover estimation based on visual interpretation of the images in their true colour. All the imageries used for the study were downloaded from the Planet Explorer Beta website in June 2017 and had < 50% cloud cover. PlanetScope satellite imagery is state-of-the-art optical products with up to 3 m spatial resolution from the PlanetScope satellite constellation with a daily capacity of covering the entire landmass. PlanetScope Ortho Tile images of the study sites, which were acquired between January–May 2017 were downloaded. On average, 13.0 images were available for each location. RapidEye Ortho Take product (3B) of RapidEye imageries with high (i.e. 5 m) spatial resolution were also used for the study. The images were acquired between December 2015 to May 2017 where on average 4.5 RapidEye images were available for interpretation at each location. Sentinel-2 images are freely available data for the public from the European Space Agency since June 2015. Sentinel-2 images have a spatial resolution of up to 10 m. Level 2A product of Sentinel-2 images acquired between December 2016 and May 2017 were used for this study and on average 5.6 images were available for each location.

In each of the seven sites 228 sample points, arranged systematically in a 3 km square grid, were observed. Two observers were involved and each interpreted 4788 observation points (i.e. 228 sample points x 7 sites x 3 image types). The images were clipped into 1 km x 1 km tiles for each of the 228 points and centred at each point to have a better overview of the surrounding land cover during the interpretation. Graphical user interface that was based on the R software used to display images for each point in a completely randomized manner, and to record and save the results of the image interpretation (i.e. LULC type, canopy cover, date of acquisition for the image used, time elapsed for the interpretation). Having each sample point at the centre, a square of 70 m x 70 m (~ 0.5 ha) observation window was superimposed and used as a unit of interpretation for LULC classes. The LULC type within the 0.5 ha (with ≥ 20% cover threshold) was determined visually based on decision tree according to the IPCC definitions of LULC categories (Penman et al., 2003). For canopy cover estimation, within the 0.5 ha observation window, a square grid consisting of 49 squares of 2 m x 2 m in size, was arranged. These small squares were used in the visual interpretation to observe the presence/absence of tree crowns,

and then used for canopy cover determination. The canopy cover for a single box of 0.5 ha was determined using the count of points that coincided with the crowns of trees divided by 49.

Table 2. Satellite image types and their characteristics that are used in Paper I and IV studies.

Image type	Spatial resolution (m)	Product level used		Spectral bands used for Paper IV*
		Paper I	Paper IV	
PlanetScope	3	3A-Visual	3B-Analytic	B, G, R, NIR
RapidEye	5	3B	-	-
Sentinel-2	10 and 20	2A	Level-1C	B, G, R, ReE, NIR, SWIR1
Landsat 8	30	-	L1-TP	B, G, R, NIR, SWIR1

* B, G, R, NIR, SWIR1 and ReE represent the blue, green, red, near-infrared, shortwave infrared-1 and red-edge spectral bands, respectively.

In Paper IV, Landsat 8, Sentinel-2 and PlanetScope optical satellite images (Table 2) were used to enhance the efficiency of biomass estimation. Single tile images of Landsat 8 (path 168, row 055) and Sentinel-2 (T37NDJ) were downloaded from USGS Earth explorer website; while for PlanetScope six scenes of orthorectified images that cover the entire study site were downloaded from Planet Explorer website. All the downloaded images were acquired within the period that coincide with the field inventory time and the dry season of the year. In addition, only images with < 5% of cloud cover were downloaded. After the required image pre-processing was conducted, for all the 111 field sample plots mean and standard deviation of relevant spectral band values were extracted from all images. Similarly, mean and standard deviation were computed for some important vegetation indices. In addition, for PlanetScope imagery mean and standard deviation of some textural variables were calculated based on grey level co-occurrence matrix using the Sentinel Application Platform software (ESA, 2019). For population level estimation of AGB, the entire study site was tessellated into cells of size equivalent to the field plot (31.64 m × 31.64 m) and resulted in N = 141604 cells. All image processing and variable extraction were done using the QGIS software.

5.3. Data analyses

For forest area estimation in Paper I, observations at each point were coded as 1 if forest and 0 otherwise. Both forest area and canopy cover estimation computations were done for the seven sites from the three types of images (i.e. PlanetScope, RapidEye and Sentinel-2). In addition, canopy cover was estimated by LULC classes. The mean ($\widehat{\overline{Y}}_i$) and its variance ($\widehat{Var}\left(\widehat{\overline{Y}}_i\right)$) of forest area and canopy cover were estimated for all the seven sites (i = 1, 2, ..., 7) using the respective estimators. The standard error (SE) of the mean was computed as the square root of the

variance. To assess the effects of the number of observations, bootstrap sampling with replacement was carried out for both forest area and canopy cover estimates using four resample sizes (m = 50, 100, 150 and 200). The standard errors of the bootstrap sampling statistics ($SE_{boot,\ \bar{x}}$) were computed and compared with the SE of the original sample (n = 228).

In Paper II, data from the sample trees (n = 1345) were used for modelling ht-dbh, dbh-dsh and bt-dbh tree biometric properties, while volume modelling and wbd documentation were based on the 63 destructively sampled trees data. For the ht-dbh, dbh-dsh and bt-dbh relationships different nonlinear model forms were tested. First the data were divided into training and test dataset. The models were fitted to the training dataset and then validated using the test dataset. The best performing models were finally fitted to the full dataset and performances were assessed using root mean squared error (RMSE), mean prediction error (MPE), pseudo-R^2 and Akaike information criteria (AIC).

For total tree and sections volume modelling, weighted least square regression was applied. Four model forms, two with dbh only and two with dbh and ht independent variables were tested for all V_{tot}, V_{ms} and V_{br}. In addition, two more models with dbh and crw were tested for V_{br}. Site-specific total volume models were also developed for the two sites. Weighting was applied to cope with the heteroscedasticity in the data (Picard et al., 2012). For models' performance assessment a leave one out cross validation (LOOCV) approach was employed to compute performance indicator metrics: RMSE (%), MPE (%) and pseudo-R^2. Also, AIC was computed for all models. Application of the commonly used form factor 0.5 ($f_{0.5}$) and observed mean form factor (f_{mean}) as well as some previously developed potential volume models from neighbouring countries in the region (Mauya et al., 2014; Kachamba and Eid, 2016; Mugasha et al., 2016) were evaluated by means of RMSE (%) and MPE (%).

The mean wbd values of stem and branch samples were further aggregated by weighting them by their respective volumes to get a volume weighted wbd at the tree and then species level. Analysis of variance was carried out to assess the presence of significant variations in wbd among the tree species and between the sites. Also, differences in wbd among stem sections (breast height, middle and upper stem positions) and branch sizes (big, mid and small branch) were tested. Presence of significant wbd differences between stems, branches, values at breast height and volume weighted means were assessed using pair-wise t-test.

In Paper III, total tree and sections biomass modelling were carried out using weighted nonlinear least square regression as for volume modelling in Paper II. For all AGB_t, B_{ms}, B_{br} and

B$_f$ response variables, generally eight different model forms were tested by first using dbh as sole predictor and then combined with ht, wbd and crw in a stepwise inclusion. Model performances were assessed by means of AIC along with the computed RMSE (%), MPE (%) and pseudo-R^2 following a LOOCV approach. Some previously developed models that could potentially be applied in our study sites were identified from Ethiopia (Eshete and Ståhl, 1998; Mokria et al., 2018; Ubuy et al., 2018b and Tetemke et al., 2019), elsewhere in Africa (Mugasha et al., 2016; Djomo et al., 2016) and the entire tropical region (Chave et al., 2005; 2014), and their performances were evaluated on our dataset. Furthermore, the indirect biomass prediction option from total tree and merchantable stem volume along with different wbd options (i.e. species-specific, study sites mean and national mean) and BEF options (i.e. species-specific and study sites mean), was tested. The BEFs were obtained by dividing the total observed tree biomass to the product of observed volume and wbd. Total tree and merchantable stem volumes were used separately. Individual tree BEFs were aggregated and averaged to yield species-specific and study sites mean. Comparisons were made based on the RMSE (%) and MPE (%) computed, and t-tests run to see whether MPEs were significantly different from zero.

For the biomass estimation in Paper IV, the observed AGB (Mg ha^{-1}) of each plot was determined using allometric biomass model from Paper III. Best predictor variables from each image type were selected based on the results of correlation analysis with the observed AGB. Then regression models of generalized linear model form were developed by relating the field observed AGB with the selected predictor variables from each type of images independently. To assess the performance of the models for each remotely sensed data source, LOOCV was conducted. Then RMSE (%), MPE (%) and R^2 were computed and used to assess the prediction accuracy of models for each imagery type. The best models from the respective image types were then applied for the AGB estimation in the whole study site. Population mean and variance were computed for field based ($\hat{\mu}_{field}$, $\hat{V}_{field}$) and remote sensing-assisted, i.e. model-assisted, ($\hat{\mu}_{image}$, $\hat{V}_{image}$) AGB estimation approaches. The relative efficiency (RE) between remote sensing-assisted estimation technique and purely field-based estimation approach was determined as the ratio of the variance estimates of the field-based option (i.e. design-based) relative to remote sensing-assisted option. The RE values were then used to assess the efficiency gain when using either Landsat 8, Sentinel-2 or PlanetScope to assist in the biomass estimation for the entire area.

6.0. Main findings and discussion

6.1. Forest area and canopy cover estimations

In Paper I forest area and canopy cover information, that are important in forest management activities including quantification of emissions and removals for REDD+ activities (IPCC, 2006; Korhonen et al., 2006), were generated. On average 83 seconds were spent for the whole interpretation task at each location with the longest (107 seconds) and shortest (68 seconds) average time elapsed at each point for PlanetScope and RapidEye, respectively. Relatively the required average interpretation time per site increased with an increase in proportion of forest. The study demonstrated efficiency of visual image interpretation practice enabling to survey vast areas of interest with less time as compared to field-based surveys. Sites B, D and E were ranked from 1st to 3rd, respectively, according to proportion of forest and site F was the one with the smallest proportion of forest in all the three image types consistently. Estimates from PlanetScope and RapidEye images showed similarities consistently over the seven study sites. On the other hand, the estimates from Sentinel-2 images differed from the other two, and the differences were much larger and statistically significant ($p < 0.01$) in most of the study sites that had larger proportion of forests. This indicates the importance of using finer resolution images for densely forested sites. Similarly, for the canopy cover estimate the largest and smallest values were recorded for sites B and F respectively from all image types. Mostly similar trends were observed for forest area and canopy cover across the sites in terms of how the estimates from all the three image types change. Analysis of canopy cover by LULC class, showed that estimates from all image types were very similar to each other except for the Settlements, Wetlands, and Other land classes. It seems that if a given LULC class is a homogenous one such as Forest land, Cropland, or Grassland, any of the images could produce reasonably comparable estimates of canopy cover. Generally, estimates from PlanetScope and RapidEye images were similar in many aspects, perhaps due to the higher spatial resolution of the images. Some studies (e.g. Churches et al., 2014; Draksler, 2017) have also reported improvement in accuracy of estimates as the images got finer in spatial resolution. Missing data could also reduce the number of observations and hence affect the quality of estimates (Lohr, 2009) where most of the missing data during image interpretation (NAs) were recorded for Sentinel-2 images.

Regarding optimum sample size, bootstrap resampling exercise showed that reducing the current sample size (i.e. 228) to 200 resulted in a marginal increase of the SEs for all image types and all sites cases. On the other hand, reducing the sample size to only 50 observations increased the SEs by more than 100% in all the cases. Therefore, it is important to look for and determine optimal sample sizes that will result in a precise estimate with the possible minimum resource (Jayaraman, 2000).

6.2. Models and data for basic tree biometric properties

In paper II, models for quantifying tree biometric properties such as ht, dbh, bt and volume were developed and wbd data documented. Model for ht based on dbh only as independent variable explained large variations in ht (pseudo-R^2 = 0.72). This result is similar to some studies from tropical natural forests elsewhere in Africa (e.g. Mugasha et al., 2013a) and such ht models may play a vital role to reduce measurement errors and costs (Larjavaara and Muller-Landau, 2013). A strong dbh-dsh relationship was observed and the model explained most of variation in dbh (pseudo-R^2 = 0.98), which is also in line with other findings (Corral-Rivas et al., 2007; Özçelik et al., 2010). Unlike ht and dbh models, the bt-dbh relationship was relatively weak and only 42% of the variation in bt was explained by the model. Nevertheless, the model is useful for quantifying tree properties such as volume of solid wood and volume of bark (Kershaw et al., 2017).

The general total tree and merchantable stem volume models performed well. From the LOOCV results the pseudo-R^2 of the total tree volume and merchantable stem volume models varied between 0.93-0.95 and 0.96-0.98, respectively and all with MPEs not significantly different from zero ($p > 0.05$). For both total tree and merchantable stem volume, models with dbh only as independent variable performed best and had RMSE% of 37.4 and 19.3, respectively. Inclusion of ht in the models revealed no improvements, and this conforms with studies in natural forest elsewhere in eastern Africa (e.g. Mauya et al., 2014; Mugasha et al., 2016). Branch volume models performed poorer than total tree and merchantable stem volume models and had pseudo-R^2 ranging from 0.74 to 0.89. Relatively poor performance of branch volume models is also previously reported (e.g. Mauya et al., 2014; Kachamba and Eid, 2016). The site-specific total tree volume models with dbh only as independent variable produced RMSE% of 19.3 and 51.4% for Degaga-Gambo and Wondo Genet, respectively. Since site-specific models performed best, they are recommended to be applied in their respective sites. For the Dry Afromontane forests, application of the general models with dbh only as independent variable are recommended in each total tree and sections volume cases. The models produce reasonably accurate predictions while reducing the inventory cost since ht is not required. However, for branch volume more accurate prediction can be obtained by a model with dbh and crw as independent variables.

Application of both commonly used form factor $f_{0.5}$ and the mean form factor f_{mean} resulted in large prediction errors. Similar and contrary findings were reported elsewhere by Masota et al. (2014) and Adekunle et al. (2013), respectively. Previously developed volume models in the region (Mauya et al., 2014; Kachamba and Eid, 2016; Mugasha et al., 2016) with a potential to

be applied in Ethiopia were evaluated on our data, and mostly large MPEs were obtained. Figure 3 shows the trend of how some of these models underpredict the total volume, particularly for medium and large diameter trees.
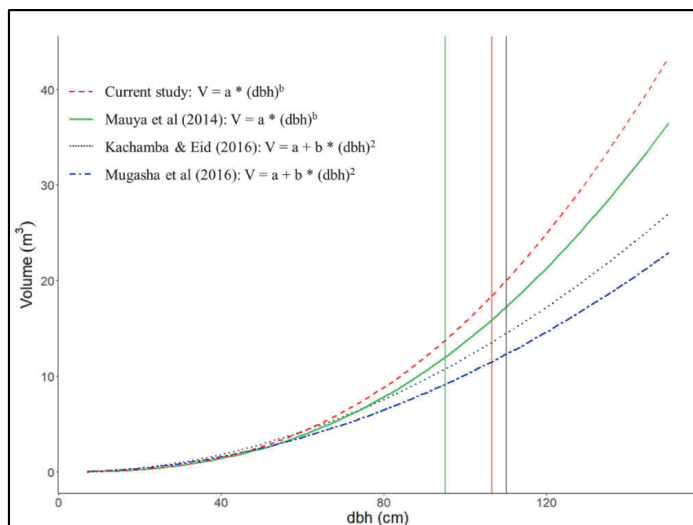
Figure 3. Diameter at breast height against predicted total volume of selected previously developed models and the model developed in Paper II (current study). Vertical lines indicate the maximum dbh used in the modelling by Mauya et al. (2014), Paper II and Kachamba and Eid (2016), respectively.

Volume weighted wbd values of the 30 tree species were also documented in Paper II. The mean wbd was 0.588 g cm^{-3} and ranged between 0.426 and 0.979 g cm^{-3}. The top three species with the largest wbd values were *Teclea nobilis*, *Dodonaea angustifolia* and *Olea capensis* with 0.979, 0.816, and 0.779 g cm^{-3}, respectively; while *Afrocarpus falcatus, Pittosporum viridiflorum* and *Vernonia amygdalina* were the three species with the smallest wbd values with 0.426, 0.441 and 0.457 g cm^{-3}, respectively. The wbd values were significantly different among species as also reported in some studies (Ubuy et al., 2018a; Tesfaye et al., 2019). There was no significant difference between the two sites in wbd values, which is an indication for the possibilities of using the wbd values for other similar forests. Similarities in wbd values of some species from other similar forest (Tesfaye et al., 2019) were seen; while also noticeable differences were detected from Ubuy et al. (2018a). Wood basic density showed no significant difference along the stem sections (dbh, mid and upper positions) and different branch sizes (big, medium and small). Mean wbd values for stems and branches were not significantly different, and this result was contrary to for example Okai et al., (2003), while in agreement with others (e.g. Swenson and Enquist, 2008).

6.3. Aboveground tree biomass prediction options

Different options for tree biomass prediction, directly using allometric models and indirectly using BEF, wbd and volume data were evaluated in Paper III. The new and previously developed models were considered for direct biomass prediction. All the new models with significant parameter estimates were considered as viable models, and based on LOOCV analysis, none of the models had MPEs significantly different from zero. From the LOOCV results, the AGB_t models had pseudo-R^2 ranging between 0.87 to 0.96 and the best performing model with the smallest AIC was the one with dbh, ht, crw and wbd as independent variables. Likewise, for B_{ms} the same independent variables as in the AGB_t resulted in best model with the smallest AIC and pseudo-R^2 = 0.96. For B_{br} and B_f models the pseudo-R^2 generally varied from 0.63 to 0.84 and in both cases models with dbh, crw and wbd as independent variables performed best in terms of AICs. While dbh explained a significant proportion of variations in both total and section biomass, addition of ht into the models did not improve the models' performances, which also confirms with previous findings (e.g. Fayolle et al., 2018; Ubuy et al., 2018b; Tetemke et al., 2019). On the contrary to ht, addition of crw considerably improved model performance. This result is also in agreement with some previous research (e.g. Goodman et al., 2014; Ubuy et al., 2018b; Tetemke et al., 2019). Evaluation of all the viable AGB_t models over the specific sites generally yielded smaller MPEs indicating that the models are feasible for application in similar forest types. Covariance matrices for the parameter estimates are also documented for the viable AGB_t models in Paper III.

The evaluation of some previously developed total AGB models that have been applied or potentially considered in our study site, resulted in large RMSEs and MPEs significantly different from zero. Exceptions are the pantropical models (Chave et al., 2005; 2014) that yielded relatively small MPEs, but still larger than our newly developed models. Figure 4 shows how some of these models either over- or underpredict biomass in relation to our current model in Paper III. In the indirect biomass prediction approach less biased prediction results were obtained when either species-specific or study area mean BEFs were used in line with only species-specific wbd for both total tree and merchantable stem volume cases. Though species-specific BEFs produced smaller MPEs than study site mean BEF, in practice this is not a feasible option since it is not likely that specie-specific BEFs are available for all species. Therefore, the study site mean BEF should be used along with species-specific wbd, which may also be obtained from the Global Wood Density database (Chave et al., 2009; Zanne et al., 2009) in cases of no local wbd availability. This approach generally overpredicted biomass and was less accurate when compared with the newly developed models. Previous researchers have also reported

poorer performance for the indirect biomass prediction method (e.g. Petersson et al., 2012; Njana, 2017; Lisboa et al., 2018).
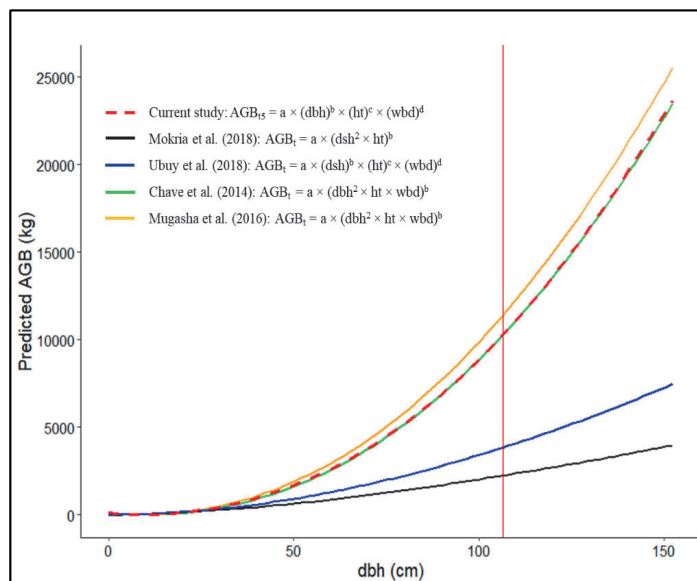
Figure 4. Total tree AGB over dbh based on the model developed in Paper III (AGB_{t5}), by Mokria et al. (2018), Ubuy et al. (2018b), Chave et al. (2014) and Mugasha et al. (2016). The vertical line indicates the maximum dbh in our dataset used for modelling. For graphical display of the models, AGB was predicted using ht derived from a ht-dbh model, as well as the mean wbd from Paper II. In addition, for displaying Mokria et al. (2018) and Ubuy et al. (2018b), that used dsh in their models, the corresponding dbh was determined using a dbh-dsh model from Paper II.

6.4. Forest AGB estimation using remotely sensed data

The exploratory study on identifying potential spectral and textural variables for AGB prediction in Paper IV, revealed that all the mean values of the spectral bands reflectance were moderately and negatively correlated with AGB, whereas most of the mean values of the vegetation indices had moderate positive correlation with AGB in all Landsat 8, Sentinel-2 and PlanetScope cases, which is in line with for example Gizachew et al. (2016), Macedo et al. (2018) and Bao et al. (2019). Some standard deviation values of vegetation indices from Sentinel-2 appeared to be also moderately correlated with AGB. On the other hand, the mean and standard deviation values of some textural variables of PlanetScope showed moderate correlation with AGB, but slightly lower than the spectral band reflectance and vegetation indices values. Most of the independent variables extracted from each image type were also intercorrelated, hence the number of variables selected for AGB prediction models were limited to a maximum of two so that the problem of overfitting was reduced. The best models were selected based on the LOOCV results. For Landsat 8, a model with one variable only using mean of shortwave infrared-1 band

reflectance performed best with RMSE of 73.2%. For Sentinel-2, a model with two variables using mean of shortwave infrared-1 band reflectance and standard deviation of green leaf index was found to perform best (RMSE = 67.1%), because these two variables were less intercorrelated with each other while strongly correlated with the observed AGB. For PlanetScope, a one variable model was fitted using mean of green reflectance band and it was a better performing model than the two variables model that used mean of green reflectance band and standard deviation of a textural variable (i.e. angular second moment of near infrared band). Some previous studies identified normalized difference vegetation index as predictor variable for AGB (e.g. Gizachew et al., 2016); however, it didn't perform well in our case. Overall the predictive power of the Sentinel-2 model prevailed over the other models (Figure 5), perhaps due to its optimized spatial resolution (better than Landsat 8) and spectral resolution (better than PlanetScope).
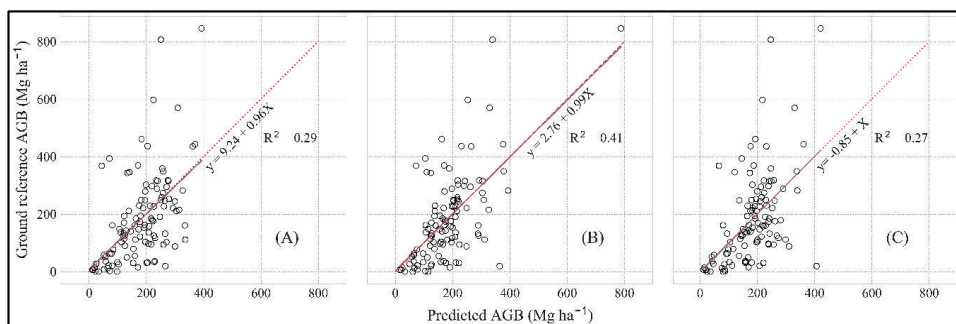
Figure 5. Relationship of ground reference (observed) versus predicted AGB using selected models of (A) Landsat 8, (B) Sentinel-2, and (C) PlanetScope data. The dashed red and solid grey lines represent the identity and the correlation function, respectively.

The best performed models of the respective satellite image types were applied to estimate AGB over the entire areas of the study site. The field-based estimate of mean (and SE) AGB ($\hat{\mu}_{field}$) was 184.35 (14.79) Mg ha^{-1}. Similarly, when using the Landsat 8, Sentinel-2 and PlanetScope prediction models the estimated mean (and SE) AGB ($\hat{\mu}_{images}$) were 179.67 (12.49), 177.79 (11.40) and 184.27 (12.62) Mg ha^{-1}, respectively. Despite the presence of large AGB variations in the study site, all the model-assisted estimates were reasonably precise and had smaller SEs than the field-based estimate. Furthermore, the estimate based on the Sentinel-2 model was the most precise among the three model-assisted AGB estimates, as a result, the RE of the mean AGB estimate using the Sentinel-2 model (i.e. 1.68) was greater than what we obtained by using the Landsat 8 (1.40) and PlanetScope (1.37) models. However, the models generally predicted a limited range of the observed AGB, may be due to saturation problem (e.g. Lu et al., 2005). The results of Paper IV in this thesis will have strong practical implications for forest biomass and carbon stock assessment in forest management efforts including REDD+ program in Ethiopia.

7.0. Conclusion and future perspectives

The studies in this thesis are among the very few initiatives in Ethiopia towards modelling and quantifying tree and forest resources applying field-based and remotely sensed data. The studies used ground reference data collected through sample plot inventories as well as destructive sampling to develop models for predicting volume and aboveground biomass with different options for independent variables. The development and use of the models will enable to follow the higher Tier approaches of the IPCC to estimate carbon stocks and changes in carbon stocks in Dry Afromontane forests of south-central Ethiopia. The studies will also contribute to enrich the national and regional databases on biomass and volume models and wood basic density data. Furthermore, the studies evaluated the use of remotely sensed data for forest resource estimation, particularly forest area, canopy cover and aboveground biomass. In general, this thesis provided data and tools to the local and national level efforts towards effective forest management. The studies will also assist the country to report its contribution to the global efforts of mitigating climate change through the implementation of programs such as REDD+ in which regular periodic reporting of the GHG inventory results are required under the UNFCCC.

Specifically, in Paper I, forest area and canopy cover estimation options of using satellite images based on visual interpretation were assessed. The visual image interpretation method is technically less complex and can best serve the purpose in most developing countries such as Ethiopia where capacities are limited in several aspects. Large areas can be covered with less time consumption compared to the field-based approach. When using finer resolution imageries such as PlanetScope and RapidEye more precise estimates can be obtained than relatively coarser resolution images such as Sentinel-2. Satellite imagery to be used for visual interpretation for forest area and canopy cover estimation should be selected carefully considering densities of the forest. Also, homogeneity within a given LULC type should be considered when selecting image type for canopy cover estimation. Costs may be reduced by employing a sampling approach as used in the current study, instead of large-scale wall-to-wall observation, to obtain reliable estimates at a lower cost of image procurement, especially for dense forest areas where low-resolution images have deficiencies.

Paper II and III provided relevant models and data for quantifying tree biometric properties. The models and data were totally lacking for the Dry Afromontane forests of the study sites. Therefore, the results of this thesis are timely and of paramount importance and will significantly contribute towards sustainable management and utilization of the forests including in the REDD+ MRV implementations. The ht-dbh model is relevant to obtain accurate ht

estimates while reducing measurement cost. The dbh-dsh model facilitates quantifications of previous losses of biomass or volume as a forest degradation. The bt-dbh model serves quantification of bark for various uses (e.g. bioenergy) or quantifying wood dimension without bark (e.g. wood for construction purposes). Wood basic density data were documented for the dominant tree species in the forest and may be used for enriching the national and Global Wood Density databases in addition to be useful in routine forest management activities locally. Furthermore, total tree, merchantable stem and branch volume models for the study forest were provided in the thesis. The models support planning and implementations of forest management actions by enabling provision of accurate estimates of the forest growing stock in terms of total tree or sections volume. The volume estimates can also be used along with BEFs and wbd data for estimating biomass indirectly. This is particularly important for situations where only volume data available from previous inventories. Nevertheless, biomass should be predicted directly using more accurate allometric models if available. Such biomass prediction models are provided in Paper III for total tree, merchantable stem, branch and foliage biomass with number of options for choosing models based on the availability of data from an inventory. Individual tree biomass prediction is crucial for generating forest biomass estimates that are fundamental for estimating existing forest carbon stock and changes over time in order to assess contributions of forests to climate change mitigation. All the models and wbd data given in this thesis may also be applied in other similar forests in Ethiopia; however, thorough evaluation of species composition, growing conditions and data ranges should be done carefully before using the models outside their data ranges.

Furthermore, Paper IV has provided the first empirical evidence that optical satellite images can potentially be used for estimation of AGB in the Dry Afromontane forests of Ethiopia, despite a wide range of variation in biomass density per unit area. Potential spectral variables for biomass prediction were derived, explored and identified for each of the Landsat 8, Sentinel-2 and PlanetScope image cases. Model-assisted estimation approaches that combine the prediction model and design-based sampling procedure provide the required reliable estimates. Sentinel-2 images, a freely accessible data source, can be used for AGB estimation with reasonable precision and estimation efficiency. This practical exercise may offer baseline information for similar feature studies including designing and implementation of a REDD+ MRV programs.

Generally, the four studies in this thesis have provided data, models and methodological information that can be used to improve assessment and quantification methods of forest resources in the study sites. Nevertheless, there are still research gaps that should be further addressed.

In Paper I, we analysed interpretation results from the three satellite image types and compared them against each other. In order to consolidate results and further verify the robustness of the method, incorporating samples of ground-based observations as reference data might be useful, hence, future researches would be encouraged to consider this.

The models developed in Paper II and III were based on samples from two sites of Dry Afromontane forests in south-central Ethiopia. We have also recommended these models to be applied in other Dry Afromontane forests, which lack site-specific models. However, the recent NFI report (MEFCC, 2018a) indicated the presence of high variabilities in the Dry Afromontane forests of the country. In line with this, the observed large prediction errors when testing a model by Tetemke et al. (2019) from Dry Afromontane forest in northern Ethiopia on the data from the present study sites, confirms this variability. Thus, future studies should consider developing comprehensive models with additional data from other forests sites together with the existing data from this study and other similar studies, for example from Tetemke et al. (2019), for developing models that can better represent all Dry Afromontane forests in Ethiopia. Some biomass modelling studies (e.g. Huy et al., 2019) have applied a seemingly unrelated regression modelling approach when developing total tree and sections biomass models simultaneously, as suggested by Parresol, (2001), to cater for the additivity challenge of nonlinear section biomass equations. This could be an interesting issue to consider and evaluate in a future study. The present study has only considered aboveground tree biomass. Belowground biomass is also one of the vital carbon pools in forests. Currently default conversion factors have been used in Ethiopia (e.g. UN-REDD, 2017; MEFCC, 2018a). However, for more accurate estimation, country- or site-specific belowground models are preferred (IPCC, 2006). Therefore, belowground biomass models should be developed also for Dry Afromontane forests in Ethiopia, although collecting belowground biomass data are demanding and costly.

In Paper IV, the use of optical satellite imageries for biomass estimation were tested, which might be influenced by factors such as saturation, shadow effect and topographic variations. Alternatively, the use of information such as 3D data from UAV imagery and airborne laser scanner sources have been used to improve the quality of estimates widely in most boreal forests (e.g. Næsset and Gobakken, 2008) and few cases in sub-Saharan Africa (e.g. Mauya et al., 2015; Kachamba et al., 2016a). Thus, future research should consider such options for the current study forest as well as other forest types in Ethiopia. In addition, effects of different sizes of the field inventory plots should be studied since it may have implications for estimation efficiency (e.g. Næsset et al., 2015).

This thesis has generally provided models, data and methods that are relevant for estimating tree and forest resources from which the ongoing implementations of different forest management schemes in Ethiopia would benefit. Sustainable management and utilization aspects in participatory forest management programs should be guided by proper and accurate information, towards which the results from this thesis contribute significantly. In REDD+ MRV programs, biomass and carbon stocks and their change over time need to be quantified and reported along with the uncertainties involved. The models and methods provided in Papers I to IV are means for estimating biomass and carbon stock at any point in time and for quantifying and documenting uncertainties. In particular, the covariance matrices for the parameter estimates of the developed biomass models that are provided in this thesis opens up for interesting research related to error propagation in biomass and carbon stock estimation where errors related to model parameters along with errors related to sampling design (e.g. number and distribution of sample points) and response design (e.g. size and shape of the plot and measurements in the plot) can be considered (Chave et al, 2004; Clark and Kellner, 2012).

References

Adekunle, V.A.J., Nair, K.N., Srivastava, A.K., Singh, N.K., 2013. Models and form factors for stand volume estimation in natural forest ecosystems: a case study of Katarniaghat wildlife sanctuary (KGWS), Bahraich District, India. *Journal of Forestry Research*, 24:217–226.

Angelsen, A., Brockhaus, M., 2009. Realising REDD+: National strategy and policy options. Centre for International Forestry (CIFOR), Bogor, Indonesia.

Asner, G.P., Mascaro, J., Muller-Landau, H.C., Vieilledent, G., Vaudry, R., Rasamoelina, M., Hall, J.S., van Breugel, M., 2012. A universal airborne LiDAR approach for tropical forest carbon mapping. *Oecologia*, 168, 1147-1160.

Ayele, G., Mezmur, S., Hussien, S., 2018 Guideline for sustainable timber harvesting in participatory forest management forests. Farm Africa, Addis Ababa.

Baloloy, A.B., Blanco, A.C., Candido, C.G., Argamosa, R.J.L., Dumalag, J.B.L.C., Dimapilis, L.L.C., et al., 2018. Estimation of Mangrove Forest Aboveground Biomass Using Multispectral Bands, Vegetation Indices and Biophysical Variables Derived from Optical Satellite Imageries: Rapideye, Planetscope & Sentinel-2. *ISPRS Annals of Photogrammetry, Remote Sensing and Spatial Information Sciences*. IV-3, 29-36.

Bao, N., Li, W., Gu, X., Liu, Y., 2019. Biomass Estimation for Semiarid Vegetation and Mine Rehabilitation Using Worldview-3 and Sentinel-1 SAR Imagery. *Remote Sensing,* 11.

Barij, N., Stokes, A., Bogaard, T., Van Beek, R., 2007. Does growing on a slope affect tree xylem structure and water relations? *Tree Physiology,* 27:757–764.

Bekele, M., Zewdie, S., Boissière, M., Atmadja, S., 2018. *REDD+ MRV implementation in Ethiopia*: Review of the context, framework and progress. Occasional Paper 192. CIFOR: Bogor, Indonesia.

Bey, A., Díaz, A.S.-P., Maniatis, D., Marchi, G., Mollicone, D., Ricci, S., et al., 2016. Collect Earth: Land Use and Land Cover Assessment through Augmented Visual Interpretation. *Remote Sensing*, 8, 807.

Brandon, K., 2014. Ecosystem Services from Tropical Forests: Review of Current Science. CGD Working Paper 380, Centre for Global Development, Washington DC.

Bollandsås, O.M., Zahabu, E., Katani, J.Z., 2016. Background on the development of biomass and volume models; In: *Allometric tree biomass and volume models in Tanzania. Department of forest mensuration and management.* Malimbwi, R.E., Eid, T., Chamshama, S.A.O., (eds). Sokoine University of Agriculture, Morogoro, pp 9-18.

Brown, S., 1997. Estimating biomass and biomass change of tropical forests: a primer. FAO Forestry paper, 134 p. ISBN 92-5-103955-0. http://www.fao.org/3/w4095e/ w4095e00.htm. Accessed on October 2019.

Brown, S., 2002. Measuring carbon in forests: current status and future challenges. *Environmental Pollution*, 116 (3): 363-372.

Chave, J., Andalo, A., Brown, S., Cairns, M.A., Chambers, J.Q., Eamus, D., et al., 2005. Tree allometry and improved estimation of carbon stocks and balance in tropical forests. *Oceologia* 145, 87–99.

Chave, J., Condit, R., Aguilar, S., Hernandez, A., Lao, S., Perez, R., 2004. Error propagation and scaling for tropical forest biomass estimates. *Philosophical Transactions of the Royal Society B*. 359:409-420.

Chave, J., Coomes, D.A., Jansen, S., Lewis, S.L., Swenson, N.G., Zanne, A.E., 2009. Towards a worldwide wood economics spectrum. *Ecology Letters*, 12 (4): 351-366.

Chave, J., Muller-Landau, H.C., Baker, T.R., Easdale, T.A., Steege, H.T., Webb, C.O., 2006. Regional and phylogenetic variation of wood density across 2456 neotropical tree species. *Ecological Applications,* 16:2356–2367.

Chave, J., Réjou-Méchain, M., Búrquez, A., Chidumayo, E., Colgan, M.S., Delitti, W.B., et al., 2014. Improved allometric models to estimate the above ground biomass of tropical forests. *Global Change Biology*, 20:3177–3190.

Chen, L., Ren, C., Zhang, B., Wang, Z., Xi, Y., 2018. Estimation of forest above-ground biomass by geographically weighted regression and machine learning with Sentinel imagery. *Forest*, 9, 582.

Churches, C.E., Wampler, P.J., Sun, W., Smith, A.J., 2014. Evaluation of forest cover estimates for Haiti using supervised classification of Landsat data. *International Journal of Applied Earth Observation and Geoinformatics*, 30, 203–216.

Clark, M.L., Aide, T.M. 2011. Virtual Interpretation of Earth Web-Interface Tool (VIEW-IT) for collecting land-use/land-cover reference data. *Remote Sensing*, 3, 601–620.

Clark, D.B., Kellner, J.R., 2012. Tropical forest biomass estimation and the fallacy of misplaced concreteness. *Journal of Vegetation Science*, 23(6):1191-1196.

Corral-Rivas, J.J., Barrio-Anta, M., Aguirre-Calderon, O.A., Dieguez-Aranda, U., 2007. Use of stump diameter to estimate diameter at breast height and tree volume for major pine species in El Salto, Durango (Mexico). *Forestry*, 80:29-40.

Deppe, F., 1998. Forest area estimation using sample surveys and Landsat MSS and TM data. *Photogrammetric Engineering and Remote Sensing*, 64:4.

Daba, D.E., Soromessa, T., 2019. Allometric equations for aboveground biomass estimation of *Diospyros abyssinica* (Hiern) F. White tree species. *Ecosystem Health and Sustainability*, 5(1), 86-97.

Djomo, N.A., Picard, N., Fayolle, A., Henry, M., Ngomanda, A., Ploton, P., et al., 2016. Tree allometry for estimation of carbon stocks in African tropical forests. *Forestry: International Journal of Forestry Research*, 89(4), 446-455.

Draksler, A., 2017. The Effect of Satellite Image Resolution and Minimum Mapping Unit on the Accuracy of Forest Cover *Maps*; Technische Universität München: Munich, Germany.

Erikson, H., Stern, M., 1987. *A soil study at Wondo Genet Forestry Resource Institute, Ethiopia*. Swedish University of Agricultural Science, International Rural Development Centre-Uppsala, ISSN 0280-4301.

Eshete, G., Ståhl, G., 1998. Functions for multi-phase assessment of biomass in acacia woodlands of the Rift Valley of Ethiopia. *Forest Ecology and Management*, 105, 79–90.

FAO, 2010. Global Forest Resources Assessment 2010 - Country Report Ethiopia. FAO: Rome, Italy.

FAO, 2020. Global Forest Resources Assessment 2020 – Key findings. FAO: Rome.

FAO and UNEP, 2020. *The State of the World's Forests 2020. Forests, biodiversity and people*. Rome.

Fayolle, A., Ngomanda, A., Mbasi, M., Barbier, N., Bocko, Y., Boyemba, F., et al., 2018. A regional allometry for the Congo basin forests based on the largest ever destructive sampling. *Forest Ecology and Management*, 430, 228-240.

FDRE - Federal Democratic Republic of Ethiopia. 2011. Ethiopia's Climate-Resilient Green Economy, Green Economy Strategy. FDRE: Addis Ababa, Ethiopia.

Friis, I., Demissew, S., Breugel, P.V., 2010. Atlas of the potential vegetation of Ethiopia. Det Kongelige Danske Videnskabernes Selskab. Denmark, Copenhagen.

Fritz, S., McCallum, I., Schill, C., Perger, C., See, L., Schepaschenko, D., et al., 2012. Geo-Wiki: An online platform for improving global land cover. *Environmental Modelling and Software*, 31, 110–123.

Fritzsche, F., Zech, W., Guggenberger, G., 2007. Soils of the main Ethiopian Rift Valley escarpment: A transect study. *Catena* 70:209-219.

Gebeyehu, G., Soromessa, T., Bekele, T., Teketay, D., 2019. Carbon stocks and factors affecting their storage in dry Afromontane forests of Awi Zone, north-western Ethiopia. *Journal of Ecology and Environment*, 43, 7.

Gebre-Egziabher, T.-B., 1991. Diversity of Ethiopian flora. In *Plant Genetic Resources of Ethiopia*; Engles, J., Hawkes, J.G., Worede, M., Eds.; Cambridge University Press: Cambridge, UK, 1991; pp. 75–81.

Githiomi, J.K., Kariuki, J.G., 2010. Wood basic density of *Eucalyptus grandis* from plantations in Central Rift Valley, Kenya: variation with age, height level and between sapwood and heartwood. *Journal of Tropical Forest Science*, 22:281–286.

Gizachew, B., Astrup, R., Vedeld, P., Zahabu, E.M., Duguma, L.A., 2017. REDD+ in Africa: context and challenges. *Natural Resources forum*, 2017.

Gizachew, B., Solberg, S., Næsset, E., Gobakken, T., Bollandsas, O.M., Breidenbach, J., et al., 2016. Mapping and estimating the total living biomass and carbon in low-biomass woodlands using Landsat 8 CDR data. *Carbon Balance Management,* 11:1-14.

Goetz, S., Hansen, M., Houghton, R.A., Walker, W., Laporte, N.T., Busch, J., 2015. Measurement and monitoring for REDD+: The needs, current technological capabilities, and future potential. Centre for Global Development Working Paper.

Goodman, R.C., Phillips, O.L., Baker, T.R., 2014. The importance of crown dimensions to improve tropical tree biomass estimates. *Ecological Applications*, 24(4):680–698.

Grace J., Morison J.I.I., Perks M.P. 2014. Forests, forestry and climate change. In: *Challenges and opportunities for the world's forests in the 21st century*; Fenning T. (ed). Springer, The Netherlands, Dordrecht, pp 241-266.

Hailemariam, S.N., Soromessa, T., Teketay, D., 2016. Land Use and Land Cover Change in the Bale Mountain Eco-Region of Ethiopia during 1985 to 2015. *Land*, 5, 41.

Henry, M., Besnard, A., Asante, W.A., Eshun, J., Adu-Bredu, S., Valentini, R., et al., 2010. Wood density, phytomass variations within and among trees, and allometric equations in a tropical rainforest of Africa. *Forest Ecology and Management*, 260:1375–1388.

Henry, M., Picard, N., Trotta, C., Manlay, R.J., Valentini, R., Bernoux, M., et al., 2011. Estimating tree biomass of sub-Saharan African forests: a review of available allometric equations. *Silva Fennica*, 45:477-569.

Hewson, J., Steininger, M., Pesmajoglou, S., 2014. REDD+ Measurement, Reporting and Verification (MRV) Manual, Version 2.0. USAID-supported Forest Carbon, Markets and Communities Program. Washington, DC, USA.

Huy, B., Tinh, N.T., Poudle, K.P., Frank, B.M., Temesgen, H., 2019. Taxon-specific modelling systems for improving reliability of tree aboveground biomass and its components estimates in tropical dry dipterocarp forests. *Forest Ecology and Management*, 437:156-174.

IPCC, 2006. *IPCC Guidelines for National Greenhouse Gas Inventories*, Prepared by the National Greenhouse Gas Inventories Programme, Eggleston H.S., Buendia L., Miwa K., Ngara T. and Tanabe K. (eds). IGES, Japan.

Jayaraman, K.A., 2000. *Statistical Manual for Forestry Research*. FORSPA, FAO, Bangkok.

Kachamba, D., Eid, T., 2016. Total tree, merchantable stem and branch volume models for miombo woodlands of Malawi. *Southern Forest: A Journal of Forest Science*, 78:41–51.

Kachamba, D., Eid, T., Gobakken, T., 2016b. Above- and belowground biomass models for trees in the miombo woodlands of Malawi. *Forests,* 7(2), 38.

Kachamba, D.J., Ørka, H.O., Gobakken, T., Eid, T., Mwase W., 2016a. Biomass estimation using 3D data from unmanned aerial vehicle imagery in a tropical woodland. *Remote Sensing*, 8, 968.

Kebede, B., Soromessa, T., 2018. Allometric equations for aboveground biomass estimation of *Olea europaea* L. subsp. *cuspidata* in Mana Angetu forest. *Ecosystem Health and Sustainability*, 4(1):1-12.

Kershaw, J.A., Ducey, M.J., Beers, T.W., Husch, B., 2017. Forest mensuration, Fifth edition. John Wiley & Sons; UK, Chichester; NJ, Hoboken.

Kindu, M., Schneider, T., Teketay, D., Knoke, T., 2013. Land Use/Land Cover Change Analysis Using Object-Based Classification Approach in Munessa-Shashemene Landscape of the Ethiopian Highlands. *Remote Sensing*, 5: 2411–2435.

Korhonen, L., Korhonen, K.T., Rautiainen, M., Stenberg, P., 2006. Estimation of forest canopy cover: A comparison of field measurement techniques. *Silva Fennica*, 40:577–588.

Kouba, J., 2009. A guide to using international GNSS service (IGS) products. http://acc.igs.org/UsingIGSProductsVer21.pdf. Accessed January 2018.

Köhl, M., Magnussen, S., Marchetti, M., 2006. Sampling methods, remote sensing and GIS multiresource forest inventory. Berlin, Springer. 373pp.

Kumar, L., Sinha, P., Taylor, S., Alqurashi, A., 2015. Review of the use of remote sensing for biomass estimation to support renewable energy generation. *Journal of Applied Remote Sensing*, 9(1):1-29.

Larjavaara, M., Muller-Landau, H.C., 2013. Measuring tree height: quantitative comparison of two common field methods in a moist tropical forest. *Methods in Ecology and Evolution*, 4:793-801.

Lemenih, M., Allan, C., Biot, Y., 2015. Making forest conservation benefit local communities: Participatory forest management in Ethiopia. Farm Africa. https://www.farmafrica.org/downloads/resources/pfmfinalweb.pdf. Accessed. August 2019.

Lemenih, M., Kassa, H., 2014. Re-greening Ethiopia: history, challenges and lessons. *Forests,* 5(8):1896–1909.

Lindner, M., Karjalainen, T., 2007. Carbon inventory methods and carbon mitigation potentials of forests in Europe: a short review of recent progress. *European Journal of Forest Research*, 126:149–156.

Lisboa, S.N., Guedes, B.S., Ribeiro, N., Sitoe, A., 2018. Biomass allometric equation and expansion factor for a mountain moist evergreen forest in Mozambique. *Carbon Balance Management*, 13(23).

Lohr, S., 2009. *Sampling: Design and Analysis*; Nelson Education: Scarborough, ON, Canada.

Lu, D., 2006. The potential and challenge of remote sensing-based biomass estimation. *International journal of remote sensing*, 27:1297-1328.

Lu, D., Batistella, M., Moran, E., 2005. Satellite estimation of aboveground biomass and impacts of forest stand structure. *Photogrammetric Engineering and Remote Sensing,* 71: 967-974.

Macedo, F.L., Sousa, A.M.O., Gonçalves, A.C., Marques da Silva, J.R., Mesquita, P.A., Rodrigues, R.A.F., 2018. Above-ground biomass estimation for *Quercus rotundifolia* using vegetation indices derived from high spatial resolution satellite images. *European J. Remote Sens. 51*, 932-944.

Masota, A.M., Zahabu, E., Malimbwi, R.E., Bollandsås, O.M., Eid, T.H., 2014. Volume models for single trees in tropical rainforests in Tanzania. *Journal of Energy and Natural Resource*, 3:66–76.

Mattsson, E., Persson, U.M., Ostwald, M., Nissanka, S., 2012. REDD+ readiness implications for Sri Lanka in terms of reducing deforestation. *Journal of Environmental Management,* 100:29-40.

Mauya, E., Ene, L., Bollandsås, O., Gobakken, T., Næsset, E., Malimbwi, R. et al., 2015. Modelling aboveground forest biomass using airborne laser scanner data in the miombo woodlands of Tanzania. *Carbon Balance and Management*, 10(28):116.

Mauya, E.W., Mugasha, W.A., Zahabu, E., Bollandsås, O.M., Eid, T., 2014. Models for estimation of tree volume in the miombo woodlands of Tanzania. *Southern Forests: Journal of Forest Science*, 76(4):209-219.

MEFCC, 2018a. Ethiopia's national forest inventory final report. Ministry of Environment Forest and Climate Change, Addis Ababa, Ethiopia.

MEFCC, 2018b. National Forest Sector Development Program, Ethiopia. Volume I: Situation Analysis. Ministry of Environment Forest and Climate Change, MEFCC: Ethiopia.

Malenovský, Z., Rott, H., Cihlar, J., Schaepman, M.E., García-Santos, G., Fernandes, R., et al., 2012. Sentinels for science: Potential of Sentinel-1, -2, and -3 missions for scientific observations of ocean, cryosphere, and land. *Remote Sensing of Environment*, 120, 91-101.

Missanjo, E., Matsumura, J., 2016. Wood density and mechanical properties of *Pinus kesiya* Royle ex Gordon in Malawi. *Forests,* 7:7–35.

Mokria, M., Mekuria, W., Gebrekiristos, A., Aynekulu, E., Belay, B., Gashaw T., et al., 2018. Mixed species allometric equations and estimation of aboveground biomass and carbon stocks in restoring degraded landscape in northern Ethiopia. *Environmental Research Letters*, 13(2).

Mugasha, W.A., Bollandsås, O.M., Eid, T., 2013a. Relationships between diameter and height of trees in natural tropical forest in Tanzania. *Southern Forest: Journal of Forest Science*, 75(4):221-237.

Mugasha, W.A., Eid, T., Bollandsås, O.M., Malimbwi, R.E., Chamshama, S.A.O., Zahabu, E., et al., 2013b. Allometric models for prediction of above- and belowground biomass of trees in the miombo woodlands of Tanzania. *Forest Ecology and Management,* 310: 87-101.

Mugasha, W.A., Mauya, E.W., Njana, A.M., Karlsson, K., Malimbwi, R.E., Ernest, S., 2019. Height-diameter allometry for tree species in Tanzania mainland. *International Journal of Forestry Research,* 2019:1-17.

Mugasha, W.A., Mwakalukwa, E.E., Luoga, E., Malimbwi, R.E., Zahabu, E., Silayo, D.S., et al., 2016. Allometric models for estimating tree volume and aboveground biomass in lowland forests of Tanzania. *International Journal of Forestry Research*, 2016:1–13.

Muller-Landau, H.C., 2004. Interspecific and inter-site variation in wood specific gravity of tropical trees. *Biotropica,* 36:20–32.

NABU, 2017. NABU's Biodiversity Assessment at the Kafa Biosphere Reserve. The Nature and Biodiversity Conservation Union (NABU), Berlin, Addis Ababa.

Næsset, E., Bollandsås, O.M., Gobakken, T., Solberg, S., McRoberts, R.E. 2015.The effects of field plot size on model-assisted estimation of aboveground biomass change using multitemporal interferometric SAR and airborne laser scanning data. *Remote Sensing of Environment*, 168:252–264.

Næsset, E., and Gobakken, T. 2008. Estimation of above- and below-ground biomass across regions of the boreal forest zone using airborne laser. *Remote Sensing of Environment,*112: 3079–3090.

Næsset, E., Ørka, H.O., Solberg, S., Bollandsås, O.M., Hansen, E.H., Mauya, E., et al., 2016. Mapping and estimating forest area and aboveground biomass in miombo woodlands in Tanzania using data from airborne laser scanning, TanDEM-X, RapidEye, and global forest maps: A comparison of estimated precision. *Remote Sensing of Environment*, 175: 282–300.

Njana, M.A., 2017. Indirect methods of tree biomass estimation and their uncertainties, *Southern Forests: Journal of Forest Science*, 79(1):41-49.

Njana, M.A., Meilby, H., Eid, T., Zahabu, E., Malimbwi, R.G., 2016. Importance of tree basic density in biomass estimation and associated uncertainties: a case of three mangrove species in Tanzania. *Annals of Forest Science*, 73:1073–1087.

Okai, R., Frimpong-Mensah, K., Yeboah, D., 2003. Characterization of moisture content & specific gravity of branch wood & stem wood of *Aningeria robusta* & *Terminalia ivorensis*. *Holz Roh-Werkst,* 61:155–158.

Özçelik, R., Brooks, J.R., Diamantopoulou, M.J., Wiant, H.V., 2010. Estimating breast height diameter and volume from stump diameter for three economically important species in Turkey. *Scandinavian Journal of Forest Research*, 25:32–45.

Pan, Y., Bridsey, R.A., Fang, J., Houghton, R., Kauppi, P.E., Kurz, W.A., et al., 2011. A large and persistent carbon sink in the world's forests. *Science*, 333:988–993.

Parresol, B.R., 2001. Additivity of nonlinear biomass equations. *Canadian Journal of Forest Research*, 31(5):865–878.

Penman, J., Gytarsky, M., Hiraishi, T., Krug, T., Kruger, D., Pipatti, R., et al., 2003. *Good Practice Guidance for land use, land-use change and forestry*. IPCC: Geneva, Switzerland.

Petersson, H., Holm, S., Ståhl, G., Alger, D., Fridman, J., Lehtonen, A., et al., 2012. Individual tree biomass equations or expansion factors for assessment of carbon stock changes in living biomass – a comparative study. *Forest Ecology and Management*, 270: 78-84.

Petrokofsky, G., Kanamaru, H., Achard, F., Goetz, S.J., Joosten, H., Holmgren, P., et al., 2012. Comparison of methods for measuring and assessing carbon stocks and carbon stock changes in terrestrial carbon pools. How do the accuracy and precision of current methods compare? Asystematic review protocol. *Environmental Evidence*, 1,6.

Picard, N., Saint-André, L., Henry, M., 2012. Manual for building tree volume and biomass allometric equations: from field measurement to prediction. Food and Agriculture Organization of the United Nations, Rome; Centre de Coopération Internationale en Recherche Agronomique pour le Développement, Montpellier.

Potapov, P.V., Dempewolf, J., Talero, Y., Hansen, M.C., Stehman, S.V., Vargas, C., et al. 2014. National satellite-based humid tropical forest change assessment in Peru in support of REDD+ implementation. *Environmental Research Letters*, 9, 124012.

Puliti, S., Saarela, S., Gobakken, T., Ståhl, G., Næsset, E., 2018. Combining UAV and Sentinel-2 auxiliary data for forest growing stock volume estimation through hierarchical model-based inference. *Remote Sensing of Environment*. 204:485-497.

Saarela, S., Grafström, A., Ståhl, G., Kangas, A., Holopainen, M., Tuominen, S., et al., 2015. Model-assisted estimation of growing stock volume using different combinations of LiDAR and Landsat data as auxiliary information. *Remote Sensing of Environment,* 158: 431-440.

Sannier, C., McRoberts, R.E., Fichet, L.-V., Makaga, E.M., 2014. Using the regression estimator with Landsat data estimate proportion forest cover and net proportion deforestation in Gabon. *Remote Sensing of Environment,* 151:138-148.

Sinha, S., Jeganathan, C., Sharma, L., Nathawat, M., 2015. A review of radar remote sensing for biomass estimation. *International Journal of Environmental Science and Technology,* 1-14.

Singh, K.D., 2013. Capacity building for the planning, assessment, and systematic observations of forests: with special reference to tropical countries. Springer: Heidelberg, Germany.

Sisay, K., Thurnher, C., Belay, B., Lindner, G., Hasenauer, H., 2017. Volume and carbon estimates for the forest area of the Amhara region in the north western Ethiopia. *Forests*, 8(4):122.

ESA, 2019. European Space Agency, SNAP version 7.0.0. Available online: http://step.esa.int/main/ download/snap-download/ (accessed on August 2019).

Swenson, N.G., Enquist, B.J., 2008. The relationship between stem and branch wood specific gravity and the ability of each measure to predict leaf area. *American Journal of Botany*, 95:516–519.

Tesfaye, M.A., Bravo-Oviedo, A., Bravo, F., Pando, V., de Aza, C.H., 2019. Variation in carbon concentration and wood density for five most commonly grown native tree species in central highlands of Ethiopia: The case of Chilimo dry Afromontane forest. *Journal of Sustainable Forestry*, 38(8):769-790.

Tesfaye, M.A., Bravo-Oviedo, A., Bravo, F., Ruiz-Peinado, R., 2016. Aboveground biomass equations for sustainable production of fuelwood in a native dry tropical afro-montane forest of Ethiopia. *Annals of Forest Science*, 73:411-423.

Temesgen, H., Affleck, D., Poudel, K., Gray, A., Sessions, J., 2015. A review of the challenges and opportunities in estimating above ground forest biomass using tree-level models. *Scandinavian Journal of Forest Research*, 30(4):326-335.

Tetemke, B.A., Birhane, E., Rannestad, M.M., Eid, T., 2019. Allometric models for predicting aboveground biomass of trees in the dry Afromontane forests of northern Ethiopia. *Forests*, 10(12):1114.

Ubuy, M.H., Eid, T., Bollandsås, O.M., 2018a. Variation in wood basic density within and between tree species and site conditions of exclosures in Tigray, northern Ethiopia. *Trees* 32:967–983.

Ubuy, M.H., Eid, T., Bollandsås, O.M., Birhane, E., 2018b. Aboveground biomass models for trees & shrubs of exclosures in the drylands of Tigray, northern Ethiopia. *Journal of Arid Environment*, 156:9–18.

UN-REDD, 2017. Ethiopia's Forest Reference Level Submission to the UNFCCC. https://redd.unfccc.int/ files/ethiopia_frel_3.2_final_modified_submission.pdf. Accessed August 2019.

Vanclay, J.K., 1994. Modelling forest growth and yield, Application to mixed tropical forests. CAB International, UK, Wallingford.

van Laar, A., Akça, A., 2007. Forest mensuration. Springer, The Netherlands, Dordrecht.

Venter, O., Koh, L.P., 2012. Reducing emissions from deforestation and forest degradation (REDD+): game changer or just another quick fix? *Annals of the New York Academy of Sciences*, 1249:137-150.

Vivero, J.L., Ensermu, K., Sebsebe, D., 2006. Progress on the Red List of plants of Ethiopia and Eritrea: conservation and biogeography of endemic flowering taxa. In: Taxonomy and ecology of African plants, their conservation and sustainable use; Ghazanfar S.A., Beentje, H.J. (eds). pp 761–778. Royal Botanic Gardens, Kew.

WBISPP, 2005. A national strategy plan for the biomass sector. Addis Ababa, Ethiopia.

Weiskittel, A.R., Hann, D.W., Kershaw, J.A., Vanclay, J.K., 2011. Forest growth and yield modelling. John Wiley and Sons, UK, The Atrium, Southern Gate, Chichester, West Sussex.

West, P.W., 2015. Tree and Forest Measurement, 3rd Edition. Springer, Switzerland. 214pp.

Williamson, G.B., Wiemann, M.C., 2010. Measuring wood specific gravity correctly. *American Journal of Botany*, 97(3):519–524.

Woodcock, C.E., Allen, R., Anderson, M., Belward, A., Bindschadler, R., Cohen, W., et al., 2008. Free access to Landsat imagery. *Science Letters*, 320:1011-1012.

Zanne, A.E., Lopez-Gonzalez, G., Coomes, D.A., Ilic, J., Jansen, S., Lewis, S.L., et al., 2009. Data from: Towards a worldwide wood economics spectrum: Dryad Data Repository.

Paper I

Article

Estimation of Forest Area and Canopy Cover Based on Visual Interpretation of Satellite Images in Ethiopia

Zerihun Asrat [1], Habitamu Taddese [2], Hans Ole Ørka [1], Terje Gobakken [1],*, Ingunn Burud [2] and Erik Næsset [1]

1 Faculty of Environmental Sciences and Natural Resource Management, Norwegian University of Life Sciences, P.O. Box 5003, 1432 Ås, Norway; zerihun.asrat.kutie@nmbu.no (Z.A.); hans.ole.orka@nmbu.no (H.O.Ø.); erik.naesset@nmbu.no (E.N.)
2 Faculty of Science and Technology, Norwegian University of Life Sciences, P.O. Box 5003, 1432 Ås, Norway; habitamu.taddese.berie@nmbu.no (H.T.); ingunn.burud@nmbu.no (I.B.)
* Correspondence: terje.gobakken@nmbu.no; Tel.: +47-67-23-17-55

Abstract: Forests, particularly in the tropics, are suffering from deforestation and forest degradations. The estimation of forest area and canopy cover is an essential part of the establishment of a measurement, reporting, and verification (MRV) system that is needed for monitoring carbon stocks and the associated greenhouse gas emissions and removals. Information about forest area and canopy cover might be obtained by visual image interpretation as an alternative to expensive fieldwork. The objectives of this study were to evaluate different types of satellite images for forest area and canopy cover estimation though visual image interpretation, and assess the influence of sample sizes on the estimates. Seven sites in Ethiopia with different vegetation systems were subjectively identified, and visual interpretations were carried out in a systematical design. Bootstrapping was applied to evaluate the effects of sample sizes. The results showed that high-resolution satellite images ($\leq$5 m) (PlanetScope and RapidEye) images produced very similar estimates, while coarser resolution imagery (10 m, Sentinel-2) estimates were dependent on forest conditions. Estimates based on Sentinel-2 images varied significantly from the two other types of images in sites with denser forest cover. The estimates from PlanetScope and RapidEye were less sensitive to changes in sample size.

Keywords: land cover; land use; visual interpretation; high resolution imagery; estimation; design-based inference

1. Introduction

Forests constitute the largest terrestrial ecosystem, and they provide a variety of services and functions [1,2]. One of the services that forests offer is carbon sequestration; approximately 2.5 billion tons carbon are absorbed annually [3–5]. Despite their contributions to carbon sequestration, much of the world's forests, particularly tropical forests, are suffering from severe deforestation and degradation, contributing to increased carbon emission [5–7]. About 12% of the total anthropogenic carbon emissions come from deforestation [5,8]. The pressure from deforestation and degradation on forests is larger particularly in tropical, developing countries due to heavy dependence on the resource for livelihoods [9].

The world has been acting continuously from the Kyoto Protocol in 1992 to the recent Paris Agreement in 2015 to halt the global warming through various means, one of which is the REDD+ mechanism (Reducing Emissions from Deforestation and forest Degradation). The REDD+ mechanism gives financial incentives to countries decreasing their deforestation and forest degradation. Ethiopia is one of the tropical countries that has lost much of its forest resources in the past [10]. Historically,

the forest cover of Ethiopia was reported to be more than 30–40% of the area [10,11]. However, the origin of this number is uncertain, and the amount itself is questionable [12]. Either way, there has been severe deforestation and forest degradation in the country the last century [11–14]. The pressure to convert forests into land for food production to support the increasing human population and provide socio-economic benefits to the nature-based livelihoods of the majority of the people has been huge. The use of wood for fuel has also aggravated the rate of deforestation [10,11].

Ethiopia is currently in the process of implementing REDD+, and one of the prerequisites for implementing the REDD+ mechanism is to develop a robust measuring, reporting, and verification (MRV) system following the Intergovernmental Panel on Climate Change (IPCC) Good Practice Guidelines [15]. Information about forest area and canopy cover are required for a MRV system in the REDD+ process and sustainable forest management practices. Forest area is the proportion of an area that is covered with trees and other perennial components of a forest land. The definition of forest varies among countries, the contexts of institutions, and of course the purpose [16]. The Food and Agriculture Organization (FAO) of the United Nations defines forest as land spanning more than 0.5 hectares with trees higher than 5 m and a canopy cover of more than 10%, or trees that are able to reach these thresholds in situ [17]. In Ethiopia, the working definition of forest describes it as any land spanning at least 0.5 hectares covered by trees (including bamboo) attaining a height of at least 2 m and a canopy cover of at least 20%, or trees with the potential to reach these thresholds in situ in due course. Canopy cover is the proportion of the forest floor covered by the vertical projection of the tree crowns [15,18,19]. Canopy cover plays a significant role in forest management for various decisions related to silviculture and the utilization of the forests [20].

In REDD+, developing countries rehabilitate and preserve their forests, and in turn get paid for the extra amount of CO_2 sequestered beyond a certain agreed level following MRV after their commitment [21]. The REDD+ system, of course, requires accurate measurement and estimation methods to be carried out through a properly established MRV system [22]. In the course of quantifying the amount of CO_2 by sink and source, reliable forest area and canopy cover estimations are key attributes [15,23]. However, according to the IPCC, information on forest area and deforestation in tropical countries is highly uncertain, often up to 50% of error [24]. This is because tropical countries are constrained by a lack of technical capacity and lack of both trained human power as well as infrastructure. In such situations, when and where there are technical inefficiencies, it would be important to critically scrutinize and choose the most feasible methods and technologies [23].

Past and current practices of forest cover assessment as well as land-use and land-cover (LULC) mapping in Ethiopia, digital image classification, and mapping methods are practiced, such as supervised, unsupervised, and object-based classification (e.g., [13,14]). However, digital image classification and mapping methods in general require a high level of technical skill, and in most cases, technical software [25,26]. Furthermore, the spectral similarity of land-cover classes is also challenging. As a result, the wider application and use of such methodologies for large-scale activities such as nationwide assessment could be problematic. For instance, Ethiopia's historical data on LULC changes between 2000–2013 for forest reference level (FRL) submission to the United Nations Framework Convention on Climate Change (UNFCCC) were generated through digital image classification and mapping using Landsat data. Nevertheless, the report underlined the need for the further reduction of uncertainties of the estimates [27]. In response to the drawbacks of digital image classification and mapping mentioned above, some platforms of free and open source software such as Geo-Wiki, VIEW-IT, and Sky Truth are developed by different bodies, including academic institutions [26,28]. The software support visual satellite image interpretation and LULC map validation by non-remote sensing experts, while some of the programs can also be used for other advanced applications by professional users [26,29]. The application of these software packages is associated with the use of very high-resolution images, which are often known to have a small geographic scope and an irregular time interval of acquisition, in turn limiting its utility for large areas. On the other hand, using Landsat images will provide a global coverage with bi-monthly acquisitions; however, interpretation is limited

by its low spatial resolution. FAO designed the software system Collect Earth as an open source tool that helps to collect, analyze, and compile reports on LULC through visual image interpretation based on freely available satellite images mainly with the Google Earth platform [25]. The tool has been adopted, and many countries have used it around the world for activities such as national forest inventory, LULC mapping, and the estimation of activity data for REDD+ [25].

The mentioned software supporting visual satellite image interpretation are efficient tools for gathering reference data. Such reference data gathered using interpretation of satellite imagery with different spatial resolutions under different forest conditions has been used to provide forest area and forest cover change estimates [30,31]. However, forest conditions and properties of the imagery, such as spatial resolution and revisit times, could potentially influence estimates. Hence, it is important to evaluate different types of satellite images under different forest conditions in order to provide guidelines for using such tools at a national level.

Thus, the aim of this study was to identify and evaluate different and alternative types of satellite images to minimize the level of uncertainties of the estimation of forest area and canopy cover in different forest conditions in Ethiopia. The specific objectives of the study were to: (1) evaluate the use of PlanetScope, RapidEye, and Sentinel-2 satellite images for forest area and canopy cover estimation through visual interpretation; and (2) assess the influence of sample sizes on the estimates. Accordingly, efforts were made to see if there is variation in the pattern of the estimates and the uncertainty of estimates from the three types of satellite images over the different areas of interest (sites of the study), which are characterized by having different biomes. Thus, such efforts would provide insight on the robustness of the method when applied to different forest conditions. The time elapsed for interpretation was assessed to evaluate the effectiveness of the method. In general, the study sites were selected so that they covered the important carbon storage areas of the country. Therefore, the study is helpful for gaining knowledge and contributing to improving Ethiopia's REDD+ MRV system in practice.

2. Materials and Methods

2.1. Description of the Study Sites

Ethiopia is located in eastern Africa, geographically extending from 3° to 15° north latitude and from 33° to 48° east longitude. It is known for its topographic diversity, stretching from the lowest Danakil depression 125 m below sea level to the highest peak of the Simien Mountains, which is over 4500 m above sea level. The great East African rift valley that runs from northeast to southwest divides the country into north, northwest, and southwest highlands and the western lowlands on one side, and the eastern and southeastern highlands and the associated lowlands on the other side [32]. This topographic diversity favored the country to have a wide range of climate and a diverse flora and fauna, with a considerable amount of it being endemic [33].

For this study, seven sites were identified to represent the major biomes of the country, as well as their tree gain or loss conditions (Table 1). The selection of sites was subjective in order to have sites covering a range of forest conditions. The size of each site was 2052 km^2 (36 km × 57 km). The major biomes were used in activity data compilation for FRL submission to the UNFCCC, and stratification during the national forest inventory planning and implementation [27]. The major biomes include (1) Dry Afromontane: includes undifferentiated Afromontane forest; dry single dominant Afromontane forest of the Ethiopian highland; Afromontane woodland, wooded grassland, and grassland. In addition, transition between Afromontane vegetation and *Acacia-Commiphora* bushland on the eastern escarpment, as well as Ericaceous and Afroalpine belts, are included. (2) Moist Afromontane: comprises mainly primary or mature secondary moist evergreen Afromontane forest. Also contains edges of moist evergreen Afromontane forest, bushland, woodland, and wooded grassland, as well as transitional rain forest. (3) *Combretum-Terminalia*: *Combretum-Terminalia* woodland and wooded grassland is a major component. Furthermore, it includes wooded grassland of

the western Gambela region. (4) *Acacia-Commiphora*: *Acacia-Commiphora* woodland and bushland proper; Acacia wooded grassland of the rift valley as well as desert and semi-desert vegetation [32]. Accordingly, dry Afromontane forests cover the north, central, and eastern highlands of the country; moist Afromontane forests dominate the southwest and south-central areas. *Combretum-Terminalia* covers the northwest, west, and southwest lowlands; *Acacia-Commiphora* includes the northeast, east, and south lowlands of the country, while the rest that is categorized as others included water bodies and wetlands (Figure 1).

Table 1. Description of the study sites.

Site	Biome Type	Condition of Forest in the Area *
A	*Acacia-Commiphora* and partly dry Afromontane	Both tree gain and loss of similar magnitude
B	Moist Afromontane	Characterized by tree loss
C	Partly moist Afromontane and partly *Acacia-Commiphora*	Characterized by tree loss and very little gain
D	Moist Afromontane	Characterized by tree loss
E	Moist Afromontane	Both tree gain and loss of similar magnitude
F	Dry Afromontane	Characterized by tree gain
G	*Combretum-Terminalia*	Characterized by tree loss

* Source: Global Forest Watch (www.globalforestwatch.org).
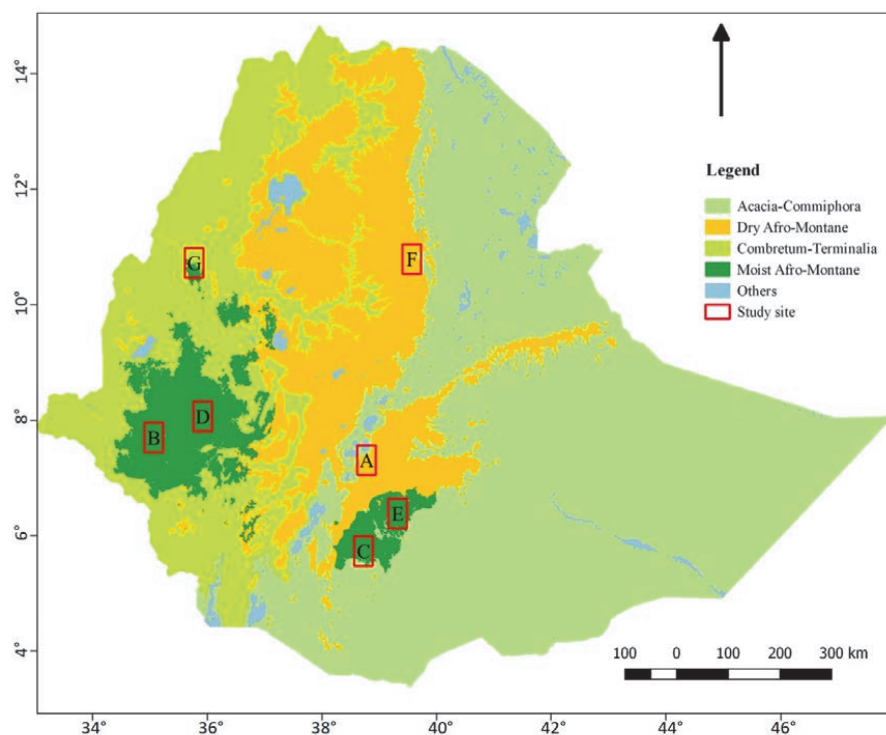
Figure 1. The major biomes in Ethiopia and the seven sites (A, B, . . . , G) selected for the study.

2.2. Satellite Imagery

Satellite images upon which the visual interpretation was based were PlanetScope, RapidEye, and Sentinel-2, which were all in their true color image (red, blue, and green).

2.2.1. PlanetScope

PlanetScope image products are available in three different forms. PlanetScope Basic Scene (1B) is a product with radiometric and sensor corrections only, which is designed for users with advanced knowledge of image processing. PlanetScope Ortho Scene (3B) is an orthorectified product that is projected to a cartographic projection. PlanetScope Ortho Tile (3A) products are orthorectified as individual 25 km × 25 km tiles, and can serve a wide range of applications that need accurate geolocation and cartographic projection. PlanetScope satellite imagery is state-of-the-art optical products with up to 3-m spatial resolution. Unlike other optical satellites, the PlanetScope satellite constellation consists of multiple launches of groups of individual satellites (also called "Doves") with continuous improvements of on-orbit capacity. The complete PlanetScope constellation of about 175 satellites (by 2 April 2018) covers the entire earth's landmass every day, and has a daily collection capacity of about 300 million km^2. PlanetScope Ortho Tile images of the study sites were downloaded from the Planet Explorer Beta website in June 2017. Only images with cloud cover <50% and images acquired between January–May 2017 were used. On average, 13.0 images were available for each location. The minimum number of images per location was four, and the maximum was 24.

2.2.2. RapidEye

RapidEye and PlanetScope imagery products are currently acquired and supplied by the same private company, Planet Labs Inc. RapidEye provides optical imagery from a constellation of five earth-imaging satellites. It has a large area coverage with frequent revisit time (one-day interval), which allows one to get cloud-free images for almost all areas. The images have high spatial (5-m pixel size) resolution. RapidEye image products can be obtained in different forms (RapidEye basic (1B): least processed product; RapidEye Ortho (3A): orthorectified and other required corrections made at individual 25 km × 25 km tiles; and RapidEye Ortho Take (3B): large-scale orthorectified product based on RapidEye Image Takes), depending on the users' needs and image processing capability (Planet, 2017). Recent RapidEye Ortho Take (product level 3B) images of the study sites were obtained from the same source as PlanetScope. Only images with a cloud cover <50% and images from December 2015 to May 2017 were used. The minimum number of images per location was one, and the maximum was 12 images; on average, 4.5 RapidEye images were available for interpretation for each location.

2.2.3. Sentinel-2

Sentinel-2 is owned by the European Space Agency (ESA); it was launched to support activities such as land monitoring, emergency management, security, and climate change issues. In order to fulfill such objectives, the mission was designed in such a way that it has high revisit frequency (five days at the equator), high spatial resolution (up to 10 m in some bands), and having wider swath (290 km). It has been providing unprecedented freely available data to the public since June 2015. The Sentinel-2 product level 2A images (Table 2) used for this study were also downloaded from the Planet Explorer Beta. Only images with a cloud cover <50% and images from December 2016 to May 2017 were used. The average number of Sentinel-2 images available for interpretation at each location was 5.6 with a range from two to 10 images.

Table 2. Satellite images used in this study.

Satellite	Spatial Resolution (m)	Product Level
Planet Scope	3	3B
RapidEye	5	3B
Sentinel-2	10	2A

2.3. Data Collection Techniques

For each of the seven sites, a 3 km × 3 km grid of systematically distributed points were prepared and overlaid the images. This resulted in 228 sample points within each site. Systematic sampling design was used because of its potential to uniformly cover the entire sites and thereby produce more precise estimates [15]. Each of the two observers interpreted a total of 4788 observation points (228 observation points per site per image type × seven sites × three image types). Having the grid point at the center, a square of 0.5 ha (about 70 m × 70 m) was created for all of the 228 grid points within each site. This cell layer was the unit of interpretation of the LULC class. This cell size was chosen to match with the minimum area of the national and FAO definitions of forest. Within these 0.5 ha cells, a systematic grid consisting of 49 squares of 2 m × 2 m in size, was arranged. These small squares were used in the visual interpretation to observe the presence/absence of tree crowns, and then used for canopy cover determination. The canopy cover of a single cell of 0.5 ha was determined using the count of points that coincided with the crowns of trees divided by 49. The images were clipped to 1 km × 1 km tiles for each of the 228 points, and centered at each point to have a better overview of the surrounding land cover during the interpretation. A package was written in R language to develop a graphical user interface that was used to display images for each point in a completely randomized manner, and record and save the results of the image interpretation. The 0.5-ha cell with 49 grid points was enabled to be zoomed in and displayed together with the clipped image (Figure 2). In addition, the land-cover type, time of acquisition for the selected image, and elapsed time (time from launching a location to saving results) were recorded.

A given LULC type within the 0.5 ha was determined visually based on the IPCC definitions of LULC categories [15] i.e., forest land, cropland, grassland, wetland, settlements, and other land; see the IPCC guidelines for details. The thresholds for forest land were 0.5 ha area and 20% canopy cover in the current study. Furthermore, interpretation decisions were made following a hierarchy of rules [34] (Figure 3). The proportions of points that fell on tree crowns (if any) were determined, regardless of the LULC class types. Among the potential images for interpretation, the newest image was used. Two persons performed the interpretation, and the average of the interpretation results was used in further analyses.

Figure 2. The graphical user interface used for visual image interpretation. (**A**) A window for opening new image and recording the interpreted data; (**B**) 1 km × 1 km image with a point at the center; (**C**) a zoomed into 0.5-ha cell with the 49 points (2 m × 2 m squares).
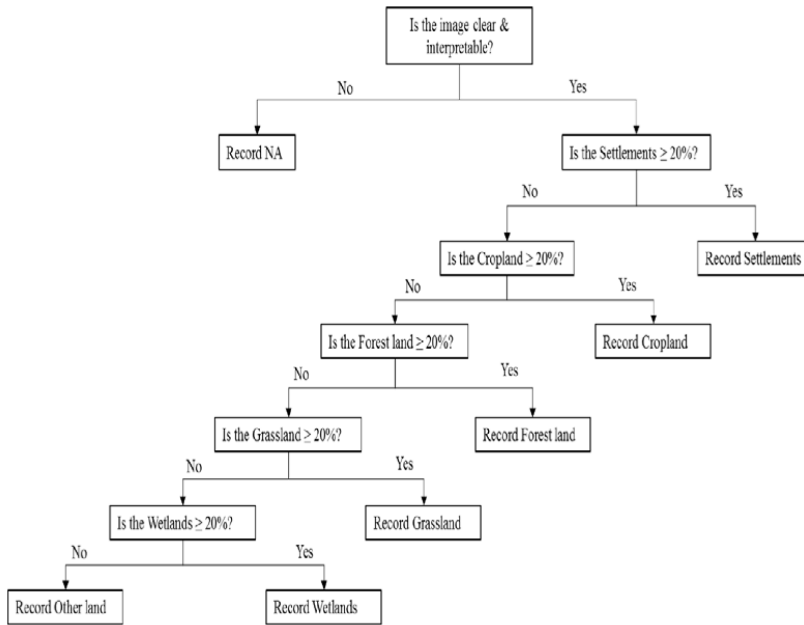
Figure 3. Decision tree based on the hierarchy of rules.

2.4. Estimation

Forest area estimates were computed for the three image types in all seven sites. Observation points were coded as 1 if they were forest and 0 otherwise, and then the mean forest area was estimated using the expression in Equation (1). Canopy cover estimates were also computed for the different image types in the seven respective sites, as well as each LULC class, applying the estimator in Equation (2):

$$\hat{\bar{X}}_i = \frac{\sum_{j=1}^{n} x_{ij}}{n}, \tag{1}$$

where $\hat{\bar{X}}_i$ is the mean forest area estimate of site *i*; x_{ij} is the proportion of forest area observed in site *i* at sample point *j*; and *n* is the number of observations in a site *i*.

$$\hat{\bar{Y}}_i = \frac{\sum_{j=1}^{n} y_{ij}}{n}, \tag{2}$$

where $\hat{\bar{Y}}_i$ is the estimated mean canopy cover of site *i*; and *n* is the number of observations.

The uncertainty of each estimate was computed using Equations (3) and (4) for forest area and canopy cover, respectively. The standard error (SE) of the mean of each estimate was computed by taking the square root of the error variance. An analysis of variance was then performed to assess the presence of significant differences among the forest area and canopy cover estimates from each image type.

$$\widehat{Var}\left(\hat{\bar{X}}_i\right) = \frac{\sum_{j=1}^{n}\left(x_{ij} - \hat{\bar{X}}_i\right)^2}{n(n-1)}, \tag{3}$$

where $\widehat{Var}\left(\hat{\bar{X}}_i\right)$ is the estimated error variance of the mean forest area estimate of site *i*.

$$\widehat{Var}\left(\hat{\bar{Y}}_i\right) = \frac{\sum_{j=1}^{n}\left(y_{ij} - \hat{\bar{Y}}_i\right)^2}{n(n-1)}, \tag{4}$$

where $\widehat{Var}\left(\hat{\bar{Y}}_i\right)$ is the error variance of the mean canopy cover estimate of site *i*.

Analysis was carried out on the data that were averaged between the two observers, as given in Table 3.

Table 3. Observation results of forest and non-forest classes from the three image types.

Observation	PlanetScope	RapidEye	Sentinel-2
Forest	819	824	602
Non-Forest	774	772	947
NA *	3	0	47
Total	1596	1596	1596

* Not recorded due to clouds or missing imagery.

In order to assess the effects of the number of observations, bootstrap sampling was carried out for each of the forest area and canopy cover estimates of the three image types and the seven respective sites. Four different resample sizes (*m* = 50, 100, 150, and 200) were used in the bootstrapping with replacement, and the standard deviation of the boot statistics (Equation (5)), which is an estimate of the standard error [35], was computed and compared with the standard error of the original sample:

$$SE_{boot,\,\bar{x}} = \sqrt{\frac{1}{m-1}\sum\left(\bar{x}* - \frac{1}{m}\sum\bar{x}*\right)^2} \tag{5}$$

where $SE_{boot,\,\bar{x}}$ is the standard error of an estimate, and $\bar{x}*$ is the mean of each resample.

3. Results

3.1. Dates and Time Elapsed for Interpretation

There was a substantial difference between the acquisition dates of the images selected for interpretation for the different image types. For PlanetScope imagery, 85% of the images used were from May 2017, and only 2.4% were from March and earlier. For Sentinel-2 imagery, 51% were from May and April, and only a marginal number were from pre-2017 (<1%). Meanwhile, for RapidEye, none of the images interpreted was from April and May 2017, and only 23% were acquired in 2017. However, most of the images were acquired during the dry season (December–May), except for 13% of the images from RapidEye, which were acquired in October and November. There was no identified effect of any differences in the time of acquisitions.

On average, 83 s were used for each location to record the LULC class and canopy coverage. The difference between RapidEye and Sentinel-2 was minor (68 s versus 73 s), while for PlanetScope, 107 s on average were needed to carry out the interpretation for each location. The seven sites were forming three clusters with respect to time consumption. The time consumption for the three groups were 67–75 s (sites A, F, and G), 87–89 s (sites C, D, and E) and 103 s (site B).

3.2. Forest Area Estimation

Mean forest area estimates from the three image types for all of the study sites are displayed in Figure 4. Sites B, D, and E were the three densely forested sites with estimated proportions of forest area of 0.89, 0.77, and 0.60 from PlanetScope, 0.88, 0.76, and 0.56 from RapidEye, and 0.55, 0.48, and 0.41 from Sentinel-2, respectively. On the other hand, site F has the least forest cover, with an estimated proportion of forest area of 0.03, 0.07, and 0.05 from the PlanetScope, RapidEye, and

Sentinel-2 images, respectively. Forest area estimates from PlanetScope and RapidEye images showed similarities consistently over the seven study sites, although there were marginal differences, where estimates from RapidEye image were smaller in most cases. The estimates from Sentinel-2 images differed from the other two image types in most of the study sites, and these differences in mean forest area were much larger and statistically significant ($p < 0.01$) for sites B, D, E, and G. However, the magnitude of the differences in mean forest area estimates decreased as the overall forest cover of the sites decreased. Thus, no significant differences were observed among the different image types for the three study sites A, C, and F, which had relatively smaller forest cover. It appears that when an area has a small proportion of forest such as sites A, C, and F, Sentinel-2 images, having relatively coarser resolution than PlanetScope and RapidEye images, would produce a reasonably comparable estimate.
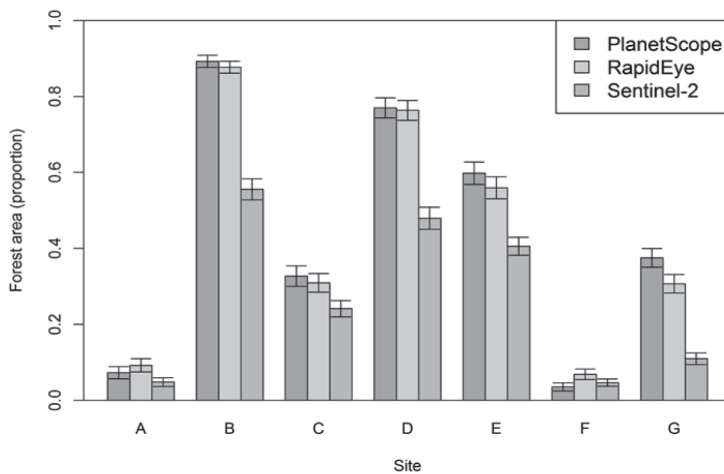
Figure 4. Forest area (proportion) estimates from PlanetScope, RapidEye, and Sentinel-2 images for each study site (A–G). Error bars represent the estimated standard error of the mean.

3.3. Canopy Cover Estimation

Estimates of proportions of canopy cover from the three image types for all of the study sites are shown in Figure 5 and for LULC classes in Figure 6. The largest canopy cover estimate was recorded for site B as 0.59, 0.56, and 0.34 using PlanetScope, RapidEye, and Sentinel-2 images, respectively. By contrast, site F showed the smallest estimates of all of the sites with canopy cover estimates of 0.05, 0.09, and 0.07 from PlanetScope, RapidEye, and Sentinel-2 images. Estimates from PlanetScope and RapidEye images again appeared to be comparable, with a slightly larger difference between them than those of the forest area estimates. Nevertheless, no statistically significant difference was seen in any site between the two software packages. In sites A, C, and F, all of which had less forest cover, Sentinel-2 produced quite similar estimates to the other image types. In contrast, in sites B, D, E, and G, which had large forest cover where one also could expect large canopy cover, the estimates from Sentinel-2 significantly varied ($p < 0.01$) from the rest. This shows that the estimates from Sentinel-2 images provided smaller canopy cover values where forests tended to be denser compared to PlanetScope and RapidEye. In terms of overall performance, when taking into account the magnitude of the standard errors of canopy cover estimates of all of the sites, although the differences were not that big, PlanetScope seemed to produce a precise estimate since it on average had the smallest value, whereas RapidEye and Sentinel-2 resulted in slightly less precise estimates (Figure 7).
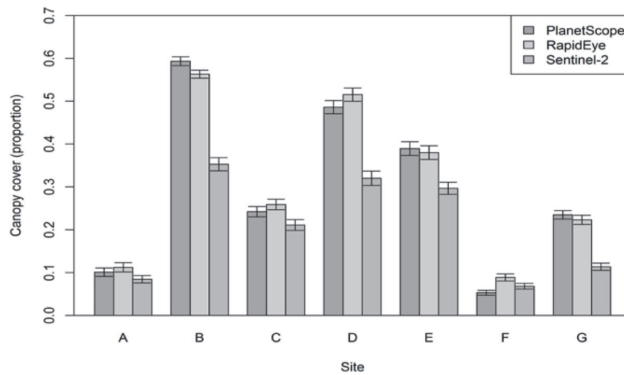
Figure 5. Canopy cover (proportion) estimates from PlanetScope, RapidEye, and Sentinel-2 images for each study site (A–G). Error bars represent the estimated standard error of the mean.

When analyses of estimates of tree canopy cover were carried out for each LULC class using the three image types (Figure 6) the largest proportion of canopy cover estimate was, as expected, obtained in the Forest land category, with a magnitude of 0.57 from PlanetScope, 0.59 from RapidEye, and 0.58 from the Sentinel-2 images. According to the estimates from PlanetScope, Settlements (0.10), Cropland (0.09), and Grassland (0.08) were the second, third, and fourth LULC classes in terms of their canopy coverage. Within each LULC class, the different image types resulted in estimates that were very similar to each other except for the Settlements, Wetlands, and Other land classes. However, even in these classes, the differences were not significant in the statistical sense. It seems that if a given LULC class is a homogenous one such as Forest land, Cropland, or Grassland, then any of these images could produce reasonably comparable estimates of canopy cover. Whereas on the contrary, in heterogeneous LULC scenarios, coarser resolution images tended to either overestimate or underestimate canopy cover as compared with estimates from finer resolution images. Considering overall standard errors for each image type, it was observed that PlanetScope resulted in a smaller overall variability, showing a better precision of estimates, whereas the largest variability of estimates was seen for RapidEye (Figure 7).
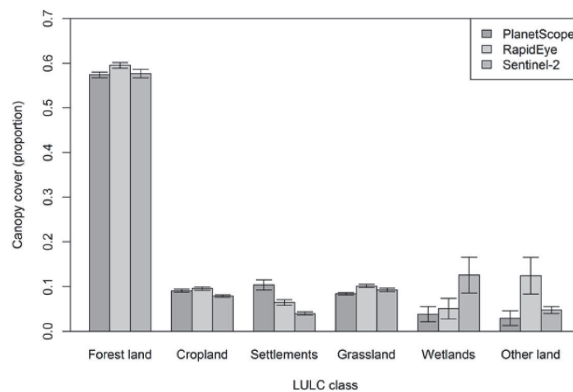
Figure 6. Canopy cover (proportion) estimates from PlanetScope, RapidEye, and Sentinel-2 images by land-use and land-cover (LULC) classes. Error bars represent the estimated standard error of the mean.
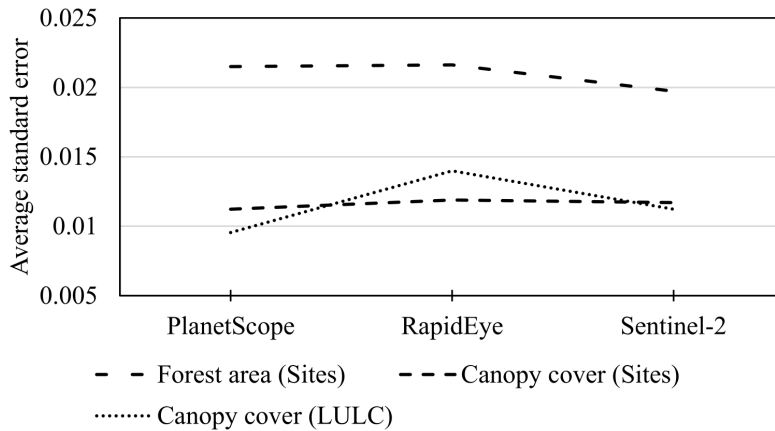
Figure 7. Average standard error for forest area and canopy cover estimates by sites as well as for canopy cover estimates by LULC classes from the three image types.

3.4. Optimal Sample Size Determination

The results from the bootstrapping showed increasing standard errors as the sample size decreased for both forest area and canopy cover estimates, regardless of site and image type (Figure 8). Resampling with a sample size of 200 observations resulted in estimates that were very close to the original sample size of 228, followed by 150, 100, and 50 as the second, third, and fourth closest estimates, respectively. On average, the increase in standard error when using 200 instead of 228 sample observations was 6.7%, 6.5%, and 4.9% for forest area and 8.7%, 6.0%, and 4.2% for canopy cover estimates from PlanetScope, RapidEye, and Sentinel-2, respectively. Similarly, samples of 150 observations on average generated estimates with a standard error inflation of less than 24.0% for all of the image types and both forest area and canopy cover estimations. Furthermore, when the sample size was reduced to 100 observations, the standard error increased almost by 50%.

The standard errors were consistently smaller for site F than for the rest of the study sites. In addition, the standard error values of sites A and F were entirely below the average curve, while those of sites D and E were constantly above the average curve for both the forest area and canopy cover estimates of the three image types (Figure 8). Reducing the sample size to only 50 observations resulted in a steeper curve and increased the standard errors by more than 100% in all of the cases. In general, considering the sample sizes, overall estimates of PlanetScope and RapidEye were found to be less sensitive to the reduction of sample size for forest area and canopy cover estimations, and the ranges of percentage increment across the sites were smaller in each respective case. Meanwhile, the Sentinel-2 estimates were highly sensitive in both cases with larger range values across the sites, regardless of having some smaller values.
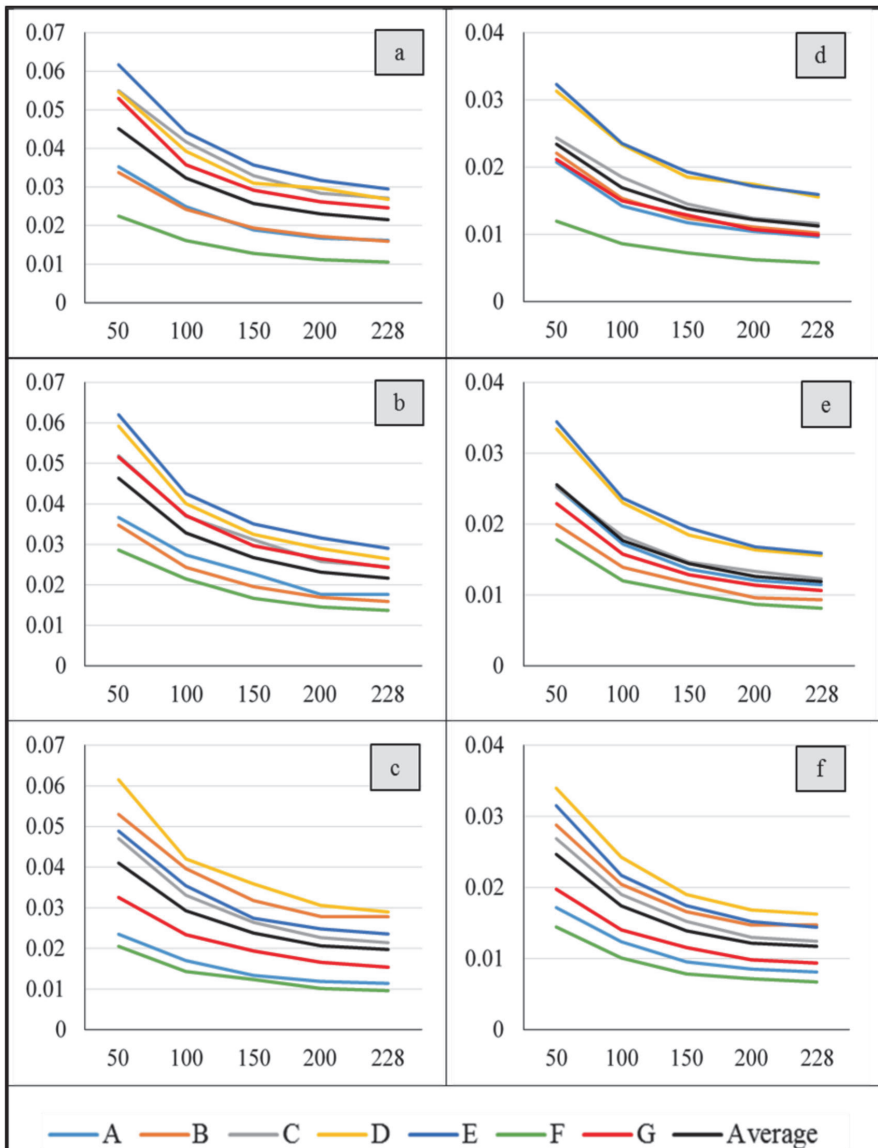
Figure 8. Standard error (*y*-axis) for forest area and canopy cover estimates in connection with sample size (*x*-axis). The results were determined through bootstrapping, except for 228 obtained from the original sample. (**a**–**c**) are for forest area; and (**d**–**f**) are for canopy cover estimates from PlanetScope, RapidEye, and Sentinel-2 images, respectively.

4. Discussion

4.1. Visual Image Interpretation in a REDD+ MRV

Visual image interpretation was adopted in this study to estimate the proportion of forest area and crown cover in seven subjectively selected sites in Ethiopia that have different forest and

vegetation types. Satellite images of PlanetScope, RapidEye, and Sentinel-2 were examined for their performance of producing estimates of forest area and canopy cover across the variety of site conditions. In addition, the study evaluated how sample size affected the uncertainty of the estimates from different image types.

The proportion of forest cover within an area of interest can be used to estimate the area of the forest by multiplying it with the total size of the area. Such information are of paramount importance for LULC change analysis as well as the quantification of emissions and removals for REDD+ activities [23,36]. Likewise, canopy cover information is used in several forest management applications. For instance, it serves as an important ecological indicator such as for habitat, microclimate, and light condition assessment [18], and it is used as a criterion in forest definitions [17].

In the current study, it was possible to record data representing 390 km^2 per hour on average. Meanwhile, for field surveys, only moving to a field plot representing 9 km^2 could be difficult within the same amount of time. Thus, the efficiency of visual interpretation is the major advantage. However, a disadvantage is the amount of subjectivity that is allowed in the interpretation. In this study, the average interpretation between two interpreters was used. However, if multiple interpreters are available, the difference between them could be calculated and thus calibrated for. Hence, multiple interpreters can mitigate systematic errors occurring due to individual decisions. In addition, it is problematic that the interpreted value could also have errors when trained and experienced interpreters are carrying out the work. Experience form Tanzania showed that tree cover and the amount of woody biomass is not necessarily a good indicator of land-use or land-cover classification in field [37]. Thus, a major confine of the current study is that we did not have any ground-measured value. However, indicating that differences between the imagery exist is important. A natural assumption is that higher resolution imageries provide a more accurate interpretation.

In this study, design-based estimates were the focus, and only the interpretations for the observation points were used to create estimates. The next step for implementing REDD+ MRV could be to include complete cover information e.g., from PlanetScope, RapidEye, or Sentinel, and combine the complete cover information with the interpretations making a wall-to-wall map that can be used in model-assisted estimation [37,38]. This will be a natural extension of the current study, as capacity building are taking place in the REDD+ countries.

4.2. Factors Influencing Estimates

Proportions of forest area estimated using PlanetScope and RapidEye images were very similar across the seven sites, regardless of their differences in spatial resolution. On the other hand, estimates from Sentinel-2 images for most of the sites differed significantly from those of both PlanetScope and RapidEye images. Exactly the same pattern of similarities and differences occurred as well for canopy cover estimates. It seemed that PlanetScope and RapidEye estimates were robust and capable of producing reliable results in different biomes with different forest types and magnitudes of forest coverage. However, the performance of Sentinel-2 images seemed to be dependent on the magnitude of forest cover. It produced similar estimates to those of PlanetScope and RapidEye for areas with less forest cover, and varied as the forest cover of the area increased. Each land-cover category has its own property that needs to be considered when selecting methods, including the images to be used for land-cover classification and mapping [39]. Accordingly, the discrepancy among estimates from these image types is perhaps due to a number of factors, one of which is the differences in the resolution of the images. Draksler [40] investigated the effect of satellite image resolution and minimum mapping unit on the accuracy of forest cover mapping in two different sites using RapidEye, Sentinel-2, and Landsat-8, and reported a declining trend in overall accuracy as the resolution got coarser. A similar trend was reported by Churches et al. [41], who compared forest cover estimates of Haiti using different satellite images.

Another factor contributing to the differences could be missing data, which will reduce the number of observations and hence affect the quality of estimates [42]. Most of the missing data during

image interpretation (NAs) were recorded for Sentinel-2 images (Table 3). Out of the total NAs in Sentinel-2, more than 70% were in sites B and D. These are the sites that are known to have denser forest cover and be accompanied by the presence of heavy cloud cover during most of the year. Therefore, its relatively coarser resolution coupled with the cloud cover might have affected the interpretation result, since it failed to sufficiently capture the existing variability within the study sites. The revisit frequency also directly influences the availability at cloudy locations. The frequent revisits of PlanetScope is highly favorable for REDD+ MRV, since 85% of the images used for the interpretations were acquired within a time period of one month, May 2017, while for RapidEye and Sentinel-2, a maximum of 34% and 40% of the images originated from one single month, respectively.

The majority of the images used for interpretation was acquired during the dry season. One reason for this is that cloud coverage is smaller in this season compared with the rainy season. It is likely that the phenology of the trees and other vegetation influences the interpretation. A tree crown with more leaves could potentially lead to a larger interpreted crown cover compared with when the tree has less or no leaves. The design of this study did not provide data to analyze the effect of seasonality in a statistical sense.

Satellite imagery used for the visual interpretation of forest area and canopy cover should be carefully selected. For low-density forest areas, say, somewhere below 30% canopy cover, Sentinel-2 images may be safely used, whereas for denser forest areas, higher resolution images such as PlanetScope and RapidEye should be considered. Of course, the choice may depend on the purpose of the study and available resources. To reduce costs, sampling instead of large-scale wall-to-wall observation could be used [43,44]. The method used in this study is such an alternative to obtain reliable estimates at a lower cost of image procurement, especially for dense forest areas where low-resolution images have deficiencies, and the quality of information pays off.

4.3. Sample Size

When resources allocated for data collection are limited, it is important also to apply appropriate sampling designs and use adequate sampling intensities [45,46]. Hence, it would be necessary to look for and determine optimal sample sizes that will result in a precise estimate with the possible minimum resource [45]. The bootstrapping technique allowed us to repeatedly sample from a given set of observations and assess the uncertainty of an estimate under certain circumstances, such as for example with different sample sizes, as in our case. As indicated in Figure 8, the precision of the estimates is sensitive to changes in the number of observations in the sample. The sensitivity also differs depending on the parameter of interest to be estimated as well as the types of images to be used. Hence, depending on the purpose of the study, the available resources, and the precisions that are required, one may decide on the number of observations accordingly. From the analysis of sample size in the current study, it seems possible to reduce the sample size slightly without substantially affecting the obtained accuracy. Perhaps a sample plot spacing of 3.5 km or 4 km between sample locations could have been considered.

5. Conclusions

Forest area and canopy cover estimates are among the most essential information in any forest management practice. One of the approaches to derive such information is through visual image interpretation techniques using satellite images. The technique is particularly quick, less costly, and helpful when the technical capacities to use digital image classification and mapping are limited. In this study, visual image interpretation was applied, and the use of PlanetScope, RapidEye, and Sentinel-2 satellite images for forest area and canopy cover estimation was evaluated. PlanetScope and RapidEye images produced similar estimates for all of the study sites and all of the LULC classes. Sentinel-2 image estimates varied significantly from the two other types of images in study sites with relatively denser forest cover, but resulted in similar estimates in sites with less dense forests. In visual image interpretation practices, very high-resolution images should be given priority. The choice of

image type can be influenced by the condition of the forest on the ground as well as the costs of the images. In case of using expensive and very high-resolution images, a sampling approach could reduce the overall costs compared to wall-to-wall acquisitions. Furthermore, the precision of the estimate is dependent on the sample size. Therefore, by taking the purpose of the assessment as well as the available resources into account, one should aim for sample sizes that balance the inventory costs and the required precision of an estimate.

Author Contributions: Z.A. and H.T. performed the experiments, analyzed the data and wrote the paper; H.O.Ø. conceived and designed the experiments, supervised all the research work that led to this paper and reviewed the manuscript; T.G. supervised the research work that led to this paper and reviewed the manuscript; I.B. reviewed the manuscript; E.N. provided inputs to the experiments and reviewed the manuscript.

Conflicts of Interest: The founding sponsors had no role in the design of the study; in the collection, analyses, or interpretation of data; in the writing of the manuscript, and in the decision to publish the results.

References

1. Dudley, N.; Stolton, S. Running Pure: The Importance of Forest Protected Areas to Drinking Water. World Bank/WWF Alliance for Forest Conservation and Sustainable Use, 2003. Available online: http://d2ouvy59p0dg6k.cloudfront.net/downloads/runningpurereport.pdf (accessed 16 November 2017).

2. McMahon, P. A Burning Issue: Tropical Forests and the Health of Global Ecosystems. In *Challenges and Opportunities for the World's Forests in the 21st Century*; Fenning, T., Ed.; Springer: Dordrecht, The Netherlands, 2014; pp. 23–35.

3. Le Quéré, C.; Raupach, M.R.; Canadell, J.G.; Marland, G.; Bopp, L.; Ciais, P.; Conway, T.J.; Doney, S.C.; Feely, R.A.; Foster, P.; et al. Trends in the sources and sinks of carbon dioxide. *Nat. Geosci.* **2009**, *2*, 831–836.

4. Canadell, J.G.; Le Quéré, C.; Raupach, M.R.; Field, C.B.; Buitenhuis, E.T.; Ciais, P.; Conway, T.J.; Gillett, N.P.; Houghton, R.A.; Marland, G. Contributions to accelerating atmospheric CO_2 growth from economic activity, carbon intensity, and efficiency of natural sinks. *Proc. Natl. Acad. Sci. USA* **2007**, *104*, 18866–18870. [CrossRef] [PubMed]

5. Pan, Y.; Birdsey, R.A.; Fang, J.; Houghton, R.; Kauppi, P.E.; Kurz, W.A.; Phillips, O.L.; Shvidenko, A.; Lewis, S.L.; Canadell, J.G.; et al. A large and persistent carbon sink in the world's forests. *Science* **2011**, *333*, 988–993. [CrossRef] [PubMed]

6. Baccini, A.; Friedl, M.A.; Woodcock, C.E.; Warbington, R. Forest biomass estimation over regional scales using multisource data. *Geophys. Res. Lett.* **2004**, *31*, L10501. [CrossRef]

7. Kim, D.-H.; Sexton, J.O.; Townshend, J.R. Accelerated Deforestation in the Humid Tropics from the 1990s to the 2000s. *Geophys. Res. Lett.* **2015**. [CrossRef] [PubMed]

8. Van der Werf, G.R.; Morton, D.C.; DeFries, R.S.; Olivier, J.G.J.; Kasibhatla, P.S.; Jackson, R.B.; Collatz, G.J.; Randerson, J.T. CO_2 emissions from forest loss. *Nat. Geosci.* **2009**, *2*, 737–738. [CrossRef]

9. Noriko, H.; Martin, H.; Veronique De, S.; Ruth, S.D.F.; Maria, B.; Louis, V.; Arild, A.; Erika, R. An assessment of deforestation and forest degradation drivers in developing countries. *Environ. Res. Lett.* **2012**, *7*, 044009. [CrossRef]

10. Pohjonen, V.; Pukkala, T. Eucalyptus globulus in Ethiopian forestry. *For. Ecol. Manag.* **1990**, *36*, 19–31. [CrossRef]

11. Bishaw, B. Deforestation and Land Degradation in the Ethiopian Highlands: A Strategy for Physical Recovery. *Northeast Afr. Stud.* **2001**, *8*, 7–25. [CrossRef]

12. McCann, J.C. The Plow and the Forest: Narratives of Deforestation in Ethiopia, 1840–1992. *Environ. Hist.* **1997**, *2*, 138–159. [CrossRef]

13.   Kindu, M.; Schneider, T.; Teketay, D.; Knoke, T. Land Use/Land Cover Change Analysis Using Object-Based Classification Approach in Munessa-Shashemene Landscape of the Ethiopian Highlands. *Remote Sens.* **2013**, *5*, 2411–2435. [CrossRef]

14.   Hailemariam, S.N.; Soromessa, T.; Teketay, D. Land Use and Land Cover Change in the Bale Mountain Eco-Region of Ethiopia during 1985 to 2015. *Land* **2016**, *5*, 41. [CrossRef]

15.   Penman, J.; Gytarsky, M.; Hiraishi, T.; Krug, T.; Kruger, D.; Pipatti, R.; Buendia, L.; Miwa, K.; Ngara, T.; Tanabe, K.; et al. *Good Practice Guidance for Land Use, Land-Use Change and Forestry*; IPCC: Geneva, Switzerland, 2003.

16.   Chazdon, R.L.; Brancalion, P.H.S.; Laestadius, L.; Bennett-Curry, A.; Buckingham, K.; Kumar, C.; Moll-Rocek, J.; Vieira, I.C.L.G.E.; Wilson, S.J. When is a forest a forest? Forest concepts and definitions in the era of forest and landscape restoration. *Ambio* **2016**, *45*, 538–550. [CrossRef] [PubMed]

17.   FAO. *Global Forest Resources Assessment 2000*; Forestry Paper No. 140; UN Food and Agricultural Organization: Rome, Italy, 2001.

18.   Jennings, S.B.; Brown, N.D.; Sheil, D. Assessing forest canopies and understorey illumination: Canopy closure, canopy cover and other measures. *Forestry* **1999**, *72*, 59–73. [CrossRef]

19.   Gschwantner, T.; Schadauer, K.; Vidal, C.; Lanz, A.; Tomppo, E.; di Cosmo, L.; Robert, N.; Duursma, D.E.; Lawrence, M. Common Tree Definitions for National Forest Inventories in Europe. *Silva Fenn.* **2009**, *43*, 303–321. [CrossRef]

20.   Korhonen, L.; Korhonen, K.T.; Rautiainen, M.; Stenberg, P. Estimation of forest canopy cover: A comparison of field measurement techniques. *Silva Fenn.* **2006**, *40*, 577–588. [CrossRef]

21.   Mbow, C.; Skole, D.; Dieng, M.; Justice, C.; Kwesha, D.; Mane, L.; El Gamri, M.; Von Vordzogbe, V.; Virji, H. *Challenges and Prospects for REDD+ in Africa: Desk Review of REDD+ Implementation in Africa*; Global Land Project Reports; GLP International Project Office: Copenhagen, Denmark, 2012; Volume 5.

22.   Herold, M.; Skutsch, M. Monitoring, reporting and verification for national REDD + programmes: Two proposals. *Environ. Res. Lett.* **2011**, *6*, 014002. [CrossRef]

23.   IPCC. *2006 IPCC Guidelines for National Greenhouse Gas Inventories*; IGES: Berlin, Germay, 2006.

24.   IPCC. *Land Use, Land Use Change, and Forestry*; Cambridge University Press: Cambridge, UK, 2000.

25.   Bey, A.; Díaz, A.S.-P.; Maniatis, D.; Marchi, G.; Mollicone, D.; Ricci, S.; Bastin, J.-F.O.; Moore, R.; Federici, S.; Rezende, M.; et al. Collect Earth: Land Use and Land Cover Assessment through Augmented Visual Interpretation. *Remote Sens.* **2016**, *8*, 807. [CrossRef]

26.   Clark, M.L.; Aide, T.M. Virtual Interpretation of Earth Web-Interface Tool (VIEW-IT) for Collecting Land-Use/Land-Cover Reference Data. *Remote Sens.* **2011**, *3*, 601–620. [CrossRef]

27.   MEFCC. *Ethiopia's Forest Reference Level Submittssion to the UNFCCC*; Ministry of Environment, Forestry and Climate Change: Addis Ababa, Ethiopia, 2017.

28.   Fritz, S.; McCallum, I.; Schill, C.; Perger, C.; See, L.; Schepaschenko, D.; van der Velde, M.; Kraxner, F.; Obersteiner, M. Geo-Wiki: An online platform for improving global land cover. *Environ. Model. Softw.* **2012**, *31*, 110–123. [CrossRef]

29.   Fritz, S.; McCallum, I.; Schill, C.; Perger, C.; Grillmayer, R.; Achard, F.; Kraxner, F.; Obersteiner, M. Geo-Wiki.Org: The Use of Crowdsourcing to Improve Global Land Cover. *Remote Sens.* **2009**, *1*, 345–354. [CrossRef]

30.   Sannier, C.; McRoberts, R.E.; Fichet, L.-V.; Makaga, E.M.K. Using the regression estimator with Landsat data to estimate proportion forest cover and net proportion deforestation in Gabon. *Remote Sens. Environ.* **2014**, *151*, 138–148. [CrossRef]

31.   Potapov, P.V.; Dempewolf, J.; Talero, Y.; Hansen, M.C.; Stehman, S.V.; Vargas, C.; Rojas, E.J.; Castillo, D.; Mendoza, E.; Calderón, A.; et al. National satellite-based humid tropical forest change assessment in Peru in support of REDD+ implementation. *Environ. Res. Lett.* **2014**, *9*, 124012. [CrossRef]

32.   Ib, F.; Sebsebe, D.; Breugel, P.V. *Atlas of the Potential Vegetation of Ethiopia*; The Royal Danish Academy of Science and Letters: Copenhagen, Denmark, 2010; Volume 58.

33.   Egziabher, T.B.G. Diversity of Ethiopian flora. In *Plant Genetic Resources of Ethiopia*; Engles, J., Hawkes, J.G., Worede, M., Eds.; Cambridge University Press: Cambridge, UK, 1991; pp. 75–81.

34.   Martínez, S.; Mollicone, D. From Land Cover to Land Use: A Methodology to Assess Land Use from Remote Sensing Data. *Remote Sens.* **2012**, *4*, 1024–1045. [CrossRef]

35. Hesterberg, T.; Moore, D.S.; Monaghan, S.; Clipson, A.; Epstein, R. Bootstrap methods and permutation tests. In *Introduction to the Practice of Statistics*; W.H. Freeman & Company: New York, NY, USA, 2003.

36. Köhl, M.; Magnussen, S.; Marchetti, M. *Sampling Methods, Remote Sensing and GIS Multiresource Forest Inventory*; Springer: Berlin/Heidelberg, Germany, 2006.

37. Næsset, E.; Ørka, H.O.; Solberg, S.; Bollandsås, O.M.; Hansen, E.H.; Mauya, E.; Zahabu, E.; Malimbwi, R.; Chamuya, N.; Olsson, H.; et al. Mapping and estimating forest area and aboveground biomass in miombo woodlands in Tanzania using data from airborne laser scanning, TanDEM-X, RapidEye, and global forest maps: A comparison of estimated precision. *Remote Sens. Environ.* **2016**, *175*, 282–300. [CrossRef]

38. McRoberts, R.E. Probability- and model-based approaches to inference for proportion forest using satellite imagery as ancillary data. *Remote Sens. Environ.* **2010**, *114*, 1017–1025. [CrossRef]

39. King, R.B. Land cover mapping principles: A return to interpretation fundamentals. *Int. J. Remote Sens.* **2002**, *23*, 3525–3545. [CrossRef]

40. Draksler, A. *The Effect of Satellite Image Resolution and Minimum Mapping Unit on the Accuracy of Forest Cover Maps*; Technische Universität München: Munich, Germany, 2017.

41. Churches, C.E.; Wampler, P.J.; Sun, W.; Smith, A.J. Evaluation of forest cover estimates for Haiti using supervised classification of Landsat data. *Int. J. Appl. Earth Obs. Geoinf.* **2014**, *30*, 203–216. [CrossRef]

42. Lohr, S. *Sampling: Design and Analysis*; Nelson Education: Scarborough, ON, Canada, 2009.

43. Böttcher, H.; Eisbrenner, K.; Fritz, S.; Kindermann, G.; Kraxner, F.; McCallum, I.; Obersteiner, M. An assessment of monitoring requirements and costs of 'Reduced Emissions from Deforestation and Degradation'. *Carbon Balanc. Manag.* **2009**, *4*, 14. [CrossRef] [PubMed]

44. Falkowski, M.J.; Wulder, M.A.; White, J.C.; Gillis, M.D. Supporting large-area, sample-based forest inventories with very high spatial resolution satellite imagery. *Prog. Phys. Geogr.* **2009**, *33*, 403–423. [CrossRef]

45. Jayaraman, K. A Statistical Manual for Forestry Research. FORSPA, 2000. Available online: http://www.fao.org/3/a-x6831e.pdf (accessed on 10 November 2017).

46. Lenth, R.V. Some Practical Guidelines for Effective Sample Size Determination. *Am. Stat.* **2001**, *55*, 187–193. [CrossRef]

Paper II

Modelling and quantifying tree biometric properties of Dry Afromontane forests of south-central Ethiopia

Zerihun Asrat[1,2]*, Tron Eid[1], Terje Gobakken[1], Mesele Negash[2]

[1] Faculty of Environmental Sciences and Natural Resource Management, Norwegian University of Life Sciences, P.O. Box 5003, 1432, Ås, Norway.

[2] Wondo Genet College of Forestry and Natural Resources, P. O. Box 128, Shashemene, Ethiopia.

*correspondence: zerihun.asrat.kutie@nmbu.no or zerasrat@gmail.com

Key Message: Models for quantifying tree biometric properties, imperative for forest management decisions-making, including height, diameter, bark thickness and volume were developed, and wood basic density was documented for Dry Afromontane forests of south-central Ethiopia.

Abstract

Tree biometric properties such as height (ht), diameter at breast height (dbh), bark thickness (bt), volume and wood basic density (wbd) are imperative for forest management decisions-making. For Dry Afromontane forests in south-central Ethiopia, models for quantifying such tree properties are totally lacking. This study therefore aimed at developing models for ht based on dbh, for dbh based on stump height diameter (dsh), for bt based on dbh, for volume based on dbh, ht and crown width (crw), as well as documenting wbd data. Comprehensive and representative datasets were collected from Degaga-Gambo and Wondo Genet forests. The ht, dbh and bt modelling were based on 1345 sampled trees during forest inventories, while the volume modelling and wbd documentation were based on 63 destructively sampled trees from 30 species covering 87% of the total basal area in the study sites. Weighted least squares regression was applied for modelling and leave one out cross-validation was used for evaluation. The ht-dbh and dbh-dsh models performed well (pseudo-R^2 = 0.72 and 0.98), while bt-dbh performed poorer (pseudo-R^2 = 0.42). Models for the total tree, merchantable stem and branches volume were developed with different options for independent variables, where pseudo-R^2 varied from 0.74 to 0.98, with smallest values for the branches models The models may be applied to forests outside the present study sites provided that the growing conditions are carefully evaluated. The species-wise wbd was ranging from 0.426-0.979 g cm^{-3}, with the overall mean of 0.588 g cm^{-3}. The wbd data will be useful for building up a national wbd database and may also be included in the Global Wood Density database. The study represents a significant step towards sustainable forest management including REDD+ MRV practices in the Dry Afromontane forests of south-central Ethiopia.

Key words: Dry Afromontane forests, Height-diameter and bark models, Volume models, Wood basic density

Introduction

Forest management decisions can be affected by the availability of relevant tree biometric information. In the course of acquiring information for decision-making in the whole continuum from single trees to forests, the use of appropriate models and data plays an immense role (Vanclay 1994; van Laar and Akça 2007). The availability of tree biometric data like wood basic density (wbd), tree height (ht), diameter at breast height (dbh), bark thickness (bt), volume and biomass are critical for supporting forest management decision-making and reducing costs for ground based forest resource assessment (van Laar and Akça 2007; West 2009). Such data and models are also the basis for assessing changes over time, which is linked to a successful implementation of measurement reporting and verification (MRV) practices in reducing emissions from deforestation and forest degradation (REDD+) programs (Penman et al. 2003).

Diameter at breast height and tree height are core variables describing trees. In the tropics, tree height measurement is very challenging compared to dbh (Mokria et al. 2015). Hence, tree height is mostly determined by means of models describing ht-dbh relationships (West 2009; Mugasha et al. 2013; Mokria et al. 2015; Mugasha et al. 2019). To this line, studies have also reported 10-30% errors in ht measurements in tropical forests (Larjavaara and Muller-Landau 2013). Hence, the presence of appropriate ht-dbh models may therefore reduce both the inventory costs and the uncertainty in height estimates, especially in tropical forests with complex tree architecture (Feldpausch et al. 2011). When assessing previous harvests or damages in a forest, only stump diameter (dsh) can usually be measured. For such cases it is therefore important to establish a dbh-dsh relationship, where dbh, and subsequently volume or biomass can be estimated by measuring dsh only (Corral-Rivas et al. 2007; Özçelik et al. 2010). Furthermore, quantifying bark thickness of trees by means of an established bt-dbh relationship might be useful either to assess the volume of solid wood to be used for construction materials or volume of bark to be used for energy purposes, spices or medicine (van Laar and Akça 2007; Kershaw et al. 2017).

Volume data are used to describe present forest resources, as a variable in growth and yield models for predicting future growing stocks and impacts of harvest as well as to assist in evaluating silvicultural practices (Vanclay 1994; Weiskittel et al. 2011). Volume data may also be used to determine biomass using expansion and conversion factors (Lindner and Karjalainen 2007; Bollandsås et al. 2016). Models predicting volume of trees based on dbh, ht and other tree properties measured in the field have been developed for decades. The development of such models, however, continues to attract attention, because no single theory exists for developing volume models that can be used satisfactorily for all tree species and forest types (Muhairwe 1999).

Wood basic density (g cm^{-3}) of trees, i.e. the ratio of oven dry mass to the green volume of the wood (Williamson and Wiemann 2010), is the basis for characterizing tree species from a wood utilization point of view (Chave et al. 2009; Missanjo and Matsumura 2016). Information on wbd may have management implications since larger wbd indicates better wood quality for fuel (Githiomi and Kariuki 2010) and better resistance to severe abiotic disturbance factors (Chave et al. 2009). Wood basic density may also be used to predict biomass either when using allometric models (Chave et al. 2014; Njana et al. 2016) or along with biomass expansion factors and volume data (Bollandsås et al. 2016). The magnitude of wbd is reported to vary with tree height and age (Githiomi and Kariuki 2010), tree section (Njana et al. 2016; Tesfaye et al. 2019), and between species, sites, and other environmental factors (Henry et al. 2010; Ubuy et al. 2018a).

The present study was conducted in Dry Afromontane forest, which is a dominant forest type in Ethiopia (UN-REDD 2017). Dry Afromontane forests are characterized by high levels of biodiversity and species endemism (Mittermeier et al. 2004; Friis et al. 2010) and are found in most highland areas in north-central, central and south-central parts at elevations between 1500 and 3400 m. Having about 460 woody species recorded, the Dry Afromontane is the second most diverse forest type in the country following the *Acacia-Commiphora* forest (Friis et al. 2010). The upper canopy of the remaining patches of these forests are dominated by *Juniperus procera*, *Afrocarpus falcatus*, *Olea europaea*, *Croton macrostachyus* and *Ficus species,* while the middle and lower canopy are usually occupied by *Allophylus abyssinicus*, *Apodytes dimidiata*, *Bersama abyssinica*, *Cassipourea malosana*, *Celtis africana*, *Chionanthus mildbraedii*, and *Dombeya torrida* (Friis et al. 2010).

Forests in Ethiopia and their management have been given attention recently from different stakeholders, mainly in line with the growing concern on climate change and its mitigation issues (UN-REDD 2017). In response, the country is striving to improve its forest management by implementing new approaches like Participatory Forest Management (PFM) (Lemenih et al. 2015), area exclosures (Lemenih and Kassa 2014), and REDD+ (UN-REDD 2017). Dry Afromontane forests, like most other natural forest types in the country, have none or little active management (Guillozet et al. 2014). However, recently, the longstanding concern that such forests should be managed and used sustainably rather than mere protection is gaining momentum, and thus some efforts to implement PFM regimes which integrate sustainable timber harvesting have been seen (Lemenih et al. 2015; Ayele et al. 2018). This may provide sufficient incentives and motivate to a better forest management scheme, as opposed to the status-quo protection-oriented system, which favours illegal and uncontrolled harvests of

timber and other forest products (MEFCC 2018). The forest policy amendment in 2018 and the development of guidelines for sustainable timber harvesting from forests under PFM (Ayele et al. 2018) are steps forward towards a shift in management.

Models and data which are basic for informed decision-making and facilitating a shift in forest management for Dry Afromontane forests in Ethiopia, however, are very scarce or totally lacking. Kebede et al. (2013) and Wondrade et al. (2015), for example, spent much time measuring both dbh and ht of all trees in their study area due to lack of any models describing ht-dbh relationships. No studies have been found specifically dealing with the dbh-dsh relationship, although several studies from natural forests in Ethiopia have used dsh instead of dbh to estimate biomass (e.g. Mokria et al. 2018, Ubuy et al. 2018b). Except for Eriksson et al. (2002), who partly dealt with bark from a fire resistance point of view, no studies have been found quantifying bt of trees in Ethiopia. Despite having diverse forest types, models estimating tree volume for natural forests in Ethiopia are lacking (Henry et al. 2011). In the literature we found volume models only for plantations (Pohjonen 1991; Teshome 2005; Berhe 2009). Hence, a general volume formula that uses tree basal area, ht and form factor (f) has been applied. Form factor is a correction value that characterizes the shape of the tree stem and adjusts the assumed cylindrical volume value to the actual stem volume (Laar and Akça 2007). However, this approach requires knowing species-specific f values, which are totally lacking for natural forests in Ethiopia. Instead, a generalised f value of 0.5 is usually applied (Sisay et al. 2017). Despite the importance of wbd in describing wood properties and the presence of the high number of tree species as well as diverse environmental conditions in Ethiopia, only a limited number of wbd studies are found in the literature (Desalegn et al. 2012; Ubuy et al. 2018a; Tesfaye et al. 2019). As a result, biomass estimations in the Ethiopian forest reference level (FRL) report submitted to the United Nations Framework Convention on Climate Change (UN-REDD 2017) were based on wbd values obtained from the Global Wood Density (GWD) database (Chave et al. 2009; Zanne et al. 2009), comprising very little data from Ethiopia.

The main objective of this study was therefore to provide models and data that can be used as tools for quantifying biometric tree properties and facilitating a sustainable use of resources in the Dry Afromontane forests of south-central Ethiopia. Specifically, the study aimed at i) developing models for ht based on dbh, dbh based on dsh and bt based on dbh, ii) developing models for merchantable stem, branches and total tree volume, and iii) determining and documenting the wbd values and their variability for different tree species.

Materials and methods

Study sites

The study was conducted in Degaga-Gambo and Wondo Genet Dry Afromontane forests in south-central Ethiopia (Fig. 1), situated along the eastern escarpment of the Great East African Rift Valley. The sites receive a biannual rainfall with the short rainy season between March and May and the main rainy season between July and September. The surrounding landscapes are composed of mosaics of land use/land covers including plantations, woodlands, settlements and water bodies. The sites are habitat for several wildlife species and source of several tributary rivers. The vegetation at both sites are remnants of previously dense Dry Afromontane forests (Friis et al. 2010).

In Degaga-Gambo, the district authorities simply conserve the natural forests, while maintaining plantation forests of exotic tree species for economic wood production purposes. During the forest inventory we observed many stumps from illegal harvesting in the natural forests. Currently, there is an ongoing effort of transferring the natural forests into a PFM system as a means to reduce deforestation and forest degradation in the area. Degaga-Gambo forest extends from 38°45' to 38°56' E longitude and from 7°13' to 7°33' N latitude, with an area of 12580 ha. The elevation ranges from about 2100 to 2700 m a.s.l. The mean annual rainfall and temperature are 1245 mm and 14.9 °C, respectively. The soils are generally classified as Mollic Nitisols and Humic Umbrisols, respectively, at lower and upper altitudes (Fritzsche et al. 2007). The Wondo Genet site is under the concession areas of Wondo Genet College of Forestry and Natural Resources, which gives the forest protection and guarding services against illegal logging and fire incidences. The natural forest has no management plan, and no silvicultural interventions are carried out except some occasional planting activities. It extends from 38°37' to 38°39' E longitude and from 7°6' to 7°7' N latitude. The forest has an area of 390 ha with an altitudinal range from about 1850 to 2400 m a.s.l, and the soils are mainly classified as Mollic Andosols (Erikson and Stern 1987). The mean annual rainfall and temperature are 1123 mm and 17.6 °C, respectively.
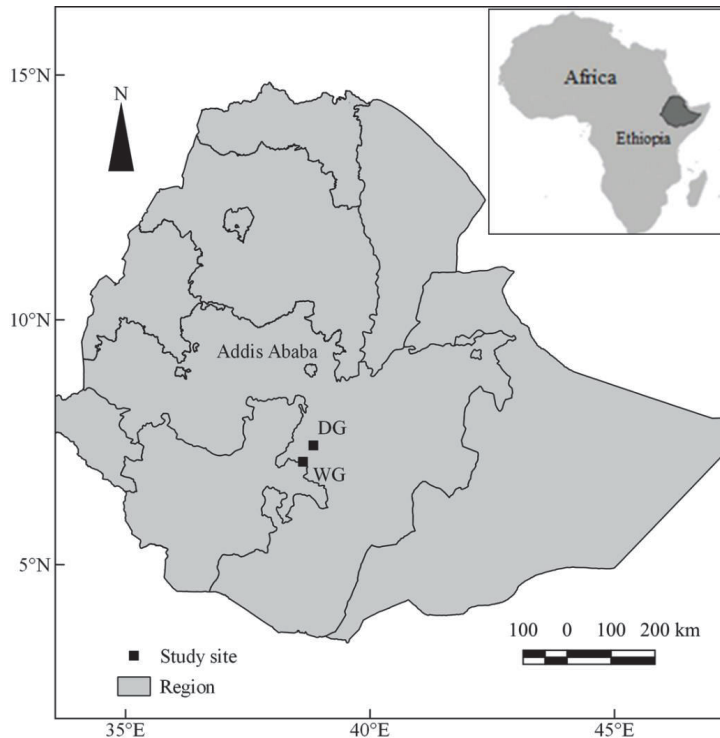
Fig. 1 Map of study sites; DG: Degaga-Gambo, WG: Wondo Genet

Data collection

Forest inventories

Forest inventories were carried out in 2018 to obtain information required for the tree selection in the destructive sampling (e.g. Mauya et al. 2014). A systematic square grid was overlaid with the sampling frame (map of the respective sites) that resulted in 65 and 42 sample plots for Degaga-Gambo and Wondo Genet, respectively. Circular plots with a size of 1000 m² and 400 m² were used for the inventories in Degaga-Gambo and Wondo Genet, respectively. All trees in the plot with dbh ≥ 5 cm were identified by species and measured for dbh. Up to 10 trees were then randomly sampled for each plot and measured for dsh (at 0.30 m above ground), ht, and bt (at breast height). Where there were only 10 or less trees in the plot, all trees were measured for dbh, dsh, ht and bt. For buttressed trees dsh was measured at the top of the buttress, and then dbh measured 0.3 m above this point if the buttress extended beyond one meter (West 2009). Tree diameters were measured using diameter tape or calliper, while ht was measured using a Haglöf VL5 hypsometer. For the sample plots, 45 and 50 tree species were identified in Degaga-Gambo and Wondo Genet, respectively, while in total there were 71 tree species. The maximum dbh encountered was 270 cm for Degaga-Gambo and 197 cm for Wondo Genet. A total of 1345

sample trees representing 60 tree species were measured and used for modelling of ht, dbh and bt. The mean (and range) values of these trees were 24.7 cm (5.0-270.0 cm), 20.9 cm (5.0-270.0 cm), 10.9 m (2.1-69.4 m) and 9.9 mm (2.0-50.0 mm) for dsh, dbh, ht and bt, respectively.

Selection of trees for destructive sampling

Based on the forest inventory data, a total of 63 trees representing 30 species (11 unique from each site and eight common from both) were selected for destructive sampling (Tables 1, 8 in Appendix). The dominant tree species, that constituted about 85% of the total basal area, were first included into the sample proportional to their basal area. The remaining trees were selected randomly among all species, meaning that 87% of the total basal area was represented in the dataset. An effort was made to proportionally select the trees throughout the 11 diameter classes considered from 5 cm to ≥ 105 cm (i.e. 5-15, 15-25, ..., ≥ 105), as this will help to ensure better and more stable models (Bollandsås et al. 2016). In addition, we tried to have a fair representation of large trees (10 trees with dbh > 75 cm) to try to avoid extrapolation in model applications (Bollandsås et al. 2016). Moreover, during destructive sampling, efforts were made in the selection to represent the altitudinal variation and spatial coverage over both sites to capture as much variability as possible in tree properties.

Before felling, we measured dbh over bark with a diameter tape or a calliper, depending on the size and shape of the stem. Tree height was measured with Haglöf VL5 hypsometer. In addition, mean crown width (crw) was recorded by taking two measurements using a measuring tape, one for maximum and one for minimum crown width. At the position of each tree, elevation (m), slope (%) and aspect (N, E, S, W) were measured, and basal area (m^2 ha^{-1}) was determined by means of relascope. Our hypotheses regarding wbd were that slope and basal area positively affect wbd because of slower growth, while elevation negatively affects wbd because precipitation increases with elevation and hence growth will be faster. In contrast, north and south facing aspects affect wbd positively and negatively, respectively, because of slower and faster growth.

Destructive sampling procedures

The selected trees were felled at stump height (0.3 m) using a chainsaw and each tree was sorted into merchantable stem, branches, and leaves and twigs sections (Table 1). The main stem up to the minimum useable top diameter (≥ 10 cm) was considered as merchantable stem. This cut off point was applied since it has been practiced as a rule of thumb at the sawmill of Wondo Genet College of Forestry and Natural Resources. However, trees with dbh < 15 cm were included in the branches section since they are considered to have insignificant merchantable

value. As a result, the merchantable stem volume analysis was based on 45 out of the 63 trees (Table 1). The branches section included the top log with diameter < 10 cm and all branches with diameter ≥ 2 cm. Twigs with diameter < 2 cm were set aside together with leaves for a separate biomass study. The stem was crosscut into shorter logs (from 0.5 m to 2.5 m) to facilitate the mid diameter and length measurement as well as to reduce taper effects. Similarly, branches were cut into pieces mostly shorter than 2 m and measured for length and mid diameter. The volume of each log was determined by multiplying the middle cross-sectional area of the log by its length (e.g. Bollandsås et al. 2016). Tree merchantable stem volume (V_{ms}) and branches volume (V_{br}) were obtained by summing up volumes for all logs in each section, respectively. Total tree volume (V_{tot}) was determined by summarizing merchantable stem and branches volumes (Table 1; Fig. 3 in appendix).

Table 1 Descriptive summary of destructively sampled trees

	Both sites (n = 63)			Degaga-Gambo (n = 32)			Wondo Genet (n = 31)		
	Mean	Range	SD	Mean	Range	SD	Mean	Range	SD
dbh (cm)	37.8	7.0-106.5	29.9	37.4	7.0-105.5	30.0	38.3	8.0-106.5	30.3
ht (m)	17.9	5.2-38.8	9.1	17.6	5.4-36.0	8.9	18.2	5.2-38.8	9.4
crw (m)	8.4	2.4-23.9	5.0	7.9	2.3-20.0	4.7	8.9	2.4-23.9	5.3
V_{tot} (m³)	3.066	0.014-22.537	5.230	2.897	0.014-17.252	4.918	3.242	0.031-22.537	5.611
V_{ms} (m³) [1]	2.687	0.074-11.865	3.559	2.683	0.076-11.865	3.671	2.691	0.074-11.579	3.525
V_{br} (m³)	1.147	0.014-10.958	2.140	0.969	0.014-6.113	1.654	1.332	0.031-10.958	2.564

[1] V_{ms} for trees with dbh ≥ 15 cm only, n = 23, 22 and 45 for Degaga-Gambo, Wondo Genet and both sites, respectively; SD = standard deviation

Sub-samples for wood basic density and laboratory work

For determining wbd, Chave et al. (2006) recommended collecting wood sub-samples from all parts of the tree. Accordingly, for each tree we collected three wood discs from the stem (i.e. one from breast height position, and one from each of the middle and upper parts) and three wood discs from the branches (one disc at a random point from a small, medium and large branch, respectively). The sizes of most discs were about 3-4 cm in length. For smaller trees with few and small sized branches, only one sub-sample was collected for the branch section. For larger trees, where it was not practical to take the whole wood disc, sub-samples were taken in such a way that they represent both the sapwood and heartwood sections (Williamson and Wiemann 2010). In total, we collected 364 sub-samples of wood, which correspond to an average of 5.8 sub-samples per tree. All sub-samples were put in an airtight plastic bag and brought to a laboratory, where green volumes were determined by the water displacement method after peeling off the bark. Then the sub-samples were oven dried at a temperature of about 103 ℃ until a constant mass was guaranteed by checking through recurrent measurements with a sensitive digital balance. Often this was attained within 48 or 72 hours, depending on the size of

the sub-sample. Finally, wbd was determined as the ratio of dry mass (g) to the green volume (cm³) for each sub-sample.

Data analyses

All data analyses were done with the R software (R Core Team 2019). The 'nlstools' package (Baty et al. 2015) in the R software was used for non-linear regression. Model fitting and performance evaluation were carried out based on two different datasets. To develop the ht-dbh, dbh-dsh and bt-dbh relationships, we used the sample trees' data (n=1345) from the inventories. To develop models for V_{tot}, V_{ms} and V_{br}, and to document wbd values and their variability, we used the destructively sampled trees (n=63).

For establishing the ht-dbh relationship five different non-linear models were tested. The data were first divided randomly into equal sized training and test datasets. Models were fitted to the training dataset, then applied on the test dataset for evaluation. Their performances were assessed using root mean squared error (RMSE), mean prediction error (MPE) and pseudo-R^2 (Eq. 7-11), where generally the smallest (close to zero) RMSE and MPE values and largest pseudo-R^2 values (close to 1), indicating a better model fit (James et al. 2013). The best performing model was finally recalibrated to the full dataset. The dbh-dsh and bt-dbh models were developed in a similar way as ht-dbh model.

For volume modelling, the data were first visually explored by plotting volume against the potential explanatory variables (Fig. 3 in appendix) to examine their functional relationships. Several textbooks suggest the use of dbh and ht together or separately as independent variables in volume modelling (e.g. West 2009; Kershaw et al. 2017). We were not able to find volume models developed for natural forests in Ethiopia, hence potential models for further testing were picked from the general literature (Schumacher and Hall 1933; van Laar and Akça 2007; West 2009) and from previous research on tree volume in natural forests in Tanzania (Mauya et al. 2014; Mugasha et al. 2016) and Malawi (Kachamba and Eid 2016). In addition, we tested two models for prediction of V_{br}, where crw was included as independent variable. The following six models were tested;

$$V_{tot,ms,br} = a + b \times (dbh)^2 \qquad (1)$$
$$V_{tot,ms,br} = a \times (dbh)^b \qquad (2)$$
$$V_{tot,ms,br} = a \times (dbh^2 \times ht)^b \qquad (3)$$
$$V_{tot,ms,br} = a \times (dbh)^b \times (ht)^c \qquad (4)$$
$$V_{br} = a \times (dbh^2 \times crw)^b \qquad (5)$$
$$V_{br} = a \times (dbh)^b \times (crw)^c \qquad (6)$$

where a, b, and c are model parameters.

Weighted ordinary least square regression was applied for Model 1 and non-linear least square regression for the remaining. Weights were applied to account for heteroscedasticity in the data, i.e. non-constant variance of the residuals with increasing values of the response variable. This is a common phenomenon that often occurs when modelling biological entities like trees (van Laar and Akça 2007; Zeng and Tang 2011). The error variances were inversely proportional to the dbh^2, and hence a weight of $1/(dbh^w)^2$ was used, where w is the weighting factor. The initial value for w was determined as explained in Picard et al. (2012), and finally after an iterative procedure the value which resulted in the smallest possible prediction error was selected as weighting factor. In addition, following recommendations by Kelly and Beltz (1987) for models with dbh and ht as independent variables, a weighting factor of $1/(dbh^w{\times}ht)^2$ was tested, and the obtained prediction error was compared with the prediction error of $1/(dbh^w)^2$. Eventually, the one with the smallest prediction error was used for weighting.

The basic requirement when testing the models was that all parameter estimates should be significantly different from zero. For further evaluation of the model performances, a leave one out cross-validation approach was applied (James et al. 2013), where one observation was put aside as test data and the model fitted to all remaining observations (i.e. n -1, training data) and then prediction was done on the test data (n=1) at a time. The procedure was repeated n times until all observations in the data were tested. The residuals, difference between the observed and predicted, were then used to calculate the performance indicators RMSE, RMSE%, MPE, MPE% and pseudo-R^2 as shown in Eq. 7–11, respectively. Akaike information criterion (AIC) was also computed.

$$\text{RMSE} = \sqrt{\frac{\sum_{i=1}^{n}(Y_i - \widehat{Y}_i)^2}{n}} \qquad\qquad (7)$$

$$\text{RMSE } (\%) = \left(\frac{\text{RMSE}}{\overline{Y}}\right) \times 100 \qquad\qquad (8)$$

$$\text{MPE} = \frac{\sum_{i=1}^{n}(Y_i - \widehat{Y}_i)}{n} \qquad\qquad (9)$$

$$\text{MPE } (\%) = \left(\frac{\text{MPE}}{\overline{Y}}\right) \times 100 \qquad\qquad (10)$$

$$\text{pseudo} - R^2 = 1 - \left(\frac{\text{SSR}}{\text{CSST}}\right) \qquad\qquad (11)$$

where Y_i and $\widehat{Y}_i$ are observed and predicted ht, dbh, bt or volume (either total, merchantable stem or branch) of observation i respectively; $\overline{Y}$ is mean observed ht, dbh, bt or volume (either total, merchantable or branch); SSR is sum of squared residuals; and CSST is corrected total sum of squares.

We also investigated consequences of using form factors in determining total volume by means of Eq. 12;

$$V_{tot} = g \times ht \times f_{0.5,mean,pred} \qquad (12)$$

where g is the basal area of a tree calculated using dbh; $f_{0.5}$, f_{mean} and f_{pred} are different form factors. We first applied the frequently used form factor of 0.5 ($f_{0.5}$) and the mean form factor observed in our data (f_{mean}). The f_{mean} is the average of all observed form factors calculated as the ratio of observed total volume and the volume of a cylinder with a diameter dbh and length of ht. In addition, we wanted to test the application of a predicted form factor (f_{pred}) for each tree by fitting a model based on dbh and ht (Tenzin et al. 2016) to the observed form factors in our data. However, this approach failed because of insignificant parameter estimates in the model. Finally, since no previously developed relevant volume models exist for Ethiopia, the performance of some previously developed models for natural forests elsewhere in east-Africa (Mauya et al. 2014; Kachamba and Eid 2016; Mugasha et al. 2016) were tested on our dataset.

The wbd values obtained from stem and branch sub-samples were averaged to get mean stem and branch wbd. These mean values were further aggregated by weighting them by their respective volumes to obtain a volume weighted wbd at tree and species level. The wbd data were organized and summarized using descriptive statistics. In addition, analysis of variance was carried out to assess the presence of significant variations in wbd among the tree species and between the sites. Differences among stem sections (breast height, middle and upper stem positions) and branch sizes (big, mid and small branch) for wbd were also tested by means of analysis of variance. Furthermore, pair-wise t-tests were applied to determine if there were significant wbd differences between stems, branches, values at breast height and volume weighted means. As wbd is expected to vary depending on growing conditions we fitted a linear regression to explore effects of elevation (m), slope (%), aspect (N, E, S, W) and basal area (m^2 ha^{-1}) on wbd variations.

Results

The model parameters and model performance indicators for the relationships between ht-dbh, dbh-dsh and bt-dbh are shown in Table 2. The ht-dbh relationship was relatively strong (pseudo-R^2 = 0.72). A very strong dbh-dsh relationship was found (pseudo-R^2 = 0.98) while the bt-dbh relationship was weaker. Generally, none of the MPEs for the models were significantly different from zero.

The model parameters and performance indicators for the general total (GT), merchantable stem (GMS) and branch (GB) volume models are shown in Table 3. The pseudo-R^2 of the total volume and merchantable stem volume models varied between 0.93-0.95 and 0.96-0.98, respectively. Moreover, none of these models had MPEs significantly different from zero and all had significant model parameters. For total volume, Model GT2 performed best (pseudo-R^2 = 0.95, RMSE = 37.4%) for the models with only dbh as independent variable, while Model GT3 performed best (pseudo-R^2 = 0.95, RMSE = 37.7%) for the models with both dbh and ht as independent variables. Likewise, for merchantable stem volume, Model GMS2 and GMS4 with dbh only and with dbh and ht independent variables, respectively, were performing best regarding pseudo-R^2 and RMSE. In general, the addition of ht into the total and merchantable stem volume models did not improve the performance indicators. The branch volume models in general had larger RMSEs compared to the total and merchantable stem volume models. For the models with dbh only as independent variable, Model GB2 was found to perform best (pseudo-R^2 = 0.74, and RMSE = 94.1%). Models with dbh and ht predictor variables either had poorer performance (Model GB3) or insignificant parameter estimates (Model GB4). Inclusion of crw instead of ht reduced the RMSEs to some extent. For the models with dbh and crw as independent variables, Model GB6 was found to perform best (pseudo-R^2 = 0.89, RMSE = 62.2%). None of the branch volume models had MPEs significantly different from zero.

Site-specific total volume models for Degaga-Gambo (DT) and Wondo Genet (WT) were also developed (Table 4). As for the general total volume models, Model DT2 and WT2 were found to be the best among models with dbh only in both sites Degaga-Gambo (pseudo-R^2 = 0.99, RMSE = 19.3%) and Wondo Genet (pseudo-R^2 = 0.91, RMSE = 51.4%) respectively. Inclusion of ht into the models improved performance marginally for Degaga-Gambo, but not for Wondo Genet. All the models for Degaga-Gambo performed better than the corresponding models in Wondo Genet. We also tested the general Model GT2 on the specific data from the two sites, but MPE was not significantly different from zero for any of them.

Table 2 Model parameters and performance indicators for different tree variable models

Tree variable	Model	Parameters a	b	c	Pseudo -R²	RMSE (*)	(%)	MPE (*)	(%)
ht	ht = 1.3 + a × [1- exp (-b × (dbh)^c)]	41.498221	0.023370	0.849478	0.72	3.96	36.4	-0.01	-0.1
dbh	dbh = a × (dsh)^b	0.6720320	1.062245		0.98	3.36	16.1	0.14	0.7
bt	bt = a × (dbh)^b	2.4743200	0.489150		0.42	4.90	49.7	0.00	0.0

* RMSE and MPE in cm, m and mm for dbh, ht and bt respectively; n=1345; all parameters $p < 0.001$

Table 3 Model parameters and performance indicators for general total, merchantable stem and branch volume models

Tree section	Model	Parameters a	b	c	Pseudo-R²	RMSE (m³)	(%)	MPE (m³)	(%)	AIC
Total volume (n = 63)	GT1	-0.1591000	0.0014030		0.93	1.326	43.2	-0.0027	-0.1	199
	GT2	**0.0001228**	**2.5500000**		**0.95**	**1.146**	**37.4**	**-0.0004**	**-0.0**	**187**
	GT3	**0.0000605**	**0.9789000**		**0.95**	**1.156**	**37.7**	**-0.0009**	**-0.0**	**193**
	GT4	0.0000891	2.4090000	0.2795000 [1]	0.95	1.158	37.8	0.0053	0.2	187
Merchantable stem volume (n = 45)	GMS1	-0.2715391	0.0009319		0.96	0.675	25.2	-0.0024	-0.1	86
	GMS2	**0.0000954** [2]	**2.5020000**		**0.98**	**0.518**	**19.3**	**0.0017**	**0.1**	**67**
	GMS3	0.0000369 [1]	0.9811000		0.97	0.642	23.9	-0.0006	-0.0	85
	GMS4	**0.0000596** [2]	**2.2480000**	**0.4701000** [2]	**0.98**	**0.557**	**20.7**	**0.0008**	**0.0**	**68**
Branch volume (n = 63)	GB1	-0.0036570*	0.0004964		0.78	0.997	86.9	0.0036	0.3	179
	GB2	**0.0000663** [1]	**2.4660000**		**0.74**	**1.079**	**94.1**	**0.0019**	**0.2**	**178**
	GB3	**0.0000421** [1]	**0.9227000**		**0.74**	**1.085**	**94.5**	**0.0721**	**6.3**	**177**
	GB4	0.0000771*	2.7130000	-0.3671000*	0.72	1.124	98.0	0.0054	0.5	179
	GB5	0.0000423 [1]	0.9829000		0.88	0.752	65.5	-0.0056	-0.5	129
	GB6	**0.0000773** [1]	**1.4980000**	**1.5070000**	**0.89**	**0.714**	**62.2**	**0.0020**	**0.2**	**120**

*Non-significant parameter ($p > 0.05$); [1]$p < 0.05$; [2]$p < 0.01$; all other parameters $p < 0.001$; Best performed models shown in bold

Table 4 Model parameters and performance indicators for site-specific total volume models

Site	Model	Parameters			Pseudo-R²	RMSE		MPE		AIC
		a	b	c		(m³)	(%)	(m³)	(%)	
Degaga-Gambo (n = 32)	DT1	-0.15170000 [2]	0.0013560		0.97	0.897	31.0	-0.0002	-0.1	70
	DT2	**0.0001306**	**2.5280000**		**0.99**	**0.558**	**19.3**	**-0.0003**	**-0.0**	**51**
	DT3	0.0000411 [2]	1.0080000		0.99	0.587	20.3	-0.0001	-0.0	51
	DT4	**0.0000744**	**2.1840000**	0.6144000 [2]	**0.99**	**0.519**	**17.9**	**0.0001**	**0.0**	**46**
Wondo Genet (n = 31)	WT1	-0.18660000 [1]	0.0014720		0.90	1.773	54.7	-0.0011	-0.0	115
	WT2	**0.0001190**	**2.5650000**		**0.91**	**1.665**	**51.4**	**0.0005**	**0.0**	**112**
	WT3	**0.0000608** [2]	**0.9811000**		**0.91**	**1.680**	**51.8**	**0.0042**	**0.1**	**115**
	WT4	0.0000880 [2]	2.5520000	0.1071000*	0.89	1.846	57.0	0.0027	0.1	113

*Non-significant parameter ($p > 0.05$); [1] $p < 0.05$; [2] $p < 0.01$; all other parameters $p < 0.001$; Best performed models shown in bold

Table 5 shows the results when testing the use of form factor approach and the previously developed models to predict total volume for our data. With $f_{0.5}$, total volume is significantly ($p > 0.05$) underpredicted (16.1%), while when applying f_{mean} (0.64), volume tended to be overpredicted, although not significantly. Generally, the previously developed models over- or underpredict volume, although the difference between observed and predicted volume is not significantly different from zero when applying the models developed by Mauya et al. (2014) and Mugasha et al. (2016) with both dbh and ht as independent variables. Figure 2 illustrates how all the models developed by Mauya et al. (2014), Kachamba and Eid (2016) and Mugasha et al. (2016), using only dbh as independent variable underpredicted volume consistently for medium and larger dbh sizes as compared to the corresponding model developed in the present study (Model GT2, Table 3).

Table 5 Testing the use of form factor and previously developed models for predicting total tree volume from our data

Model type	Predicted volume (m^3)	RMSE		MPE	
		(m^3)	(%)	(m^3)	(%)
$f_{0.5}$	2.574	1.423	46.4	0.493**	16.1
f_{mean} (0.64)	3.296	1.169	38.1	-0.229	-7.5
Mauya et al. (2014): dbh only	2.727	1.264	41.2	0.339*	11.1
Kachamba and Eid (2016): dbh only	2.675	1.655	54.0	0.391	12.8
Mugasha et al. (2016): dbh only	2.318	2.214	72.2	0.749**	24.4
Mauya et al. (2014): dbh and ht	3.081	1.020	33.3	-0.015	-0.5
Kachamba and Eid (2016): dbh and ht	4.103	1.957	63.8	-1.036***	-33.8
Mugasha et al. (2016): dbh and ht	2.870	1.073	35.0	0.196	6.4
Current study (GT2)	3.030	1.021	33.3	0.006	0.2

n = 63; observed total volume is 3.066 m^3; * $p < 0.05$, ** $p < 0.01$, *** $p < 0.001$
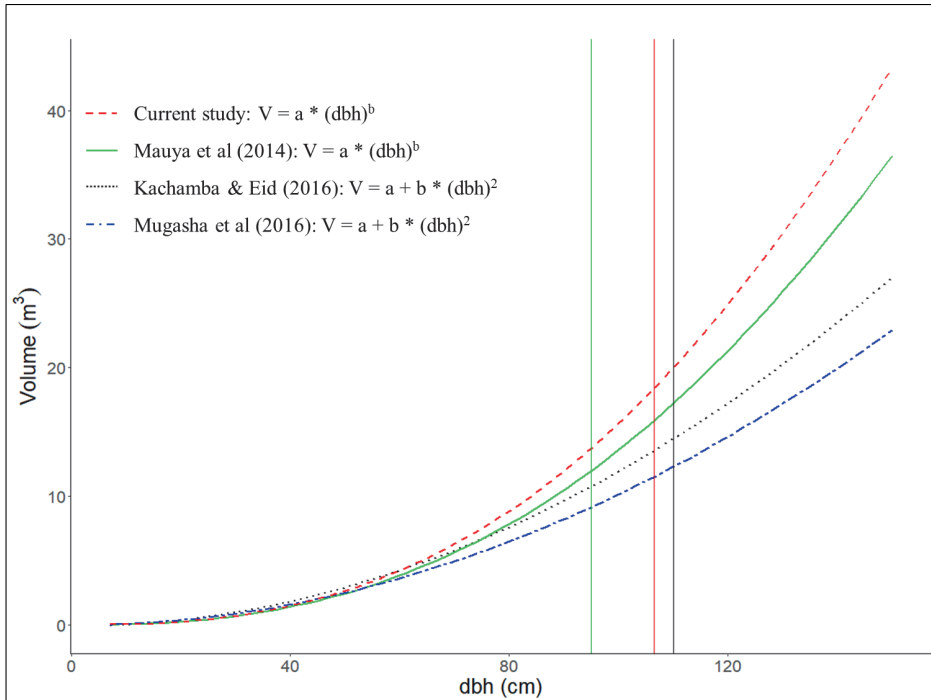
Fig. 2 Relationship of tree diameter against predicted total volume of selected previous models and the current study (Model GT2). Vertical lines indicate the maximum dbh used in the studies by Mauya et al. (2014), the current study, and Kachamba and Eid (2016), respectively

Volume weighted wbd values for 30 different tree species are documented in Table 6. The species-wise overall volume weighted mean (n=30 species) wbd was 0.588 g cm^{-3} and ranged between 0.426 and 0.979 g cm^{-3}. At individual tree level (n=63), the overall volume weighted mean wbd was 0.553 g cm^{-3} and ranged between 0.380 – 0.979 g cm^{-3}. Among the species, *T. nobilis*, *D. angustifolia* and *O. capensis* were found to be the top three with the largest wbd values of 0.979, 0.816, and 0.779 g cm^{-3}, respectively; while *A. falcatus, P. viridiflorum* and *V. amygdalina* were the three species with the smallest wbd values with 0.426, 0.441 and 0.457 g cm^{-3}, respectively.

Analysis of variance revealed that wbd values were significantly different ($p < 0.001$) among the tree species, while they were not significantly different ($p > 0.05$) between sites. In addition, analyses showed that there were no significant differences in wbd among the three samples collected from the stem sections (at breast height, at midpoint and at upper part) or among the three branch sizes (small, medium and large branches). The species-wise overall mean wbd for samples from stem, branch, and breast height position were also determined, and found to be 0.590, 0.589 and 0.576 g cm^{-3}, respectively (Table 8 in Appendix); and analyses of variance revealed no significant differences between these means ($p > 0.05$).

Table 6 Mean and range of volume weighted wbd values by tree species

Scientific name	No. of sample trees	wbd (g cm^{-3})	
		Mean	Range
Acokanthera schimperi (A. DC.) Schweinf.	1	0.621	
Afrocarpus falcatus (Thumb.) Mirb.	9	0.426	0.401 – 0.480
Albizia gummifera (J.F.Gmel.) C. A. Sm.	3	0.534	0.499 – 0.598
Allophylus abyssinicus Radlk.	2	0.509	0.509 – 0.515
Apodytes dimidiata E. Mey ex Am.	1	0.556	
Bersama abyssinica Fresen.	1	0.576	
Canthium oligocarpum Hiern	1	0.473	
Cassipourea malosana Alston	2	0.663	0.605 – 0.683
Celtis africana Burm. F.	5	0.631	0.615 – 0.658
Combretum molle R. Br. ex. G. Don	1	0.701	
Croton macrostachyus Hochst. ex. Delile.	5	0.511	0.430 – 0.521
Dodonaea angustifolia L. f.	1	0.816	
Ekebergia capensis Sparm.	1	0.532	
Ficus thonningii Blume	1	0.471	
Galiniera coffeoides Delile	1	0.563	
Maesa lanceolata Forssk.	3	0.483	0.457 – 0.536
Maytenus arbutifolia (Hochst. ex. A. Rich) R. Wilczek	2	0.615	0.615 – 0.622
Millettia ferruginea Hochst	4	0.550	0.380 – 0.554
Nuxia congesta R. Br.	2	0.537	0.498 – 0.603
Olea capensis L.	1	0.779	
Olea welwitschii (Knobl.) Gilg. & Schellenb.	1	0.700	
Olinia rochetiana A. Juss.	1	0.544	
Osyris quadripartita Salzam. ex Decne.	1	0.690	
Pittosporum viridiflorum Sims	1	0.441	
Pouteria adolfi-friedericii (Engl.) Baehni	4	0.460	0.458 – 0.567
Prunus africana (Hook.f.) Kalkman	3	0.609	0.608 – 0.615
Syzygium guineense (Willd.) DC.	2	0.580	0.579 – 0.590
Teclea nobilis Delile	1	0.979	
Vepris dainellii (Pic. Serm.) Kokwaro	1	0.631	
Vernonia amygdalina Del	1	0.457	

The outputs from regression analysis of wbd against variables describing growing conditions revealed non-significant parameter estimates for all the tested variables (Table 7) and a very small value of coefficient of determination. Still, when considering the signs of the parameter estimates, wbd was negatively influenced by elevation and basal area but positively influenced by slope. Concerning aspect, trees facing to the south tend to have higher wbd than the trees facing north.

Table 7 Parameter estimates and *p*-values from linear regression analysis of wbd as a dependent variable and some growing factors as independent variables

	Parameters	*p*-value
Intercept	0.762300	< 0.0000
Elevation (m)	- 0.000103	0.1950
Slope (%)	0.000317	0.7960
Basal area (m^2 ha^{-1})	- 0.000262	0.9030
Aspect (South)	0.009509	0.7730

Discussion

Models for tree biometric properties

The present study reported multi-species ht-dbh, dbh-dsh and bt-dbh models (Table 2), based on 1345 trees and 60 tree species, representing the study Dry Afromontane forests. Our ht-dbh model explained about 72% of the variation in ht, which is similar to models developed for four different natural forest types in Tanzania (Mugasha et al. 2013). Tree height measurement is challenging and susceptible to errors in tropical forests with complex tree architecture. Thus, the presence of local ht-dbh models may play a considerable role in reducing measurement errors (Larjavaara and Muller-Landau 2013; Mugasha et al. 2019).

The dbh-dsh model explained 98% of the variance. Similarly, other studies have reported strong dbh-dsh relationship (Corral-Rivas et al. 2007; Özçelik et al. 2010). This indicates that the model is important for volume or biomass quantification, particularly where there is only dsh data. More importantly, the model is helpful to estimate the magnitude of forest degradation and carbon loss from remaining stumps, which is presently a challenge in REDD+ MRV practices (UN-REDD 2017).

The bt-dbh model explained only 42% of the variation in bt. The model has a larger RMSE (49%) than some similar previously developed models, e.g. by Zeibig-Kichas et al. (2016) in the USA (RMSE of about 25%), but the MPE was not significantly different from zero, indicating that the model has an appropriate behaviour. Although some uncertainty will be involved in application due to the large RMSE, the model can be used for predicting bt at breast height, which may be useful in itself. Based on the bt predicted from the model, it is also possible indirectly to quantify tree properties relevant to forest management, such as volume of solid wood and volume of bark (van Laar and Akça 2007; Kershaw et al. 2017).

Tree and forest volume may be used for planning and monitoring of forest management practices (West 2009). Merchantable stem volume is needed to evaluate trees from a timber production perspective, but may also be useful when determining compensations for timber loss due to several reasons such as road construction (Melemez 2012). Branch volume estimates, particularly for big trees that have been used for timber production, maybe useful to estimate fuelwood quantities. Thus, our models remain crucial for the aspired sustainable utilization of the natural forests in Ethiopia (Ayele et al. 2018).

Generally, the total tree volume models explained about 93 - 95% of the variation in volume (Table 3). Model GT2, with dbh only as independent variable performed better than the other

models, i.e. Model GT3 with dbh and ht as independent variables revealed a marginally larger RMSE than Model GT2. The same applies to the merchantable stem volume models, i.e. Model GMS2 with dbh only and Model GMS4 with both dbh and ht, where the differences in RMSE again were marginal. The fact that inclusion of ht in the models revealed none or marginal improvements, conforms with studies in natural forest elsewhere in eastern Africa (e.g. Mauya et al. 2014; Mugasha et al. 2016). The branch volume models generally exhibited poorer performance than the total and merchantable stem volume models. Among the six branch volume models, Model GB2 with dbh and Model GB6 with dbh and crw had significant model parameters and the smallest MPE with pseudo-R^2 of 0.74 and 0.89, respectively. The relatively poor performance of the branch volume models might be attributed to the different branching habits of the different species. Similar findings regarding poor performance of branch volume models are also previously reported (Mauya et al. 2014; Kachamba and Eid 2016).

We also developed site-specific total volume models for Degaga-Gambo and Wondo Genet (Table 4). Site-specific models usually provide more accurate site-specific results than general models developed with data from multiple sites (Penman et al. 2003). Accordingly, we recommend the site-specific models to be applied for their respective sites. Furthermore, we recommend to use Models DT2 and DT4 for Degaga-Gambo and Models WT2 and WT3 for Wondo Genet with dbh only and with dbh and ht entries, respectively, depending on the availability of data.

No previous volume models have been developed in Ethiopia, neither for Dry Afromontane forests in particular, nor in general for natural forests. When applying the most relevant volume models from elsewhere in eastern Africa (Mauya et al. 2014; Kachamba and Eid 2016; Mugasha et al. 2016) on our data, the results showed that the MPEs in many cases were quite large (Table 5; Fig. 2). This is not surprising since these models were applied outside the ecological range they are developed for. Form factor $f_{0.5}$, along with dbh and ht, is often used in Ethiopia to determine tree volume (e.g. Sisay et al. 2017). Our result on the use of $f_{0.5}$ and f_{mean} showed that both form factors produced large MPEs, although the use of f_{mean} performed relatively better (Table 5). A study in Tanzania (Masota et al. 2014) conforms with our results, while a study in India (Adekunle et al. 2013) found volume estimates using mean form factors similar to estimates using volume models. However, in our case the use of form factors should be avoided since the models provide much better results.

Since no other appropriate options exist, we recommend the general models developed in this study also to be applied for Dry Afromontane forests elsewhere in the country. The fact that the

test of the general Model GT2 on data from the two specific sites did not reveal significant MPEs for any of the sites, is also indicating that this could be a viable option. Still, however, it is important to carefully evaluate species composition, and growing conditions related to altitude, rainfall, temperature and edaphic factors before utilizing our models. We also recommend applying Models GT2, GMS2 and GB2, based on only dbh as independent variable, in volume predictions for total, merchantable stem and branch, respectively. This will provide reasonably accurate predictions, and since these models do not require ht data, the inventory costs will be reduced. However, it is important to note that for branch volume, more accurate predictions can be made using Model GB6 if crw data are available besides dbh.

Wood basic density data

The wbd data of this study (Table 6) together with data from other studies (e.g. Ubuy et al. 2018a; Tesfaye et al. 2019) will help to develop a national wbd database for Ethiopia. Wood basic density data for 420 tree species have previously been compiled in Ethiopia's FRL report (UN-REDD 2017), but only a few of the wbd values were based on data from Ethiopia. The remaining were obtained mainly from the GWD database. In addition, the locally determined wbd values in the national database were determined at air dry basis (Desalegn et al. 2012), which means that some distortion may occur when converting them into oven dry basis (Vieilledent et al. 2018). Among the locally determined wbd values in the national database, we noted that for the 12 species also found in our study sites, they all had larger values as compared to our values. We have also recognized that 11 of the species in our list were not included in the GWD database (Chave et al. 2009; Zanne et al. 2009). Since our procedure in wbd determination is congruent with the requirement stated by Chave et al. (2006) and Williamson and Wiemann (2010), there is a possibility to incorporate the new Ethiopian wbd values into the GWD database.

The wbd values in our study varied significantly among species. The same was reported in some previous studies in Ethiopia (Ubuy et al. 2018a; Tesfaye et al. 2019). It is so because all species have inherent genetic makeup that governs its characteristics (Chave et al. 2006). Interestingly, there was no significant difference between our two sites in terms of mean wbd; perhaps due to the fact that they both belong to the same forest type. This is in fact a good indication that the wbd values also can be applied elsewhere in a similar forest type. This can be further consolidated by comparing wbd of two species *A. abyssinicus* (0.510 g cm^{-3}) and *O. rochetiana* (0.560 g cm^{-3}) from Tesfaye et al. (2019), a study conducted in a Dry Afromontane forest of central Ethiopia, with our findings that happened to be quite similar (i.e. 0.509 and 0.544 g cm^{-3}, respectively). On the other hand, when comparing the wbd of seven common species from

Ubuy et al. (2018a), the values were generally larger than ours and the differences ranged from 0.001 to 0.218 g cm^{-3}. Although some studies (e.g. Chave et al. 2009; Tesfaye et al. 2019) stated that wbd varies along the stem, we did not find any significant wbd differences along the stems, or among different branch sizes. Similarly, the overall stem and branch wbd values were not significantly different. This finding was contrary to some studies (e.g. Okai et al. 2003), while being in agreement with others (e.g. Swenson and Enquist 2008).

Many previous studies have found that wbd is influenced by growing conditions (e.g. Muller-Landau 2004; Ubuy et al. 2018a). In our study, no significant parameter estimates were found when we tested a few variables describing growing conditions by means of regression analysis (Table 7). Still, the signs of the parameter estimates might provide an indication of the effects. Elevation, for example, influenced wbd negatively. This confirms our hypothesis that both precipitation and growth will increase with elevation, and accordingly wbd will be smaller. Such a result is also in agreement with previous findings (Chave et al. 2006). Similarly, the effect of slope confirms our hypothesis, because increasing slope inclination might be associated with moisture stress, as water drains quickly, leading to slow growth and higher wbd. A similar finding was reported by Barij et al. (2007). Furthermore, we hypothesized that as basal area increases, the competition among trees becomes more intense, leading to slower growth and higher wbd. The results from the analyses, however, showed an opposite effect. Similarly, the result derived from the effect of aspect was the opposite of our hypothesis since trees on south facing slopes tended to have higher wbd than trees on north facing slopes. This could be due to more moisture stress due to higher evapotranspiration caused by longer exposure to sunlight for south facing slopes, implying slow growth, but denser wood. The work by Diaconu et al. (2016) also showed that south-west facing trees tend to have larger wbd.

Conclusions

This study provided the first comprehensive biometric datasets and models that can be used when working towards sustainable forest management including REDD+ MRV practices in the Dry Afromontane forests of south-central Ethiopia. Applying the ht-dbh model may have dual advantages of obtaining accurate ht estimates and of reducing costs in ht measurements while the dbh-dsh model may significantly contribute to estimation of biomass loss from forest degradation. The volume models are the first ones developed based on destructive sampling for natural forests in Ethiopia and facilitate a significant step forward for the management. The models may also be applied to Dry Afromontane forest areas outside the present study sites. It is, however, important to carefully evaluate the growing conditions in such areas before model application. The documented wbd data were based on a robust sampling scheme that

represented the whole tree. The absence of significant differences between the two sites in terms of wbd, and comparisons with findings from other studies indicate that the wbd data are applicable to other Dry Afromontane forests as well. The wbd data from the present study will be useful for building up a national wbd database and may potentially also be included in the GWD database.

Conflict of interest: The authors declare that they have no conflict of interest.

Appendix
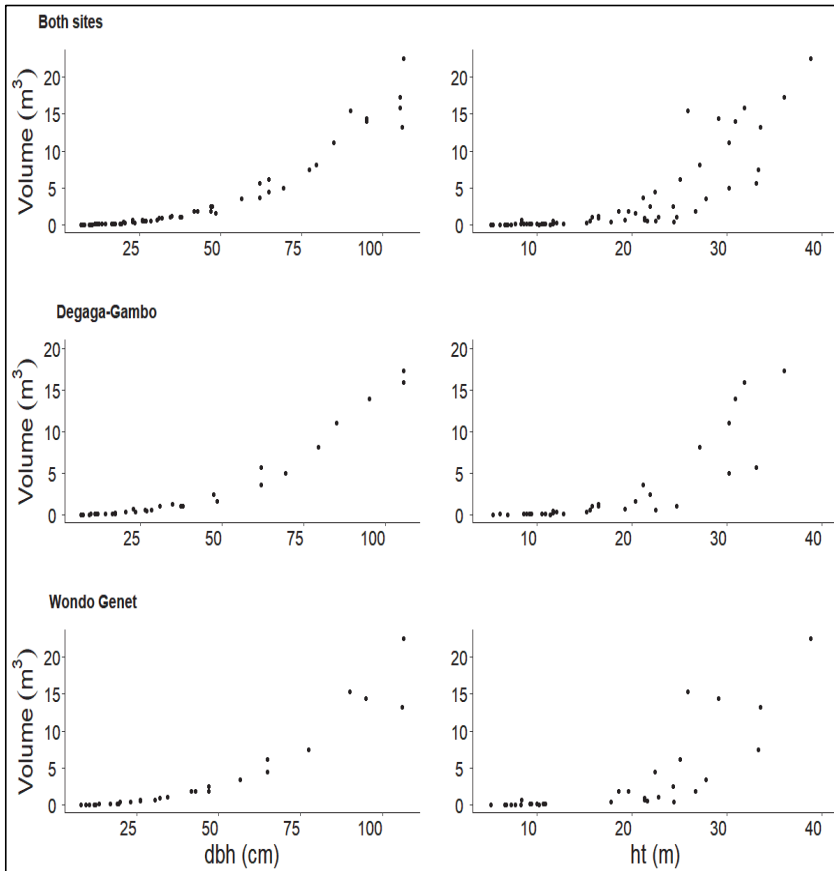
Fig. 3 Scatter plot of total volume against dbh (left) and ht (right) panel for both study sites, Degaga-Gambo and Wondo Genet (from top to bottom)

Table 8 Mean and range for dbh (cm), ht (m), crw (m) and wbd (g cm^{-3}) of stem, branch and at breast height position by species

Scientific name	Local name *	n	dbh (cm) Mean	dbh (cm) Range	ht (m) Mean	ht (m) Range	crw (m) Mean	crw (m) Range	Stem wbd Mean	Stem wbd Range	Branch wbd Mean	Branch wbd Range	Breast height wbd Mean	Breast height wbd Range
A. schimperi	Qeraru (S)	1	17.0		9.4		5.9		0.756		0.481		0.602	
A. falcatus	Birbirsa (O)	9	47.2	9.5–105.5	19.7	6.9–36.0	9.6	3.4-17.7	0.419	0.373–0.451	0.504	0.383–0.610	0.425	0.348–0.513
A. gummifera	Sesa (A)	3	87.2	65.0–106.5	29.9	25.1–38.8	20.3	16.1-23.9	0.522	0.474–0.611	0.548	0.525–0.582	0.552	0.413–0.795
A. abyssinicus	Hirqqammuu (O)	2	36.3	10.5–62	14.0	6.8–21.2	8.5	4.5-12.5	0.505	0.489–0.522	0.503	0.466–0.540	0.467	0.465–0.469
A. dimidiata	Arabdotteesaa (O)	1	37.5		24.7		6.1		0.548		0.596		0.540	
B. abyssinica	Koraqqaa (O)	1	27.0		11.7		6.7		0.577		0.575		0.563	
C. oligocarpum	Amshiqqaa (O)	1	28.5		15.6		5.7		0.463		0.499		0.440	
C. malosana	Xiillo (O)	2	10.0	8.0–12.0	8.0	6.6–9.4	5.1	4.9-5.4	0.618	0.551–0.684	0.724	0.680–0.768	0.669	0.660–0.677
C. africana	Amalaqa (O)	5	49.2	20.0–95.0	24.6	21.3–29.1	10.4	8.1-16.3	0.635	0.614–0.656	0.622	0.561–0.663	0.604	0.502–0.681
C. molle	Abalo (A)	1	12.0		7.7		3.6		0.701		0.702		0.784	
C. macrostachyus	Mokkoniisa (O)	5	43.6	11.5–85.0	22.1	10.5–30.2	11.3	3.6-20.0	0.479	0.426–0.511	0.521	0.468–0.561	0.482	0.436–0.565
D. angustifolia	Kitkita (A)	1	13.5		9.3		6.8		0.776		0.869		0.780	
E. capensis	Ononu (O)	1	62.0		33.1		12.9		0.521		0.554		0.530	
F. thonningii	Dimbicho (S)	1	47.0		18.6		8.2		0.472		0.469		0.428	
G. coffeoides	Korallaa (O)	1	11.3		8.6		4.1		0.572		0.545		0.535	
M. lanceolata	Abbayyi (O)	3	23.3	14.5–38.0	12.0	9.2–15.8	5.0	3.5-6.8	0.489	0.455–0.538	0.492	0.460–0.532	0.477	0.430–0.520
M. arbutifolia	Kombolcha (O)	2	12.3	7.0–17.5	8.6	5.4–11.7	4.2	3.4-4.9	0.629	0.628–0.630	0.581	0.580–0.583	0.672	0.668–0.675
M. ferruginea	Dhaadhaatu (O)	4	47.4	8.0–77.5	24.1	10.2–33.3	8.9	2.4-13.1	0.496	0.378 – 0.551	0.520	0.470–0.574	0.526	0.487–0.580
N. congesta	Bixxannaa (O)	2	21.3	19.0–23.5	11.1	10.0–12.1	4.7	4.3-5.0	0.552	0.505–0.599	0.549	0.490–0.608	0.558	0.526–0.590
O. capensis	Sigeda (O)	1	23.0		19.3		7.1		0.788		0.771		0.794	
O. welwitschii	Wolincho (S)	1	19.5		10.9		5.9		0.724		0.678		0.635	
O. rochetiana	Gunaa (O)	1	7.5		11.4		2.4		0.546		0.498		0.602	
O. quadripartita	Kaaro (O)	1	30.5		8.4		7.8		0.724		0.660		0.749	
P. viridiflorum	Aaraa (O)	1	10.5		5.2		3.8		0.432		0.480		0.440	
P. adolfi-friedericii	Sudubaa (O)	4	42.1	13.5–106.0	20.9	10.7–33.5	7.6	3.7-15.9	0.501	0.454–0.593	0.406	0.329–0.474	0.478	0.430–0.530
P. africana	Sukkee (O)	3	53.3	11.5–105.5	21.4	12.8–31.9	8.4	5.3-13.3	0.603	0.599–0.606	0.652	0.613–0.688	0.603	0.593–0.621
S. guineense	Baddeessa (O)	2	53.0	26.5–79.5	24.8	22.5–27.1	10.7	6.9-14.6	0.585	0.584–0.586	0.584	0.569–0.599	0.532	0.516–0.549

25

Table 8 Continued

Scientific name	Local name*	n	dbh (cm)		ht (m)		crw (m)		Stem wbd		Branch wbd		Breast height wbd	
			Mean	Range	Mean	Range	Mean	Range	Mean	Range	Mean	Range	Mean	Range
T. nobilis	Hadhesaa (O)	1	9.5		7.3		5.2		0.962		0.994		0.763	
V. dainellii	Lela (S)	1	12.5		8.3		5.7		0.619		0.645		0.584	
V. amygdalina	Ebicha (O)	1	10.0		6.1		2.9		0.471		0.433		0.473	

*Local name (A): in Amharic, (O): in Oromifa, and (S): in Sidaamu Afoo; n: No. of sample trees

References

Adekunle VAJ, Nair KN, Srivastava AK, Singh NK (2013) Models and form factors for stand volume estimation in natural forest ecosystems: a case study of Katarniaghat wildlife sanctuary (KGWS), Bahraich District, India. J For Res 24:217–226. https://doi.org/10.1007/s11676-013-0347-8

Ayele G, Mezmur S, Hussien S (2018) Guideline for sustainable timber harvesting in participatory forest management forests. Farm Africa, Addis Ababa

Barij N, Stokes A, Bogaard T, Van Beek R (2007) Does growing on a slope affect tree xylem structure and water relations? Tree Physiol 27:757–764. https://doi.org/10.1093/treephys/27.5.757

Baty F, Ritz C, Charles S, Brutsche M, Flandrois JP, Delignette-Muller ML (2015) A Toolbox for Nonlinear Regression in R: The Package nlstools. J Stat Software 66(5):1-21. http://www.jstatsoft.org/v66/i05/

Berhe L (2009) Volume and implicit taper functions for *Cupressus lusitanica* and *Pinus patula* tree plantations in Ethiopia. Eth J Environ Stud Manage 2:12-28. http://dx.doi.org/10.4314/ejesm.v2i1.43498

Bollandsås OM, Zahabu E, Katani JZ (2016) Background on the development of biomass and volume models; In(eds): Malimbwi RE, Eid T, Chamshama SAO. Allometric tree biomass and volume models in Tanzania. Department of forest mensuration & management, Sokoine University of Agriculture, Morogoro, pp 9-18

Chave J, Coomes D, Jansen S, Lewis SL, Swenson NG, Zanne AE (2009) Towards a worldwide wood economics spectrum. Ecol Lett 12:351–366. https://doi.org/10.1111/j.1461-0248.2009.01285.x

Chave J, Muller-Landau HC, Baker TR, Easdale TA, Steege HT, Webb CO (2006) Regional and phylogenetic variation of wood density across 2456 neotropical tree species. Ecol Appl 16:2356–2367. https://doi.org/10.1890/1051-0761(2006)016[2356:RAPVOW]2.0.CO;2

Chave J, Réjou-Méchain M, Búrquez A, Chidumayo E, Colgan MS, Delitti WB, Duque A, Eid T, Fearnside PM, Goodman RC, Henry M, Martínez-Yrízar A, Mugasha WA, Muller-Landau HC, Mencuccini M, Nelson BW, Ngomanda A, Nogueira EM, Ortiz-Malavassi E, Pélissier R, Ploton P, Ryan CM, Saldarriaga JG, Vieilledent G (2014) Improved allometric models to estimate the above ground biomass of tropical forests. Glob Chang Biol 20:3177–3190. https://doi.org/10.1111/gcb.12629

Corral-Rivas JJ, Barrio-Anta M, Aguirre-Calderon OA, Dieguez-Aranda U (2007) Use of stump diameter to estimate diameter at breast height and tree volume for major pine species in El Salto, Durango (Mexico). Forestry 80:29-40. https://doi.org/10.1093/forestry/cpl048

Desalegn G, Abegaz M, Teketay D, Gezahgne A (2012) Commercial Timber Species in Ethiopia: Characteristics and uses. A handbook for forest Industries, Construction and energy Sectors, foresters and Other Stakeholders. Addis Ababa University press, Addis Ababa. http://publication.eiar.gov.et:8080/ xmlui/handle/123456789/2920. Accessed August 2019

Diaconu D, Wassenberg M, Spiecker H (2016) Variability of European beech wood density as influenced by interactions between tree-ring growth and aspect. For Ecosyst 3:6. https://doi.org/10.1186/s40663-016-0065-8

Erikson H, Stern M (1987) A soil study at Wondo Genet Forestry Resource Institute, Ethiopia. Swedish University of Agricultural Science, International Rural Development Centre, Uppsala

Eriksson I, Teketay D, Granstrom (2002) Response of plant communities to fire in an *Acacia* woodland and dry Afromontane forest, southern Ethiopia. For Ecol Manage 177:39-50. https://doi.org/10.1016/S0378-1127(02)00325-0

Feldpausch T, Banin L, Phillips O, Baker T, Lewis S, Quesada C, Affum-Baffoe K, Arets E, Berry N, Bird M, et al. (2011) Height-diameter allometry of tropical forest trees. Biogeosciences 8:1081–1106. https://doi.org/10.5194/bg-8-1081-2011

Friis I, Demissew S, Breugel PV (2010) Atlas of the potential vegetation of Ethiopia. Det Kongelige Danske Videnskabernes Selskab. Denmark, Copenhagen

Fritzsche F, Zech W, Guggenberger G (2007) Soils of the main Ethiopian Rift Valley escarpment: A transect study. Catena 70:209-219. https://doi.org/10.1016/j.catena.2006.09.005

Githiomi JK, Kariuki JG (2010) Wood basic density of *Eucalyptus grandis* from plantations in Central Rift Valley, Kenya: variation with age, height level and between sapwood and heartwood. J Trop For Sci 22:281–286. https://www.jstor.org/stable/23616657

Guillozet K, Bliss JC, Kelecha TS (2014) Degradation in an Afromontane forest in highland Ethiopia, 1969 – 2010. Small-scale For 14:121–137. https://doi.org/10.1007/s11842-014-9277-3

Henry M, Besnard A, Asante WA, Eshun J, Adu-Bredu S, Valentini R, Bernoux M, Saint-André L (2010) Wood density, phytomass variations within and among trees, and allometric equations in a tropical rainforest of Africa. For Ecol Manage 260:1375–1388. https://doi.org/10.1016/j.foreco.2010.07.040

Henry M, Picard N, Trotta C, Manlay RJ, Valentini R, Bernoux M, Saint-André L (2011) Estimating tree biomass of sub-Saharan African forests: a review of available allometric equations. Silva Fenn 45:477–569. https://doi.org/10.14214/sf.38

James G, Witten D, Hastie T, Tibshirani R (2013) An introduction to statistical learning: with Applications in R. Springer, New York

Kachamba D, Eid T (2016) Total tree, merchantable stem and branch volume models for miombo woodlands of Malawi. South For J For Sci 78:41–51. https://doi.org/10.2989/20702620.2015.1108615

Kebede M, Kanninen M, Yirdaw E, Lemenih M (2013) Vegetation structure characteristics and topographic factors in the remnant moist Afromontane forest of Wondo Genet, south central Ethiopia. J For Res 24:419–430. https://doi.org/10.1007/s11676-013-0374-5

Kershaw JA, Ducey MJ, Beers TW, Husch B (2017) Forest mensuration, Fifth edition. John Wiley & Sons; UK, Chichester; NJ, Hoboken

Kelly JF, Beltz RC (1987) A comparison of tree volume estimation models for forest inventory. Research paper SO-233, USDA Forest serve, Southern forest experiment station. New Orleans, Louisiana. https://doi.org/10.2737/SO-RP-233

Larjavaara M, Muller-Landau HC (2013) Measuring tree height: quantitative comparison of two common field methods in a moist tropical forest. Method Ecol Evol 4:793-801. https://doi.org/10.1111/2041-210X.12071

Lemenih M, Allan C, Biot Y (2015) Making forest conservation benefit local communities: Participatory forest management in Ethiopia. Farm Africa. https://www.farmafrica.org/downloads/resources/pfmfinalweb.pdf. Accessed August 2019

Lemenih M, Kassa H (2014) Re-greening Ethiopia: history, challenges and lessons. Forests 5:1896–1909. https://doi.org/10.3390/f5081896

Lindner M, Karjalainen T (2007) Carbon inventory methods and carbon mitigation potentials of forests in Europe: a short review of recent progress. Eur J For Res 126:149–156. https://doi.org/10.1007/s10342-006-0161-3

Masota AM, Zahabu E, Malimbwi RE, Bollandsås OM, Eid TH (2014) Volume models for single trees in tropical rainforests in Tanzania. J Energy Nat Resour 3:66–76. http://doi: 10.11648/j.jenr.20140305.12

Mauya EW, Mugasha WA, Zahabu E, Bollandsås OM, Eid T (2014) Models for estimation of tree volume in the miombo woodlands of Tanzania. South For J For Sci 76:209–219. https://doi.org/10.2989/20702620.2014.957594

MEFCC (2018) National Forest Sector Development Program, Ethiopia. Volume I: Situation Analysis. Ministry of Environment Forest and Climate Change. https://www.et.undp.org/content/ethiopia/en/home/library/ten-year-national-forest-sector-development-programme.html. Accessed August 2019

Melemez K (2012) An environmental assessment of forest stands damages caused by excavators during road construction in Beech forests. Int J Environ Sci Technol 10:645-650. https://doi.org/10.1007/s13762-012-0125-8

Missanjo E, Matsumura J (2016) Wood density and mechanical properties of *Pinus kesiya* Royle ex Gordon in Malawi. Forests 7:7–35. https://doi.org/10.3390/f7070135

Mittermeier RA, Robles Gil P, Hoffman M, Pilgrim J, Brooks T (2004) Hotspots revisited: Earth's biologically richest and most endangered terrestrial ecoregions. University of Chicago Press, Chicago

Mokria M, Gebrekirstos A, Aynekulu E, Bräuning A (2015) Tree dieback affects climate change mitigation potential of a dry afromontane forest in northern Ethiopia. For Ecol Manage 344:73-83. https://doi.org/10.1016/j.foreco.2015.02.008

Mokria M, Mekuria W, Gebrekiristos A, Aynekulu E, Belay B, Gashaw T, Brauning A (2018) Mixed species allometric equations and estimation of aboveground biomass and carbon stocks in restoring degraded landscape in northern Ethiopia. Environ Res Lett 13(2). https://doi.org/10.1088/1748-9326/aaa495

Mugasha WA, Bollandsås OM, Eid T (2013) Relationships between diameter and height of trees in natural tropical forest in Tanzania. South For J For Sci 75(4):221-237. http://dx.doi.org/10.2989/20702620.2013.824672

Mugasha WA, Mauya EW, Njana AM, Karlsson K, Malimbwi RE, Ernest S (2019) Height-diameter allometry for tree species in Tanzania mainland. Int J For Res. https://doi.org/10.1155/2019/4832849

Mugasha WA, Mwakalukwa EE, Luoga E, Malimbwi RE, Zahabu E, Silayo DS, Sola G (2016) Allometric models for estimating tree volume and aboveground biomass in lowland forests of Tanzania. Int J For Res 2016:1–13. https://doi.org/10.1155/2016/8076271

Muhairwe CK (1999) Taper equation for *Eucalyptus pilularis* and *Eualyptus grandis* for the north coast in New South Wales, Australia. For Ecol Manage 113:251–269. https://doi.org/10.1016/S0378-1127(98)00431-9

Muller-Landau HC (2004) Interspecific and inter-site variation in wood specific gravity of tropical trees. Biotropica 36:20–32. https://doi.org/10.1111/j.1744-7429.2004.tb00292.x

Njana MA, Meilby H, Eid T, Zahabu E, Malimbwi RG (2016) Importance of tree basic density in biomass estimation and associated uncertainties: a case of three mangrove species in Tanzania. Ann For Sci 73:1073–1087. https://doi.org/10.1007/s13595-016-0583-0

Okai R, Frimpong-Mensah K, Yeboah D (2003) Characterization of moisture content and specific gravity of branch wood and stem wood of *Aningeria robusta* and *Terminalia ivorensis.* Holz Roh-Werkst 61:155–158. https://doi.org/10.1007/s00107-002-0360-7

Özçelik R, Brooks JR, Diamantopoulou MJ, Wiant HV (2010) Estimating breast height diameter and volume from stump diameter for three economically important species in Turkey. Scand J For Res 25:32–45. https://doi.org/10.1080/02827580903280053

Penman J, Gytarsky M, Hiraishi T, Krug T, Kruger D, Pipatti R, Buendia L, Miwa K, Ngara T, Tanabe K, Wagner F (2003) IPCC Good Practice Guidance for land use, land-use change and forestry. http://www.ipcc-nggip.iges.or.jp. Accessed August 2019

Pohjonen VM (1991) Volume equations and volume tables of *Juniperus procera* Hocht. ex. Endl. J For Ecol Manage 44:185–200. https://doi.org/10.1016/0378-1127(91)90007-I

Picard N, Saint-André L, Henry M (2012) Manual for building tree volume and biomass allometric equations: from field measurement to prediction. Food and Agriculture Organization of the United Nations, Rome; Centre de Coopération Internationale en Recherche Agronomique pour le Développement, Montpellier

R Core Team (2019) R: A language and environment for statistical computing. R Foundation for Statistical Computing, Vienna, Austria. https://www.R-project.org/

Schumacher FX, Hall FS (1933) Logarithmic expression of timber-tree volume. J Agric Res 47:719-734. https://naldc.nal.usda.gov/download/IND43968352/PDF

Sisay K, Thurnher C, Belay B, Lindner G, Hasenauer H (2017) Volume and carbon estimates for the forest area of the Amhara region in the north-western Ethiopia. Forests 8(4):122. https://doi.org/10.3390/f8040122

Swenson NG, Enquist BJ (2008) The relationship between stem and branch wood specific gravity and the ability of each measure to predict leaf area. Am J Bot 95:516–519. http://doi.org/10.3732/ajb.95.4.516

Tenzin J, Wangchuk T, Hasenauer H (2016) Form factor functions for nine commercial trees in Bhutan. Forestry 90:359–366. https://doi.org/10.1093/forestry/cpw044

Tesfaye MA, Bravo-Oviedo A, Bravo F, Pando V, de Aza CH (2019) Variation in carbon concentration and wood density for five most commonly grown native tree species in central highlands of Ethiopia: The

case of Chilimo dry Afromontane forest. J Sustainable For.
https://doi.org/10.1080/10549811.2019.1607754

Teshome T (2005) Analysis of individual tree volume equations for *Cupressus lusitanica* in Munessa forest, Ethiopia, S Afr For J 203:27–32. https://doi.org/10.2989/10295920509505215

Ubuy MH, Eid T, Bollandsås OM (2018a) Variation in wood basic density within and between tree species and site conditions of exclosures in Tigray, northern Ethiopia. Trees 32:967–983. https://doi.org/10.1007/s00468-018-1689-9

Ubuy MH, Eid T, Bollandsås OM, Birhane E (2018b) Aboveground biomass models for trees and shrubs of exclosures in the drylands of Tigray, northern Ethiopia. J Arid Environ 156:9–18. https://doi.org/10.1016/j.jaridenv.2018.05.007

UN-REDD (2017) Ethiopia's Forest Reference Level Submission to the UNFCCC. https://redd.unfccc.int/files/ethiopia_frel_3.2_final_modified_submission.pdf. Accessed August 2019

Vanclay JK (1994) Modelling forest growth and yield, Application to mixed tropical forests. CAB International, UK, Wallingford

van Laar A, Akça A (2007) Forest mensuration. Springer, The Netherlands, Dordrecht

Vieilledent G, Fischer FJ, Chave J, Guibal D, Langbour P, Gérard J (2018) New formula and conversion factor to compute basic wood density of tree species using a global wood technology database. Am J Bot. https://doi.org/10.1002/ajb2.1175

Weiskittel AR, Hann DW, Kershaw JA, Vanclay JK (2011) Forest growth and yield modelling. John Wiley and Sons, UK, The Atrium, Southern Gate, Chichester, West Sussex

West PW (2009) Tree and Forest Measurement, 2nd Edition. Springer-Verlag, Berlin Heidelberg

Williamson GB, Wiemann MC (2010) Measuring wood specific gravity correctly. Am J Bot 97(3):519–524. https://doi.org/10.3732/ajb.0900243

Wondrade N, Dick ØB, Tveite H (2015) Estimating above ground biomass and carbon stock in the Lake Hawassa Watershed, Ethiopia by integrating remote sensing and allometric equations. Forest Res 4:151. doi:10.4172/2168-9776.1000151

Zanne AE, Lopez-Gonzalez G, Coomes DA, Ilic J, Jansen S, Lewis SL, Miller RB, Swenson NG, Wiemann MC, Chave J (2009) Data from: towards a worldwide wood economics spectrum. Dryad Digital Repository. https://doi.org/10.5061/dryad.234

Zeibig-Kichas NE, Ardis CW, John-Pascal Berrill JP, King JP (2016) Bark thickness equations for mixed-conifer forest type in Klamath and Sierra Nevada mountains of California. Int J For Res. http://dx.doi.org/10.1155/2016/1864039

Zeng WS, Tang SZ (2011) Bias correction in logarithmic regression and comparison with weighted regression for nonlinear models. Nat Precedings. https://doi.org/10.1038/npre.2011.6708.1

Paper III

379

FOREST
ECOLOGY AND
MANAGEMENT
SCIENCE TO SUSTAIN THE WORLD'S FORESTS

Aboveground tree biomass prediction options for the Dry Afromontane forests in south-central Ethiopia

Check for updates

Zerihun Asrat[a,b,*], Tron Eid[a], Terje Gobakken[a], Mesele Negash[b]

[a] *Norwegian University of Life Sciences, Faculty of Environmental Sciences and Natural Resource Management, P.O. Box 5003, 1432 Ås, Norway*
[b] *Wondo Genet College of Forestry and Natural Resources, P.O. Box 128, Shashemene, Ethiopia*

ABSTRACT

Biomass of trees may be predicted either directly applying allometric models or indirectly from volume and biomass expansion factors (BEFs). For the Dry Afromontane forests, the second largest biomass pool in Ethiopia, such methods are not devised and properly documented. The main objective of this study was to explore different aboveground tree biomass prediction options based on destructively sampled tree biomass data. We explored the direct method by means of 1) new mixed-species general biomass models developed in the present study, and 2) some previously developed models including the pan-tropical models, and the indirect method by means of 3) volume and BEFs. From two sites in south-central Ethiopia, based on information from systematic sample plot inventories, 63 trees from 30 different species that contributed about 87% to the total forest basal area, were destructively sampled. Weighted nonlinear regression was applied to fit new models and their performance was assessed using root mean squared error (RMSE, %), mean prediction error (MPE, %) and pseudo-R^2 based on leave-one-out-cross-validation. Previously developed models and the indirect method were also evaluated by means of RMSE and MPE. The new general total biomass models performed well with pseudo-R^2 ranging between 0.87 and 0.96 and are presented along with covariance matrices for the parameter estimates enabling error propagation in biomass estimation. Most previously developed models resulted in significant MPEs up to 78%, while the best pan-tropical model performed much better with an MPE of about 7%. The indirect method also showed poor performance with MPEs ranging between 5% and 30%. Generally, the new models are accurate and flexible, thus, preferred over all previously developed models and the indirect method for application. However, their application to Dry Afromontane forests outside the study sites should be made only after thoroughly evaluating growing conditions and species composition. The results are step forward to enhance decisions made towards sustainable forest management including the REDD + implementation for Dry Afromontane forests in Ethiopia.

1. Introduction

Forests are biologically rich and diverse ecosystems and cover about one third (30.6%) of the global land area (FAO, 2016). Forests are sources of livelihoods to millions of people and contribute to economic development in many countries. In addition, by being sources and sinks of carbon, forests influence the magnitude and rate of climate change (Brown, 2002; Agrawal et al., 2011; Köhl et al., 2015). Tropical forests are particularly important as they store 55% of the carbon accumulated in the global forest ecosystems, out of which 56% is found in the live tree biomass (Pan et al., 2011). Despite their ecological and socio-economic significance, tropical forests have been under severe challenges due to deforestation and forest degradation (e.g. Gibbs et al.,

2010; FAO, 2016).

Forests in Ethiopia have also experienced deforestation and forest degradation over the last century (McCann, 1997). The major natural forest types in Ethiopia include Dry Afromontane forests, which is the focus of the present study, Moist Afromontane forests, *Acacia-Commiphora* forests and *Combretum-Terminalia* forests (UN-REDD, 2017). The Dry Afromontane forests of sub-Saharan Africa have been deforested and degraded heavily over many years due to an increasing population accompanied by high demands of wood for fuel and farmland for food production (Chidumayo and Marunda, 2010). The Dry Afromontane forests of Ethiopia, which also are heavily degraded (MEFCC, 2018a), are distributed over north-central, central and south-central parts of the country, mostly between altitudinal ranges from 1500 to 3400 m a.s.l.

They are the second largest harbour of aboveground biomass in the country (UN-REDD, 2017), and most diverse next to *Acacia-Commiphora* forests, with *Juniperus procera, Afrocarpus falcatus, Olea europaea, Croton macrostachyus* and *Ficus* species dominating in the upper canopy and *Allophylus abyssinicus, Apodytes dimidiala, Bersama abyssinica, Cassipourea malosana, Celtis africana, Chionanthus mildbraedii* and *Dombeya torrida* dominating in the middle and lower canopies (Friis et al., 2010).

Management and utilization of natural forests in Ethiopia in general, and of Dry Afromontane forests in particular, have been given little attention in the past, except for mere protection measures. Recently, however, the issue of sustainable forest utilization has been raised (Lemenih et al., 2015; MEFCC, 2018a). Various approaches such as participatory forest management, establishment of biosphere reserves and exclosures, as well as carbon financed projects such as clean development mechanisms and reducing emissions from deforestation and forest degradation (REDD +) mechanism have been implemented for enhancing sustainable management of natural forests in the country (Winberg, 2011; Lemenih and Kassa, 2014; NABU, 2017; UN-REDD, 2017).

In line with climate change and subsequent efforts to mitigate that, accurate biomass estimation methods have become a concern of the global community (e.g. Brown, 2002; IPCC, 2006; Temesgen et al., 2015). Aboveground tree biomass, i.e. the dry weight of the whole aboveground part of a tree or its sections (stem, branch, and foliage), and then of that of a forest per unit area, are information often used in forestry as an input for forest management decisions (e.g. Burkhart and Tomé, 2012). Information on biomass can be used to understand how tree growth occur by producing biomass through photosynthesis, to quantify products such as wood for fuel or pulp and to determine how much carbon is sequestered in forests as a result of trees taking carbon dioxide from the atmosphere (Köhl et al., 2006; West, 2015). Information for section biomass, such as branch and foliage, are also important to assess the potential availability for extraction of fuelwood and fodder products (Brown, 1997; Balehegn et al., 2012; Burkhart and Tomé, 2012).

The biomass of a tree may be directly predicted by applying allometric models based on easily measured tree variables or indirectly using a biomass expansion factor (BEF) to convert tree volume into tree biomass (Brown, 1997). Allometric biomass prediction models are usually developed by regressing tree variables such as diameter at breast height (dbh), total tree height (ht) and other tree variables with observed tree biomass based on destructive sampling (e.g. Brown, 1997; Chave et al., 2005, 2014; Bollandsås et al., 2016). Such models can be developed for a single species or a mixture of species as well as for one site and multiple sites. Species-specific biomass models are preferred for their accurate prediction for that given species, but they are constrained by the narrow range of application due to the large number of species in tropical forests (Penman et al., 2003; Gibbs et al., 2007; Picard et al., 2012). Many mixed-species biomass models have therefore been developed for tropical forests, among these are the pan-tropical models by Brown (1997) and Chave et al. (2005, 2014), which are based on comprehensive datasets collected throughout the tropical region. Since the pan-tropical models developed by Chave et al. (2005, 2014) offer the opportunity of application over large areas and different forest types, there are many examples where they have been tested on local data from destructive sampling in sub-Saharan African (viz. Afrotropics) natural forests. A number of such tests, for example in miombo woodlands (Mugasha et al., 2013), dry forests (Vieilledent et al., 2012; Tetemke et al., 2019) and moist forests (Vieilledent et al., 2012; Fayolle et al., 2013, 2018), have shown that the models are almost as good as the local ones, but there are also several cases where large prediction errors have been detected, for example Mugasha et al. (2013) and Kachamba et al. (2016) in miombo woodlands, Tesfaye et al. (2016) and Ubuy et al. (2018) in dry forests, and Ngomanda et al. (2014) and Lisboa et al. (2018) in moist forests.

The Intergovernmental Panel on Climate Change (IPCC) requires

uncertainties to be identified, documented and reported along with biomass and carbon stock estimates when reporting under the REDD + mechanism (IPCC, 2014). Uncertainties in biomass estimation can among others arise due to measurements of individual tree properties (e.g. dbh and ht), sample plot design (e.g. number, size and distribution of plots), applied remote sensing platform and methods, and biomass model application (e.g. Chave et al., 2004; Clark and Kellner, 2012; Mavouroulou et al., 2014; Næsset et al., 2016). The uncertainty related to biomass model application in this context could be due to model misspecifications, residual variability and uncertainty in the model parameter estimates (e.g. McRoberts and Westfall, 2013; Mavouroulou et al., 2014; Magnussen and Negrete, 2015). The uncertainty in the model parameter estimates, which can be documented by means of the covariance structure of the parameter estimates of the developed models, has large influence on the uncertainty, but are seldom reported (Breidenbach et al., 2014; Magnussen and Negrete, 2015). A necessary step forward to be able to propagate the totality of the uncertainty in biomass estimation is therefore to document this when developing new models. To our knowledge, the biomass models developed by Kachamba et al. (2016) are the only ones from east-Africa where this has been done.

In the indirect biomass prediction method, wood basic density (wbd) and BEF are used to convert volume into biomass. The biomass expansion factor, which is unitless, is usually determined as the ratio of biomass for the whole tree (kg) to stem volume (m^3) multiplied with the wbd (kg m^{-3}) of the stem (Brown, 1997; IPCC, 2006; Hewson et al., 2014). Both total stem volume (Nogueira et al., 2008; Petersson et al., 2012; Magalhães and Seifert, 2015a) and merchantable stem volume (Brown, 2002; Magalhães and Seifert, 2015a, 2015b; Njana, 2017; Lisboa et al., 2018) have been used to calibrate BEFs. Since the application of the indirect biomass prediction method relies on BEFs not directly measured in ordinary forest inventories, the uncertainties in biomass estimation for this method, as compared to the direct method using allometric biomass models, have been the concern of several authors (Petersson et al., 2012; Magalhães and Seifert, 2015a, 2015b; Njana, 2017).

A review by Henry et al. (2011) on biomass models in sub-Saharan Africa showed that most of the available models in Ethiopia are limited to a few *Eucalyptus* species in plantations, while about 98% of the species were uncovered. Recently some species-specific models for natural forests have been developed (e.g. Tesfaye et al., 2016; Kebede and Soromessa, 2018; Daba and Soromessa, 2019). A few mixed-species general biomass models also exist in some parts of the country and forest conditions (Eshete and Ståhl, 1998; Mokria et al., 2018; Ubuy et al., 2018). There are no mixed-species models for the Dry Afromontane forests in general, except the very recently published models by Tetemke et al. (2019) in northern Ethiopia. As a result, pan-tropical models (Brown, 1997; Chave et al., 2005, 2014) have been commonly used (e.g. MEFCC, 2018b; Gebeyehu et al., 2019). It is also worth mentioning that the implementation of the REDD + programme in Ethiopia is in progress and that the country has submitted its first forest reference level report to the United Nations Framework Convention on Climate Change (UN-REDD, 2017). This report recommends the pan-tropical biomass model developed by Chave et al. (2014) to be applied across all forest types due to lack of existing biomass models in the country.

The main objective of this study was therefore to explore different aboveground tree biomass prediction options for Dry Afromontane forests in south-central Ethiopia. The options considered were; using the direct method by means of 1) new mixed-species general biomass models developed in the present study, and 2) some previously developed models including the pan-tropical models, and using the indirect method by means of 3) volume and expansion factors. The performance of the all three options were evaluated using root mean squared error and mean prediction error derived from destructively sampled tree biomass data. New mixed-species general tree section biomass models
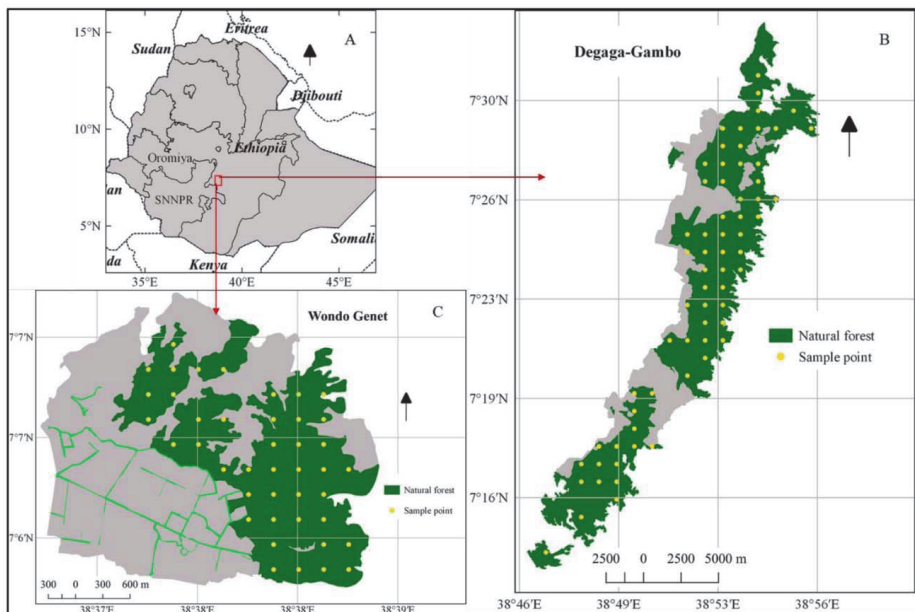
Fig. 1. Map of the study sites; (A) location of the study sites in Ethiopia; (B) Deggaga-Gambo site; and (C) Wondo Genet site. In both sites, areas outside the natural forests (grey) are mosaics of plantations, cropland, grassland and settlement land cover types.

were also developed. The developed general aboveground biomass models were accompanied by information on the covariance structure of the parameter estimates.

2. Materials and methods

2.1. Study sites

Degaga-Gambo and Wondo Genet forest sites were chosen to represent the Dry Afromontane forests in south-central Ethiopia (Fig. 1). These forests are remnants from extensive montane forests in the highlands of north-central, central and south-central parts of the country (Friis et al., 2010). The standing scattered big trees on the surrounding farmlands indicate the severity of the deforestation happened in the past. There is still a continued pressure on the forests manifested in different ways; clearing trees for farmland; illegal logging for lumber processing and extraction of wood for fuel. Forest fire is also a common phenomenon, particularly in Wondo Genet. Despite all the pressures, the forests serve as source of food, fodder and water supporting numerous people in the surrounding and downstream areas. Both sites have a bimodal rainfall with the short rainy season between March and May and the main rainy season between July and September.

Degaga-Gambo is located in the Oromia regional state about 240 km south of Addis Ababa and belongs to the state-owned Oromia Forest and Wildlife Enterprise. The forest area considered for this study extends longitudinally from 38°45′ to 38°56′ E and latitudinally from 7°13′ to 7°33′ N, with an area of about 12580 ha. As it is located along the eastern escarpment of the main Ethiopian Rift Valley the elevation ranges from about 2100 to 2700 m.a.s.l. Based on climate data registered at a station inside the forest in the period 2001 to 2011, the mean annual rainfall and temperature were 1245 mm and 14.9 °C, respectively. The soils are generally classified as Mollic Nitisols and Humic Umbrisols, respectively, at lower (2300 m) and upper (2600 m) parts of the forest (Fritzsche et al., 2007).

Wondo Genet is located about 270 km south of Addis Ababa, and extends longitudinally from 38°37′ to 38°39′ E and latitudinally from 7°6′ to 7°7′ N. The forest covers an area of about 390 ha with an altitudinal range from about 1850 to 2400 m.a.s.l. The mean annual rainfall and temperature are 1123 mm and 17.6 °C, respectively. The soils are mainly classified as Mollic Andosols (Erikson and Stern, 1987). The forest is managed by Wondo Genet College of Forestry and Natural Resources.

2.2. Data collection

2.2.1. Systematic sample plot inventories

Tree allometry varies with location, tree species and size. Thus, trees to be selected for destructive sampling and biomass modelling should reflect such variations in order to minimize extrapolations in model application. For appropriate selection of trees, a ground-based forest inventory representative for the target population therefore needs to be conducted (e.g. Jara et al., 2014; Bollandsås et al., 2016). Systematic sample plot inventories were done for both sites with 65 circular plots of 1000 m^2 at Degaga-Gambo and 42 circular plots of 400 m^2 at Wondo Genet. Following tree species identification, all trees on the plots with dbh ≥ 5 cm were measured for dbh. Species were identified with the help of local guides and identification keys (Tesemma, 2007). A total of 71 species were identified with 45 and 50 species in Degaga-Gambo and Wondo Genet, respectively. The most frequently occurring species were *Afrocarpus falcatus* and *Celtis africana*. *Afrocarpus falcatus* trees were the largest measured in both sites with dbh of 270 cm in Degaga-Gambo and 197 cm in Wondo Genet. The mean basal areas for all sample plots in Degaga-Gambo and Wondo Genet, respectively, were 14 and 17 m^2 ha^{-1} while number of stems were 129 and 416 ha^{-1}.

2.2.2. Selection of sample trees for destructive sampling

Based on information from the sample plot inventories we selected a total of 63 trees (32 in Degaga-Gambo and 31 in Wondo Genet)
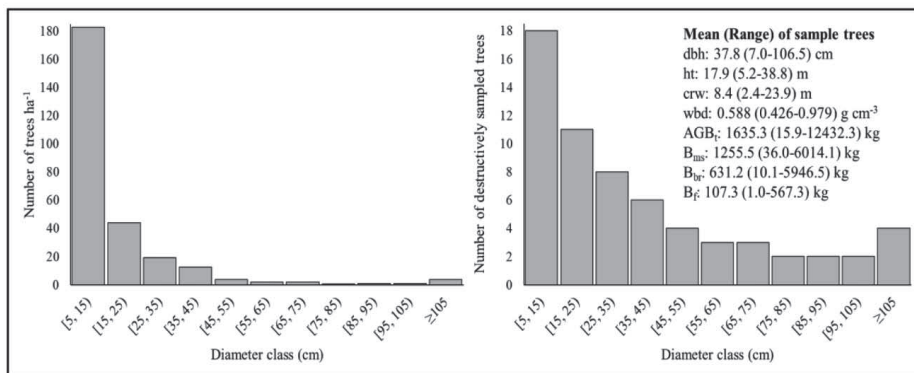
Fig. 2. Distribution of trees ha^{-1} from sample plot inventories (left) and number of destructively sampled trees (right) by diameter classes. Summary of the sample trees from both sites: dbh – diameter at breast height, ht – total height, crw – crown width, wbd – wood basic density; AGB$_t$, B$_{ms}$, B$_{br}$ and B$_f$ are total tree aboveground, merchantable stem, branch, and foliage biomass respectively. Sample size for merchantable stem was n = 45. The wbd values were obtained from Asrat et al. (2020).

representing 30 different species (11 unique from each site and eight common from both) (Fig. 2 and Table A1). For each site we first selected according to dominant tree species, and subsequently the rest was selected randomly among the remaining species. The dominant species accounted for 85% of the total basal area of the forests while in total 87% was covered. Furthermore, the selection of trees aimed at having a fair distribution across the diameter classes which also included a relatively high number of larger trees (Fig. 2) because in general a few individuals of the larger trees accumulate a relatively large part of the biomass in forests (Brown, 2002). Finally, when in field, we also aimed at selecting trees representing the population in terms of tree forms and spatial coverage.

Prior to felling the selected tree was verified for correct species name. Subsequently, diameter at stump height (dsh, 0.3 m above ground) and dbh were measured either with calliper or diameter tape (for irregular shape or bigger size stems) while ht was measured using Haglöf Vertex Laser 5. In addition, average crown width (crw) was determined by measuring maximum and minimum widths of the crown with measuring tape (Fig. 2 and Table A1).

2.2.3. Destructive sampling procedures

After measurements of the selected trees were completed, they were felled with a chainsaw at stump height (0.3 m above ground). The trees were divided into three sections: merchantable stem, branch and foliage. The merchantable stem section included the main trunk up to a minimum of 10 cm top diameter, a dimension beyond which local sawmills do not consider the wood for processing. The stems of all trees with dbh < 15 cm were included in the branch section because they are not considered as suitable for wood processing. The merchantable stem section also included the stump, i.e. the part of the stem from ground to 0.3 m above ground. The volume of the stump was determined from the mid-diameter and length of the stump part. Later the biomass of the stump was determined from volume and wbd (Brown, 1997; IPCC, 2006). The branch section comprised all branches with diameter ≥ 2 cm, stem tops with diameter < 10 cm and the stems of all trees with dbh < 15 cm. The foliage section included branches < 2 cm, and all twigs, flowers, fruits, seeds and leaves. For practical reasons the stem was crosscut into smaller logs and then fresh weight of each log was determined using a hanging balance scale (0–200 kg capacity). Similarly, branches were cut into shorter pieces and measured for fresh weights. The foliage was collected in bundles and weighed using a plastic sheet. Merchantable stem, branch and foliage fresh weights were obtained by summing up the fresh weights of all respective pieces.

2.2.4. Sub-samples for wood basic density and dry weight biomass

For determining wbd of the trees, separate wood sub-samples were collected from stem and branches. A detailed description of sub-sampling procedures and determination of wbd values are given by Asrat et al. (2020). For dry weight biomass determination of the trees, three wood sub-samples from the stem were collected, i.e. one at breast height, and one from middle and upper positions, respectively. Three sub-samples for each tree were also collected from the branches, i.e. one from a large, medium and small branch. However, for some smaller trees, which just had a few branches of similar size, only one branch sub-sample was taken. The sub-samples were mostly wood discs representing the whole cross-section, except for some large trees where a smaller representative (from pith to bark) wood sub-sample was taken. Small bundles of foliage samples were also taken from each sample tree. In total, 427 sub-samples (6.8 per tree) were collected. All the sub-samples were brought to laboratory with an airtight plastic bag where fresh weights first were determined using sensitive digital balance scale. The sub-samples were then dried in an oven to two to three days at a temperature of 103 °C. The sub-samples were monitored and weighed recurrently every 24 h to check if a constant mass was attained. Finally, the average dry to fresh weight biomass ratios were determined for the stem, branch and foliage sections. These ratios were used to convert the fresh weights of their respective sections into dry weights. For the merchantable stem section of each tree the dry weight of the stump, derived by multiplying the volume of the stump with the wbd of the tree (Asrat et al., 2020), was added. The total tree aboveground dry weight biomass (AGB$_t$) was aggregated from merchantable stem biomass (B$_{ms}$), branch biomass (B$_{br}$) and foliage biomass (B$_f$) (Fig. 2 and Fig. A1).

2.3. Model fitting and evaluation

All analyses were done with the R statistical software (R Core Team, 2019). The potential predictor variables considered to describe variations in biomass were dbh, ht, wbd and crw. The scatter plots of biomass versus dbh and ht indicated non-linear relationships (Fig. A1). To cope with non-linearity, power functions have been widely applied in biomass modelling (e.g. Chave et al., 2005, 2014; Picard et al., 2015; Mugasha et al., 2016; Mokria et al., 2018; Ubuy et al., 2018; Tetemke et al., 2019). In all these models, dbh and ht were used as predictor variables, either separately (Picard et al., 2015; Ubuy et al., 2018;

Tetemke et al., 2019) or by combining dbh and ht as dbh^2 × ht (Chave et al., 2005, 2014; Picard et al., 2015; Mugasha et al., 2016; Mokria et al., 2018). Using dbh^2 × ht as one entry in the regression is usually practiced to overcome problems of collinearity (Picard et al., 2015; Ductă et al., 2019). The reasoning behind using dbh^2 × ht is that aboveground biomass is proportional to the volume of a cylinder with a diameter dbh and length of ht. However, a limitation of this approach is that the dbh^2 × ht as predictor constrains the model to produce parameter estimates for dbh and ht that have a fixed ratio, in this case equal to 2.0. Picard et al. (2015) compared the approaches with separate and combined predictors and concluded that separate predictors performed better than combined. Similarly, when Ductă et al. (2019) compared the two approaches they concluded that the dbh^2 × ht predictor becomes less efficient in predicting biomass when the Q-ratio, i.e. the ratio of the parameter estimates for dbh and ht when used separately, deviates from 2.0. Therefore, they recommend the combined approach only when the Q-ratio is between 1.5 and 2.5. Since collinearity between dbh and ht was not a problem in our case (i.e. variance inflation factor was 5.0), and since previous models developed for natural forests in Ethiopia (Ubuy et al., 2018; Tetemke et al., 2019) produced Q-ratios outside the interval of 1.5–2.5, we decided to apply the separate predictor approach in our modelling. We formulated eight different model forms (Eqs. (1)–(8)) for testing the general biomass models, by using dbh as sole predictor and combined with a stepwise inclusion of ht, wbd and crw in the following way;

$$Y = a \times (dbh)^b \tag{1}$$

$$Y = a \times (dbh)^b \times (ht)^c \tag{2}$$

$$Y = a \times (dbh)^b \times (wbd)^c \tag{3}$$

$$Y = a \times (dbh)^b \times (crw)^c \tag{4}$$

$$Y = a \times (dbh)^b \times (ht)^c \times (wbd)^d \tag{5}$$

$$Y = a \times (dbh)^b \times (ht)^c \times (crw)^d \tag{6}$$

$$Y = a \times (dbh)^b \times (crw)^c \times (wbd)^d \tag{7}$$

$$Y = a \times (dbh)^b \times (ht)^c \times (crw)^d \times (wbd)^f \tag{8}$$

where Y is biomass (dry weight respectively of total aboveground, merchantable stem, branch and foliage biomass) in kg, dbh in cm, ht in m, wbd in g cm^{-3} and crw in m; and a, b, c, d and f are parameter estimates.

Weighted nonlinear least square regression was applied. The nls function in the R programme was used to fit models. Weighting by 1/(dbh)$^{2\delta}$ was used to account for heteroscedasticity in the residuals (Kelly and Beltz, 1987), where δ is a weighting factor determined by following the procedures of Picard et al. (2012). The models were assessed for their performance based on root mean squared error (RMSE, %), mean prediction error (MPE, %) and pseudo-R^2 all determined from leave-one-out cross-validation. In a leave-one-out cross-validation one observation (x$_1$, y$_1$) is used as validation data after a model is calibrated based on the rest of the data {(x$_2$, y$_2$), …., (x$_n$, y$_n$)} at a time. This procedure is repeated n (number of observations) times (James et al., 2013). The obtained n residuals (observed minus predicted) from leave-one-out-cross-validation were used to compute the model performance indicators;

$$RMSE = \sqrt{\frac{1}{n}\sum_{i=1}^{n}(Y_i - \widehat{Y_i})^2}; \quad RMSE\% = \frac{RMSE}{\bar{Y}} \times 100$$

$$MPE = \frac{1}{n}\sum_{i=1}^{n}(Y_i - \widehat{Y_i}); \quad MPE\% = \frac{MPE}{\bar{Y}} \times 100$$

$$Pseudo - R^2 = 1 - \frac{\sum_{i=1}^{n}(Y_i - \widehat{Y_i})^2}{\sum_{i=1}^{n}(Y_i - \bar{Y})^2}$$

where Y$_i$ is observed biomass of a tree, $\widehat{Y_i}$ is predicted biomass of a tree and $\bar{Y}$ is the mean observed biomass of all trees. Models with non-significant parameter estimates were ignored and the final judgements on the models were based on Akaike Information Criterion (AIC) along with RMSE, MPE and pseudo-R^2.

Some previously developed aboveground biomass models that have been or potentially could be applied for Dry Afromontane forests in Ethiopia (Table A2), were tested based on our dataset. First, some mixed-species models from Ethiopia were tested (Eshete and Ståhl, 1998; Mokria et al., 2018; Ubuy et al., 2018; Tetemke et al., 2019). We also tested two relevant models from tropical dry forests elsewhere in Africa (Djomo et al., 2016; Mugasha et al., 2016), and the pan-tropical models developed by Chave et al. (2005) for dry forest including ht, and Chave et al. (2014). The performance of the models was evaluated by means of RSME and MPE. Mean prediction errors were statistically tested by means of t-tests.

For testing the indirect biomass prediction method, we first determined BEF$_t$ and BEF$_{ms}$ for all the individual trees with dbh ≥ 15 cm (n = 45) based on total tree volume (i.e. stem and large branches) and merchantable stem volume, respectively;

$$BEF_t = \frac{AGB_{t\_obs}}{V_{t\_obs} \times wbd}; \quad BEF_{ms} = \frac{AGB_{t\_obs}}{V_{ms\_obs} \times wbd}$$

where AGB$_{t\_obs}$ are observed total aboveground biomass (kg), V$_{t\_obs}$ and V$_{ms\_obs}$ are observed total and merchantable stem volume (m^3) and wbd are wood basic density (kg m^{-3}). Details on the determination of observed total volume, merchantable stem volume and wbd for the trees are described by Asrat et al. (2020).

Secondly, we used these biomass expansion factors (BEF$_{t,ms}$), along with predicted volumes (V$_{t,ms\_pred}$) based on mixed-species total and merchantable stem volume models and wbd from Asrat et al. (2020), to mimic application of the indirect biomass prediction method for individual trees;

$$AGB_t = BEF_{t,ms} \times V_{t,ms\_pred} \times wbd$$

where AGB$_t$ are predicted total aboveground biomass. For each of two BEFs we applied two options, i.e. species-specific means (Table A1) and study sites means (BEF$_t$ = 1.10, BEF$_{ms}$ = 1.80). In addition, we applied species-specific wbd values (Table A1), study sites mean wbd value (0.588 g cm^{-3}) as well as national mean wbd value (0.612 g cm^{-3}) from the national wbd database (UN-REDD, 2017). Finally, the residuals (observed minus predicted biomass) were used to compute RMSE and MPE. Mean prediction errors were statistically tested by means of t-tests.

3. Results

Parameter estimates and performance indicators of the general total aboveground and section biomass models are displayed in Table 1. No models with MPE significantly different from zero were found. All models, where all the parameter estimates are different from zero, are regarded as viable options, except Model B$_{f3}$, which was ruled out due to the negative parameter estimate for wbd implying that biomass is decreasing with increasing wbd. For the general total aboveground biomass models, pseudo-R^2 ranged from 0.87 to 0.96, and Model AGB$_{t8}$, with dbh, ht, crw and wbd as predictor variables, best according to AIC. For the merchantable stem models, pseudo-R^2 varied from 0.88 to 0.96, and Model B$_{ms8}$, with dbh, ht, crw and wbd as predictor variables, was best in terms of AIC. The performance of the branch and foliage biomass models in general appeared to be relatively poorer compared to the total aboveground and merchantable stem biomass models. Using dbh as sole predictor explained 68% and 83% of the variations in branch and foliage biomass, respectively. Inclusion of ht in any form of combinations in the branch and foliage models resulted in non-significant parameter estimates. On the other hand, including crw as predictor variable improved the model performances.

Table 1
Model parameters and performance indicators for general total tree aboveground, merchantable stem, branch and foliage biomass models.

Section	Model	Pseudo-R^2	RMSE (kg)	RMSE (%)	MPE (kg)	MPE (%)	AIC
Total above-ground (n = 63)	$AGB_{t1} = 0.15895 \times (dbh)^{2.34670}$	0.87	995.5	60.9	0.1	0.0	1041.6
	$AGB_{t2} = 0.13648 \times (dbh)^{2.09997} \times (ht)^{0.35775NS}$	0.87	975.0	59.6	45.2	2.8	1043.6
	$AGB_{t3} = 0.26136 \times (dbh)^{2.40291} \times (wbd)^{1.15019}$	0.90	874.7	53.5	−0.0	−0.0	1020.3
	$AGB_{t4} = 0.21170 \times (dbh)^{1.69530} \times (crw)^{0.95050}$	0.93	741.8	45.4	0.0	0.0	1010.7
	$AGB_{t5} = 0.19250 \times (dbh)^{2.21060} \times (ht)^{0.35380} \times (wbd)^{1.21890}$	0.89	887.6	54.3	5.9	0.4	1019.8
	$AGB_{t6} = 0.17587 \times (dbh)^{1.51600} \times (ht)^{0.27451} \times (crw)^{0.96145}$	0.92	757.0	46.3	23.9	1.5	1010.9
	$AGB_{t7} = 0.29628 \times (dbh)^{1.89139} \times (crw)^{0.78636} \times (wbd)^{1.14705}$	0.96	528.1	32.3	0.1	0.0	946.5
	$\mathbf{AGB_{t8} = 0.21765 \times (dbh)^{1.77660} \times (ht)^{0.33242} \times (crw)^{0.65575} \times (wbd)^{1.07739}}$	**0.96**	**531.6**	**32.5**	**0.1**	**0.0**	**943.6**
Merchant-able stem (n = 45)	$B_{ms1} = 0.12106 \times (dbh)^{2.27313}$	0.89	534.3	42.6	−0.7	−0.1	688.7
	$B_{ms2} = 0.04031 \times (dbh)^{1.82014} \times (ht)^{0.91345}$	0.88	553.3	44.1	0.0	0.0	690.7
	$B_{ms3} = 0.18572 \times (dbh)^{2.35380} \times (wbd)^{1.20824}$	0.95	369.0	29.4	−4.4	−0.4	651.3
	$B_{ms4} = 0.14609 \times (dbh)^{1.84083} \times (crw)^{0.63428}$	0.90	502.7	40.0	−0.2	−0.0	683.9
	$B_{ms5} = 0.10785 \times (dbh)^{2.07564} \times (ht)^{0.53631} \times (wbd)^{1.27653}$	0.95	361.3	28.8	0.1	0.0	646.6
	$B_{ms6} = 0.05873 \times (dbh)^{1.60756} \times (ht)^{0.74407} \times (crw)^{0.41969}$	0.89	534.8	42.6	−0.1	−0.0	685.7
	$B_{ms7} = 0.20867 \times (dbh)^{1.97553} \times (crw)^{0.52935} \times (wbd)^{1.01514}$	0.96	317.9	25.3	−0.4	−0.0	624.6
	$\mathbf{B_{ms8} = 0.10447 \times (dbh)^{1.74198} \times (ht)^{0.60139} \times (crw)^{0.42886} \times (wbd)^{1.07777}}$	**0.96**	**312.9**	**24.9**	**0.0**	**0.0**	**615.9**
Branch (n = 63)	$B_{br1} = 0.06505 \times (dbh)^{2.33062}$	0.68	680.9	107.9	8.2	1.3	991.9
	$B_{br2} = 0.11906 \times (dbh)^{2.43578} \times (ht)^{-0.32368NS}$	0.67	689.1	109.2	24.2	3.8	993.9
	$B_{br3} = 0.11022 \times (dbh)^{2.43841} \times (wbd)^{1.54887}$	0.63	722.4	114.5	3.2	0.5	985.6
	$B_{br4} = 0.06888 \times (dbh)^{1.44535} \times (crw)^{1.41522}$	0.80	531.0	84.1	3.6	0.6	956.0
	$B_{br5} = 0.16117 \times (dbh)^{2.43394} \times (ht)^{-0.10224NS} \times (wbd)^{1.60134}$	0.65	708.0	112.2	15.3	2.4	986.7
	$B_{br6} = 0.14685 \times (dbh)^{1.62725} \times (ht)^{-0.52177NS} \times (crw)^{1.48618}$	0.80	538.3	85.3	11.3	1.8	955.9
	$\mathbf{B_{br7} = 0.10787 \times (dbh)^{1.60737} \times (crw)^{1.41226} \times (wbd)^{1.79041}}$	**0.82**	**511.0**	**81.0**	**5.7**	**0.9**	**932.1**
	$B_{br8} = 0.14173 \times (dbh)^{1.61959} \times (ht)^{-0.09043NS} \times (crw)^{1.38634} \times (wbd)^{1.71448}$	0.82	512.2	81.2	7.2	1.1	932.7
Foliage (n = 63)	$B_{f1} = 0.12031 \times (dbh)^{1.77544}$	0.83	62.1	57.9	0.0	0.0	696.6
	$B_{f2} = 0.16246 \times (dbh)^{1.94930} \times (ht)^{-0.31582NS}$	0.83	62.6	58.4	0.1	0.1	697.8
	$Bf3 = 0.07122 \times (dbh)^{1.78590} \times (wbd)^{-0.72460}$	0.84	60.7	56.5	1.4	1.3	685.0
	$B_{f4} = 0.18503 \times (dbh)^{1.31755} \times (crw)^{0.57839}$	0.82	64.9	60.5	0.3	0.3	697.0
	$B_{f5} = 0.31330 \times (dbh)^{1.81360} \times (ht)^{-0.19370NS} \times (wbd)^{0.81590}$	0.73	78.2	72.8	5.2	4.8	682.6
	$B_{f6} = 0.24750 \times (dbh)^{1.53610} \times (ht)^{-0.37940NS} \times (crw)^{0.59060}$	0.82	64.7	60.3	−0.0	−0.0	697.8
	$\mathbf{B_{f7} = 0.30861 \times (dbh)^{1.20644} \times (crw)^{0.74019} \times (wbd)^{0.76903}}$	**0.74**	**76.6**	**71.4**	**4.2**	**3.9**	**686.1**
	$B_{f8} = 0.39100 \times (dbh)^{1.32770} \times (ht)^{-0.29480NS} \times (crw)^{0.81790} \times (wbd)^{0.74840}$	0.74	77.1	71.8	4.2	3.9	682.6

[NS], not significant ($p > 0.05$), viable models with lowest AIC highlighted in bold.

Models B_{br7} and B_{f7} for branch and foliage biomass, respectively, were best in terms of lowest AIC. Covariance matrices for all the viable total aboveground biomass models in Table 1 are presented in Table A3.

Fig. 3 displays observed biomass over predicted biomass for the best performing general models, i.e. total aboveground (AGB_{t8}), merchantable stem (B_{ms8}), branch (B_{br7}) and foliage (B_{f7}) biomass models, respectively.

All the general total aboveground biomass models with significant parameter estimates were applied separately over the two sites and evaluated by means of RMSE and MPE (Table 2). Except for model AGB_{t1} in Degaga-Gambo, the models produced MPEs not significantly different from zero ($p > 0.05$).

The previously developed models were also applied to our dataset and evaluated by means of RMSE and MPE (Table 3). In general, all tested models, except the pan-tropical models developed by Chave et al. (2005, 2014), yielded large MPEs significantly different from zero ($p < 0.01$). Fig. 4 displays graphically some of the previously developed models and Model AGB_{t5} from the current study.

The results of the indirect biomass prediction method, using BEFs based on total volume and merchantable stem volume, respectively are shown in Table 4. In general, predicted biomass were larger than observed biomass in all cases. MPEs not significantly different from zero ($p > 0.05$) were obtained only when species-specific wbd values were applied along with either species-specific or study sites mean BEF values. As expected, the MPEs increased as the BEF and wbd values changed from species-specific to study site mean values, and to the national mean values in the case of wbd.

4. Discussion

Quantification and related uncertainties of tree biomass prediction and biomass estimation per unit area for forests have been a main concern among researchers globally, and various approaches to this have been devised and applied under different conditions in different places. In the present study, conducted in Dry Afromontane forests in south-central Ethiopia, we considered options, challenges and uncertainties related to direct tree biomass prediction methods using both new and previously developed models, and to indirect methods using different tree volumes and BEFs. The study was based on a comprehensive dataset from destructive sampling. Destructive sampling is demanding in terms of time consumption, required equipment and financial resources (e.g. Eid et al., 2016). In our case, with a crew comprising a researcher, two assistants with forestry background, one chainsaw operator and four to seven labourers, we spent from about one hour per tree to complete measurements in the field for the smallest ones and up to five days for the largest. The data were collected from two sites with a relatively wide range of altitudinal variations and associated soils, rainfall and temperature variability. Prior to the destructive sampling, systematic sample plot inventories were conducted for each site to secure representativity for the target populations. Sixty-three trees were selected, among these 30 different tree species covering about 87% of the total basal area of the study sites were presented. We also emphasised to include wide diameter ranges and a relatively high number of large trees, as this will reduce extrapolations in model application (Bollandsås et al., 2016). No previous studies in Ethiopia have considered trees with such large diameters in tree biomass prediction models, despite the fact that these trees store large parts of the total biomass and carbon stock in tropical forests (Brown,
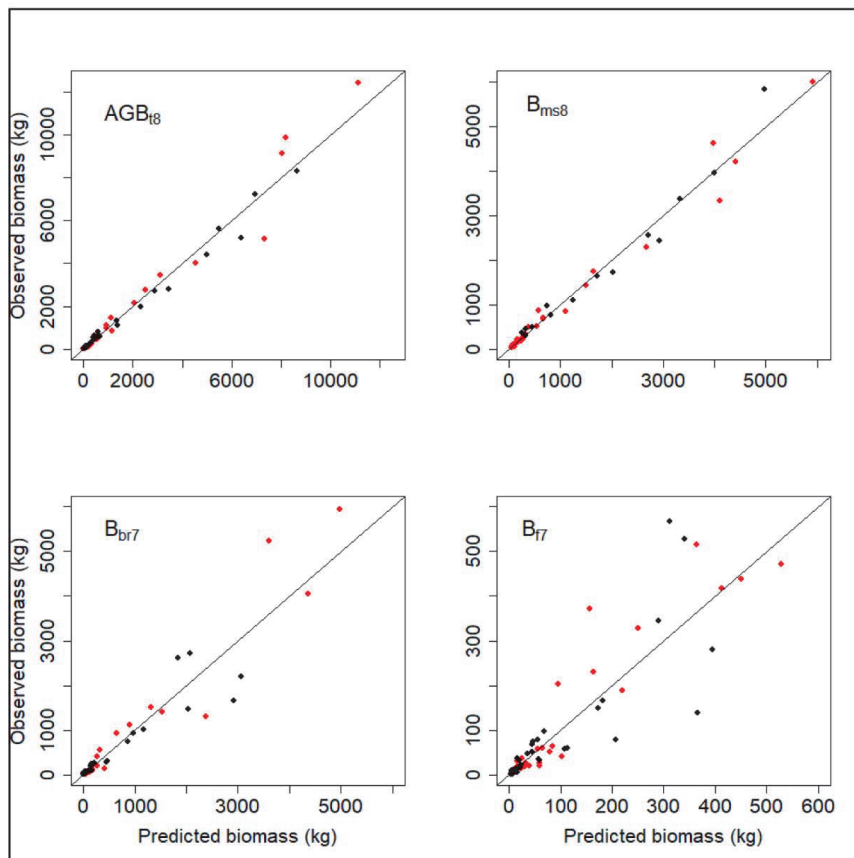
Fig. 3. Observed biomass over predicted biomass for the best performing general total aboveground (AGB$_{t8}$), merchantable stem (B$_{ms8}$), branch (B$_{br7}$) and foliage (B$_{f7}$) biomass models. The black and red colours represent sample trees from Degaga-Gambo and Wondo Genet sites, respectively. (For interpretation of the references to colour in this figure legend, the reader is referred to the web version of this article.)

Table 2
Evaluation results of the general total tree aboveground biomass models over the study sites.

Site	Model	Predicted AGB$_t$ (kg)	RMSE		MPE	
			(kg)	(%)	(kg)	(%)
Degaga-Gambo[1]	AGB$_{t1}$	1603.0	434.7	30.3	−165.5	−11.8*
(n = 32)	AGB$_{t3}$	1571.8	496.1	34.6	−137.4	−9.6
	AGB$_{t4}$	1515.1	528.7	36.9	−80.7	−5.6
	AGB$_{t5}$	1569.5	483.4	33.7	−135.0	−9.4
	AGB$_{t6}$	1491.5	523.7	36.5	−57.1	−4.0
	AGB$_{t7}$	1499.1	333.8	23.3	−64.7	−4.5
	AGB$_{t8}$	1515.1	290.5	20.3	−80.7	−5.6
Wondo Genet[1]	AGB$_{t1}$	1665.8	1203.4	65.3	176.8	9.6
(n = 31)	AGB$_{t3}$	1694.8	937.2	50.9	147.8	8.0
	AGB$_{t4}$	1761.2	826.8	44.9	81.4	4.4
	AGB$_{t5}$	1695.4	923.6	50.1	147.2	8.0
	AGB$_{t6}$	1737.8	864.4	46.9	104.8	5.7
	AGB$_{t7}$	1791.0	520.8	28.3	51.6	2.8
	AGB$_{t8}$	1773.4	596.7	32.4	69.1	3.8

[1] Observed AGB$_t$ for Degaga-Gambo and Wondo Genet were 1434.4 kg and 1842.6 kg, respectively;

* Significantly different from zero ($p < 0.05$)

Table 3
Evaluation results of previously developed models when applied on our dataset.

Reference	Predicted AGB$_t$ (kg)	RMSE		MPE	
		(kg)	(%)	(kg)	(%)
Eshete and Ståhl (1998)	361.5	2611.2	159.7	1273.8	77.9***
Mokria et al. (2018)	525.5	2378.1	145.4	1109.8	67.9***
Ubuy et al. (2018)	745.0	1976.0	120.8	890.2	54.4***
Tetemke et al. (2019)	766.1	1869.7	114.3	869.1	53.2***
Mugasha et al. (2016)	1979.7	995.2	60.9	−344.4	−21.1**
Djomo et al. (2016)	635.8	2104.7	128.7	999.5	61.1***
Chave et al. (2005)	852.5	852.5	52.1	167.0	10.2
Chave et al. (2014)	1747.8	801.8	49.0	−112.5	−6.9
Current study AGB$_{t5}$	1631.4	733.8	44.9	3.8	0.2
Current study AGB$_{t8}$	1642.2	467.0	28.6	−6.9	−0.4

n = 63; observed mean AGB$_t$ = 1635.6 kg.

** $p < 0.01$.

*** $p < 0.001$.

2002; MEFCC, 2018b).

In data analysis we applied well documented methods. For model fitting we considered the pros and cons of available power model forms (e.g. Picard et al., 2015; Ductă et al., 2019), and also included several
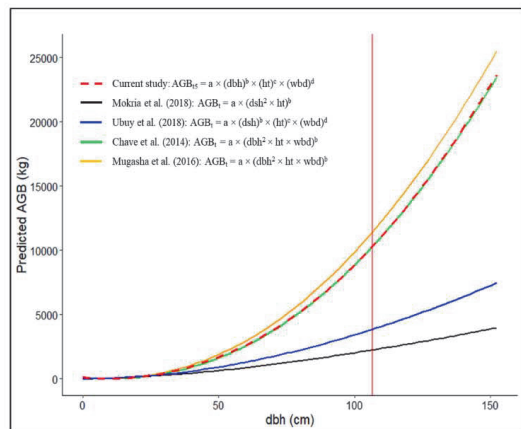
Fig. 4. A graph for total aboveground biomass (dry weight) over dbh based on the general models developed in this study (AGB$_{t5}$), by Mokria et al. (2018), Ubuy et al. (2018), Chave et al. (2014) and Mugasha et al. (2016). The vertical line indicates the maximum diameter in our dataset used for modelling. For graphical display of the models, AGB was predicted using ht derived from a ht-dbh model, as well as the mean wbd for the study sites given by Asrat et al. (2020). In addition, for displaying Mokria et al. (2018) and Ubuy et al. (2018), that used dsh in their models, the corresponding dbh was determined using a dbh-dsh model from Asrat et al. (2020).

predictor variable options. Furthermore, we applied a leave-one-out cross validation to compute model fit statistics, which enables using the entire dataset for modelling instead of splitting it into separate modelling and validation datasets (James et al., 2013). Finally, we have also in our work emphasised to document information near up the requirements on the target population, environmental conditions, sampling and laboratory procedures as well as model fitting and related uncertainties as suggested by Jara et al. (2014).

As part of exploring the direct tree biomass prediction method we developed a set of new models. To allow flexibility in practical applications, we provided different model options applicable depending on the availability of data from inventories. In the case of our general aboveground tree biomass models, Model AGB$_{t1}$ with dbh only as predictor variable explained about 87% of the variations in aboveground biomass. Adding ht into the model (Model AGB$_{t2}$) did not provide a viable model because of an insignificant parameter estimate

for ht. Similar results are also reported from elsewhere in Ethiopia (e.g. Ubuy et al., 2018; Tetemke et al., 2019) and from central Africa (e.g. Fayolle et al., 2018). On the other hand, adding wbd (Model AGB$_{t3}$) or crw (Model AGB$_{t4}$) improved the model performance considerably with pseudo-R^2 of 0.90 and 0.93, respectively. However, by using ht together with dbh, crw and wbd as predictor variables Model AGB$_{t8}$ explained 96% of the variations in biomass and produced the lowest AIC. Probably the branchy patterns of many trees in these forests, that enable accumulation of considerable biomass proportions to branches (see Fig. 2), made crw a better predictor variable than ht to explain variation in biomass. Similar poor contributions of ht as opposed to crw in explaining variations in biomass are also reported by Ubuy et al. (2018) for exclosure forests and Tetemke et al. (2019) for Dry Afromontane forest in northern Ethiopia. Apart from improving the models, crw has also the potential of being used for biomass estimation in remote sensing applications since this variable is more easily detectable from the air as compared to other variables (e.g. Eshete and Ståhl, 1998; Jucker et al., 2017).

Overall, none of the viable general AGB$_t$ models had MPEs significantly different from zero, and no obvious trends were seen for observed biomass over predicted biomass over size, indicating that extrapolation of the models within reasonable ranges are not likely to be biased. In addition, the models explained from 87% to 96% of biomass variations, which are more than some previous results from dry forests in east-Africa (e.g. Mokria et al., 2018; Ubuy et al., 2018) while similar to some others (e.g. Mugasha et al., 2013; Kachamba et al., 2016; Tetemke et al., 2019). The general conclusion is therefore these models may be applied with high certainty for tree biomass prediction in our study sites.

For biomass and carbon stock estimation over larger forest areas, particularly in REDD+ implementation, the associated uncertainties should be indicated (IPCC, 2014). Errors related to models' parameter estimates are one source of the uncertainties that need to be provided along with the developed models (Magnussen and Negrete, 2015). However, very few published papers reported these results (e.g. Breidenbach et al, 2014; Kachamba et al., 2016). Hence in order to enable the potential users of our models to determine uncertainties in biomass estimates, e.g. related to the REDD+ implementations that are underway for Ethiopia (UN-REDD, 2017), covariance matrices for the parameters estimates of all the viable general total tree aboveground biomass models in Table 1 are provided (Table A3). Breidenbach et al. (2014) and Ståhl et al. (2014) used information from covariance matrices of biomass models along with information from the sampling design and applied Monte Carlo simulations to quantify the combined effects on biomass uncertainty from both models and sampling. Both

Table 4
Evaluation results of the indirect biomass prediction method.

Volume	BEF	wbd	Predicted AGB$_t$ (kg)	RMSE		MPE	
				(kg)	(%)	(kg)	(%)
Total	Species-specific	Species-specific	2444.9	917.6	40.4	−173.4	−7.6
	Species-specific	Study sites mean	2766.1	1535.7	67.6	−494.6	−21.8*
	Species-specific	National mean	2879.3	1664.2	73.3	−607.8	−26.8*
	Study sites mean	Species-specific	2452.0	970.0	42.7	−180.6	−8.0
	Study sites mean	Study sites mean	2756.8	1436.2	63.2	−485.3	−21.4*
	Study sites mean	National mean	2869.3	1564.4	68.9	−597.8	−26.3**
Merchantable stem	Species-specific	Species-specific	2378.6	595.3	26.2	−107.2	−4.7
	Species-specific	Study sites mean	2688.5	1285.9	56.6	−417.0	−18.4*
	Species-specific	National mean	2798.7	1412.5	62.2	−527.2	−23.2**
	Study sites mean	Species-specific	2526.9	1004.4	44.2	−255.4	−11.2
	Study sites mean	Study sites mean	2840.2	1497.4	65.9	−568.7	−25.0**
	Study sites mean	National mean	2956.1	1634.7	72.0	−684.6	−30.1**

n = 45; observed mean AGB$_t$ = 2271.5 kg.

* $p < 0.05$.

** $p < 0.01$.

studies concluded that the model related effects had considerable influence. The documentation of covariance matrices of the biomass models developed in the present study therefore facilitate interesting future research related to error propagation issues when estimating biomass in an Ethiopian context.

Tree section biomass models may be useful in forest management for quantifying exploitable tree products such as fuelwood and fodder (Brown, 1997; Balehegn et al., 2012). The branch and foliage models developed in the present study in general performed poorer than the total aboveground and the merchantable stem biomass models, but most of them may still be applied to our study sites with reasonable certainty. A similar result with poorer branch biomass models than stem biomass models was found for natural forests in Tanzania (Mugasha et al., 2016) while the opposite was seen in Malawi (Kachamba et al., 2016). Tree height as a predictor variable did not bring any improvement into the branch and foliage models, i.e. best performing according to AIC were Model B_{br7} for branch and Model B_{f7} for foliage, both with dbh, crw and wbd as predictor variables.

Application of previously developed biomass models should always be considered as an option if no models exist for a certain forest area. When we tested some relevant previously developed models on our dataset, we found large MPEs significantly different from zero except for the pan-tropical models. This is of course not surprising because the models were applied outside the data ranges from which they were developed from. Even the model developed for Dry Afromontane forest in northern Ethiopia (Tetemke et al., 2019) arrived at such a result, but when considering the large variation in biomass per ha within the Dry Afromontane forests documented in a recent national forest inventory for Ethiopia (MEFCC, 2018b), this is probably what we should expect. Among the previously developed models, only the pan-tropical ones (Chave et al., 2005, 2014) yielded MPEs not significantly different from zero. This means that these models perform in an appropriate way in our study sites, although not as good as the new models. It is important to note, however, that this does not guarantee the pan-tropical models to work well in other parts of Dry Afromontane forest in Ethiopia.

There are also situations where tree biomass must be predicted indirectly from volume by the means of BEF and wbd (Brown, 1997; IPCC, 2006). By mimicking such a situation, we tested this method on our dataset. In general, this method overpredicted biomass, but not significantly when species-specific wbd values were used. Species-specific wbd values should therefore be used, probably even when local wbd values are not available they can be obtained from the Global Wood Density database (Chave et al., 2009; Zanne et al., 2009), although some additional uncertainty then is included. Species-specific BEF values, along with species-specific wbd values, produced smaller MPEs than the study sites mean BEF values. This is not a realistic situation, however, because species-specific BEFs are very likely not available for all species in a forest. The most realistic situation is therefore to apply study sites mean BEF values. Generally, the performance of indirect biomass prediction method is much influenced by the methodologies applied (Sanquetta et al., 2011). Similar to our study, also previous researchers have reported poorer performance for the indirect biomass prediction method as compared to the direct method (e.g. Petersson et al., 2012; Njana, 2017). To describe BEF values as a function of dbh and/or ht has proved to result in lower uncertainty than mean BEF values (Sanquetta et al., 2011; Magalhães and Seifert, 2015a). However, several authors have also indicated that the indirect method should be avoided if possible because the method generally is associated with larger uncertainties than the direct method (e.g. Hewson et al., 2014; Lisboa et al., 2018).

Among the options for biomass prediction explored in this study there is no doubt that the direct biomass prediction method when applying the new biomass models performed well and is associated with the lowest uncertainty. Applications of the new general models are therefore likely to enhance the bases for decision-making in forest management including REDD+ implementation for Dry Afromontane

forests in Ethiopia. For maximizing accuracy, we recommend Models AGB_{t8}, B_{ms8}, B_{br7} and B_{f7} to be used for total, merchantable stem, branch and foliage biomass, respectively. However, it is also important to note that any of the viable models still may be applied depending on the variables that are available from an inventory. The previously developed models performed poorer than the new models and most of them had MPEs significantly different from zero, generally because they were applied outside their data ranges. Similarly, the indirect method performed poorer than the new models. Application of the indirect method should be limited to situations where no biomass models are available using study sites mean BEF values, which are the most practically realistic option, and either available local specie-specific wbd values or values from Global Wood Density database.

The dataset used in this study does not cover large parts of the Dry Afromontane forests in Ethiopia. Future research should therefore aim at developing biomass models based on both existing data and additional data to better cover the entire target population including the high biomass density variation that characterize this forest type (MEFCC, 2018b). Meanwhile we rely on existing models, and in this regard, though the pan-tropical models are still viable, we recommend for the Dry Afromontane forests in Ethiopia to apply the models from the present study and from the Tetemke et al. (2019) models over the pan-tropical models (Chave et al., 2005, 2014), mainly because the latter models are limited by the fact that they are not based on any data from Ethiopia, but also because crw as an independent variable in our models improved performance considerably. However, before an application of the existing models is done, we also strongly recommend considering similarities in terms of growing conditions such as soil, rainfall and temperature, and data ranges of dbh and ht. A recent study of biomass allometry, based on two large datasets from Eurasia and Canada, found that the differences between species was a more important driver of the variability in allometric models compared to differences between sites (Dutcă, 2019). Particularly for our models therefore, the presence of dominant tree species such as *Afrocarpus falcatus*, *Celtis africana*, *Croton macrostachyus*, *Millettia ferruginea*, and *Pouteria adolfi-friedericii* is important when considering application of the models.

5. Conclusion

Choice of tree biomass prediction method is a crucial step for biomass and carbon stock estimations. Here we have evaluated direct and indirect biomass prediction methods based on destructively sampled trees data from Dry Afromontane forests in south-central Ethiopia. The direct method using the newly developed general allometric models is the best option for application in the study sites. The pan-tropical model also performed well as opposed to other previously developed models and the indirect method that are associated with larger uncertainties. The new models are flexible and any of the viable models may be chosen for application based on the availability of data from an inventory. Our general models may also be considered for application in other Dry Afromontane forests, which lack site-specific models, but only if the required conditions are carefully evaluated. The results have strong practical implications for enhanced decision-making in forest management including REDD + implementations for Dry Afromontane forests in Ethiopia.

Declaration of Competing Interest

The authors declare that they have no known competing financial interests or personal relationships that could have appeared to influence the work reported in this paper.

Acknowledgement

Appendix A

Fig. A1. Scatter plots of total aboveground, merchantable stem, branch and foliage biomass (dry weight) against dbh (left) and ht (right). The black and red colours represent sample trees from Degaga-Gambo and Wondo Genet sites, respectively.

Table A1
Tree species sampled for biomass modelling along with their mean and range values for dbh, ht, crw, wbd and BEF.

Tree species	n	dbh (cm)		ht (m)		crw (m)		wbd (g cm^{-3})*		BEF_t		BEF_{ms}	
		Mean	Range	Mean	Range	Mean	Range	Mean	Range	Mean (n_i)	Range	Mean**	Range
Acokanthera schimperi	1	17.0		9.4		5.9		0.621		1.53(1)		3.01	
Afrocarpus falcatus	9	47.2	9.5–105.5	19.7	6.9–36.0	9.6	3.4–17.7	0.426	0.401–0.480	1.28(8)	0.95–1.77	2.06	1.43–2.66
Albizia gummifera	3	87.2	65.0–106.5	29.9	25.1–38.8	20.3	16.1–23.9	0.534	0.499–0.598	1.07(3)	0.99–1.12	2.01	1.83–2.15
Allophylus abyssinicus	2	36.3	10.5–62	14.0	6.8–21.2	8.5	4.5–12.5	0.509	0.509–0.515	1.09(1)		1.77	
Apodytes dimidiata	1	37.5		24.7		6.1		0.556		1.03(1)		1.22	
Bersama abyssinica	1	27.0		11.7		6.7		0.576		1.24(1)		2.05	
Canthium oligocarpum	1	28.5		15.6		5.7		0.473		1.12(1)		1.57	
Cassipourea malosana	2	10.0	8.0–12.0	8.0	6.6–9.4	5.1	4.9–5.4	0.663	0.605–0.683	–		–	
Celtis africana	5	49.2	20.0–95.0	24.6	21.3–29.1	10.4	8.1–16.3	0.631	0.615–0.658	1.20(5)	1.10–1.40	1.93	1.45–2.37
Combretum molle	1	12.0		7.7		3.6		0.701		–		–	
Croton macrostachyus	5	43.6	11.5–85.0	22.1	10.5–30.2	11.3	3.6–20.0	0.511	0.430–0.521	1.00(4)	0.90–1.06	1.31	1.24–1.38
Dodonaea angustifolia	1	13.5		9.3		6.8		0.816		–		–	
Ekebergia capensis	1	62.0		33.1		12.9		0.532		0.91(1)		1.40	
Ficus thonningii	1	47.0		18.6		8.2		0.471		1.14(1)		1.92	
Galiniera coffeoides	1	11.3		8.6		4.1		0.563		–		–	
Maesa lanceolata	3	23.3	14.5–38.0	12.0	9.2–15.8	5.0	3.5–6.8	0.483	0.457–0.536	1.06(2)	0.99–1.13	1.67	1.48–1.85
Maytenus arbutifolia	2	12.3	7.0–17.5	8.6	5.4–11.7	4.2	3.4–4.9	0.615	0.615–0.622	0.92(1)		1.31	
Millettia ferruginea	4	47.4	8.0–77.5	24.1	10.2–33.3	8.9	2.4–13.1	0.550	0.380–0.554	1.05(3)	0.97–1.17	1.51	1.47–1.60
Nuxia congesta	2	21.3	19.0–23.5	11.1	10.0–12.1	4.7	4.3–5.0	0.537	0.498–0.603	1.14(2)	1.13–1.15	2.10	2.10–2.10
Olea capensis	1	23.0		19.3		7.1		0.779		1.11(1)		2.32	
Olea welwitschii	1	19.5		10.9		5.9		0.700		1.16(1)		2.38	
Olinia rochetiana	1	7.5		11.4		2.4		0.544		–		–	
Osyris quadripartita	1	30.5		8.4		7.8		0.690		1.06(1)		2.27	
Pittosporum viridiflorum	1	10.5		5.2		3.8		0.441		–		–	
Pouteria adolfi-friedericii	4	42.1	13.5–106.0	20.9	10.7–33.5	7.6	3.7–15.9	0.460	0.458–0.567	1.03(3)	0.85–1.17	1.18	1.07–1.30
Prunus africana	3	53.3	11.5–105.5	21.4	12.8–31.9	8.4	5.3–13.3	0.609	0.608–0.615	0.94(2)	0.86–1.01	1.18	1.15–1.21
Syzygium guineense	2	53.0	26.5–79.5	24.8	22.5–27.1	10.7	6.9–14.6	0.580	0.579–0.590	1.09(2)	0.93–1.24	1.59	1.36–1.83
Teclea nobilis	1	9.5		7.3		5.2		0.979		–		–	
Vepris dainellii	1	12.5		8.3		5.7		0.631		–		–	
Vernonia amygdalina	1	10.0		6.1		2.9		0.457		–		–	

* wbd from Asrat et al. (2020); n_i: number of individual trees per species.
** The same n_i as in BEF_t.

Table A2
Previously developed total aboveground biomass models applied on our data.

Reference	Model	n	dbh/dsh range (cm)
Eshete and Ståhl (1998)	$AGB_t = \exp(1.21 + 1.09 \times \ln(cra))$ *	83	–
Mokria et al. (2018)	$AGB_t = 0.2451 \times (dsh^2 \times ht)^{0.7038}$	84	–
Ubuy et al. (2018)	$AGB_t = 0.217 \times dsh^{1.8428} \times ht^{0.3361} \times wbd^{0.2963}$	305	2.5–29.5
Tetemke et al. (2019)	$AGB_t = 0.350 \times dbh^{1.864} \times cra^{0.171} \times wbd^{0.485}$ *	86	2.9–45.2
Mugasha et al. (2016)	$AGB_t = 0.1014 \times (wbd \times dbh^2 \times ht)^{0.9510}$	30	–
Djomo et al. (2016)	$AGB_t = \exp(-0.841 + 2.082 \times \ln(dbh) + 1.248 \times \ln(wbd))$	118	3.0–32.0
Chave et al. (2005)	$AGB_t = 0.112 \times (wbd \times dbh^2 \times ht)^{0.916}$	686	5.0–63.4
Chave et al. (2014)	$AGB_t = 0.0673 \times (wbd \times dbh^2 \times ht)^{0.976}$	4004	5.0–180.0

* cra: crown area (m^2).

Table A3
Covariance matrices for all viable general total aboveground biomass models.

Model	Model expression	Variables	Covariance matrix		
AGB_{t1}	$0.15895 \times (dbh)^{2.34670}$		Intercept	dbh	
		Intercept	0.00183		
		dbh	−0.00272	0.00414	
AGB_{t3}	$0.26136 \times (dbh)^{2.40291} \times (wbd)^{1.15019}$		Intercept	dbh	wbd
		Intercept	0.00346		
		dbh	−0.00261	0.00285	
		wbd	0.00369	0.00298	0.04423
AGB_{t4}	$0.21170 \times (dbh)^{1.69530} \times (crw)^{0.95050}$		Intercept	dbh	crw
		Intercept	0.00095		
		dbh	−0.00128	0.01137	
		crw	0.00009	−0.01548	0.02474

Table A3 (continued)

Model	Model expression	Variables	Covariance matrix				
AGB_{t5}	$0.19250 \times (dbh)^{2.21060} \times (ht)^{0.35380} \times (wbd)^{1.21890}$		Intercept	dbh	ht	wbd	
		Intercept	0.00311				
		dbh	0.00109	0.01122			
		ht	−0.00601	−0.01601	0.03099		
		wbd	0.00162	0.00034	0.00513	0.04426	
AGB_{t6}	$0.17587 \times (dbh)^{1.51600} \times (ht)^{0.27451} \times (crw)^{0.96145}$		Intercept	dbh	ht	crw	
		Intercept	0.00089				
		dbh	0.00036	0.01606			
		ht	−0.00230	−0.01043	0.01873		
		crw	0.00011	−0.01263	−0.00216	0.02291	
AGB_{t7}	$0.29628 \times (dbh)^{1.89139} \times (crw)^{0.78636} \times (wbd)^{1.14705}$		Intercept	dbh	crw	wbd	
		Intercept	0.00208				
		dbh	−0.00168	0.00657			
		crw	0.00037	−0.00775	0.01183		
		wbd	0.00151	0.00254	−0.00056	0.02370	
AGB_{t8}	$0.21765 \times (dbh)^{1.77660} \times (ht)^{0.33242} \times (crw)^{0.65575} \times (wbd)^{1.07739}$		Intercept	dbh	ht	crw	wbd
		Intercept	0.00097				
		dbh	0.00052	0.00923			
		ht	−0.00197	−0.00526	0.01111		
		crw	−0.00005	−0.00794	−0.00170	0.01397	
		wbd	0.00053	0.00426	0.00179	−0.00475	0.02254

References

Agrawal, A., Nepstad, D., Chhatre, A., 2011. Reducing emissions from deforestation and forest degradation. Annu. Rev. Environ. Resour. 36, 373–396. https://doi.org/10.1146/annurev-environ-042009-094508.

Asrat, Z., Eid, T., Gobakken, T., Negash, M., 2020. Modelling and quantifying tree biometric properties of Dry Afromontane forests in south-central Ethiopia (submitted for publication).

Balehegn, M., Eniang, E.A., Hassen, A., 2012. Estimation of browse biomass of *Ficus thonningii*, an indigenous multipurpose fodder tree in northern Ethiopia. Afr. J. Range Forage Sci. 29 (1), 25–30. https://doi.org/10.2989/10220119.2012.687071.

Breidenbach, J., Anton-Fernandez, C., Petersson, H., McRoberts, R.E., Astrup, R., 2014. Quantifying the model-related variability of biomass stock and change estimates in the Norwegian National Forest Inventory. For. Sci. 60, 25–33. https://doi.org/10.5849/forsci.12-137.

Bollandsås, O.M., Zahabu, E., Katani, J.Z., 2016. Background on the development of biomass and volume models. In: Malimbwi, R.E., Eid, T., Chamshama, S.A.O. (Eds.), Allometric Tree Biomass and Volume Models in Tanzania. Department of Forest Mensuration and Management, Sokoine University of Agriculture.

Brown, S., 1997. Estimating biomass and biomass change of tropical forests: a primer. FAO Forestry paper, 134 p. ISBN 92-5-103955-0. http://www.fao.org/3/w4095e/w4095e00.htm (accessed on October 2019).

Brown, S., 2002. Measuring carbon in forests: current status and future challenges. Environ. Pollut. 116, 363–372. https://doi.org/10.1016/S0269-7491(01)00212-3.

Burkhart, H.B., Tomé, M., 2012. Modelling Forest Trees and Stands. Springer, Dordrecht, pp. 457.

Chave, J., Andalo, A., Brown, S., Cairns, M.A., Chambers, J.Q., Eamus, D., Folster, H., Fromard, F., Higuchi, N., Kira, T., Lescure, J.-P., Nelson, B.W., Ogawa, H., Puig, H., Riera, B., Yamakura, T., 2005. Tree allometry and improved estimation of carbon stocks and balance in tropical forests. Oecologia 145, 87–99. https://doi.org/10.1007/s00442-005-0100-x.

Chave, J., Condit, R., Aguilar, S., Hernandez, A., Lao, S., Perez, R., 2004. Error propagation and scaling for tropical forest biomass estimates. Philos. Trans. Royal Soc. Lond. B 359, 409–420. https://doi.org/10.1098/rstb.2003.1425.

Chave, J., Coomes, D., Jansen, S., Lewis, S.L., Swenson, N.G., Zanne, A.E., 2009. Towards a worldwide wood economics spectrum. Ecol. Lett. 12, 351–366. https://doi.org/10.1111/j.1461-0248.2009.01285.x.

Chave, J., Mechain, M.R., Burquez, A., Chidumayo, E., Colgan, M.S., Delitti, W.B.C., Duque, A., Eid, T., Fearnside, P.M., Goodman, R.C., Henry, M, Yrizar, A.M., Mugasha, W.A., Mullerlandau, H.C., Mencuccini, M., Nelson, B.W., Ngomanda, A., Nogueira, E.M., Ortiz-Malavassi, E., Pelissier, R., Ploton, P., Ryan, C.M., Saldarriaga, J.G., Vieilledent, G., 2014. Improved allometric models to estimate the aboveground biomass of tropical trees. Glob. Change Biol. 20, 3177–3190. https://doi.org/10.1111/gcb.12629.

Chidumayo, E., Marunda, C., 2010. Dry forests and woodlands in Sub-Saharan Africa: context and challenges. In: Chidumayo, E.N., Gumbo, D.J. (Eds.), The Dry Forests and Woodlands of Africa, Managing for Products and Services. Earhscan, London UK.

Clark, D.B., Kellner, J.R., 2012. Tropical forest biomass estimation and the fallacy of misplaced concreteness. J. Veg. Sci. 23, 1191–1196. https://doi.org/10.1111/j.1654-1103.2012.01471.x.

Daba, D.E., Soromessa, T., 2019. Allometric equations for aboveground biomass estimation of *Diospyros abyssinica* (Hiern) F. White tree species. Ecosyst. Health Sustain. 5 (1), 86–97. https://doi.org/10.1080/20964129.2019.1591169.

Djomo, N.A., Picard, N., Fayolle, A., Henry, M., Ngomanda, A., Ploton, P., McLellan, J., Saborowski, J., Adamou, I., Lejeune, P., 2016. Tree allometry for estimation of carbon stocks in African tropical forests. Forestry: Int. J. For. Res. 89 (4), 446–455. https://doi.org/10.1093/forestry/cpw025.

Dutcă, I., 2019. The variation driven by differences between species and between sites in allometric biomass models. Forests 10 (11), 976. https://doi.org/10.3390/f10110976.

Ductă, I., Mcroberts, R.E., Næsset, E., Blujdea, V.N.B., 2019. A practical measure for determining if diameter (D) and height (H) should be combined in to D²H in allometric biomass models. Forestry: Int. J. For. Res. 00, 1–8. https://doi.org/10.1093/forestry/cpz041.

Eid, T., Bollandsås, O.M., Mugasha, W.A., Mauya, E., Zahabu, E., Malimbwi, R.E., 2016. Allometric biomass and volume models for Miombo Woodlands. In: Malimbwi, R.E., Eid, T., Chamshama, S.A.O. (Eds.), Allometric Tree Biomass and Volume Models in Tanzania. Department of Forest Mensuration and Management, Sokoine University of Agriculture.

Erikson, H., Stern, M., 1987. A Soil Study at Wondo Genet Forestry Resource Institute, Ethiopia. Swedish University of Agricultural Science, International Rural Development Centre-Uppsala 0280–4301 ISSN 0280-4301.

Eshete, G., Ståhl, G., 1998. Functions for multi-phase assessment of biomass in acacia woodlands of the Rift Valley of Ethiopia. For. Ecol. Manage. 105, 79–90. https://doi.org/10.1016/S0378-1127(97)00273-9.

FAO, 2016. Global forest resources assessment 2015; How are the world's forests changing? second ed. http://www.fao.org/3/a-i4793e.pdf (accessed October 2019).

Fayolle, A., Doucet, J.L., Gillet, J.F., Bourland, N., Lejeune, P., 2013. Tree allometry in Central Africa: testing the validity of pantropical multi-species allometric equations for estimating biomass and carbon stocks. For. Ecol. Manage. 305, 29–37. https://doi.org/10.1016/j.foreco.2013.05.036.

Fayolle, A., Ngomanda, A, Mbasi, M., Barbier, N., Bocko, Y., Boyemba, F., Couteron, P., Fonton, N., Kamdem, N., Katembo, J., Kondaoule, H.J., Loumeto, J., Maïdou, H.M., Mankou, G., Mengui, T., Mofack, G.I.I., Moundounga, C., Moundounga, Q., Nguimbous, L., Nchama, N.N., Obiang, D., Asue, F.O.M., Picard, N., Rossi, V., Senguela, Y.P., Sonké, B., Viard, L., Yongo, O.D., Zapfack, L., Vincent, P., Medjibe, V.P., 2018. A regional allometry for the Congo basin forests based on the largest ever destructive sampling. For. Ecol. Manage. 430, 228–240. https://doi.org/10.1016/j.foreco.2018.07.030.

Friis, I., Demissew, S., Breugel, P.V., 2010. Atlas of the Potential Vegetation of Ethiopia. Det Kongelige Danske Videnskabernes Selskab, Copenhagen V, Denmark, pp. 306.

Fritzsche, F., Zech, W., Guggenberger, G., 2007. Soils of the main Ethiopian Rift Valley escarpment: a transect study. Catena 70, 209–219. https://doi.org/10.1016/j.catena.2006.09.005.

Gebeyehu, G., Soromessa, T., Bekele, T., Teketay, D., 2019. Carbon stocks and factors affecting their storage in dry Afromontane forests of Awi Zone, north-western Ethiopia. J Ecol. Environ. 43, 7. https://doi.org/10.1186/s41610-019-0105-8.

Gibbs, H.K., Brown, S., Niles, J.O., Foley, J.A., 2007. Monitoring and estimating tropical forest carbon stocks: making REDD a reality. Environ. Res. Lett. 2 (4), 13. https://doi.org/10.1088/1748-9326/2/4/045023.

Gibbs, H.K., Ruesch, A.S., Achard, F., Clayton, M.K., Holmgren, P., Ramankutty, N., Foley, J.A., 2010. Tropical forests were the primary sources of new agricultural land in the 1980s and 1990s. PNAS 107 (38), 16732–16737. https://doi.org/10.1073/pnas.0910275107.

Henry, M., Picard, N., Trotta, C., Manlay, R., Valentini, R., Bernoux, M., Saint-André, L.,

2011. Estimating tree biomass of sub-Saharan African forests: A review of available allometric equations. Silva Fenn. 45, 477–569. https://doi.org/10.14214/sf.38.

Hewson, J., Steininger, M.K., Pesmajoglou, S., Parra, A., Shoch, D., 2014. REDD+ Measurement, Reporting and Verification (MRV) Manual, Version 2.0: Overview. USAID-supported Forest Carbon, Markets and Communities Program. Washington, DC, USA. https://rmportal.net/library/content/fcmc/publications/MRV_Manual.pdf/view (accessed December 2019).

IPCC, 2006. IPCC Guidelines for National Greenhouse Gas Inventories, Prepared by the National Greenhouse Gas Inventories Programme. In: Eggleston, H.S., Buendia, L., Miwa, K., Ngara, T., Tanabe K. (Eds.), IGES, Japan.

IPCC, 2014. Revised Supplementary Methods and Good Practice Guidance Arising from the Kyoto Protocol. In: Hiraishi, T., Krug, T., Tanabe, K., Srivastava, N., Baasansuren, J., Fukuda, M., Troxler, T.G. (Eds.), IPCC, Switzerland.

James, G., Witten, D., Hastie, T., Tibshirani, R., 2013. An Introduction to Statistical Learning with Application in R. Springer, New York, pp. 441.

Jara, M.C., Henry, M., Réjou-Méchain, M., Wayson, C., Zapata-Cuartas, M., Piotto, D., Guier, F.A., Lombis, H.C., López, E.C., Lara, R.C., Rojas, K.C., Pasquel, J.D.Á., Montoya, Á.D., Vega, J.F., Galo, A.J., López, O.M., Marklund, L.G., Fuentes, J.M.M., Milla, F., Návar Chaidez, J.J., Malavassi, E.O., Pérez, J., Zea, C.R., García, L.R., Pons, R.R., Saint-André, L., Sanquetta, C., Scott, C., Westfall, J., 2014. Guideline for documenting and reporting tree allometric equations. Ann. For. Sci. 72, 763–768. https://doi.org/10.1007/s13595-014-0415-z.

Jucker, T., Caspersen, J., Chave, J., Antin, C., Barbier, N., Bongers, F., Dalponte, M., van Ewijk, K.Y., Forrester, D.I., Haeni, M., Higgins, S., Holdaway, R.J., Ida, Y., Lorimer, C., Marshall, P.L., Momo, S., Moncrieff, G.R., Ploton, P., Poorter, L., Rahman, K.A., Schlund, M., Sonké, B., Sterck, F.J., Trugman, A.T., Usoltsev, V.A., Vanderwel, M.C., Valdner, P., Wedeux, B.M., Wirth, C., Wöll, H., Woods, M., Xiang, W., Zimmermann, N.E., Coomes, D.A., 2017. Allometric equations for integrating remote sensing imagery into forest monitoring programmes. Glob. Change Biol. 23, 177–190. https://doi.org/10.1111/gcb.13388.

Kachamba, D., Eid, T., Gobakken, T., 2016. Above- and belowground biomass models for trees in the miombo woodlands of Malawi. Forests 7 (2), 38. https://doi.org/10.3390/f7020038.

Kebede, B., Soromessa, T., 2018. Allometric equations for aboveground biomass estimation of Olea europaea L. subsp. cuspidata in Mana Angetu forest. Ecosyst. Health Sustain. 4 (1), 1–12. https://doi.org/10.1080/20964129.2018.1433951.

Kelly, J.F., Beltz, R.C., 1987. A comparison of tree volume estimation models for forest inventory. Research paper SO-233, USDA Forest serve, Southern forest experiment station. New Orleans, Louisiana. https://doi.org/10.2737/SO-RP-233.

Köhl, M., Lasco, R., Cifuentes, M., Jonsson, Ö., Korhonen, K.T., Mundhenk, P., DeJesus, J., Stinson, G., 2015. Changes in forest production, biomass and carbon: results from the 2015 UN FAO global forest resource assessment. For. Ecol. Manage. 352, 21–34. https://doi.org/10.1016/j.foreco.2015.05.036.

Köhl, M., Magnussen, S., Marchetti, M., 2006. Sampling Methods, Remote Sensing and GIS Multiresource Forest Inventory. Springer, Berlin, pp. 373.

Lemenih, M., Allan, C., Biot, Y., 2015. Making forest conservation benefit local communities: Participatory forest management in Ethiopia. Farm Africa. https://www.farmafrica.org/downloads/resources/pfmfinalweb.pdf (accessed August 2019).

Lemenih, M., Kassa, H., 2014. Re-greening Ethiopia: history, challenges and lessons. Forests 5 (8), 1896–1909. https://doi.org/10.3390/f5081896.

Lisboa, S.N., Guedes, B.S., Ribeiro, N., Sitoe, A., 2018. Biomass allometric equation and expansion factor for a mountain moist evergreen forest in Mozambique. Carbon Balance Manage. 13 (23). https://doi.org/10.1186/s13021-018-0111-7.

Magalhães, T.M., Seifert, T., 2015a. Estimates of tree biomass and its uncertainties through mean-of-ratios, ratio-of-means and regression estimators in double sampling: a comparative study of Mecrusse woodlands. Am. J. Agric. For. 3 (5), 161–170. https://doi.org/10.11648/j.ajaf.20150305.11.

Magalhães, T.M., Seifert, T., 2015b. Tree component biomass expansion factors and root-to-shoot ratio of Lebombo ironwood: measurement uncertainty. Carbon Balance Manage. 10 (9). https://doi.org/10.1186/s13021-015-0019-4.

Magnussen, S., Negrete, O.I.C., 2015. Model errors in tree biomass estimates computed with an approximation to a missing covariance matrix. Carbon Balance Manage. 10 (21). https://doi.org/10.1186/s13021-015-0031-8.

Mavouroulou, Q.M., Ngomanda, A., Obiang, N.L.E., Lebamba, J., Gomat, H., Mankou, G.S., Loumeto, J., Iponga, D.M., Ditsouga, F.K., Koumba, R.Z., Bobé, K.H.B., Lépengué, N., Mbatchi, B., Picard, N., 2014. How to improve allometric equations to estimate forest biomass stocks? Some hints from a central African forest. Can. J. For. Res. 44, 685–691. https://doi.org/10.1139/cjfr-2013-0520.

McCann, J.C., 1997. The Plow and the forest: narratives of deforestation in Ethiopia, 1840–1992. Environ. Hist. 2, 138–159. https://doi.org/10.2307/3985505.

McRoberts, R.E., Westfall, J.A., 2013. Effects of uncertainty in model predictions of individual tree volume on large area volume estimates. For. Sci. 60, 34–42. https://doi.org/10.5849/forsci.12-141.

MEFCC, 2018a. National Forest Sector Development Program, Ethiopia. Volume I: Situation Analysis. Ministry of Environment Forest and Climate Change. https://www.et.undp.org/content/ethiopia/en/home/ library/ten-year-national-forest-sector-development-programme.html (accessed August 2019).

MEFCC, 2018b. Ethiopia's national forest inventory final report. Ministry of Environment Forest and Climate Change, Addis Ababa, Ethiopia.

Mokria, M., Mekuria, W., Gebrekiristos, A., Aynekulu, E., Belay, B., Gashaw, T., Brauning, A., 2018. Mixed species allometric equations and estimation of aboveground biomass

and carbon stocks in restoring degraded landscape in northern Ethiopia. Environ. Res. Lett. 13 (2). https://doi.org/10.1088/1748-9326/aaa495.

Mugasha, W.A., Eid, T., Bollandsås, O.M., Malimbwi, R.E., Chamshama, S.A.O., Zahabu, E., Katani, J.Z., 2013. Allometric models for prediction of above- and belowground biomass of trees in the miombo woodlands of Tanzania. For. Ecol. Manage. 310, 87–101. https://doi.org/10.1016/j.foreco.2013.08.003.

Mugasha, W.A., Mwakalukwa, E.E., Luoga, E., Malimbwi, R.E., Zahabu, E., Silayo, D.S., Sola, G., 2016. Allometric models for estimating tree volume and aboveground biomass in lowland forests of Tanzania. Int. J. For. Res. 2016, 1–13. https://doi.org/10.1155/2016/ 8076271.

NABU, 2017. NABU's Biodiversity Assessment at the Kafa Biosphere Reserve. The Nature and Biodiversity Conservation Union (NABU), Berlin, Addis Ababa. http://imperia.verbandsnetz.nabu.de/imperia/md/content/nabude/international/nabu_biodiversity_assessment_15.pdf (accessed August 2019).

Næsset, E., Ørka, H.O., Solberg, S., Bollandsås, O.M., Hansen, E.H., Mauya, E., Zahabu, E., Malimbwi, R., Chamuya, N., Olsson, H., Gobakken, T., 2016. Mapping and estimating forest area and aboveground biomass in miombo woodlands in Tanzania using data from airborne laser scanning, TanDEM-X, RapidEye, and global forest maps: A comparison of estimated precision. Remote Sens. Environ. 175, 282–300. https://doi.org/10.1016/j.rse.2016.01.006.

Ngomanda, A., Obiang, N.L.E., Lebamba, J., Mavouroulou, Q.M., Gomat, H., Mankou, G.S., Loumeto, J., Iponga, D.M., Ditsouga, F.K., Koumba, R.Z., Bobé, K.H.B., Okouyi, C.M., Nyangadouma, R., Lépengué, N., Mbatchi, B., Picard, N., 2014. Site-specific versus pantropical allometric equations: which option to estimate the biomass of a moist central African forest? For. Ecol. Manage. 312, 1–9. https://doi.org/10.1016/j.foreco.2013.10.029.

Nogueira, E.M., Fearnside, P.M., Nelson, B.W., Barbosa, R.I., Keizer, E.W.H., 2008. Estimates of forest biomass in the Brazilian Amazon: New allometric equations and adjustments to biomass from wood-volume inventories. For. Ecol. Manage. 256, 1853–1867. https://doi.org/10.1016/j.foreco.2008.07.022.

Njana, M.N., 2017. Indirect methods of tree biomass estimation and their uncertainties, Southern Forests. J. For. Sci. 79 (1), 41–49. https://doi.org/10.2989/20702620.2016. 1233753.

Pan, Y., Bridsey, R.A., Fang, J., Houghton, R., Kauppi, P.E., Kurz, W.A., Phillips, O.L., 2011. A large and persistent carbon sink in the world's forests. Science 333, 988–993. https://doi.org/10.1126/science.1201609.

Penman, J., Gytarsky, M., Hiraishi, T., Krug, T., Kruger, D., Pipatti, R., Buendia, L., Miwa, K., Ngara, T., Tanabe, K., Wagner, F., 2003. IPCC Good Practice Guidance for land use, land-use change and forestry. http://www.ipcc-nggip.iges.or.jp (accessed August 2019).

Petersson, H., Holm, S., Ståhl, G., Alger, D., Fridman, J., Lehtonen, A., Lundström, A., Mäkipää, R., 2012. Individual tree biomass equations or expansion factors for assessment of carbon stock changes in living biomass – a comparative study. For. Ecol. Manage. 270, 78–84. https://doi.org/10.1016/j.foreco.2012.01.004.

Picard, N., Rutishauser, E., Ploton, P., Ngomanda, A., Henry, M., 2015. Should tree biomass allometry be restricted to power models? For. Ecol. Manage. 353, 156–163. https://doi.org/10.1016/j.foreco.2015.05.035.

Picard, N., Saint-André, L., Henry, M., 2012. Manual for building tree volume and biomass allometric equations: from field measurement to prediction. Rome: Food and Agriculture Organization of the United Nations; Montpellier: Centre de Coopération Internationale en Recherche Agronomique pour le Développement.

Core Team, R., 2019. R: A language and environment for statistical computing. R Foundation for Statistical Computing, Vienna, Austria.

Sanquetta, C.R., Corte, A.P.D., da Silva, F., 2011. Biomass expansion factor and toot-to-shoot ratio for Pinus in Brazil. Carbon Balance Manage. 6 (6). https://doi.org/10.1186/1750-0680-6-6.

Ståhl, G., Heikkinen, J., Petersson, H., Repola, J., Holm, S., 2014. Sample-based estimation of greenhouse gas emissions from forests – a new approach to account for both sampling and model errors. For. Sci. 60 (1), 3–13. https://doi.org/10.5849/forsci.13-005.

Temesgen, H., Affleck, D., Poudel, K., Gray, A., Sessions, J., 2015. A review of the challenges and opportunities in estimating above ground forest biomass using tree-level models. Scand. J. For. Res. 30 (4), 326–335. https://doi.org/10.1080/02827581.2015.1012114.

Tesemma, A.B., 2007. Useful trees of Ethiopia: identification, propagation and management in 17 agroecological zones. RELMA in ICRAF Project, Nairobi, pp. 552.

Tesfaye, M.A., Bravo-Oviedo, A., Bravo, F., Ruiz-Peinado, R., 2016. Aboveground biomass equations for sustainable production of fuelwood in a native dry tropical afro-montane forest of Ethiopia. Ann. For. Sci. 73, 411–423. https://doi.org/10.1007/s13595-015-0533-2.

Tetemke, B.A., Birhane, E., Rannestad, M.M., Eid, T., 2019. Allometric models for predicting aboveground biomass of trees in the dry Afromontane forests of northern Ethiopia. Forests 10 (12), 1114. https://doi.org/10.3390/f10121114.

Ubuy, M.H., Eid, T., Bollandsås, O.M., Birhane, E., 2018. Aboveground biomass models for trees and shrubs of exclosures in the drylands of Tigray, northern Ethiopia. J. Arid Environ. 156, 9–18. https://doi.org/10.1016/j.jaridenv.2018.05.007.

UN-REDD, 2017. Ethiopia's Forest Reference Level Submission to the UNFCCC. https://redd.unfccc.int/files/ethiopia_frel_3.2_final_modified_submission.pdf (accessed August 2019).

Vieilledent, G., Vaudry, R., Andriamanohisoa, S.F.D., Rakotonarivo, O.S., Randrianasolo, H.Z., Razafindrabe, H.N., Rakotoarivony, C.B., Ebeling, J., Rasamoelina, M., 2012. A

universal approach to estimate biomass and carbon stock in tropical forests using generic allometric models. Ecol. Appl. 22, 572–583. https://doi.org/10.1890/11-0039.1.

West, P.W., 2015. Tree and Forest Measurement, third ed. Springer, Switzerland, pp. 214.

Winberg, E., 2011. Participatory forest management in Ethiopia, practices and experiences. FAO-SFE technical paper, Addis Ababa. http://www.fao.org/3/a-aq407e.pdf (accessed August 2019).

Zanne, A.E., Lopez-Gonzalez, G., Coomes, D.A., Ilic, J., Jansen, S., Lewis, S.L., Miller, R.B., Swenson, N.G., Wiemann, M.C., Chave, J., 2009. Data from: towards a worldwide wood economics spectrum. Dryad Digital Repository. https://doi.org/10.5061/dryad.234.

Paper IV

Use of remotely sensed data to enhance estimation of aboveground biomass for the Dry Afromontane forest in south-central Ethiopia

Habitamu Taddese [a, c, *], Zerihun Asrat[b, c], Ingunn Burud[a], Terje Gobakken[b], Hans Ole Ørka[b], Øystein B. Dick[a] and Erik Næsset[b]

[a] Norwegian University of Life Sciences, Faculty of Science and Technology, P. O. Box 5003, 1432, Ås, Norway.

[b] Norwegian University of Life Sciences, Faculty Environmental Sciences and Natural Resource Management, P. O. Box 5003, 1432, Ås, Norway.

[c] Hawassa University, Wondo Genet College of Forestry and Natural Resources, P. O. Box 128, Shashemene, Ethiopia.

* Correspondence: habitamu.taddese.berie@nmbu.no; Tel: +4746718534.

Abstract

Periodic assessment of forest aboveground biomass (AGB) is essential to regulate the impacts of the changing climate. However, AGB estimation using field-based sample survey (FBSS) has limited precision due to cost and accessibility constraints. Fortunately, remote sensing technologies assist to improve AGB estimation precisions. Thus, this study assessed the role of remotely sensed (RS) data in improving the precision of AGB estimation in an Afromontane forest in south-central Ethiopia. The research objectives were to identify RS variables that are useful for estimating AGB and evaluate the extent of improvement in the precision of the remote sensing-assisted AGB estimates beyond the precision of a pure FBSS. Reference AGB data for model calibration and estimation were collected from 111 systematically distributed circular sample plots (SPs) of 1,000 m² area. Independent variables were derived from Landsat-8, Sentinel-2 and PlanetScope images acquired in January 2019. The area-weighted mean and standard deviation of the spectral reflectance, spectral index and texture (only for PlanetScope) variables were extracted for each SP. A maximum of two independent variables from each image type was fitted to a generalized linear model for AGB estimation using model-assisted estimators. The results of this study revealed that the Landsat-8 model with predictor variable of shortwave infrared band reflectance and the PlanetScope model with predictor variable of green band reflectance had estimation efficiency of 1.40 and 1.37, respectively. Similarly, the Sentinel-2 model, which had predictor variables of shortwave infrared reflectance and standard deviation of green leaf index, improved AGB estimation with the relative efficiency of 1.68. Utilizing freely available Sentinel-2 data seems to enhance the AGB estimation efficiency and reduce cost and extensive fieldwork in inaccessible areas.

Keywords: aboveground biomass; Sentinel-2; generalized linear model; model-assisted estimation; relative efficiency

1. Introduction

Forests are paramount in regulating the global environment, mainly through sequestering carbon [1]. They are particularly important these days to combat the changing climate, which affects people's life in many aspects. Due to the multiple significance of forest resources, information about the resource base, its spatial distribution and spatio-temporal changes have become a global concern. The information is a basis to make decisions when planning and assessing impacts regarding mitigation and adaptation to global climate change [2-4]. As a result of a series of international dialogues, the conference of the parties to the United Nations Framework Convention on Climate Change (UNFCCC) have passed several decisions to combat the impacts of climate change through sequestering carbon in the living biomass, which mainly includes forests. Incentivizing the REDD+ (Reducing Emission from Deforestation and Forest Degradation, Sustainable Forest Management and Conservation) programs was one of the main issues in the Paris agreement in 2015 [4]. All these programs, initiatives and treaties require information about the resource stock and trends of changes over time.

The current tradition of measurement, monitoring and change estimation for forest resources relies mainly on field-based sample surveys (FBSSs). The FBSS methods of data collection are limited in developing countries due to high costs, logistical challenges and limited field access[5]. As a result, many of the national forest inventory programs in developing countries are still dependent on field inventories conducted with relatively small sample sizes and thus, have high uncertainties in the estimates[6]. Studies about uncertainties of emission reduction in Ethiopia indicated that the estimates based on FBSSs with small sample size are not sufficiently precise to support decision-making [7]. Therefore, it is important to look for alternative approaches that can reduce costs and contribute to improving precision of estimates from pure FBSSs. In recent years, remotely sensed (RS) data and associated estimation techniques have become viable options to support quantification of resource stocks in a cost-effective way in areas inaccessible for traditional FBSS [8-10]. Previous research has shown that RS data can help reducing FBSS efforts without loss of precision of estimates [11].

RS data and technologies have improved over the last few decades and are becoming vital tools for enhancing quality and ensuring accessibility of spatial information to users across the world. Following the developments, there are many sources of useful satellite RS data for estimation of forest resource parameters including aboveground biomass (AGB). Landsat and Sentinel are some examples of such satellite programs, which provide freely available data [12,13]. Images of Landsat-8 (L8) and Sentinel-2 (S2) are useful for AGB estimation in various forest ecosystems [14-18]. However, data with higher spatial resolution are often considered better [19,20].

PlanetScope (PS) images are among potentially applicable commercial satellite RS data, which have 3 m spatial resolution and are acquired daily. These characteristics of the images make the PS data suitable for REDD+ MRV (measurement, reporting and verification) systems [20]. Compared to the L8 and S2 images, fewer studies have been carried out on biomass estimation using the PS images [21].

Various studies used either SB reflectance values, SIs or texture solely or in combination for AGB modelling. A study by [22] on AGB estimation using Landsat TM data in the Brazilian Amazon indicated that a combination of SB and texture variables improved AGB estimation. The study showed the importance of texture information particularly in primary forests where there are complex forest structures. The visible and shortwave infrared-1 bands correlate strongly with AGB, particularly in forests with simple stand structures. Therefore, the visible, near-infrared, Red-edge (for S2) and shortwave infrared-1 SB of each satellite mission and the texture variables of the PS SB reflectance are among the independent variables subject to analysis in the current study. The texture information of L8 and S2 images were not used due to the courser resolution of these images as compared to the PS images.

A study of AGB estimation using Landsat images in North-western Turkey revealed that SIs were better in estimating AGB in that forest type as compared to SB reflectance values [23]. However, sensitivity of SIs to biomass vary between environments and forest types [24-27]. According to the research findings by [24] in India, a significant correlation was observed between AGB and simple ratio (SR), difference vegetation index (DVI), normalized difference vegetation index (NDVI), soil adjusted vegetation index (SAVI) and modified soil adjusted vegetation index (MSAVI). Gizachew et al. [14] found that NDVI, enhance vegetation index (EVI), SAVI, MSAVI, and normalized difference moisture index (NDMI) had significant correlation with total AGB in the Miombo woodlands of Tanzania. Furthermore, atmospherically resistant vegetation index (ARVI) of L8 imagery was used for AGB estimation in Mount Tai, China [17]. A similar study in southern Portugal indicated that SIs are useful as predictors of AGB [28]. Imran et al. [29] in their study in Pakistan found that red-edge normalized difference vegetation index (RENDVI) has greater correlation with AGB than the individual SBs. Together with other SIs mentioned above, the red-edge simple ratio (SRRE) index was used for estimating AGB of mangrove forest in the Philippines [21]. Motohka et al. [30] studied normalized difference green index (NDGI) as a good phenological indicator of various ecosystems in Japan. According to the study by [31], data collected using unmanned aerial vehicles for monitoring post-fire recovery of pine forests in the Mediterranean areas indicated excessive green index (ExGI) as a useful variable for estimating DBH, which is a default predictor of AGB allometry. In another study, ExGI was used

for discriminating vegetation types in the USA and Canada [32]. Furthermore, SIs that are indicators of leaf greenness and used in different applications including crop monitoring and discriminating vegetation like the green leaf index (GLI) and vegetation index (VI), were included in the current list of potential predictor variables to test if they relate to AGB. Table 1 shows detailed descriptions of the SIs explored in this study.

Table 1. Description of spectral indices (SIs) used as candidate independent variables for aboveground biomass (AGB) modelling in this research.

SI	Expression[c]	Reference(s)	
		General	Relationship with AGB
NDVI	$\dfrac{(NIR - R)}{(NIR + R)}$	[33,34]	[14,24]
SR	NIR/R	[35]	[24,28]
VI	G/R	[36]	
DVI	NIR − R	[37]	[24]
ExGI	$2 \times G - (B + R)$		
GLI	$\dfrac{(G - R) + (G - B)}{2 \times G + R + B}$	[38]	
EVI	$2.5 \times \dfrac{(NIR - R)}{(NIR + 6 \times R - 7.5 \times B + 1)}$	[39]	[14]
SAVI	$\dfrac{(NIR - R)}{(NIR + R + 0.5)} \times (1.5)$	[40]	[24]
MSAVI	$\dfrac{2 \times NIR + 1 - \left(\sqrt{(2(NIR) + 1)^2 - 8(NIR - R)}\right)}{2}$	[41]	[24]
NDMI	$\dfrac{(NIR - SWIR1)}{(NIR + SWIR1)}$	[42]	[14]
NDGI	$\dfrac{(G - R)}{(G + R)}$	[30]	
ARVI	$\dfrac{(NIR - (2 \times R - B))}{(NIR + (2 \times R - B))}$	[43]	[17]
SRRE	NIR/RE	[44,45]	[21]
RENDVI	$\dfrac{(NIR - RE)}{(NIR + RE)}$	[46]	[29]

[c] See Table 2 for description of the acronyms of the SBs used in the expressions of the SIs in this table.

Image texture analysis was carried out for the high-resolution PS images to assess the role of pixel resolution in identifying spatial variations of image values and thus providing potentially useful variables for AGB modelling. Several studies indicated that image texture variables can improve AGB estimation, especially in dense tropical forests [17,22,47]. The most common method of calculating image texture variables is the grey level co-occurrence matrix (GLCM).

The dry Afromontane forests in Ethiopia are attributed to areas with an altitude range from 1500 to 3400 m above sea level; mean annual temperature of 14 - 25℃; and mean annual precipitation of 400 - 1700 mm [48]. These forests are of great ecological and economic importance [49,50]. They contribute to the national and international initiatives towards biodiversity conservation and to the mitigation of the global climate change [49]. Although the dry Afromontane forests are important forest types in Ethiopia and have various purposes [51], they are under pressure from the local community for expansion of agriculture, settlement and fuelwood collection [50,52].

Some studies (e.g. [11,14,53]) evaluated the use of RS data for biomass estimation in small study areas in the region of east Africa. However, to the best of our knowledge, except some efforts related to the use of Landsat images for land cover classification and mapping, data from the mentioned satellite missions subject to analysis in the current study have never been used to assess AGB of Afromontane forests in Ethiopia. AGB of trees is the weight of all living material of trees above the soil surface including the stem, stump, branches, bark, seeds and leaves. AGB estimates, which can be converted to carbon stock estimates, are required in forest management, and particularly in implementation of the REDD+ programs that are underway in Ethiopia. Therefore, this study was initiated with the aim of introducing the possibility of supporting and enhancing the estimation of AGB from traditional FBSSs with data from the three satellite programs. The image-derived data were used to construct AGB prediction models. These models will serve as non-destructive spatially explicit tools for AGB prediction and estimation.

Because there is little current experience with what types of variables extracted from the satellite systems in question that would be useful for AGB modelling, the first objective of this study was to explore what kind of variables extracted from the different satellite programs might be useful for AGB modelling in the dry Afromontane forest. The second objective was to evaluate to what extent such RS data could help improving the precision of AGB estimates beyond the precision of a pure FBSS in these forests.

2. Materials and Methods

2.1. Description of the study area

The study was conducted in Degaga-Gambo forest in south-central Ethiopia. It belongs to a state-owned enterprise, Oromia Forest and Wildlife. The study area is located on the eastern escarpment of the central rift valley of Ethiopia, in the Horn of Africa (Figure 1). It extends geographically from 38°45' to 38°56' E longitude and from 7°13' to 7°33' N latitude. The forest has an area of 14,176 ha. The altitude of the study area ranges from 2100 to 2730 m above sea level. The study area has a bimodal rainfall distribution. The main rainy season is from July to September while the short rainy season is from March to May [54]. The mean annual precipitation and temperature in the area are 1245 mm and 14.9℃.

The forest area has both natural and plantation forest types. The major species of plantation forest compartments, which are mostly found in the lower elevations, are *Cupressus lucitanica*, *Pinus patula*, *Grevillea robusta* and different *Eucalyptus* species. The natural forest has high tree species diversity. The dominant tree species observed in the natural forest include *Syzygium guineense, Afrocarpus falcatus, Juniperus procera, Pitosporum viridiflorum, Maesa lanceolate, Millettia ferruginea, Croton macrostachyus* and *Maytenus arbutifolia*. The objectives of the enterprise are production of lumber and poles from the plantations and conserving the natural forests. The natural forests are home to a wide range of wildlife species and are source of water for the downstream areas. Nevertheless, the forests are under severe pressure. Illegal cutting of trees and land use change for settlement and farmland expansion are the common problems in the area.

The forest has complex vertical and horizontal structures. Besides the species diversity, there is large variability in tree height and wood basic density of the study forest. The mean (and range) of observed tree height was 13.9 m (4.9-40.1 m); while the mean (and range) of wood basic density (g cm^{-3}) for tree species in the forest was 0.588 (0.426-0.979) [55].
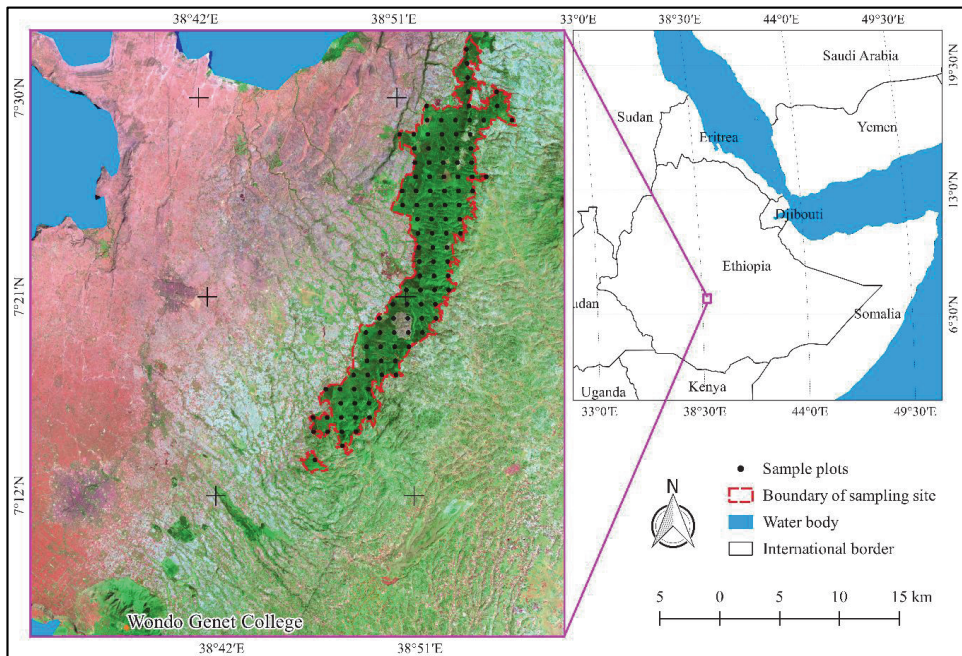
Figure 1. Location of the study area and distribution of the field sample plots (SPs). A band combination of SWIR-NIR-R (in the order of R-G-B) of L8 image was used to enhance the appearance of vegetated areas (in green).

2.2. Field data collection

The sampling frame was defined to include the Degaga-Gambo forest territory, which contains both the natural and plantation forest types. Circular sampling plots (SPs) of 17.85 m radius aligned in a systematic grid at an interval of 1.2 km were used for field data collection (Figure 1). One hundred and eleven plots (from the natural forests, plantation forests and other categories like clear-cut, cropland, settlement and grassland cover types) were sampled from February 2018 to January 2019. Handheld global positioning system (GPS) receiver was used to navigate to the pre-defined locations of the SPs. Then, precise coordinates of the plot centres were determined using differential GPS and global navigation satellite system (GLONASS) measurements. Two Topcon legacy-E + 40 dual frequency receivers were used for this purpose [56]; one serving as base station and the other as a rover field unit. The receivers record pseudo-range and carrier phase of GPS and GLONASS.

The base station was set up at Wondo Genet College of Forestry and Natural Resources campus. The Euclidean distance between the base station and the plot centres ranged between 21.7 and 57.2 km with an average distance of 41.8 km. In order to determine the position of the base

station using precise point positioning, the GPS and GLONASS data were recorded continuously for 24 hours [57]. At the plot centres, the rover was mounted on a 2.98 m carbon rod and recorded for 41.5 minutes on average using a one-second logging rate. The recordings were post-processed using the Magnet tools software [58]. The standard error of the post-processed planimetric plot coordinates ranged from 0.017 to 1.111 m with a mean of 0.232 m.

In each of the SPs, we recorded species names and measured diameter at breast height (DBH), i.e. the diameter of trees at 1.3 m above the ground, for all the trees with DBH ≥ 5 cm. Calliper or diameter tape was used for DBH measurement depending on tree size. Tree height measurements were carried out for 10 trees selected systematically in each of the plots using a Haglöf vertex laser 5 instrument [59]. Height of the trees for which height were not measured were predicted using height-diameter models developed based on the sample trees [14].

2.3. Plot level AGB estimation

Plot level AGB (Mg ha^{-1}, mega grams per hectare) was estimated by aggregating the predicted individual tree AGB in the respective plots. For predicting tree AGB in the natural forests, the allometric model constructed by [55] was used. This model has DBH, height and wood basic density as predictor variables. Wood basic density values were obtained from [60]. For plantation forests, tree AGB was estimated using species-specific allometric models. Accordingly, for *Cupressus lusitanica,* we used the model by [61] with DBH and height as predictor variables. For *Eucalyptus* species and *Grevillea robusta,* models by [62,63] were used, respectively, having DBH and height as predictor variables. The plot level AGB values ranged from 0 to 845.7 Mg ha^{-1} with a mean and standard deviation of 184.35 Mg ha^{-1} and 155.8 Mg ha^{-1}, respectively.

2.4. Satellite image acquisition

Satellite images acquired in January 2019 were considered since this is the dry season when most of the undergrowth vegetation dries up and is easier to distinguish from the trees. This time window was also within the field inventory period. Additionally, selected images were restricted to those with cloud cover < 5%. A detail description of the images used in this study is given in Table 2. Single tiles of each of the L8 and S2 products were downloaded from the USGS Earth Explorer website [64]. Both images were Level-1C products, which means that the images were corrected for any possible topographic and geometric errors. The processing level of the L8 image used in this study was L1-TP, which is a Level-1 precision and terrain corrected product. Besides terrain and topographic correction, radiometric correction has already been done for S2 products prior to delivery. The SB (spectral band) used in this study (i.e., blue (B),

green (G), red (R), near infrared (NIR), shortwave infrared-1 (SWIR1) (for both L8 and S2), red-edge (RE) (only for S2)) have spatial resolutions of 30 m for L8 and 10 or 20 m for S2.

We downloaded the PS Ortho Scene Product (Level-3B) from the Planet Explorer website [65]. Six scenes of orthorectified scaled Top of Atmosphere Radiance (at sensor) image were downloaded to cover the study area. These images contain information about the B, G, R and NIR SBs.

Table 2. Major characteristics of Landsat-8 (L8), Sentinel-2 (S2) and PlanetScope (PS) systems and properties of images used in this study.

Satellite	Sensor	Path/row or tile number	Date of acquisition	Cloud cover (%)	Product processing level	Spectral bands[b]	Spatial resolution
L8	OLI[a]	168/055	16/01/2019	0	L1-TP	B, G, R, NIR, SWIR1	30 m: all SB
S2	MSI	T37NDJ	14/01/2019	3	Level-1C	B, G, R, RE, NIR, SWIR1	10 m: visible, NIR; 20 m: RE, SWIR1
PS	4-band frame imager; NIR filter	Scene-based frames	27/01/2019	0	3B-Analytic-MS	B, G, R, NIR	3 m: all SB

Source: USGS Earth Explorer [64] for L8 and S2; Planet Explorer [65] for PS.
[a] OLI stands for operational land imager.
[b] B, G, R, NIR, SWIR1 and RE represent the blue, green, red, near-infrared, shortwave infrared-1 and red-edge spectral bands, respectively.

2.5. Image processing and independent variable definition

In the current study, we first evaluated a great number of potential candidate variables that could be useful for AGB modelling. A series of image processing techniques were applied on the satellite images to get the independent variables. First, atmospheric correction was done using the QGIS software version 3.1.0 [66] and python codes. For L8 and S2 images, the semi-automatic classification plugin (SCP) of QGIS was used for running the dark-object subtraction (DOS-1) algorithm, which removes the dark pixels that result from atmospheric scattering. The satellite images were transformed from spectral radiance to top of atmosphere reflectance values based on the conversion factors in the metadata file that comes along with the image files. However, the PS images were processed using the empirical line correction for conversion of radiance to reflectance values indicated in Equation 1:

Reflectance = Gain × Radiance (Input data) + Offset   (1)

The radiances of the input images were converted to reflectance values and atmospheric correction applied since variables from multiple images were compared. In addition to variation

in the sensors, the three sets of images were acquired in different dates although within 13 days of maximum gap among them. Furthermore, six scenes of the PS imagery covered the area of interest. After atmospheric correction, all the images became Level-2A products, which have pixels with surface reflectance values suitable for calculating SIs (spectral indices) and texture variables used in this study. Atmospherically corrected SBs, which were used for creating SIs and texture variables shown in Table 1 and Table 3, respectively, were selected for this study. Descriptions of the GLCM image texture data derived from the PS images are presented in Table 3. Texture information of the L8 and S2 images were not used due to the coarse spatial resolutions. Sentinel Application Platform (SNAP) software version 7.0.0 [67] was used for calculating the texture variables. Processing parameters of window size of 11 pixels × 11 pixels, angle in all directions, probability quantization with level of 128 were set to obtain the texture data used in the current study. This processing window size was set to provide an equivalent area to the field SPs.

Table 3. General description of the GLCM texture features used in this study.

GLCM Texture[d]	Expression[e]	Description
Contrast	$\sum_{i,j=0}^{N-1} p_{i,j} \times (i-j)^2$	Contrast and dissimilarity indicate the amount of local grey level (GL) variation in an image. Large values mean presence of edges, noise or wrinkled features.
Dissimilarity	$\sum_{i,j=0}^{N-1} p_{i,j} \times \lvert i-j \rvert$	
Homogeneity (IDM)	$\sum_{i,j=0}^{N-1} \dfrac{p_{i,j}}{1+(i-j)^2}$	Measures the smoothness (homogeneity) of the GL distribution of an image.
ASM	$\sum_{i,j=0}^{N-1} (p_{i,j})^2$	ASM measures the degree of orderliness of pixel values in an image.
Energy	$\sqrt{ASM}$	Energy is a measure of uniformity.
Maximum probability	$maximum\ (p_{i,j})$	Maximum probability of the GL values.
Entropy	$\sum_{i,j=0}^{N-1} p_{i,j} \times (-\ln^{p_{i,j}})$	It measures the degree of randomness of pixel values in an image. Entropy is inversely related to uniformity.
GLCM mean	$\mu_i = \sum_{i,j=0}^{N-1} i \times (p_{i,j})\ ;\ \mu_j = \sum_{i,j=0}^{N-1} j \times (p_{i,j})$	Mean of GL distribution of the image.
GLCM variance	$s^2_i = \sum_{i,j=0}^{N-1} p_{i,j} \times (i-\mu_i)^2;$ $s^2_j = \sum_{i,j=0}^{N-1} p_{i,j} \times (j-\mu_j)^2$	GLCM variance is a measure of dispersion of GL distribution.
Correlation	$\sum_{i,j=0}^{N-1} p_{i,j} \times \left[\dfrac{(i-\mu_i) \times (j-\mu_j)}{\sqrt{s^2_i \times s^2_j}} \right]$	Correlation indicates linear dependency of GL on their neighbouring pixels.

[d] IDM and ASM stand for inverse difference moment and angular second moment, respectively.
[e] Where $p_{i,j}$ is the probability of finding the GLCM relationship at cell (i, j) and is calculated as:

$p_{i,j} = \dfrac{V_{i,j}}{\sum_{i,j=0}^{N-1} V_{i,j}}$; such that $\sum_{i,j=0}^{N-1}(p_{i,j}) = 1$; $V_{i,j}$ = grey level value in a cell (i, j) of the image window,

N = Number of grey levels in the image as specified by number of levels in the quantization

Area-weighted mean and standard deviation (hereafter referred to as mean and standard deviation, respectively) of all the variables were extracted to each SP using QGIS. These were used as independent variables of the models constructed from each RS data, the details of which are explained in the following sections.

2.6. Variable selection and model fitting

The purpose of the AGB regression modelling was to construct models with variables from the RS data as predictors and which could be used to enhance the precision of the overall AGB estimates for the study area. For the AGB estimation we used a model-assisted approach to inference (see details in section 2.8) because that would allow a direct comparison of the uncertainty of the AGB estimate with similar uncertainty estimates obtained for the pure field-based estimate. In model-assisted estimation, the model form and the predictors selected for the model should be determined independent of the sample at hand [68]. In model-assisted inference, no claim of a true model is necessary. A poor choice of model form and predictors would have negative consequences in terms of efficiency [69](p. 238), but would not invalidate the unbiasedness of the estimator. If, however, the choice of model form and the choice of predictors were sample-based, e.g. by choosing predictors by optimizing the predictive power of the model for the sample at hand, there would be a risk of overfitting and underreporting of uncertainty [70].

On this background, we found ourselves in a dilemma in this study. On one hand, we had no prior information about useful variables derived from the given RS data for AGB modelling for the particular forest types under study. Neither had we any experience with suitable model forms for the study area. On the other hand, if model selection and variable selection were optimized for the given sample, overfitting would be a likely consequence.

To balance these conflicting requirements, we first did a screening of the variables mentioned above to gain first-hand experience with the three types of satellite data for the current forest types. We then chose a model-form a priori and allowed only a small number of predictors to be included in the model. In the modelling phase, we paid special attention to any sign of overfitting.

Thus, in the first phase of the analysis, Pearson's correlation coefficient was used to explore the relationships of individual independent variables with AGB. Those variables that had significant correlation with AGB were used as potential variables for the AGB model fitting. Furthermore, correlation analysis was done for each pair of independent variables within each satellite data

source to evaluate the level of intercorrelation between them. Results of the correlation analysis indicated that most of the variables were strongly intercorrelated (Figure 2). Hence, variable screening was employed to reduce the redundant information emanating from those strongly intercorrelated variables. Results of the initial analysis using more complex models showed overfitting problems, which was manifested in accuracy difference between training and validation results for each model. Such sever overfitting was observed for models with more than two variables. Because of the risk of overfitting, we restricted selection of independent variables in the models to a maximum of two variables only. The results from the analysis of models with more than two variables are not documented any further.

The relevant variables of each satellite data source were related to plot-level AGB using the logarithmic link function in a generalized linear model (GLM) of the form:

$$\ln(y_i) = \beta_0 + \sum_{i=1}^{i} \beta_i X_i \qquad (2)$$

where y_i is ground reference AGB (Mg ha^{-1}), β_0 is intercept, β_i is coefficient of the independent variable (X_i), and i is index of an individual independent variable.

This model form was chosen since it provides valid estimates where true zeroes are included in the estimate of AGB, which has positive continuous numerical values. A study of AGB prediction using topographic variables in human-impacted tropical dry forest landscapes of Mexico indicated that GLM estimation technique improved predictions [71]. Thus, the mean of SBs and SIs of L8 image were candidate independent variables for the L8 model. The mean and standard deviation of the SBs and SIs of S2 image were candidate independent variables for the S2 model. The mean and standard deviation of SBs, SIs and texture features of PS bands were used as candidate independent variables for the PS model.

2.7. Model validation

We evaluated the performance of the models using a leave one out cross-validation technique. The cross-validation was used to assess overfitting. Each model was validated in terms of coefficient of determination (R^2), root mean squared error (RMSE, %), mean deviation (MD, %), and Akaike Information Criterion (AIC) as determined by Equations 3 - 8. The AIC was used to evaluate the maximum likelihood of the model parameters.

$$R^2 = 1 - \frac{\text{Residual deviance}}{\text{Null deviance}} \qquad (3)$$

$$\text{RMSE} = \sqrt{\frac{1}{n}\sum_{i=1}^{n}(y_i - \hat{y}_i)^2} \qquad\qquad (4)$$

$$\text{RMSE\%} = \frac{\text{RMSE}}{\bar{y}} \times 100 \qquad\qquad (5)$$

$$\text{MD} = \frac{1}{n}\sum_{i=1}^{n}(y_i - \hat{y}_i) \qquad\qquad (6)$$

$$\text{MD\%} = \frac{\text{MD}}{\bar{y}} \times 100 \qquad\qquad (7)$$

$$\text{AIC} = -2\ln L[\hat{\beta}(k)] + 2k \qquad\qquad (8)$$

where y_i and $\hat{y}_i$ are the ground reference and predicted AGB (Mg ha-1) in the ith SP, and $\bar{y}_i$ is the mean of ground reference AGB (Mg ha-1) of all SPs; n is the sample size; $L[\hat{\beta}(k)]$ is the likelihood function of the observations, $\hat{\beta}(k)$ is the maximum likelihood estimation of the parameter β, given the number of parameters of k within the model. The maximum likelihood estimation enables choosing the parameter that makes the likelihood of having the observed data a maximum fit with the dependent variable (AGB) without causing an overfitting issue. When comparing models, the model with a smaller AIC is better than the one with a higher AIC. In addition to the validation metrics indicated above, we did qualitative evaluation based on visual comparison between the predictions using the selected models in each satellite data source and false-colour composite (i.e. band combination of NIR-R-G in the R-G-B channels) depiction of the S2 image.

2.8. Population level estimation and efficiency assessment

Based on the SP inventory data, for the sample size of 111 plots of about 1,000 m2 area, the estimator of the mean AGB for the population and estimator of its variance were calculated by Equations 9 and 10, respectively [69]:

$$\hat{\mu}_{\text{field}} = \frac{1}{n}\sum_{i=1}^{n} y_i \qquad\qquad (9)$$

$$\widehat{\text{var}}(\hat{\mu}_{\text{field}}) = \frac{1}{n(n-1)}\sum_{i=1}^{n}(y_i - \hat{\mu}_{\text{field}})^2 \qquad\qquad (10)$$

where y_i is AGB (Mg ha-1) of the ith SP in the sample and n is the sample size.

The 95% confidence interval (CI) of $\hat{\mu}_{\text{field}}$ was calculated using Equation 11:

$$\text{CI} = \hat{\mu}_{\text{field}} \pm t \times \text{SE}(\hat{\mu}_{\text{field}}) \qquad\qquad (11)$$

where $\text{SE}(\hat{\mu}_{\text{field}}) = \sqrt{\widehat{\text{var}}(\hat{\mu}_{\text{field}})}$ is the standard error (SE) of $\hat{\mu}_{\text{field}}$ and t is student's t at significance level of 0.05.

Similarly, we estimated the mean AGB for the entire study area using the selected regression model for each satellite data source. For this purpose, the study area was tessellated into grid cells of 31.64 m × 31.64 m providing a total of N (141,604) population units. The size of the grid cell size was chosen to be equivalent to the SPs. Area-weighted mean and standard deviation of the variables used in the regression models were extracted for each grid cell using QGIS. AGB was predicted for each population unit (i) in the map of the tessellated granules using the selected regression models for each satellite data source and is represented by $\hat{y}_i$. Because the prediction relied on field data collected based on probability sampling inside the population of interest, we adopted generalized model-assisted regression estimators. The mean and the variance estimates were computed using Equations 12 and 13, respectively [69] (p.231):

$$\hat{\mu}_{image} = \frac{1}{N}\sum_{i=1}^{N}\hat{y}_i + \frac{1}{n}\sum_{i=1}^{n}(y_i - \hat{y}_i) \qquad (12)$$

where $\hat{\mu}_{image}$ is the mean remote sensing-assisted estimate of AGB (either L8, S2 or PS). The first term in this estimator $(\frac{1}{N}\sum_{i=1}^{N}\hat{y}_i)$ is the mean of the model predictions $(\hat{y}_i)$ for all population units, and the second term $(\frac{1}{n}\sum_{i=1}^{n}(\hat{y}_i - y_i))$ is an estimate of the mean error calculated over the sample units and compensates for systematic model prediction errors.

$$\widehat{var}(\hat{\mu}_{image}) = \frac{1}{n(n-1)}\sum_{i=1}^{n}(\varepsilon_i - \overline{\varepsilon})^2 \qquad (13)$$

The SE of the mean AGB estimators (i.e. $SE(\hat{\mu}_{field})$ and $SE(\hat{\mu}_{image})$) were calculated by taking the square root of the respective variance estimators $\widehat{var}(\hat{\mu}_{field})$ and $\widehat{var}(\hat{\mu}_{image})$.

The study assessed the gain in precision of AGB estimation with the use of the three types of RS data. The measure of quantifying such a gain in precision of using RS data over the pure field-based estimates was expressed using relative efficiency (REf). REf quantifies the magnitude of estimated variance of a remote sensing-assisted estimate of mean AGB to a field-based estimate. It was computed by Equation 14 as the ratio of the variance of the field-based estimates to the remote sensing-assisted estimates:

$$REf = \frac{\widehat{var}(\hat{\mu}_{field})}{\widehat{var}(\hat{\mu}_{image})} \qquad (14)$$

When REf is greater than one, it is interpreted as the amount of additional precision gained due to the use of the RS data for estimating mean AGB.

3. Results

3.1. Relationship of independent variables with AGB

Examination of the relationship of individual RS variables with AGB demonstrated that many of the candidate variables were reasonably related with AGB. Correlation coefficients were translated to descriptors like 'weak', 'moderate' and 'strong' relationships according to the scheme used by [72]. The mean SB reflectance values of the three satellite data sources had negative moderate correlation with AGB (Table 4). On the other hand, the mean values of most SIs tend to show moderate positive relationship with AGB with some exceptions (for instance, mean ExGI of S2). It was revealed from the exploratory analysis that standard deviation of SIs of S2 and PS images and texture variables of PS images had moderate relationships with AGB.

For the L8 category of independent variables, the mean SIs were less correlated with AGB as compared to those of the SBs. Table 4 shows that from the SIs, the mean NDMI had considerable relationship while that of ARVI, NDVI and SR have weaker performance. The mean values of all SBs were moderately related to AGB with correlation coefficients ranging from -0.38 (NIR_mean) to -0.48 (SWIR1_mean). The strength of association of AGB with NIR_mean was equivalent to that observed with the strongly correlated SI (i.e. the NDMI_mean), which was 0.39.

From the S2 variables, the mean of both SBs and SIs showed reasonable association with AGB. Similar to the L8 variables, the mean of SBs had stronger relationship than that of the SIs except the mean ExGI, which had the strongest relationship. The peculiar behavior of ExGI comes from the fact that it is just a difference of SBs. Likewise; standard deviation of the SIs (namely GLI, NDGI and VI) had strong positive association with the dependent variable.

Similarly, for the PS variables, the mean of SBs of G, R and B showed the strongest relationship with AGB followed by that of VI and NDGI SIs. The mean and standard deviation of the texture data had moderate relationship with AGB (Table 4).

Table 4. Correlation of relevant independent variables (see Tables 1, 2 and 3 for definitions) derived from L8, S2 and PS images with AGB. The notations for SB and SI variables of all the image types are MMM_mean or MMM_std representing the mean and standard deviation of the variable MMM, in respective order. For texture variables of the PS data, BnXXX_mean is the mean of the mentioned (XXX) texture variable of the SB Bn where n =1, 2, 3, 4 for B, G, R, NIR, respectively. Similarly, BnXXX_std is the standard deviation of the texture variable as described above.

L8		S2		PS	
Variable	**correlation**	**Variable**	**correlation**	**Variable**	**correlation**
NDMI_mean	0.39***	GLI_std	0.44***	VI_mean	0.44***
ARVI_mean	0.27**	NDGI_std	0.43***	NDGI_mean	0.44***
NDVI_mean	0.23*	VI_std	0.43***	B4ASM_std	0.37***
SR_mean	0.19*	NDMI_mean	0.31***	B4ENE_std	0.35***
NIR_mean	-0.38***	NIR_mean	-0.42***	NIR_mean	-0.38***
B_mean	-0.41***	R_mean	-0.43***	B3VAR_mean	-0.39***
R_mean	-0.42***	B_mean	-0.46***	B2VAR_mean	-0.39***
G_mean	-0.45***	RE_mean	-0.48***	B1VAR_mean	-0.39***
SWIR1_mean	-0.48***	G_mean	-0.49***	B3MEA_mean	-0.40***
		SWIR1_mean	-0.49***	B2MEA_mean	-0.40***
		ExGI_mean	-0.51***	B1MEA_mean	-0.40***
				B_mean	-0.46***
				R_mean	-0.46***
				G_mean	-0.48***

* p-value < 0.05; ** p-value < 0.01; *** p-value < 0.001.

3.2. Variable selection for the prediction models

Correlation analysis indicated that independent variables of each satellite data source were strongly intercorrelated (Figure 2). Therefore, the variables that fit well with AGB in the GLM, and which had no significant collinearity problem, were selected for the AGB prediction models. As a result, the means of NDMI and NIR variables were less intercorrelated and became predictor variables for one of the L8 models. Besides, a simple model with the most strongly correlated variable (SWIR1) with AGB was considered as another candidate model in this category.

Similarly, the mean of SWIR1 and standard deviation of GLI were selected as predictor variables for the two-variable S2 model. The standard deviation of GLI had strong positive correlation with AGB (Table 4) and was less correlated with the mean of SWIR1 variable (Figure 2), which was already in the model. Moreover, the single variable model with a predictor variable of mean of ExGI and another one with mean of SWIR1 SB were other candidate models of the S2 category.

From the PS data, the mean of G reflectance had the strongest correlation with AGB. Thus, one of the PS models contains independent variables composed of the mean reflectance of G SB and

standard deviation of the ASM texture variable of the NIR SB. The mean of B4ASM was the least intercorrelated with the mean of G SB. The other simple model was the model with a predictor variable of the mean of G SB reflectance only.
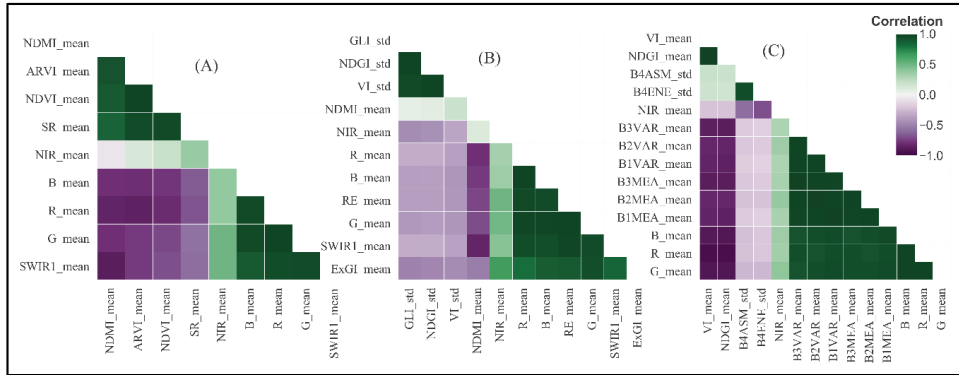
Figure 2. Intercorrelation among independent variables derived from (A) L8, (B) S2, and (C) PS images. See Table 4 for description of the notations used to represent the independent variables.

3.3. Selected AGB models for each image type

Table 5 shows detailed description of the candidate AGB models for each image type. Two candidate models were obtained from the L8 data. There was marginal difference between the single and two-variable models with AIC of 1403.31 and 1402.68, respectively. The model calibration RMSE of the single and two-variable models were 70.22% and 71.06% of the mean AGB, respectively. Likewise, the respective model validation RMSE values were 73.23% and 73.31% of the mean AGB. As clearly revealed in these model metrics, there is concern of less responsiveness of the selected variables for the AGB estimates in the two-variable model. The presence of two variables in the model did not significantly improve the model performance. Therefore, the model with the mean of SWIR1 reflectance as the only predictor variable was selected for AGB estimation.

Three models were selected as candidates from the S2 variables. Two of them were with single predictor variable while the third has two variables (Table 5). The model with the mean of ExGI as a predictor variable had a larger validation RMSE (73.80%) than the other models and had an overfitting problem. The model with predictor variable of the mean of SWIR1 was better than the one with the mean of ExGI. However, the two-variable model had even greater performance among the S2 category of models. The two-variable S2 model with predictor variables of the mean of SWIR1 and standard deviation of GLI had the least AIC value among the models (1385.06) and minimal overfitting problem (Table 5). Additional indicators of the model fit and

validation results of this model were also better than the other models in the category. This model explained 40.96% of the variability in the ground reference AGB unlike the selected L8 and PS models, each of which explained less than 30%.

Two candidate models were obtained from the PS data. The two-variable PS model contains the mean of G reflectance and standard deviation of B4ASM texture as predictor variables. However, this model revealed a severe overfitting problem. The model RMSE and validation RMSE were 70.19% and 79.48%, respectively. Thus, the single variable model with the mean of G reflectance was selected for AGB estimation in this category. It had model calibration and validation RMSE of 71.79% and 75.17%, respectively. Overall performance of the selected PS model was slightly lower than the S2 models but similar to that of the selected L8 model (Table 5). The validation results of all the three selected models for AGB estimation indicated that the models have sensible performance in predicting AGB for the data with which they were not trained. The scatter plot of fitted versus ground reference AGB values shown in Figure 3 indicates a reasonable predictive power of the models given the complex settings of the study area. Pearson's correlation coefficients of the model predicted and ground reference AGB in the SPs revealed that the S2 model predictions were more correlated with the ground reference AGB than the other two models. The S2 model predictions had correlation coefficient of 0.64 with the ground reference AGB.

Table 5. Models and performance indicators for mean AGB estimation in the Degaga-Gambo forest using independent variables from L8, S2 and PS images.

Image	Model	AIC	Calibration RMSE (%)	Validation RMSE (%)	Prediction Correlation[f]
L8	$\widehat{AGB} = \exp(6.0703 - 9.3781 \times NIR\_mean + 3.5489 \times NDMI\_mean)$	1402.68	129.46 (70.22)	135.20 (73.31)	0.55
	$\widehat{AGB}^{@} = \exp(6.9967 - 16.1492 \times SWIR1\_mean)$	1403.31	131.00 (71.06)	135.00 (73.23)	0.54
S2	$\widehat{AGB}^{@} = \exp(6.1310 - 11.4874 \times SWIR1\_mean + 12.7865 \times GLI\_std)$	1385.06	119.58 (64.87)	123.70 (67.12)	0.64
	$\widehat{AGB} = \exp(7.1200 - 51.3576 \times ExGI\_mean)$	1400.00	128.97 (69.96)	136.01 (73.80)	0.56
	$\widehat{AGB} = \exp(6.9968 - 15.2480 \times SWIR1\_mean)$	1402.00	130.33 (70.69)	134.70 (73.06)	0.54
PS	$\widehat{AGB} = \exp(10.0593 - 56.0248 \times G\_mean + 1.1545 \times B4ASM\_std)$	1402.55	129.40 (70.19)	147.30 (79.48)	0.55
	$\widehat{AGB}^{@} = \exp(11.7696 - 75.2766 \times G\_mean)$	1406.00	132.34 (71.79)	138.58 (75.17)	0.52

Mean and std refer to the area-weighted mean and standard deviation of the image-derived variables within the grid cells.

@ Selected model for AGB prediction from each image type.

f Pearson correlation coefficient between ground reference and model-predicted values of AGB for the models in each image type. The square of these coefficients is the same as the R2 of the models, which was determined using Equation 3.

The L8 and PS models had equivalent performance and explained a considerable amount of the variation in the FBSS estimate of mean AGB with R^2 of 29% and 27%, respectively, given the complex forest structure and topography in the study area.
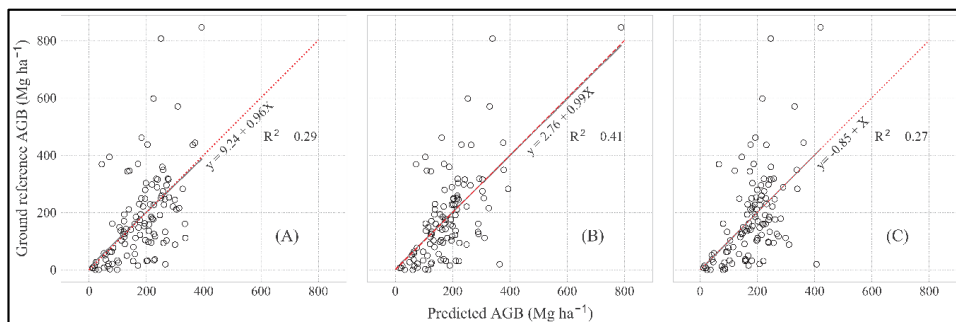
Figure 3. Relationship of ground reference versus predicted AGB using selected models of (A) L8, (B) S2, and (C) PS data. The dashed red and grey solid lines (overlapping) represent the identity and the correlation function, respectively.

Although the general trend of the error distribution of the three selected models looks similar, prediction errors of the L8 and PS models spread out at small and large AGB more than the S2 model did (Figure 3). The extents of deviation of predicted values from the ground reference AGB differ for each model especially at the smaller and larger AGB values. With this variability maintained, the selected models of all the three image data inflated predictions of small AGB, particularly those below approximately 300 Mg ha^{-1}. For SPs with large AGB, the predictions using all the three models were smaller than the ground reference values.

Figure 4. Understory vegetation in a forest SP. The understory vegetation that was not measured during the forest inventory could have influenced the image values and thus their relationship with AGB.

The L8 and S2 models had smaller prediction error at the smaller AGB end than at the large AGB levels. Generally, the predictive power of the S2 model prevailed over that of the other models.

### 3.4. Estimation and mapping of AGB using the selected models

Table 6 shows the estimated mean AGB, estimates of mean deviation, SE of the mean AGB estimates and REf for the selected models of the three image categories presented in Table 5. The estimates of mean AGB were 179.67 Mg ha^{-1}, 177.79 Mg ha^{-1} and 184.27 Mg ha^{-1} when using the L8, S2 and PS model predictions, respectively. The model-assisted estimates of the mean AGB for all the three categories of models were within 95% CI of the mean AGB estimate based the field data only (i.e. 155.15 - 213.76 Mg ha^{-1}). The estimated mean AGB using the PS model was closer to the field-estimated mean AGB (i.e. 184.35 Mg ha^{-1}) than the estimates using the other models. The estimated mean AGB using the L8 and PS models had the largest and smallest MDs, respectively. The AGB estimate based on the PS model was relatively less precise followed by the L8 model. The estimation results revealed that the L8 and PS models resulted in equivalent estimation efficiencies (i.e., 1.40 and 1.37, respectively).

The estimate based on the S2 model was the most precise among the three model-assisted AGB estimates with SE of 11.40 Mg ha^{-1}. As a result, the REf of the mean AGB estimate using the S2 model (i.e. 1.68) was greater than what we obtained by using the other two models.

Table 6. Estimated mean AGB (Mg ha^{-1}), mean deviation (MD) in Mg ha^{-1}, standard error (SE) of the mean estimates (Mg ha^{-1}) and relative efficiency (REf) when using the selected models to assist in the estimation.

Estimator data source	Estimated mean AGB	Estimated MD	SE	REf
Model-assisted; L8-model	179.67	1.71	12.49	1.40
Model-assisted; S2-model	177.79	0.62	11.40	1.68
Model-assisted; PS-model	184.27	-0.13	12.62	1.37
Field-based	184.35	-	14.79	-

Visual inspection of the predicted AGB using the three selected models and the false colour composite of the S2 image shows convincing AGB distribution across the landscape. As expected, the patches of bare land in the study area (shown in different shades of grey in Figure 5-D) have small AGB predictions using all the models while the dense forest areas (coloured red in Figure 5-D) yielded greater predicted AGB values. The map revealed that AGB predictions using the selected models had many similarities, which also was confirmed by similarities in the estimated uncertainties (Table 6). The proportion of each category of AGB predictions and their distribution patterns in the maps clearly indicated the spatial consistency of AGB predictions across the area for the selected models.
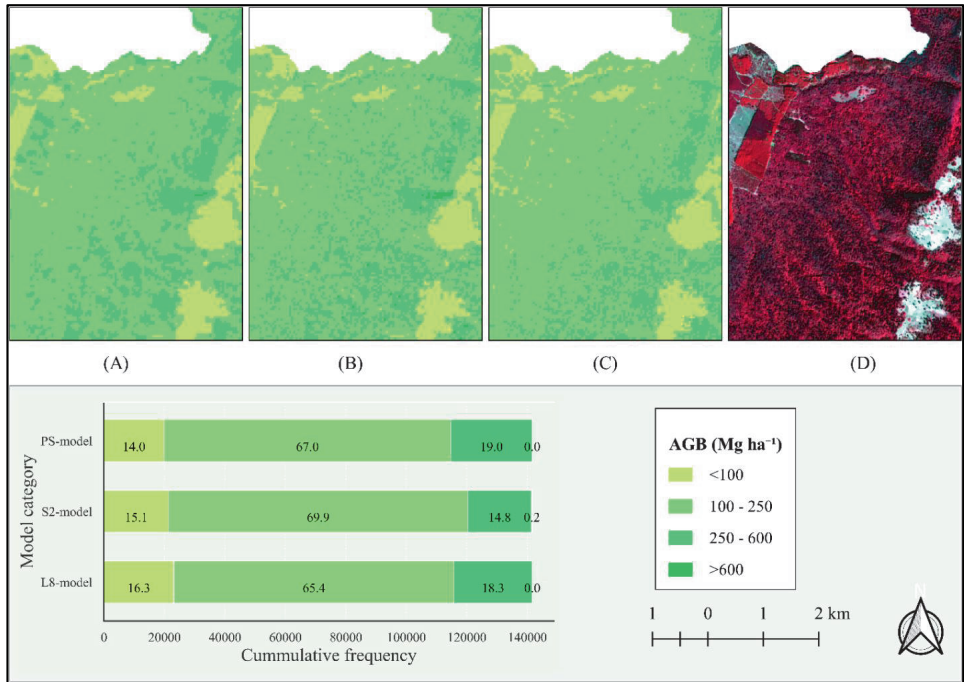
Figure 5. Visual representation of a portion of the predicted AGB using the selected models of (A) L8, (B) S2, (C) PS and (D) false colour composite (NIR-R-G in the R-G-B channels) of the S2 image of the study area acquired on 14 January 2019. Values within the bar graph are area proportions of predicted AGB for each class of AGB (shown in the legend) for the population.

4. Discussion

4.1. Variable exploration for estimating AGB and model selection

The observed moderate relationships of independent variables of the RS data with AGB demonstrated the potential of optical RS data for developing models to enhance AGB estimation. The observed negative correlation coefficients between the mean of SB reflectance and AGB agree with results of similar studies conducted in various forest types [14,73,74]. The negative correlation coefficients indicate the inverse relationship between reflectance values from the SBs and AGB. This relationship in the current study could be explained by a shadow effect within the complex forest stands where AGB is large [75, 76]. The presence of scattered big trees in SPs with large AGB result in large shadows. Additionally, such an effect might be related to large canopy water content, which is directly linked to photosynthetic efficiency [77]. The reflectance of the SBs from uniform forest stands like young plantations is large but they have relatively small AGB.

The positive relationship of most of the SIs with AGB found in this study is in accordance with previous research findings [14,28,74]. Besides the mean of SIs in each SP, the standard deviation of some SIs had also remarkable potential to relate with AGB. Næsset et al. [11] got similar results in Tanzania. Reviewed literature indicated that application of some of the SIs like the GLI, ExGI and NDGI have been limited to assessing grass biomass and crop cover or yield estimation. However, the current study showed that they had great potential to predict AGB in this type of forest. Thus, an in-depth study is required to understand the potential of such SIs for AGB estimation in different forest types.

It was revealed from the correlation analysis that most of the predictor variables in each satellite data were intercorrelated. Lu et al. [78] found a similar result for estimation of AGB in wheat using unmanned aerial vehicle. Among the SBs, the visible and the shortwave infrared bands, which are affected by atmospheric interference and shadow, were more strongly intercorrelated [75]. Besides, SIs and texture variables were derived from these interrelated SBs. Therefore, the observed intercorrelation among the independent variables was likely to happen. This suggests the importance of a careful screening of RS variables for AGB modelling.

Furthermore, inter-resolution comparison of SBs showed that the limited spectral properties of the PS images might have restricted their potential to characterize AGB. For example, AGB correlated similarly with the G SB from each of the three image sources regardless of the differences in spatial resolution. The study results showed that the same SB across the resolution gradient characterized AGB similarly, indicating only a minor impact of pixel

resolution on the quality of the AGB models if only SBs are related to AGB (Table 4). We observed that the S2 data contain a range of SBs that were more sensitive to AGB than the PS data, which have a higher spatial resolution.

Based on the relationship of the independent variables with AGB, we identified useful variables and models for each satellite data source. For example, exploration of the L8 data revealed that the NDMI showed a stronger correlation with AGB than other SI variables including the NDVI. This might be due to the improvements in the NDMI to detect leaf water content at the canopy level [50]. Previous research indicated that NDMI is useful for predicting forest attributes, including biomass [29,64]. The NDVI, which is the most popular SI for AGB modelling mostly in the temperate and boreal forests, was not a good predictor of AGB in the current study. Sader et al. [26] got similar results indicating unsuitability of NDVI for estimating AGB in tropical dense forests.

However, for the L8 data, AGB had a stronger correlation with SBs than the SIs mentioned above. Even among the SBs, AGB strongly correlated with the mean of SWIR1. The significance of the SWIR1 variable for AGB modelling was according to the results of other studies [18]. A study of biomass estimation using RS data in India indicated that biomass models using the SWIR bands were more reliable than those using short-wavelength SBs like the visible bands, which are more sensitive to atmospheric effects [79, 80]. For green vegetation, reflectance in the SWIR spectral regions is controlled by the amount of water in the leaf biomass of the canopy. There is low diffuse of light at the SWIR wavelengths, and hence shadows are contrasted. The presence of thick layers of fragmented tree canopy and shadows in SPs with large AGB yielded low reflectance in the SBs, including the SWIR1 SB as indicated with the negative coefficient in the selected model.

The S2 model used for AGB estimation was the two-variable model with the independent variables of the mean of SWIR1 and standard deviation of GLI. Inclusion of the standard deviation of the GLI variable in the S2 model indicates the ability to capture spatial variation in canopy structure in the forest as the GLI can identify green leaves and stems from the background soil surface [38]. This variable may reflect the level of disturbance, terrain variation or presence of very big scattered trees in the natural forest. This variable signifies the importance of using measures of variability derived from higher resolution images in AGB modelling. The mean of ExGI was also another variable from the S2 data sensitive to AGB variability.

Besides the SBs and SIs, texture variables of the PS images had considerable potential for AGB modelling. The standard deviation of B4ASM that was included in one of the PS models, indicating the importance of high-resolution images for AGB modelling. Image texture variables like the ASM, describe the spatial arrangement of pixels with varying intensities that resulted in different AGB. The texture variables were able to differentiate between heterogeneous and homogenous surfaces, which prevailed in the disturbed natural forest patches and young plantation forests, respectively. This might be the reason for the observed strong positive relationship of the standard deviation of B4ASM with AGB. Improvement in the model performance by including this texture variable was in line with the findings of other studies [19, 47, 81]. Nevertheless, the two-variable model containing the standard deviation of B4ASM was subject to overfitting as compared to the reduced model with the mean of the G reflectance variable (Table 5).

4.2. Model characteristics and their contribution to enhance AGB estimation

Generally, the selected L8 and PS models explained a proportion of the variability in the ground reference AGB that was within the expected range, given the complex nature of the forest and terrain configuration. The calibration RMSEs of the L8 and PS models were 71.06% and 71.79% of the mean of the ground reference AGB, respectively. This was comparable with the results of other studies conducted even in intermediate vegetation cover conditions where it is easier to get a stronger relationship between image data and AGB [68]. The REf of the AGB estimates based on the selected L8 and PS models were 1.40 and 1.37, respectively. Consequently, there was similarity in improving the mean AGB estimates based on the L8 and PS models. The REf when using the L8 model in this study was slightly larger than the findings by Næsset et al. [11] for Miombo woodlands in Tanzania using the global Landsat products.

The selected S2 model contributed more strongly to improve the precision of the AGB estimates than the L8 and PS models. This improvement in estimation efficiency contributes to reducing the number of field SPs required to attain the same precision, to approximately 59% of the sample size required for a pure FBSS estimate.

The REf when using the S2 model was smaller than that of the RapidEye images used for AGB estimation in the Miombo woodlands in Tanzania [11]. This might be attributed to the heterogeneity of the forest in the current study, or the interaction effect of forest types and spatial resolution of the images. Besides, [11] stated that the small study area covered in their study might have resulted in overly optimistic results because the remotely sensed data were very homogenous since they came from only a single scene. On the other hand, the results of the

current study were similar to the findings by Navarro et al. [16] who studied AGB of mangrove plantations using S2 images in Senegal. Thus, the findings of the current study are reasonable given the heterogeneity of the terrain and forest conditions, which influence the relationship of image data and AGB [80].

Although there were some variations between the models in this might regard, they were able to predict only to a limited range of the ground reference AGB. This shows a saturation problem for which canopy shadow is mainly responsible in the SPs with large AGB. Similar studies in primary and successional forests in Brazil indicated that shadows were among the main factors resulting in data saturation, particularly in natural forests with large AGB [76]. Therefore, future efforts should focus on synchronizing other auxiliary variables like canopy density and canopy height from airborne laser scanning data with the identified variables to improve model performance.

During the fieldwork, understory vegetation was observed in SPs (see Figure 4). The inflated predictions at SPs with small AGB might be attributed to this phenomenon. The field inventory was limited to trees with DBH ≥ 5 cm and did not account for the understory vegetation. Dense understory vegetation composed of saplings, shrubs, lianas and herbaceous species covered most of these SPs and challenged our movement during the fieldwork. The biomass in the understory vegetation, which was not accounted for in the ground reference AGB, could have had a major influence on the SB reflectance values and hence in all the RS variables. This might partly explain the moderate improvement in precision of the model-assisted estimates of AGB compared to the pure field-based estimate. As shown in Table 6, the PS-model assisted estimates had negative MD indicating the greater effect of the inflated predictions at SPs with small AGB than the reduced predictions at the SPs with large AGB. Thus, the effect of understory vegetation on the relationship between image-derived variables and AGB was more obvious when using the high-resolution PS images. A greater compliance of the RS data with AGB would happen for homogeneous forests in which the understory vegetation cover is minimal and the forest canopy cover is uniform. Therefore, further studies are needed in pure plantation forests to attain an optimum efficiency of RS data for AGB estimation beyond the ones we got in this study.

Generally, the findings of the current study were encouraging. We identified relevant variables extracted from RS data for AGB estimation. The selected models of each satellite data source based on the identified variables provided reasonable improvements in AGB estimations, which were reinforced by other research findings. The freely available S2 data were particularly useful. The research results revealed that S2 images possess sensible spectral and spatial properties

for AGB estimation. The results of this study will help to satisfy the existing demand for forest carbon stock assessment by the national REDD+ program in Ethiopia. Enhanced forest information using the freely available data sources like the S2 would help to improve sustainable forest management and encourage results-based payments for those who properly manage their forest resources according to established principles like the REDD+ schemes.

5. Conclusion

Optical RS variables from L8, S2 and PS satellites were studied with the objective of identifying relevant RS predictor variables that could be used to enhance AGB estimation in a dry Afromontane forest. Most of the SBs, some SIs and texture variables (listed in Table 4) were found to be promising variables for predicting AGB. Although some of them were not selected in the models used for assisting AGB estimation, we identified variables including the mean of GLI, ExGI and NDGI that were seldom used for AGB modelling but are highly correlated with AGB. We recommend a detailed investigation of the importance of these variables for AGB assessment in various forest conditions.

The simple models selected for each satellite data source enhanced AGB estimation. Of the variables used in the models, the SWIR1 SB, which lacks in the PS data, was a useful variable of the L8 and S2 images for AGB estimation in this forest type despite the huge differences in pixel resolution among the image types. The study suggested that the spectral resolution of optical satellite images was more determinant of AGB estimation than the pixel size.

The use of RS data for AGB estimation improved the precision of estimates. Thus, the remote sensing-assisted estimation techniques used in this study will complement the FBSS estimates of AGB by improving accuracy. The study results provide sufficient evidence that the L8, S2 and PS model estimates could reduce sample size to 71%, 59% and 73%, respectively, of the field sample size to get the same accuracy with the FBSS estimates. However, the models used for AGB estimation in this study revealed saturation problem. Therefore, future studies should focus on refining these limitations using a synergy of different data sources to enhance estimation efficiency of AGB models beyond the ones achieved in the current study.

Conflicts of Interest: The authors declare no conflict of interest.

References

1. Bonan, G.B. Forests and climate change: forcings, feedbacks, and the climate benefits of forests. Science 2008, 320, 1444-1449, doi: 10.1126/science.1155121.

2. Anderson, J.W. The Kyoto Protocol on Climate Change; Resources for the Future: Washington DC, 1998; pp 1-21.

3. UNFCCC. Draft decision-/CP. 15. In Proceedings of Conference of the Parties to the UNFCCC, Copenhagen, 7-18 December, 2009; pp. 1-5.

4. UNFCCC. Adoption of the Paris Agreement Proposal by the President. In Proceedings of Paris Climate Change Conference – COP 21, Paris, 21 December 2015; pp. 1-32.

5. Kebede, B.; Soromessa, T. Allometric equations for aboveground biomass estimation ofOlea europaeaL. subsp.cuspidatain Mana Angetu Forest. *Ecosystem Health and Sustainability* **2018**, *4*, 1-12, https://doi.org/10.1080/20964129.2018.1433951.

6. Duncanson, L.; Rourke, O.; Dubayah, R. Small Sample Sizes Yield Biased Allometric Equations in Temperate Forests. *Sci Rep* **2015**, *5*, 1-13, https://doi.org/10.1038/srep17153.

7. Watson, C.; Mourato, S.; Milner-Gulland, E.J. Uncertain Emission Reductions from Forest Conservation: REDD in the Bale Mountains, Ethiopia. *Ecol. Soc.* **2013**, *18*, 1-16, doi:10.5751/es-05670-180306.

8. Hashim, M.; Pour, A.B.; Chong, K.W. Tropical forest degradation monitoring using ETM+ and MODIS remote sensing data in the Peninsular Malaysia. *IOP Conference Series: Earth Environ. Sci.* **2014**, *18*, 1-6, doi:10.1088/1755-1315/18/1/012011.

9. Ingole, N.A.; Ram, R.N.; Ranjan, R.; Shankhwar, A.K. Advance application of geospatial technology for fisheries perspective in Tarai region of Himalayan state of Uttarakhand. *Sustainable Water Resources Management* **2015**, *1*, 181-187, https://doi.org/10.1007/s40899-015-0012-9.

10. Koch, B. Remote Sensing supporting national forest inventories NFA. In *FAO knowledge reference for national forest assessments*, 2013; pp. 1-15.

11. Næsset, E.; Ørka, H.O.; Solberg, S.; Bollandsås, O.M.; Hansen, E.H.; Mauya, E.; Zahabu, E.; Malimbwi, R.; Chamuya, N.; Olsson, H., et al. Mapping and estimating forest area and aboveground biomass in miombo woodlands in Tanzania using data from airborne laser scanning, TanDEM-X, RapidEye, and global forest maps: A comparison of estimated precision. *Remote Sens. Environ.* **2016**, *175*, 282-300, https://doi.org/10.1016/j.rse.2016.01.006.

12. Malenovský, Z.; Rott, H.; Cihlar, J.; Schaepman, M.E.; García-Santos, G.; Fernandes, R.; Berger, M. Sentinels for science: Potential of Sentinel-1, -2, and -3 missions for scientific observations of ocean, cryosphere, and land. *Remote Sens. Environ.* **2012**, *120*, 91-101, https://doi.org/10.1016/j.rse.2011.09.026.

13. Woodcock, C.E.; Allen, R.; Anderson, M.; Belward, A.; Bindschadler, R.; Cohen, W.; Gao, F.; Goward, S.N.; Helder, D.; Helmer, E., et al. Free access to Landsat imagery. *Science Letters* **2008**, *320*, 1011-1012, doi:10.1126/science.320.5879.1011a.

14. Gizachew, B.; Solberg, S.; Naesset, E.; Gobakken, T.; Bollandsas, O.M.; Breidenbach, J.; Zahabu, E.; Mauya, E.W. Mapping and estimating the total living biomass and carbon in low-biomass woodlands using Landsat 8 CDR data. *Carbon Balance Manage.* **2016**, *11*, 1-14, https://doi.org/10.1186/s13021-016-0055-8.

15. Li, C.; Li, Y.; Li, M. Improving Forest Aboveground Biomass (AGB) Estimation by Incorporating Crown Density and Using Landsat 8 OLI Images of a Subtropical Forest in Western Hunan in Central China. *Forests* **2019**, *10*, 1-17, https://doi.org/10.3390/f10020104.

16. Navarro, J.A.; Algeet, N.; Fernández-Landa, A.; Esteban, J.; Rodríguez-Noriega, P.; Guillén-Climent, M.L. Integration of UAV, Sentinel-1, and Sentinel-2 Data for Mangrove Plantation Aboveground Biomass Monitoring in Senegal. *Remote Sens.* **2019**, *11*, 1-23, https://doi.org/10.3390/rs11010077.

17. Qiu, A.; Yang, Y.; Wang, D.; Xu, S.; Wang, X. Exploring parameter selection for carbon monitoring based on Landsat-8 imagery of the aboveground forest biomass on Mount Tai. *European J. Remote Sens.* **2019**, *52*, 1-12, https://doi.org/10.1080/22797254.2019.1686717.

18. Risdiyanto, I.; Fakhrul, M. Examination of Multi-Spectral Radiance of the Landsat 8 Satellite Data for Estimating Biomass Carbon Stock at Wetland Ecosystem. *Preprints* **2017**, *04 April 2017*, 1-14, http://dx.doi.org/10.20944/preprints201704.0020.v1.

19. Sousa, A.M.O.; Gonçalves, A.C.; da Silva, J.R.M. Above-Ground Biomass Estimation with High Spatial Resolution Satellite Images. In *Biomass Volume Estimation and Valorization for Energy*, Tumuluru, J.S., Ed. InTech: Rijeka, Croatia, 2017; Vol. 2017, pp. 47-70.

20. Sousa, A.M.O.; Gonçalves, A.C.; Mesquita, P.; Marques da Silva, J.R. Biomass estimation with high resolution satellite images: A case study of Quercus rotundifolia. *ISPRS J. Photogramm. Remote Sens.* **2015**, *101*, 69-79, https://doi.org/10.1016/j.isprsjprs.2014.12.004.

21. Baloloy, A.B.; Blanco, A.C.; Candido, C.G.; Argamosa, R.J.L.; Dumalag, J.B.L.C.; Dimapilis, L.L.C.; Paringit, E.C. Estimation of Mangrove Forest Aboveground Biomass Using Multispectral Bands, Vegetation Indices and Biophysical Variables Derived from Optical Satellite Imageries: Rapideye, Planetscope and Sentinel-2. *ISPRS Ann. Photogramm. Remote Sens. Spatial Inf. Sci.* **2018**, *IV-3*, 29-36, doi:10.5194/isprs-annals-IV-3-29-2018.

22. Lu, D. Aboveground biomass estimation using Landsat TM data in the Brazilian Amazon. *Int. J. Remote Sens.* **2007**, *26*, 2509-2525, https://doi.org/10.1080/01431160500142145.

23. Günlü, A.; Ercanli, I.; Başkent, E.Z.; Çakır, G. Estimating aboveground biomass using Landsat TM imagery: A case study of Anatolian Crimean pine forests in Turkey. *Ann. For. Res.* **2014**, *57*, 289-298, doi: 10.15287/afr.2014.278.

24. Das, S.; Singh, T.P. Correlation analysis between biomass and spectral vegetation indices of forest ecosystem. *Int. J. Eng. Res. Technol.* **2012**, *1*, 1-13.

25. Ringrose, S.; Matheson, W.; Matlala, C.J.S.S.; O'Neill, T.; Werner, P.A. Vegetation spectral reflectance along a north-south vegetation gradient in northern Australia. *J. Biogeogr.* **1994**, *21*, 33-47, https://www.jstor.org/stable/2845602.

26. Sader, S.A.; Waide, R.B.; Lawrence, W.T.; Joyce, A.T. Tropical forest biomass and successional age class relationships to a vegetation index derived from Landsat TM data. *Remote Sens. Environ.* **1989**, *28*, 143-156, https://doi.org/10.1016/0034-4257(89)90112-0.

27. Viña, A.; Gitelson, A.A.; Nguy-Robertson, A.L.; Peng, Y. Comparison of different vegetation indices for the remote assessment of green leaf area index of crops. *Remote Sens. Environ.* **2011**, *115*, 3468-3478, https://doi.org/10.1016/j.rse.2011.08.010.

28. Macedo, F.L.; Sousa, A.M.O.; Gonçalves, A.C.; Marques da Silva, J.R.; Mesquita, P.A.; Rodrigues, R.A.F. Above-ground biomass estimation for Quercus rotundifolia using vegetation indices

derived from high spatial resolution satellite images. *European J. Remote Sens.* **2018**, *51*, 932-944, https://doi.org/10.1080/22797254.2018.1521250.

29. Imran, A.B.; Khan, K.; Ali, N.; Ahmad, N.; Ali, A.; Shah, K. Narrow band based and broadband derived vegetation indices using Sentinel-2 Imagery to estimate vegetation biomass. *Glob. J. Environ. Sci. Manage.* **2020**, *6*, 97-108, doi: 10.22034/GJESM.2020.01.08.

30. Motohka, T.; Nasahara, K.N.; Oguma, H.; Tsuchida, S. Applicability of Green-Red Vegetation Index for Remote Sensing of Vegetation Phenology. *Remote Sens.* **2010**, *2*, 2369-2387, https://doi.org/10.3390/rs2102369.

31. Larrinaga, A.R.; Brotons, L. Greenness Indices from a Low-Cost UAV Imagery as Tools for Monitoring Post-Fire Forest Recovery. *Drones* **2019**, *3*, 1-16, https://doi.org/10.3390/drones3010006.

32. Sonnentag, O.; Hufkens, K.; Teshera-Sterne, C.; Young, A.M.; Friedl, M.; Braswell, B.H.; Milliman, T.; O'Keefe, J.; Richardson, A.D. Digital repeat photography for phenological research in forest ecosystems. *Agric. For. Meteorol.* **2012**, *152*, 159-177, doi: 10.1016/j.agrformet.2011.09.009.

33. Huete, A.; Justice, C.; Van Leeuwen, W. MODIS vegetation index (MOD13). Algorithm theoretical basis document. 1999; p 129.

34. Rouse, J.W.; Hass, R.H.; Schell, J.A.; Deering, D.W.; Harlan, J.C. *Monitoring the vernal advancement and netrogradation (greenwave effect) of natural vegetation*; Texas A M Univ Coll Station Texas, Texas, United States: 1974; p 390.

35. Jordan, C.F. Derivation of leaf-area index from quality of light on the forest floor. *Ecology* **1969**, *05*, 663-666, https://doi.org/10.2307/1936256.

36. Adamsen, F.J.; Pinter, P.J.; Barnes, E.M.; LaMorte, R.L.; Wall, G.W.; Leavitt, S.W.; Kimball, B.A. Measuring wheat senescence with a digital camera. *Crop Sci.* **1999**, *39*, 719-724, https://doi.org/10.2135/cropsci1999.0011183X003900030019x.

37. Richardson, A.J.; Wiegand, C.L. Distinguishing vegetation from soil background information. *Photogramm. Eng. Remote Sens.* **1977**, *43*, 1541-1552.

38. Louhaichi, M.; Borman, M.M.; Johnson, D.E. Spatially Located Platform and Aerial Photography for Documentation of Grazing Impacts on Wheat. *Geocarto International* **2001**, *16*, 65-70, https://doi.org/10.1080/10106040108542184.

39. Liu, H.Q.; Huete, A. A feedback based modification of the NDVI to minimize canopy background and atmospheric noise. *IEEE Trans. Geosci. Remote Sens.* **1995**, *33*, 457-465, https://doi.org/10.1109/36.377946.

40. Huete, A.R. A soil-adjusted vegetation index (SAVI). *Remote Sens. Environ.* **1988**, *25*, 295-309, https://doi.org/10.1016/0034-4257(88)90106-X.

41. Qi, J.; Kerr, Y.; Chehbouni, A. External factor consideration in vegetation index development. In Proceedings of The 6th International Symposium on Physical Measurements and Signatures in Remote Sensing, France, 01 January 1994; pp. 723-730.

42. Gao, B.C. NDWI - A normalized difference water index for remote sensing of vegetation liquid water from space. *Remote Sens. Environ.* **1996**, *58*, 257-266, https://doi.org/10.1016/S0034-4257(96)00067-3.

43. Kaufman, Y.J.; Tanre, D. Atmospherically resistant vegetation index (ARVI) for EOS-MODIS. *IEEE Trans. Geosci. Remote Sens.* **1992**, *30*, 261-270, doi: 10.1109/36.134076.

44. Rajah, P.; Odindi, J.; Mutanga, O.; Kiala, Z. The utility of Sentinel-2 Vegetation Indices (VIs) and Sentinel-1 Synthetic Aperture Radar (SAR) for invasive alien species detection and mapping. *Nature Conservation* **2019**, *35*, 41-61, https://doi.org/10.3897/natureconservation.35.29588.

45. Torino, M.S.; Ortiz, B.V.; Fulton, J.P.; Balkcom, K.S.; Wood, C.W. Evaluation of Vegetation Indices for Early Assessment of Corn Status and Yield Potential in the Southeastern United States. *Agron. J.* **2014**, *106*, 1389-1401, https://doi.org/10.2134/agronj13.0578.

46. Gitelson, A.; Merzlyak, M.N. Quantitative estimation of chlorophyll-a using reflectance spectra: Experiments with autumn chestnut and maple leaves. *J. Photochem. Photobiol., B: Biol.* **1994**, *22*, 247-252, https://doi.org/10.1016/1011-1344(93)06963-4.

47. Kelsey, K.; Neff, J. Estimates of Aboveground Biomass from Texture Analysis of Landsat Imagery. *Remote Sens.* **2014**, *6*, 6407-6422, https://doi.org/10.3390/rs6076407.

48. Gerhardt, K.; Hytteborn, H. Natural dynamics and regeneration methods in tropical dry forests - an introduction. *J. Veg. Sci.* **1992**, *3*, 361-364, https://doi.org/10.2307/3235761.

49. Price, M.; Gratzer, G.; Alemayehu Duguma, L.; Kohler, T.; Maselli, D. *Mountain Forests in a Changing World: Realizing Values, Adressing Challenges*; Food and Agriculture Organization of the United Nations (FAO) and Centre of Development and Environment (CDE): Rome, Italy, 2011.

50. Solomon, N.; Segnon, A.C.; Birhane, E. Ecosystem Service Values Changes in Response to Land-Use/Land-Cover Dynamics in Dry Afromontane Forest in Northern Ethiopia. *Int. J. Environ. Res. Public Health* **2019**, *16*, 1-15, https://doi.org/10.3390/ijerph16234653.

51. Lemenih, M.; Bongers, F. Dry Forests of Ethiopia and Their Silviculture. In *Silviculture in the Tropics*, Günter, S., Weber, M., Stimm, B., Mosandl, R., Eds. Springer-Verlag Berlin Heidelberg: Germany, 2011; Vol. 8, pp. 261-272.

52. Nguon, P.; Kulakowski, D. Natural forest disturbances and the design of REDD+ initiatives. *Environ. Sci. Policy* **2013**, *33*, 332-345, https://doi.org/10.1016/j.envsci.2013.04.011.

53. Otukei, J.R.; Emanuel, M. Estimation and mapping of above ground biomass and carbon of Bwindi impenetrable National Park using ALOS PALSAR data. *South African Journal of Geomatics* **2015**, *4*, doi: 10.4314/sajg.v4i1.1.

54. Duriaux, J.Y.; Baudron, F. Understanding people and forest interrelations along an intensification gradient in Arsi-Negele, Ethiopia. In *Agrarian change in tropical landscapes*, Deakin, L., Kshatriya, M., Sunderland, T., Eds. Center for International Forestry Research (CIFOR): Indonesia, 2016; pp. 14-53.

55. Asrat, Z.; Eid, T.; Gobakken, T.; Negash, M. Aboveground tree biomass prediction options for the Dry Afromontane forests in south-central Ethiopia. *Forest Ecology and Management* **2020**, *473*, 1-14, https://doi.org/10.1016/j.foreco.2020.118335.

56. Topcon Positioning Systems Inc. . Availabe online: https://www.topconpositioning.com/gb/ (accessed on 16 September 2019).

57. Kouba, J. A guide to using international GNSS service (IGS) products. 2009; p 34.

58. MAGNET Tools 1.0.; Topcon Positioning Systems Inc. Availabe online: https://www.topconpositioning.com/gb/ (accessed on 21 September 2019).

59. Haglöf Company Group. Availabe online: http://www.haglofsweden.com/index.php/en/products/instruments/height/541-the-vertex-laser-geo-all-you-need-in-a-rangefinder-hypsometer (accessed on 12 November 2019).

60. Asrat, Z.; Eid, T.; Gobakken, T.; Negash, M. Modeling and quantifying tree biometric properties of Dry Afromontane forests of South-central Ethiopia. *Trees (under review)*.

61. Berhe, L.; Assefa, G.; Teklay, T. Models for estimation of carbon sequestered by Cupressus lusitanica plantation stands at Wondo Genet, Ethiopia. *Southern Forests* **2013**, *75*, 113-122, https://doi.org/10.2989/20702620.2013.805511.

62. Ounban, W.; Puangchit, L.; Diloksumpun, S. Development of general biomass allometric equations for Tectona grandis Linn.f. and Eucalyptus camaldulensis Dehnh. plantations in Thailand. *Agriculture and Natural Resources* **2016**, *50*, 48-53, https://doi.org/10.1016/j.anres.2015.08.001.

63. Owate, O.A.; Mware, M.J.; Kinyanjui, M.J. Allometric Equations for Estimating Silk Oak (Grevillea robusta) Biomass in Agricultural Landscapes of Maragua Subcounty, Kenya. *Int. J. For. Res.* **2018**, 10.1155/2018/6495271, 1-14, https://doi.org/10.1155/2018/6495271.

64. USGS. USGS Earth Explorer. Availabe online: https://earthexplorer.usgs.gov/ (accessed on 23 August 2019).

65. Planet. Planet Explorer. Availabe online: https://www.planet.com/explorer/ (accessed on 03 September 2019).

66. QGIS Development Team. QGIS - A Free and Open Source Geographic Information System. Availabe online: https://www.qgis.org/en/site/ (accessed on 23 November 2019).

67. ESA. SNAP version 7.0.0. Availabe online: http://step.esa.int/main/download/snap-download/ (accessed on 28 August 2019).

68. Magnussen, S.; Næsset, E.; Gobakken, T. An application niche for finite mixture models in forest resource surveys. *Can. J. For. Res.* **2019**, *49*, 1453-1462, https://doi.org/10.1139/cjfr-2019-0170.

69. Särndal, C.E.; Swensson, B.; Wretman, J. *Model assisted survey sampling*; Springer: New York, USA, 1992; pp. 694.

70. Magnussen, S.; Næsset, E.; Kändler, G.; Adler, P.; Renaud, J.P.; Gobakken, T. A functional regression model for inventories supported by aerial laser scanner data or photogrammetric point clouds. *Remote Sens. Environ.* **2016**, *184*, 496-505, https://doi.org/10.1016/j.rse.2016.07.035.

71. Salinas-Melgoza, M.A.; Skutsch, M.; Lovett, J.C. Predicting aboveground forest biomass with topographic variables in human-impacted tropical dry forest landscapes. *Ecosphere* **2018**, *9*, 1-20, doi:https://doi.org/10.1002/ecs2.2063.

72. Schober, P.; Boer, C.; Schwarte, L.A. Correlation Coefficients: Appropriate Use and Interpretation. *Anesth Analg* **2018**, *126*, 1763-1768, doi: 10.1213/ANE.0000000000002864.

73. Bao, N.; Li, W.; Gu, X.; Liu, Y. Biomass Estimation for Semiarid Vegetation and Mine Rehabilitation Using Worldview-3 and Sentinel-1 SAR Imagery. *Remote Sens.* **2019**, *11*, https://doi.org/10.3390/rs11232855.

74. Lorenzen, B.; Jensen, A. Reflectance of blue, green, red and near infrared radiation from wetland vegetation used in a model discriminating live and dead above ground biomass. New phytol. 1988, 108, 345-355, https://doi.org/10.1111/j.1469-8137.1988.tb04173.x.

75. Wang, Q.; Pang, Y.; Li, Z.; Sun, G.; Chen, E.; Ni-Meister, W. The Potential of Forest Biomass Inversion Based on Vegetation Indices Using Multi-Angle CHRIS/PROBA Data. *Remote Sensing* **2016**, *8*, https://doi.org/10.3390/rs8110891.

76. Lu, D.; Batistella, M.; Moran, E. Satellite estimation of aboveground biomass and impacts of forest stand structure. *Photogramm. Eng. Remote Sens.* **2005**, *71*, 967-974, https://doi.org/10.14358/PERS.71.8.967.

77. Prasad, B.; Babar, M.A.; Carver, B.F.; Raun, W.R.; Klatt, A.R. Association of biomass production and canopy spectral reflectance indices in winter wheat. *Can. J. Plant. Sci.* **2009**, *89*, 485-496, https://doi.org/10.4141/CJPS08137.

78. Lu, N.; Zhou, J.; Han, Z.; Li, D.; Cao, Q.; Yao, X.; Tian, Y.; Zhu, Y.; Cao, W.; Cheng, T. Improved estimation of aboveground biomass in wheat from RGB imagery and point cloud data acquired with a low-cost unmanned aerial vehicle system. *Plant Methods* **2019**, *15*, 17, https://doi.org/10.1186/s13007-019-0402-3.

79. Horler, D.N.H.; Ahern, F.J. Forestry information content of Thematic Mapper data. *Int. J. Remote Sens.* **1986**, *7*, 405-428, https://doi.org/10.1080/01431168608954695.

80. Roy, P.S.a.R., S.A. Biomass estimation using satellite remote sensing data-an investigation on possible approaches for natural forest. *J. Biosciences* **1996**, *21*, 535-561, https://doi.org/10.1007/BF02703218.

81. Nichol, J.E.; Sarker, M.L.R. Improved Biomass Estimation Using the Texture Parameters of Two High-Resolution Optical Sensors. *IEEE Transactions on Geoscience and Remote Sensing* **2011**, *49*, 930-948, doi: 10.1109/TGRS.2010.2068574.

Norwegian University
of Life Sciences